REVERSE AND FORWARD GENETICS APPROACHES REVEAL THE GENE NETWORKS THAT REGULATE DEVELOPMENT OF INNER EAR NEURONS

A Dissertation

by

HUSNIYE KANTARCI

Submitted to the Office of Graduate and Professional Studies of
Texas A&M University
in partial fulfillment of the requirements for the degree of

DOCTOR OF PHILOSOPHY

Chair of Committee,	Bruce B. Riley
Committee Members,	Arne Lekven
	Luis Rene Garcia
	Vladislav Panin
Head of Department,	Tom Mcknight

August 2017

Major Subject: Biology

ABSTRACT

Stato-Acoustic Ganglion (SAG) neurons originate from the floor of the otic vesicle during a brief developmental window. They subsequently leave the otic vesicle and undergo a phase of migration and proliferation (transit-amplification). Neuroblasts finally differentiate into mature SAG neurons and extend processes to connect sensory cells of the inner ear to the information processing centers in the brain. The goal of this dissertation has been to elucidate mechanisms controlling these diverse events, which have heretofore been only poorly understood.

First we showed that a threshold level of Fgf signaling initially sets the neurogenic domain in the otic epithelium. However, the level of Fgf signaling increases during development and becomes inhibitory to otic neurogenesis. Specfically, fgf5 is expressed by accumulating SAG neurons, which serves to terminate specification of new neuroblasts and delay differentiation of transit-amplifying cells.

Second, we tested the role of transcription factor *tfap2a*, which we found is expressed in the neurogenic domain in both zebrafish and chick. Gain and loss-of-function studies revealed that Tfap2a activates expression of *bmp7a*, which in turn partially inhibits Fgf and Notch signaling. By modulating the inhibitory functions of Fgf and Notch, Tfap2a regulates the duration, amount and speed of SAG development.

Third, we investigated the mechanism by which SAG neuroblasts leave the otic epithelium. We showed that Goosecoid (Gsc) regulates epithelial-mesenchymal transition of the otic neuroblasts. Fgf signaling regulates expression of *gsc* in a region

partially overlapping with the neurogenic otic domain. The medial marker Pax2a acts in opposition to Gsc and stabilizes otic epithelia in non-neurogenic parts of the otic vesicle.

Lastly, we conducted a mutagenesis screen in zebrafish to identify ENU-induced mutations that affect SAG development. We recovered a SAG deficient mutation, termed *sagd1* that strongly reduces a subset of SAG neurons required for vestibular (balance) functions. Whole genome sequencing revealed that *sagd1* affects the glycolytic enzyme, Phosphoglycerate kinase-1 (Pgk1). Further analysis revealed that Pgk1 acts nonautonomously to augment Fgf signaling during early stages of otic neurogenesis.

Together, these studies have uncovered a number of previously unknown mechanisms for dynamic regulation of Fgf to control specification, delamination, and maturation of SAG neurons.

ACKNOWLEDGEMENTS

Firstly, I would like to express my deepest gratitude for my advisor Dr. Bruce Riley whose guidance, encouragement and support inspired me through my graduate studies at Texas A&M. I have been very fortunate to have him as my advisor. His enthusiasm, teachings, motivation and suggestions enabled me to pursue my studies and helped my professional and personal growth. His constant support, guidance and patience helped me to overcome many difficulties during my graduate career. I would also like to thank my committee members Dr. Arne Lekven, Dr. Rene Garcia and Dr. Vladislav Panin for their valuable input, suggestions and guidance.

I am extremely thankful to all past and current Riley lab members for their help and guidance over the past several years. I am very thankful to Dr. Shruti Vemaraju, Dr. Mahesh Padanad and Dr. Neha Bhat for their help and support in initiating my graduate studies. I would like to express my deepest gratitude to Dr. Shruti Vemaraju for introducing me to SAG and helping me in the early days of my work. My special thanks to Yunzi Gou for stimulating intellectual discussions of my projects over the years and for her valuable friendship. My special thanks to Jennifer Dong and Dr. Jinbai Guo for their help in my research projects. I was very fortunate to study with extremely talented udergraduates Andrea Gerberding, Kirstin Maulding and Christine Harris. My special thanks to Andrea Gerberding for her help in the Gsc project. I greatly appreciate members of Dr Lekven's lab for sharing reagents and in-depth discussions.

I am very grateful to my parents, sisters and extended family for their patience, support and love through this journey. Their support and motivation inspired me to develop into the person I am today and guided me through my studies.

I am thankful to all my friends for their support and motivation. I am especially thankful to my friend Gregory Whitaker for his support and help during my graduate studies.

CONTRIBUTORS AND FUNDING SOURCES

This work was supervised by a thesis committee consisting of Professors Bruce Riley, Arne Lekven and Rene Garcia of the Department of Biology and Professor Vladislav Panin of the Department of Biochemistry and Biophysics.

The experiments presented in Chapter III were performed by Dr. Shruti Vemaraju, Dr. Mahesh Padanad and Husniye Kantarci. The data was analyzed by Dr. Shruti Vemaraju, Dr. Mahesh Padanad and Husniye Kantarci and Dr. Bruce Riley. The chapter was written by Dr. Shruti Vemaraju, Dr. Bruce Riley and Husniye Kantarci.

The experiments presented in Chapter IV were performed by Husniye Kantarci and Dr. Renee K. Edlund. The data was analyzed by Husniye Kantarci, Dr. Bruce Riley, Dr. Renee K. Edlund and Dr. Andrew Groves. The chapter was written by Husniye Kantarci and Dr. Bruce Riley.

The experiments presented in Chapter V were performed by Husniye Kantarci and Andrea Gerberding. The data was analyzed by Husniye Kantarci and Dr. Bruce Riley. The chapter was written by Husniye Kantarci and Dr. Bruce Riley.

All the other work in this dissertation was conducted by Husniye Kantarci under the advisement of Dr. Bruce Riley from Biology department.

This work was made possible in part by NIDCD under Grant Number R01- DC 003806. Its contents are solely the responsibility of the authors and do not necessarily represent the official views of the NIDCD.

TABLE OF CONTENTS

Page

LIST OF FIGURES

LIST OF TABLES

CHAPTER I

INTRODUCTION AND LITERATURE REVIEW

CRANIAL PLACODES

In all vertebrates, cranial placodes originate from the preplacodal ectoderm (PPE) that forms at the interface between the epidermis and neural ectoderm. Distinct placodes arise from the stereotypical positions along the anterior-posterior axis of the PPE region and subsequently undergo morphological changes to form the paired sensory organs and cranial neural networks of the head (1-3). Fate maps for the cranial placodes are shown to include adenohypophyseal, olfactory, lens, trigeminal, otic, lateral line and epibranchial placodes in an anteroposterior order. The adenohypophyseal placode gives rise to the neuroendocrine cells of the pituitary gland. The olfactory placode forms the olfactory receptor cells and their afferent neurons. The lens placode forms the non-neural parts of the eye, such as the crystalline-containing cells in the lens. The trigeminal placode forms the somatosensory neurons that transmit touch, pain and temperature related information from the skin of the face, jaw and teeth. Further posteriorly, the otic placode forms alongside the hindbrain and gives rise to the morphologically complex inner ear apparatus and the associated sensory cells such as hair cells and neurons. An additional placode called the lateral line forms both anteriorly and posteriorly to the otic placode in fish and amphibian embryos and is responsible for detecting changes in the surrounding water. Epibranchial placode forms in close association to the endodermal

pharyngeal pouches and gives rise to neuroblasts that migrate and subsequently innervate heart and other visceral organs to transmit information related to, for example, heart rate and blood pressure (1-3). Distinct set of transcriptional factor families such as Eya (Eyes absent), Six (Sine oculis) and Dlx (Distal-less) mark the earliest stages of the PPE development (4-6). Some of the important signals that regulate PPE formation include BMP-antagonists, Wnt antagonists and Fgf signaling (7-9). In zebrafish the transcription factors Gata3, Foxi1 and Tfap2a/c are shown to function redundantly and provide competence throughout the non-neural ectoderm to enable placodal development (9). Formation of the distinct placodes is governed by locally acting signals emanating from the surrounding tissues (2). For example, Fgf signals originating from the adjacent hindbrain regions are shown to be an important regulator of otic placode induction (10-12). Pax family of paired domain homeobox genes are shown to mark the earliest stages of the placodal identity. For example, *pax6* marks the early lens placode progenitors, *pax8* is the earliest marker of the otic placode (13), and later, *pax2a* and *pax8* marks both otic and epibranchial placode progenitors.

DEVELOPMENT OF THE INNER EAR

In anamniotes, soon after the formation of the otic placode, otic cells began to condense as they excrete fluid to form a lumen and subsequently give rise to a fluid filled oval luminal structure, called the otic vesicle (14, 15). The otic vesicle develops by a different mechanism in mammalian and avian embryos such that otic cells invaginate to form an otic cup and subsequently break off from the surface ectoderm to

generate a vesicle (16). In all vertebrates, the otic vesicle gives rise to the interconnected semicircular canals and chambers (utricle, saccule and lagena) that provide housing for a sensory epithelium called cristae in the canals and macula in the chambers (17). Sensory epithelia detect and transmit vestibular (balance) and auditory (hearing) information. In most vertebrates, semicircular canals and the utricular macula constitutes the vestibular apparatus of the inner ear whereas saccule and lagena of the anamniotes serve as the functional homolog of the mammalian cochlea and mediate auditory information (15, 18). Sensory epithelia of the inner ear consist of ciliated sensory hair cells and support cells. Each chamber has an associated otolith, an aggregate of calcium carbonate molecules that is attached to the long cilia of the hair cells and vibrate in response to sensory stimulus. On the contrary, otoliths are lacking in the semicircular canals, hence the hair cells in the cristae sense the angular rotation and movement via their long cilium embedded in the flowing otic fluid. Support cells provide trophic support for the survival and maintenance of the hair cells. In zebrafish, lost hair cells could be replaced by transdifferentiation or proliferation of the support cells (19, 20). This ability is lost in the mammalian inner ear, possibly due to the inability of the highly differentiated support cells to reenter the cell cycle or change cell fate (20-22). Hair cells are innervated by Stato-Acoustic Ganglion (SAG) neurons that carry hearing or balance related information to the processing centers in the hindbrain (14, 15, 18). The structure of the vestibular apparatus is highly conserved among vertebrates, however, auditory structures have undergone extensive changes in shape (15). Despite the changes in the

morphology, the overall functionality of the auditory structures is highly homologous among the vertebrates, as explained below.

MECHANOTRANSDUCTION OF AUDITORY AND VESTIBULAR SIGNALS

Hair cells contain hair-like protrusions called stereocilia in numbers ranging from thirty to a few hundred and one long kinocilium on their apical surface. The kinocilium is a true ciliary structure with two central tubules circled with nine doublet tubules whereas stereocilia are composed of actin filaments. On the apical surface of the hair cells, stereocilia are arranged in parallel rows that progressively increase in height towards the kinocilium. Cadherin23 and Protocadherin 15 form extracellular tip-links that connects the parallel rows of stereocilia and link the highest row of stereocilia to the kinocilium (23). These links are crucial for the mechanotransduction of auditory and vestibular stimuli (23). In mammalia and birds, kinocilium is lost from the auditory hair cells soon after birth but it is retained in the vestibular hair cells albeit its function is not known(24, 25). During development, the kinocilium forms first and it becomes progressively linked to the newly forming stereocilium. In zebrafish, the kinocilium of the earliest forming hair cells, called tether cells, enables the attachment of the otolith particles over the developing macula (26). The kinocilium also plays a role in mechanosensation of the nascent hair cells prior to the onset of tip-link mediated mechanotransduction, but starts to regress afterwards (27).

Displacement of the hair cell cilia towards the kinocilium stretches the tip links and opens the cation selective transduction channels (28). The composition of the otic

fluid (endolymph) that contacts the apical surface of the hair cells and support cells is unique in the presence of high concentration of potassium ions (29). The flow of the potassium ions into the hair cell body causes depolarization and opens the voltage gated calcium channels in the cell membrane (29). The influx of the calcium ions into the hair cell leads to the release of the neurotransmitter glutamate at the basal side and also opens potassium channels to allow the exit of the potassium ions and repolarization. In contrast to the endolymph, basal side of the sensory cells is embedded in a low potassium containing fluid (perilymph) that allows passive flow of the potassium ions. One of the functions of the support cells is to recycle potassium ions back to endolymph via use of the sodium-potassium-chloride cotransporter channels and gap junctions (30). Unlike a conventional synapse that is governed by action potential driven neurotransmitter release, hair cell synapses are specialized in responding to a gradient of changes in membrane potential to allow detection of the stimuli with extremely varying intensities. Moreover, hair cell afferent synapses are specialized to encode long-lasting, sustained stimuli from the environment which require extensive synaptic vesicle recycling ability. To meet the requirements of the high rate and sustained neurotransmitter release, hair cells form ribbon synapses composed of an electron dense ribbon surrounded with tightly clustered synaptic vesicles (31). Ribbon synapses are thought to improve the synchronous release of several synaptic vesicles to encode precise timing and intensity of the stimulus. Ribbon synapses are also capable of immense, continuous transmission, due to the calcium dependent mechanisms that resupply synaptic vesicles (32). The location and the number of ribbon synapses vary

greatly among the hair cells, however, each ribbon lines up with a single post synaptic terminal (33).

PROPERTIES OF SAG NEURONS

Exocytosis of the synaptic vesicles releases glutamate which binds and activates receptors clustered in the post-synaptic terminal of the SAG neurons. SAG neurons are defined as bipolar and pseudomonopolar as their spindle shape displays 2 main projections stemming from the opposite poles of the soma, connecting hair cells to information processing centers in the brain. This configuration renders SAG neurons uniquely different compared to a central neuron where the information that is received by the dendrites and processed in the soma, subsequently invokes an action potential at the axon hillock. Instead, in the SAG neurons, action potential is initiated proximal to hair cells and carried along the axonal segment which is interrupted by the somatic membrane (34). The involvement of the soma in the conductor pathway of SAG neurons is likely to be important for regulation and modification of action potentials.

It is important to note that most studies that characterize the properties of the auditory SAG neurons are conducted in mammalian systems and accordingly 2 different classes of auditory neurons have been described, based on projection patterns and morphology. The first class of the auditory SAG neurons (type 1) is myelinated, constitute 95% of the overall auditory neuron population. Each type 1 SAG neuron is shown to synapse with one hair cell, however, each inner hair cell is innervated by many SAG neurons (35). The remaining 5% of the auditory neurons are classified as type 2 auditory neurons and

differ from the rest of the population as they lack myelin and synapse with the outer hair cells of the mammalian cochlea (36). Outer hair cells are an innovation of the mammalian cochlea and do not exist in other vertebrates. Even though these kinds of hair cells do not play a role in mechanotransduction of sound waves, they amplify the auditory stimulus and enhance the frequency sensing ability of the cochlea (37). Deflections in the stereocilia of the outer hair cells opens the mechanically gated transduction channels, however, the resulting change in the membrane potential creates a mechanical force that sends vibrations to increase the sensitivity of the cochlea (37). Interestingly, each type two auditory SAG neuron make synapses with multiple outer hair cells. Very little is known about the in vivo responses of type 2 auditory neurons to sound stimuli, however, some of the proposed mechanisms describe them a role in the integration of sensory signals and pain perception (38, 39). It is currently unknown if SAG neurons has similar functional diversity in other vertebrates.

It is important to note that sound waves, based on their frequency, reach their maximum amplitude at different locations along the longitudinal axis of the cochlea. Thus, different frequencies of sound are analyzed by different locations in the cochlea, such as, high frequency sounds are encoded in the base and low frequency sounds are detected at the apex of cochlea (40). A similar tonotopic map also exists in the fish auditory chamber saccule, for instance, high frequency stimulus is encoded by the anterior region and low frequency stimulus is detected by the posterior area (41). Each SAG neuron innervates one hair cell, hence transmits information related to a very narrow range of sound frequency. SAG neurons are shown to display an extensive

heterogeneity in firing patterns and respond to a different range of intensity thresholds. Thus, innervation of the hair cells by 10-30 SAG neurons, each subtly differ from another, enables a hair cell to encode a variety of sound intensities regardless of the frequency (42, 43). The number of synapses on the hair cells also varies by the tonotopical location in the cochlea; the hair cells are innervated by 10 SAG neurons in the apex of the cochlea whereas in the 15-30 synapses are present in the mid cochlear regions. Synaptic density correlates with greater hearing acuity, as increased synaptic density shown to correspond to frequencies of increased behavioral sensitivity (44).

Many morphological, anatomical and physical properties of auditory SAG neurons show heterogeneity and display a different response phenotype based on the tonotopic position (45). For example, SAG neurons are arranged along the longitudinal axis of the cochlea such that the size of the soma increases from the apex through mid-base and then increases extremely towards the basal end of the cochlea (46). Hence, SAG neurons likely have somatic specializations towards transmission of high, mid or low sound frequencies. Furthermore, electrophysiological properties of SAG neurons, such as resting membrane potential, action potential latency and duration also show extensive heterogeneity and display a frequency-based tonotopical distribution (47). SAG neurons are also graded according to their responsiveness to the intensity of the sound such that the neurons that are capable of responding to the lowest detectable intensity of the sound are located in the apex while those that require a much higher stimulus to produce a response are located towards the basal end of the cochlea (47). Moreover, the properties that show a clear tonotopic distribution from the apex to the

base of the cochlea also present a marked variation locally, within each of these regions (47). These pronounced differences in excitability and neural firing patterns of SAG neurons are partially accounted by the variation in the abundance and diversity of the potassium and calcium channels present in each SAG auditory neuron. Differential expression of electrophysiologically relevant proteins such as synaptic vesicle-associated proteins, neurofilament proteins and calcium ion binding proteins also contribute to the heterogeneity of SAG neurons (47).

Many of the distinct characteristics of the auditory SAG neurons are partially regulated and maintained by the neutrophic factors BDNF and NT3. Both factors are expressed in the sensory epithelium and important for the survival and synaptic strength of SAG neurons (48-50). Furthermore, BDNF and NT3 regulate expression of the ion channels and synaptic proteins that are known to affect response kinetics of SAG neurons (51). Interestingly, BDNF and NT3 act in opposition such that BDNF overexpression enhances basal SAG characteristics and expression profiles whereas overexpression of NT3 introduces apical SAG neuron properties (50). Accordingly, BDNF is strongly expressed in the basal sensory epithelium and neurons whereas NT3 is highly concentrated in apical hair cells and neurons (50). However, these factors are unlikely to be the sole regulators of variation among SAG population. Yet, very little is known about the other regulators of SAG development and maintenance.

Vestibular system of the inner ear transmits information to the brainstem and cerebellum and drive powerful reflexes that control gaze, direction and balance. Hair cells in the semicircular canals detect rotational acceleration and hair cells in the otolith

organ utricle are responsible for detecting linear acceleration and give information related to head position. Saccular macula detects auditory information in fish, however, in mammals and birds it serves as a vestibular endorgan. Vestibular neurons display a resting discharge, possibly to allow detection of bidirectional information towards increasing or decreasing stimulus. Very little is known about the mechanisms that regulate functional segregation and differential targeting of auditory versus vestibular neurons. Nevertheless, similar to the auditory SAG neurons, vestibular neurons also display heterogeneity in morphology and response dynamics (52, 53). Some vestibular neurons have regularly spaced action potentials with high rates and more precision whereas other vestibular neurons show huge variation in firing rates and display irregularly spaced action potentials (52). Irregular vestibular neurons are more sensitive and have been shown adapt easier to the changing stimulus whereas regular neurons detect a better range of thresholds and temporal information. These two populations are shown to differ in their location in the sensory epithelium, synaptic endings, size and axonal diameter and presence of structural or calcium binding proteins (52). How these two different types of vestibular neurons generated during development are is largely unknown.

DEVELOPMENT OF SAG NEURONS

In all vertebrates, SAG neurons originate from the otic epithelium. A long history of studies explored the possibility of the neural crest or neural tube origin of SAG neurons. However, recent experiments using Cre-recombinase to activate

expression of fluorescent proteins under the control of ear specific markers such as *pax2*, *pax8* and *foxg1* ruled out these possibilities by showing most, if not all, SAG neurons derive from the otic floor (54-56). Furthermore, similar fate mapping studies using neural epithelium markers such as *wnt1* and *pax3* did not reveal any neural crest contribution to the SAG neurons (57). However, neural crest cells do give rise to the Schwann cells that are important for the myelination of the inner ear neurons. Neural crest derived glial cells also likely to play a role in growth and guidance of the central projections of SAG (58). Studies in chick show that axonal processes of SAG neurons follow the corridor of the migratory neural crest cells in perfect concordance (58). Furthermore, removal of hindbrain rhombomere 4 from chick embryos eliminates the migratory neural crest from this region and severely disrupts central and peripheral outgrowth of SAG projections (59). However, these experiments need to be confirmed by genetic ablation of the neural crest since the observed phenotypes could also stem from the lack of signals from the removed hindbrain segment.

In birds and mammals neurogenesis precedes the development of the hair cells and the sensory epithelium, however, in zebrafish both tissues are produced concurrently in adjacent regions. Mouse and chick are estimated to have 8000-9000 SAG neurons in adulthood and humans are estimated to have 30.000 SAG neurons. However, there are only a few hundred of SAG neurons in fish species. The discrepancy for the low number of SAG neurons is very poorly understood. SAG neuroblasts mainly originate from the anteroventral part of the otic vesicle and marked by expression of the basic helix-loop-helix (bHLH) transcription factor *neurogenin1* (*ngn1*). All cranial neurons fail to form

in *ngn1* mutants (60, 61) and overexpression of *ngn1* leads to formation of ectopic cranial neurons (62, 63). Specified neuroblasts subsequently undergo epithelial-mesencyhmal transition and leave the otic epithelium by a process called delamination. Soon after delamination, neuroblasts turn off *ngn1* and upregulate a related proneural bHLH factor called *neurod* (64, 65). *Neurod* expressing neuroblasts migrate towards the hindbrain as they proliferate, and upon reaching their final destination differentiate into mature neurons (66). Mature SAG neurons are marked by the expression of neuronal markers, such as *Islet-1*(*Isl1*) or *Islet-2b* (*Isl2b*) (67, 68).

PATTERNING OF THE NEUROGENIC OTIC DOMAIN

Neuroblasts originate from mostly the anteroventral quadrant of the otic vesicle. This part of the otic vesicle is shown to produce SAG neurons when dissected and isolated in culture. However, anteroposterior patterning of the otic vesicle is initially determined by environmental signals that originate from the tissues surrounding the ear. In chick, removal of the otic vesicle from a donor embryo at the otic cup stage and transplanting into a host embryo with a reverse anterior-posterior (AP) orientation leads to formation of an otic vesicle with the axial plan of the host (69). However, a similar manipulation at later stages causes a reverse AP orientation in transplanted otic vesicles (70). This result indicates that the factors that determine the AP polarity of the otic vesicle are not intrinsic at early stages but the axis becomes fixed at later stages.

Further studies show that, underlying mesoderm and ectodermal tissues express retinoic acid (RA) which confers posterior identity in the otic vesicle (71).

Administration of high levels of RA expands the expression of posterior marker *tbx1* in the expense of the neurogenic tissue (71). Similarly, inhibition of the RA signaling in the posterior half of the otic vesicle expands expression of the neurogenic markers to the posterior region (71). However, complete inhibition of RA signaling is also detrimental to expression of *ngn1* (71). It is likely that RA signaling is graded along the AP axis of the otic vesicle where a low level is required for the patterning of the neural region, whereas, high levels are inhibitory to the neurogenesis.

Fgf signaling is important for many aspects of otic development. In zebrafish, *fgf3* and *fgf8* are expressed in the hindbrain and act redundantly to establish the otic placode and loss of both factors impairs otic development (72). Fgf signaling is also crucial for AP patterning during otic vesicle development. In zebrafish *valentine* (*val*) mutants, *fgf3* expression which is normally restricted to the hindbrain rhombomere 4, expands into the rhombomeres 5 and 6 and results in expansion of the anterior otic vesicle markers(73).Furthermore, conditional inhibition of Fgf signaling during otic development using pharmacological inhibitors leads to loss of anterior otic vesicle characteristics, indicating that Fgf signaling is necessary for the formation of anterior otic fates (74). Fgf signaling has been shown to have neural-inducing potential in many tissues. Loss of Fgf3 and Fgf8 function has also been shown to impair neurogenesis of SAG neurons in zebrafish (75).Correspondingly, pharmacological inhibition of Fgf signaling also impairs SAG neuroblast formation and overexpression of *fgf3* expands anterior otic markers and leads to formation of additional neurod positive SAG neuroblasts in zebrafish embryos (74). In chick, electroporation of an *fgf8* construct

expands neurod expression in a similar fashion (76). Moreover, overexpression of *fgf10* increases the neurogenic domain whereas inhibition of the Fgf signaling reduces *neurod* expression (77). Another Fgf ligand, *fgf19* is also expressed in delaminating SAG neuroblasts in chick, albeit its function is unknown (78). In mouse, Fgf3 from the hindbrain and Fgf10 from the subjacent tissues underlying the otic vesicle regulate otic induction and patterning. Mouse *fgf3* mutants display morphological defects in produce fewer SAG neurons (79). On the contrary, loss of *fgf10* and *fgf3* function is shown to induce ectopic and expanded *neurod* expression in the otic vesicle (80). Similarly, mouse Kreisler mutants which display lower *fgf3* and *fgf10* expression levels due to a patterning defect in rhombomeres 4 and 5 show an expansion in neurogenic domain and produce *neurod* positive cells in ectopic locations (80). Thus, the role of Fgf signaling on otic neurogenesis remains unclear, partially resulting from the lack of detailed analysis on the varying levels and timing of Fgf signals.

There are four Fgf receptors in vertebrates with many alternative splicing isoforms. Fgf receptors vary in their responsiveness due to their different affinities to the present Fgf ligands. All Fgf receptors are expressed in the otic vesicle, although they display a complex spatial and temporal pattern (81). Accordingly *fgfr3* mutation in mice leads to hearing loss and *fgfr2* mutation leads to severe morphological defects in ear development (82, 83). The importance of the differential expression and levels of many Fgf ligands and their receptors during SAG neurogenesis also remains ambiguous. Moreover Fgf signaling is likely involved in many aspects of SAG development, including proliferation and differentiation. For example, Fgf2 has been shown to induce

migration and differentiation of otic neuroblasts (84). Furthermore, addition of Fgf10 reduces proliferation of SAG neuroblasts whereas inhibition of Fgf signaling enhances this process. Despite that, loss of function of other Fgf ligands, such as Fgf9, is shown to induce a contrasting proliferation phenotype in the inner ear. It is currently unknown why Fgf antagonizes neurogenesis in some contexts but induces neurogenesis in others.

In zebrafish, the prosensory domain forms the support cells and hair cells of the sensory epithelia and the proneural domain that produces SAG neuroblasts develop concurrently, in adjacent regions. Prosensory precursors are marked by the expression of the proneural gene *atoh1a*. Development of the prosensory and proneural domain is temporally segregated in mouse and chick embryos, and common progenitors of the sensory and neural domains have been observed in these species (85, 86). Binary cell fate decisions and the pace of neurogenesis are partially regulated by Notch signaling in both progenitor pools. Initially described in Drosophila, Notch receptors interact with the Delta transmembrane ligands in the neighboring cells and induce lateral inhibition to promote acquisition of distinct cell fates within a progenitor pool. Proneural factors such as *atoh1a*, *ngn1* and *neurod* induces the expression of the Delta ligands. Binding of the Delta ligand induces the cleavage of the Notch intracellular fragment (ICD). Notch-ICD acts as a transcription factor and activates expression of the target genes within the nucleus. These target genes include basic helix-loop-helix proneural factors such as *Hairy enhancer of split* (*Hes*) and *Hairy related* (*Her*) genes known to act as transcriptional repressors of proneural genes including *atoh1a* and *ngn1*. As a result, activation of Notch pathway leads to repression of the neural fate in the receiving cell

which consequently adopts an alternate fate, for instance, to become a support cell versus a hair cell. Accordingly, inhibition of Notch signaling leads to excess production of both hair cells and SAG neurons in the zebrafish inner ear (87-89). However, the role of Notch signaling during SAG neurogenesis is very poorly described. Many Delta ligands and Notch receptors are expressed by the early otic neuroblasts, yet there is no secondary cell fate is described for the neurogenic pool. Possibly, neuroblasts that receive lateral inhibition remain in the otic epithelium and contribute to the non-neurogenic parts of the otic vesicle. Alternatively, Notch signaling could have a role in regulation of the overall pace of otic neurogenesis.

As mentioned earlier, prosensory and neural domains develop in adjacent regions in zebrafish. Since *ngn1* and *atoh1a* are required for SAG neuron and hair cell formation, it is suggested that these two transcription factors engage in mutually antagonistic interactions within the anterior otic vesicle domain to sharpen domain boundaries. Accordingly, in mouse *atoh1a* mutants produce more neural precursors whereas loss of *ngn1* function leads to excess number of hair cells precursors (86). However, induction of different proneural genes within these sensory domains is very poorly described. Expression of proper dose of Fgf signaling increases the number of hair cells, despite the effects of this regimen on SAG neurogenesis is very poorly described. Many Fgf ligands are expressed in the developing macula, exposing the prosensory domain to a higher level of Fgf signaling. Possibly, requirements for Fgf signaling or other signaling molecules differ for the induction of *ngn1* versus *atoh1a*.

During my doctoral studies, I aimed to recover novel genes that regulate development of SAG neurons and unreveal the genetic mechanisms and signaling pathways that modulate timing and size growth of SAG neurons. First we investigated the role of Fgf signaling pathway during specification and maturation of SAG neuroblasts (Chapter II). Next, we took candidate approaches to characterize the role of transcription factors Tfap2a and Gsc in SAG development (Chapter III & IV). I have also recovered a novel mutation through an ENU mutagenesis screen. Whole genome sequencing revealed the affected locus as the glycolytic enzyme Pgk1. Further analysis revealed a novel role for glycolysis during SAG development (Chapter V). Future work will focus on studying the remarkable interactions between these identified transcription factors and signaling pathways during SAG development (Chapter VI).

CHAPTER II

A SPATIAL AND TEMPORAL GRADIENT OF FGF DIFFERENTIALLY REGULATES DISTINCT STAGES OF NEURAL DEVELOPMENT IN THE ZEBRAFISH INNER EAR[1]

INTRODUCTION

Neurons of the VIIIth cranial ganglion, or the statoacoustic ganglion (SAG), innervate sensory hair cells in the inner ear. These bipolar neurons relay auditory and vestibular information to the hindbrain. During development, SAG precursors (neuroblasts) originate in the floor of the otic vesicle during a relatively brief window of time. Newly specified neuroblasts soon delaminate from the floor of the otic vesicle before continuing development outside the ear.

Neuroblast specification requires the bHLH transcription factor *neurogenin1* (*neurog1*) (60, 61). Expression of *neurog1* is transient and is followed by strong upregulation of *neurod*, which encodes a related bHLH transcription factor required for completing neuronal differentiation (61, 90). After delamination, neuroblasts migrate a short distance to become situated between the hindbrain and otic vesicle and undergo a

---

[1]Reprinted with permission from "A spatial and temporal gradient of Fgf differentially regulates distinct stages of neural development in the zebrafish inner ear." by Vemaraju S., Kantarci H., Padanad M.S., & Riley B.B., 2012, *PLoS genetics*, 8, 11,:e1003068. Copyright [2012] by Vemataju et al.

transient phase of proliferation to expand the precursor population (66, 77, 91, 92). This phase, termed transit-amplification, is characterized by co-expression of *neurod* and proliferation markers (93). Neuroblasts eventually exit the cell cycle and differentiate into mature neurons.

Numerous studies suggest a role for Fgf in otic neurogenesis. In chick, Fgf10 is expressed in the neurosensory domain of the otic placode and promotes neuroblast specification (77). Elevating Fgf2 or Fgf8 increases the number of SAG neurons (84, 94), though the mechanism of action in these cases has not been determined. In mouse, *Fgf3* is also expressed in the neurosensory domain, and SAG development is impaired in *Fgf3* null mutants . In zebrafish, *fgf3* and *fgf8* are prominently expressed in the developing utricular macula adjacent to the neurogenic domain (75, 95), and impairment of *fgf8* causes a reduction in SAG markers (75, 96). Also in zebrafish, mutations that expand the domain of *fgf3* expression in the hindbrain cause a corresponding expansion of anterior markers in the otic vesicle, including markers of the utricular macula and neurogenic domain (73, 97). Unfortunately, interpretation of these mutant phenotypes in mouse and zebrafish is clouded because morphogenesis of the inner ear is significantly altered. Additionally, previous studies have not been able to clearly distinguish effects of changing Fgf levels on different stages of SAG development.

Here we study the development of SAG and its regulation by Fgf by conditionally manipulating Fgf signaling levels. We show that Fgf signaling differentially controls distinct stages of otic neurogenesis. A moderate level of Fgf is necessary for the initial specification of neuroblasts in the floor of the otic vesicle,

whereas high levels of Fgf inhibit specification. During later stages of SAG development, Fgf5 expressed by mature SAG neurons serves two roles. First, upon accumulation of sufficient mature neurons the phase of specification is terminated. Second, ongoing Fgf signaling delays the differentiation of SAG precursor cells. This ensures maintenance of progenitors and steady production of an appropriate number of mature neurons.

MATERIALS AND METHODS

Fish strains, misexpression and inhibitor treatment

Wild-type zebrafish strains were derived from the AB line (Eugene OR). The following transgenic lines were used in this study: *Tg(hsp70:fgf8)*^{x17} (19), *Tg(hsp70I:dnfgfr1-EGFP)*^{pd1} (98) and *Tg(-17.6isl2b:GFP)*^{zc7} (99). Embryos were maintained at 28^{o}C, unless otherwise stated, and staged according to standard protocol (100). Heat shock-inducible transgenes were activated by incubating embryos for 30 minutes at elevated temperatures as indicated in the Results. In some experiments, Fgf signaling was blocked by treating wild-type embryos in their chorions with SU5402 (Tocris Bioscience) diluted from a 20mM stock in DMSO to a final concentration of 100 µM SU5402. PTU (1-phenyl 2-thiourea, 0.3mg/ml, Sigma) was added to fish water to prevent melanin formation.

Morpholino injection and RT-PCR

To block *fgf5* translation, we used *fgf5tb*-MO" 5'-CATTCTTTCCAGAGAGCGCTAGGCC-3'. To block splicing of *fgf5* transcript, we used *fgf5i1e2*-MO: 5' -GCTCCAGCACACCTAGATAGAGAAA- 3'. Approximately 5ng morpholino was injected per embryo at one-cell stage. Both morpholinos gave identical phenotypes. The efficacy of the splice blocker was assessed at 24 hpf by RT-PCR with primers P1 (forward), 5'-TCGATGGAAGAGTCAACGGGAGC-3' and P2 (reverse) 5'-GCCTTCCCCTCTTGTTCATGGC-3' (see Fig. 2.4 D, E). Expression of *ornithine decarboxylase* (*odc*) was measured as a constitutive control. Uninjected embryos from the same genetic background were used to measure control transcript levels.

In situ hybridization

Whole-mount *in situ* hybridization was carried out with methods described previously (72, 101). A shorter riboprobe was synthesized for *neurog1* using T7 RNA polymerase to avoid binding to shared vector sequences encoded by the *Tg(-17.6isl2b:GFP)*^{zc7} transgene. To improve signal and reduce background staining during in situ hybridization for *fgf5*, pre-hybridization and hybridization were performed at 70^{o}C for 12 hours and 24 hours, respectively.

Immunostaining

Antibody staining was performed as described previously (102). Primary antibodies were as follows: anti-Islet1/2 (Developmental Studies Hybridoma Bank 39.4D5, 1:100 for whole-mount, 1:250 for cryosections) and anti-BrdU (Beckton-Dickinson, 1:300). Secondary antibodies were as follows: HRP-conjugated goat anti-mouse IgG (Vector Labs PI-2000, 1:200) and Alexa 546 goat anti-mouse IgG (Invitrogen A-11003, 1: 250).

Cryosectioning and BrdU labeling

Fixed embryos were washed three times for 5 min each in 1x PBS and then soaked in 20% sucrose solution made in PBS followed by 30% sucrose until sinking to the bottom of a microcentrifuge tube. Embryos were embedded in tissue freezing medium (Triangle Biomedical Sciences, TFM-C) and transverse sections were cut at 10μm thickness using a cryostat and immunostained. Finally, slides were washed twice in 1x PBS and mounted in ProLong Gold (Invitrogen) with a coverslip. For double labeling, whole-mount *in situ* hybridization was performed first followed by immunostaining on cryosections. For BrdU labeling, dechorionated embryos were incubated in fish water containing 10mM BrdU in 1% DMSO for the indicated duration. Embryos were rinsed twice for 5 minutes each in fish water prior to fixation. For older stages (96 hpf) 2nl of 10mM BrdU/1% DMSO solution with 3% filtered green food coloring was injected into the brain ventricle of larvae anesthetized in Tricaine (Sigma). Embryos were first processed by whole-mount *in situ* hybridization for *neurod* and then

cryosectioned. Slides were washed thrice for 5 minutes each in PBT (with 0.1% Triton) and incubated in 2N HCl for 45 minutes at 37^{o}C. Slides were rinsed in PBT again, incubated in blocking solution (with 1% Triton for 36 hpf and 3% Triton for 102 hpf) for 2 hours and stained for BrdU.

Laser ablation

Maturing SAG neurons were ablated using a MicroPoint laser, under 40x objective, in *isl2b:GFP* transgenic line that labels this population of cells. Anesthetized embryos were mounted in a dorsolateral orientation beneath a #1 coverslip on a bridge slide made by stacking two #1 coverslips on either side of the embryo.

RESULTS

Development of the statoacoustic ganglion (SAG)

The paradigm for otic neurogenesis, as formalized in several recent reviews (103, 104), involves a sequential process of specification, delamination, proliferative expansion and differentiation of precursor cells to form the mature SAG. The general features of this process appear to be conserved in zebrafish, shown schematically in Fig. 2.1A. In zebrafish, SAG neuroblasts are initially specified in the floor of the late placode/nascent vesicle as early as 16 hpf (14 somites) and express *neurog1* (61, 105). Neuroblasts begin to delaminate and accumulate outside the otic vesicle by 17 hpf. The reiterative process of specification and delamination peaks at 24 hpf, continues at a more moderate pace through 30 hpf (Fig. 2.1D), then declines sharply and stops entirely by 42

hpf (14). Expression of *neurog1* is only transient. As neuroblasts delaminate they lose expression of *neurog1* and initiate expression of *neurod* (61, 106). At this point SAG precursors enter a phase of transit-amplification, as shown by co-labeling with *neurod* expression and BrdU incorporation (Fig. 2.1E, F). *neurod*$^{+}$ cells continue to proliferate through at least 4 days post fertilization (dpf), the latest stage examined (Fig. 2.1F). Surprisingly, staining with anti-phospho histone H3 shows that there are typically only 1-2 mitotic cells in the SAG at any time between 24 and 50 hpf (Fig. 2.1G, and data not shown), indicating that transit-amplifying cells cycle relatively slowly. Summing *neurod*$^{+}$ cells in serial sections revealed that the number of transit-amplifying cells remains relatively constant after 30 hpf, with a transient peak at 48 hpf followed by a return to steady state of 180-200 cells through 78 hpf (Fig. 2.1B). As precursor cells begin to differentiate they exit the cell cycle and lose expression of *neurod* (Fig. 2.1E, F) and initiate expression of *isl1/2* genes (Fig. 2.1H, I) (90). The first mature Isl1^{+} neurons appear by 20 hpf and almost immediately begin to extend processes to peripheral and central targets (data not shown). Co-staining for BrdU and Gfp in *isl2b:Gfp* transgenic embryos (99) confirms that relatively few mature neurons incorporate BrdU (Fig. 2.1H). The number of Isl1^{+} neurons increases linearly at a rate of 2-2.5 neurons per hour through at least 72 hpf, despite the cessation of specification and delamination at 42 hpf (Fig. 2.1C). The steady increase in mature neurons after 42 hpf presumably reflects ongoing differentiation from the slowly cycling pool of transit-amplifying cells. The slow mitotic rate amongst precursors presumably counterbalances production of new neurons, thereby maintaining a relatively stable transit-amplifying pool.To clarify the

spatial relationship between transit-amplifying and mature SAG cells, we examined sections co-stained for *neurod* and Isl1 (Fig. 2.1I-M). The most mature neurons accumulate in immediate contact with the ventromedial surface of the ear, while *neurod*$^{+}$ cells undergoing transit-amplification reside more distally (Fig. 2.1L, M). By 36 hpf the SAG also develops a more complex spatial distribution, forming three distinct regions along the anterior-posterior axis: The anterior-most region abuts the front end of the otic vesicle and contains only *neurod*$^{+}$ precursors (Fig. 2.1K), although mature neurons accumulate in this region at later stages (see below). The middle region forms a broad mass spreading mediolaterally beneath the utricular region and contains complementary domains of *neurod*$^{+}$ cells and Isl1^{+} cells (Fig. 2.1L). The posterior-most region forms as a narrow finger of Islet^{+} cells and abutting *neurod*$^{+}$ cells extending along the medial surface of the otic vesicle to the level of the saccular macula (Fig. 2.1M). Segregation of neurons into these three AP domains reflects emergence of the topological pattern of innervation of the inner ear: Specifically, Sapède and Pujades (107) reported that anteroventral SAG neurons (corresponding to the anterior and middle regions reported here) predominantly innervate the utricular macula and to a lesser degree anterior and lateral cristae, whereas posterior-medial SAG neurons (corresponding to the posterior region reported here) predominantly innervate the saccular macula and to a lesser degree the posterior crista.

A general model of SAG regulation and manipulation of Fgf signaling

The data presented in subsequent sections support a model in which changing levels of Fgf differentially affect SAG development: Initially, moderate Fgf from nearby

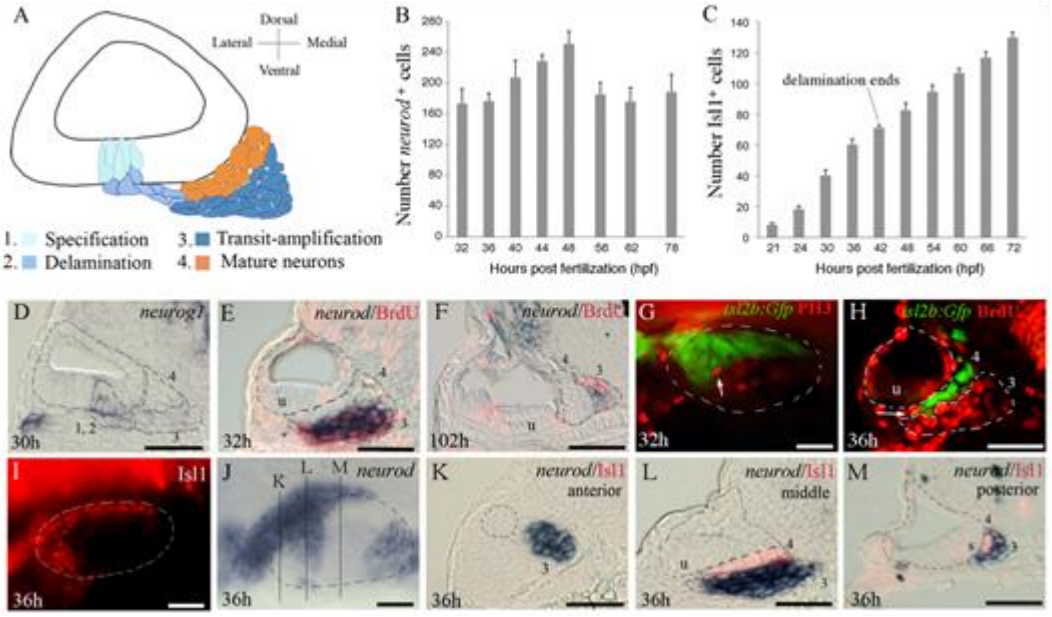

Figure 2.1. Development of Statoacoustic Ganglion (SAG). (A) Illustration showing the various stages of SAG development. Neuronal precursors (neuroblasts) are specified (1) and delaminate from (2) the floor of the otic vesicle. Neuroblasts undergo a phase of transit-amplification (3) wherein they migrate to a position between the otic vesicle and hindbrain as they continue to proliferate. Neuroblasts finally differentiate into mature neurons (4). (B) Total number of delaminated *neurod*$^{+}$ cells within the SAG counted from serial sections at the indicated times (mean ± standard deviation, n=2 or greater for each time point). (C) total number of Islet-1-positive SAG neurons at the indicated times (mean of total number ± standard deviation, n=20 for each time point). (D) *neurog1* expression at 30 hpf. (E, F) Co-staining for *neurod* (blue) and BrdU (red) in embryos exposed to BrdU for 6 hours starting at 26 hpf (E) and 96 hpf (F), and then fixed at 32 hpf and 102 hpf, respectively. (G) Co-staining for *isl2b:Gfp* (green) and phospho-histone H3 (PH3, red) at 32 hpf. Only one mitotic cell (arrow) is seen in the vicinity of the SAG. (H) Co-staining for Islet1 (green) and BrdU (red) at 36 hpf. Only one double-stained cell is visible (arrow). (I-M) Expression of *neurod* (blue) and Islet-1 (red) at 36 hpf. Mature neurons are labeled with Islet-1 (I) and delaminated progenitor cells express *neurod* (J). Positions of section-planes in K-M are indicated in (J). (K-L) Transverse sections passing through the anterior (K), middle (L) and posterior (M) regions of the SAG show mostly complementary patterns of *neurod* and Islet-1. The outer edge of the otic vesicle is outlined in all panels. SAG cells in stages 1-4 of development are indicated in sections, and the position of the utricular macula (u) is indicated. Images of whole-mount specimens (G, I, J) show dorsolateral (G, I) and dorsal (J) views with anterior to the left. Images of transverse sections (C-F, H, K-M) show dorsal to the top and lateral to the left. Scale bar, 25 µm.

cells promotes neuroblast specification in the otic vesicle. Subsequently, Fgf levels rise in part because mature SAG neurons specifically express Fgf5 and accumulate just outside the otic vesicle (Fig. 2.2).

Elevated Fgf then terminates further specification/delamination and also inhibits maturation of transit-amplifying precursors. Manipulation of Fgf to test this model was achieved by specifically knocking down *fgf5* (described below) and more generally by using two heat shock inducible transgenic lines, *hs:fgf8* and *hs:dnfgfr1* (dominant-

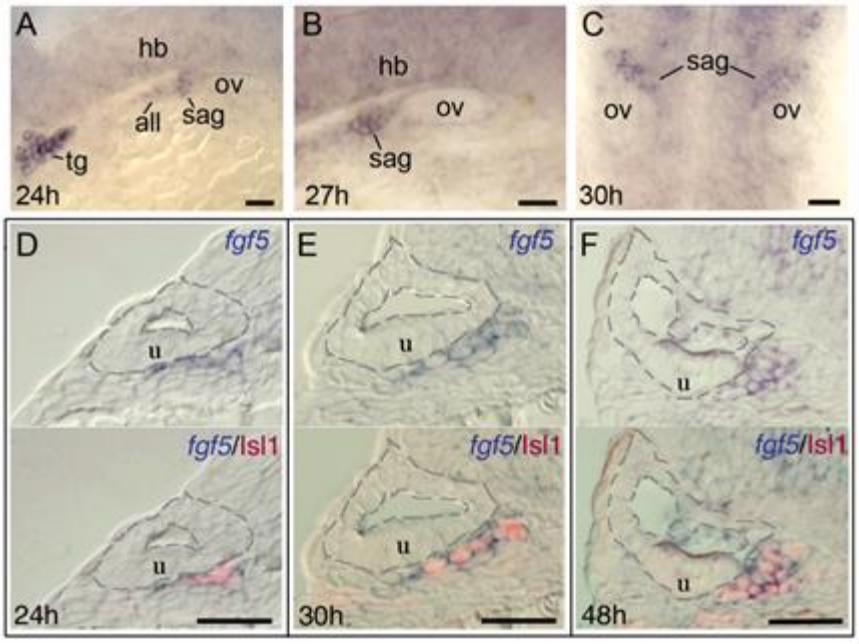

Figure 2.2. Mature SAG neurons express *fgf5*.
(A-C) Wholemount embryos showing lateral views of *fgf5* expression at 24 hpf (A) and 27 hpf (B) and a dorsal view at 30 hpf (C). During these stages, *fgf5* expression marks the trigeminal ganglion (tg), anterior lateral line ganglion (all) and SAG, and there is also weak diffuse expression in the developing hindbrain (hb). There is no detectable staining in the otic vesicle (ov). (D-F) Transverse sections (dorsal to the top and lateral to the left) of specimens co-stained for *fgf5* (blue) and Islet-1 (red) at 24 hpf (D), 30 hpf (E) and 48 hpf (F). Sections pass through the middle portion of the SAG at the level of the utricular macula (u). The inner and outer surfaces of the otic vesicle are outlined. Co-labeling confirms that *fgf5* expression in the SAG is restricted to mature neurons. Scale bar, 25 µm. During mid-somitogenesis stages *fgf5* is diffusely expressed throughout the neural tube and strongly marks the developing trigeminal ganglion (not shown).

negative Fgf receptor), to increase or decrease Fgf signaling, respectively (19, 98).

To document the efficacy of these transgenic lines, we examined expression of the Fgf-feedback gene *etv5b* (previously *erm*) (108, 109) following activation of the transgenes. Strong activation of *hs:fgf8* by heat shocking embryos at 24 hpf (30 minutes at 39°C) led to a detectable increase in *etv5b* levels by the end of the heat shock period (not shown), with maximal *etv5b* seen throughout the embryo by 26 hpf (Fig. 2.3B, E). *etv5b* levels remained elevated through 30 hpf (Fig. 2.3H) and subsequently returned to normal. In contrast, strong activation of *hs:dnfgfr1* at 24 hpf (30 minutes at 38°C) led to marked reduction of *etv5b* expression throughout the embryo by 25 hpf (not shown), and complete loss by 26 hpf (Fig. 2.3C, F). Expression first began to return by 36 hpf, though levels were still well below normal at that time (Fig. 2.3I). These transgenes were subsequently used to assess the effects of changing Fgf signaling levels at different stages of SAG development.

Fgf regulates SAG specification in a dose-dependent manner

Several Fgfs expressed in tissues near the developing SAG have been implicated in establishing a neurogenic domain in the ear (79). In zebrafish, *fgf3* is expressed in the adjacent hindbrain through placodal stages and later helps initiate expression of *fgf3* and *fgf8* in the nascent utricular macula by 18 hpf (73). We have hypothesized that sensory-neural patterning is spatially coordinated by a lateral gradient of Fgf, with high levels initiating sensory development in the medial half of the otic placode – e.g. closest to the Fgf source (95), and lower levels specifying the neurogenic domain in laterally adjacent

otic epithelium. We previously documented a stringent requirement for Fgf in sensory development (95) and here we focused on the requirement for Fgf in neurogenic specification. To bypass the early requirements of Fgf during otic induction we used the chemical inhibitor, SU5402, to block Fgf signaling at later stages of otic development.

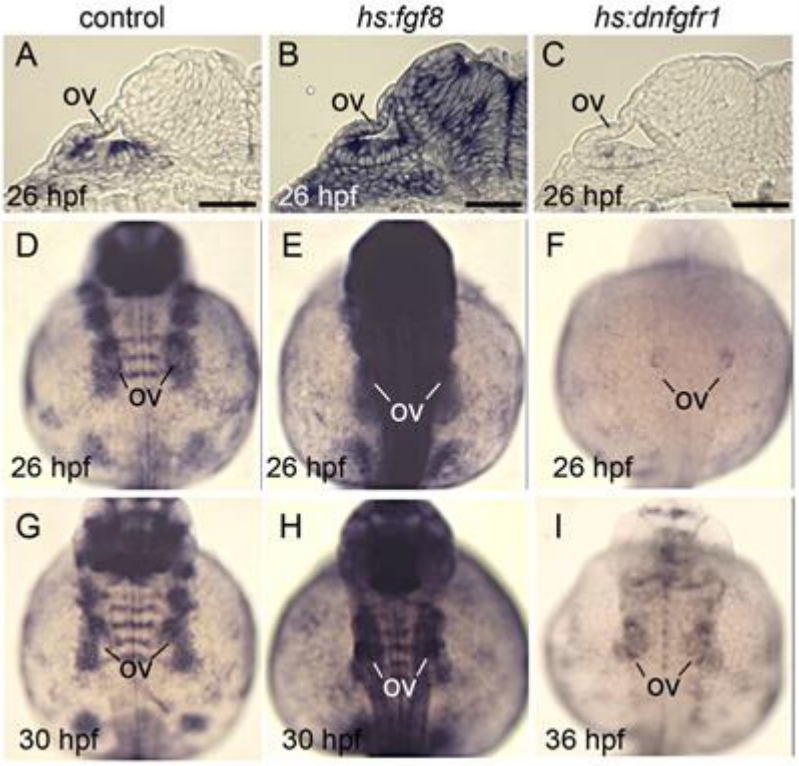

Figure 2.3. Effects of transgene activation on expression of the Fgf reporter *etv5b*.
All embryos were heat shocked for 30 minutes beginning at 24 hpf. Wild-type and *hs:fgf8* embryos were heat shocked at 39°C and *hs:dnfgfr1* embryos were heat shocked at 38°C.(A-C) Cross sections showing *etv5b* expression in wild-type (A) , *hs:fgf* (B) and *hs:dnfgfr1* (C) embryos at 26 hpf. (D-I) Dorsal views (anterior up) of wholemounts showing *etv5b* expression in wild-type (D, G), *hs:fgf8* (E, H) and *hs:dnfgfr1* (F, I) embryos at the indicated times. The otic vesicle (ov) is marked. Expression of *etv5b* remains elevated in *hs:fgf8* embryos for at least 6 hours after heat shock, whereas *etv5b* expression is downregulated in *hs:dnfgfr1* for at least 12 hours after heat shock. Scale bar, 25 µm.

Embryos treated with 100µM SU5402 from 14 hpf -18 hpf showed a strong reduction in *neurog1* expression (Fig. 2.4A, B). Likewise, impairment of Fgf signaling by strongly

activating *hs:dnfgfr1* (98) (38°C for 30 minutes) showed similar results (Fig. 2.4C). Blocking Fgf from this early stage caused widespread cell death at later stages, precluding analysis of SAG maturation. Nevertheless, these data confirm that normal specification of the neurogenic domain requires Fgf signaling. To test the hypothesis that SAG neuroblasts are specified by a specific lower level of Fgf in a signaling gradient, we manipulated Fgf levels using *hs:fgf8* (98). The level of *hs:fgf8* activity can be adjusted by heat shocking at different temperatures (110). To provide a broad shelf of low Fgf signaling, embryos were incubated at 35°C from 18 hpf to 24 hpf. This caused a marked upregulation and expansion of *neurog1* expression (Fig. 2.4D, E). Additionally, there was a notable increase in the number of delaminating neuroblasts as seen by *hmx3* expressing cells leaving the vesicle (Fig. 2.4F, G). By 42 hpf, the number of $Isl1^+$ cells in the mature SAG had increased by 37% over the control (Fig. 2.4H, 63 ± 6.0 $Isl1^+$ cells in control embryos compared to 86 ± 3.6 in *hs:fgf8* transgenic embryos, n=15). To evaluate the effects of a higher level of Fgf, *hs:fgf8* embryos were maximally induced by heat shocking them at 39°C for 30 minutes beginning at 18 hpf. Under these conditions, *neurog1* expression was reduced for several hours following heat shock but recovered to near normal by 24 hpf (data not shown). However, the number of mature $Isl1^+$ neurons at 42 hpf was reduced by 20% (51 ± 4.2 $Isl1^+$ cells, n=15; Fig. 2.4H). As summarized in Table 1, these data support the idea that Fgf acts in a concentration-specific manner, with lower levels promoting neuroblast specification and higher levels inhibiting specification.

Because the rate of neuroblast specification and delamination peaks at 24 hpf, we examined the effects of Fgf misexpression during this stage. As before, maximal activation of *hs:fgf8* (39°C) at 24 hpf reduced expression of *neurog1* in the ear by 30 hpf (Fig. 2.4I, J). However, in contrast to earlier stages, low level activation of *hs:fgf8* (35°C) at 24 hpf reduced *neurog1* expression by 30 hpf (data not shown). Fully blocking Fgf by strong activation of *hs:dnfgfr1* (38°C) at 24 hpf also diminished *neurog1* expression by 30 hpf (data not shown), in keeping with the requirement for Fgf in neuroblast specification. However, weak attenuation of Fgf signaling by activating *hs:dnfgfr1* at a low level (35^{o}C for 2 hours followed by incubation at 33^{o}C) expanded the *neurog1* expression domain at 30 hpf (Fig. 2.4K). Overall these data (summarized in Table 1) support the hypothesis that a specific low-to-moderate level of Fgf promotes neuroblast specification at both early and later stages, and either a high level of Fgf signaling or complete blockage of Fgf signaling impairs this process. At later stages, however, the process of specification becomes increasingly sensitive to inhibition by elevated Fgf. This likely reflects the finding that the level of Fgf increases during development, as described in the next section.

fgf5 **from mature neurons inhibits neuroblast specification**

Because SAG specification becomes increasingly sensitive to inhibition by elevated Fgf, we hypothesized that the process of neuroblast specification is normally terminated by a developmental increase in local Fgf signaling. To explore this possibility, we surveyed expression of all known *fgf* genes in zebrafish and identified

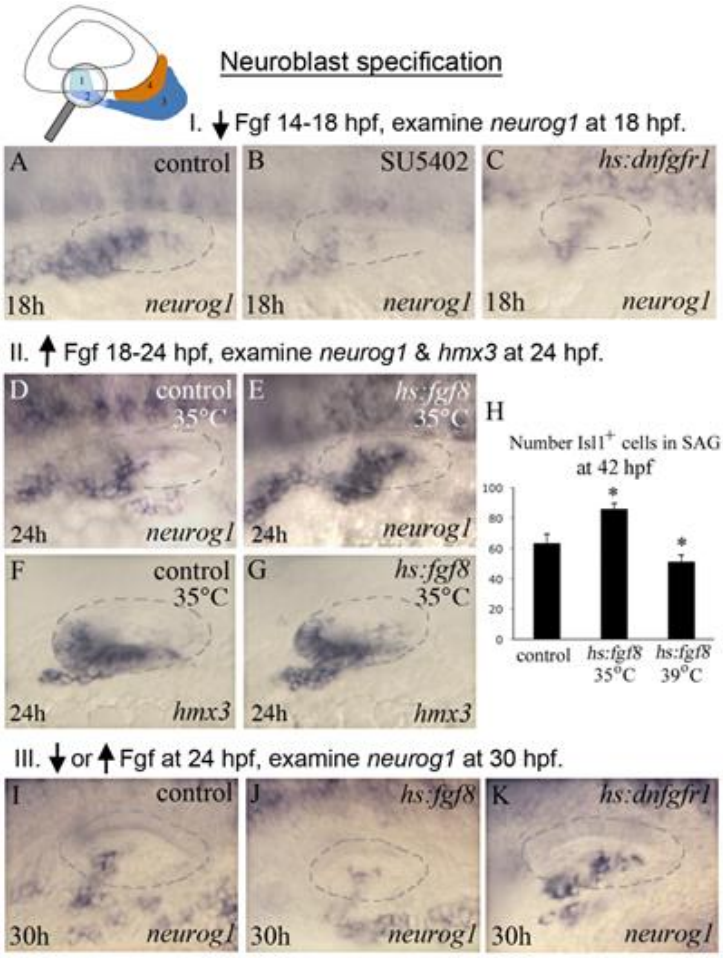

Figure 2.4. Fgf regulates neuroblast specification. The icon at the top of the figure indicates that analysis focuses on initial stages of neuroblast formation, as normally marked by *neurog1* expression. Experimental manipulations in groups I, II and III are briefly summarized at the tops of the corresponding data panels. (A-C) Experiment I, *neurog1* expression at 18 hpf in a control (A), SU5402 inhibitor treated (B) and *hs:dnfgfr1*/+ transgenic embryo heat shocked for 30 minutes at 38°C beginning at 14 hpf. Blocking Fgf strongly reduces expression of *neurog1*. (D-G) Experiment II, expression of *neurog1* (D-E) and *hmx3* (F-G) in control and *hs:fgf8*/+ embryos heat shocked at 35°C for 6 hours, from 18 hpf until 24 hpf. This regimen results in weak overexpression of Fgf8, which at this stage enhances expression of *neurog1*. (H) Experiment II, total number of Islet1-positive cells in the SAG (mean and standard deviation, n=15) at 42 hpf following heat shock activation of *hs:fgf8* at 18 hpf at indicated temperatures. Weak misexpression of Fgf8 (35°C) increases production of SAG neurons whereas strong misexpression of Fgf8 (39°C) reduces production of SAG neurons. *$p < 0.001$ in comparison to the control, analyzed with Student's *t* test. (I-K) Group III, *neurog1* expression at 30 hpf following heat shock at 24 hpf in control embryos (I), *hs:fgf8*/+ embryos heat shocked at 39°C for 30 minutes to strongly over-express Fgf (J) and *hs:dnfgfr1*/+ embryos heat shocked for 2 hours at 35°C and then shifted to 33°C to maintain low level inhibition of Fgf signaling (K). At this stage, weak impairment of Fgf enhances *neurog1* expression, consistent with the idea that Fgf levels normally increase during development and become inhibitory for neuroblast specification. All images show dorsolateral views with anterior to the left, and the otic vesicle is outlined.

fgf5 as a strong candidate for a feedback regulator of SAG development. During mid-somitogenesis stages *fgf5* is diffusely expressed throughout the neural tube and strongly marks the developing trigeminal ganglion (not shown). As mentioned above, *fgf5* shows relatively specific expression in mature SAG neurons, and several other cranial ganglia, by 24 hpf and this pattern is maintained through at least 48 hpf (Fig. 2.2). No expression is detected in the otic vesicle or other nearby tissues. We tested the role of Fgf5 by injecting morpholino oligomers to block translation (*fgf5tb*-MO) or to disrupt splicing at the intron1-exon2 splice junction (*fgf5i1e2*-MO). Injection of either MO yielded identical phenotypes: Morphants showed highly specific and fully penetrant enhancement of SAG specification and maturation, as described below, but otherwise there were no other detectable changes in embryo morphology nor was there a detectable increase in cell death. For most experiments reported here, we show results obtained with *fgf5i1e2*-MO, which proved to be highly effective in reducing mature *fgf5* transcript levels (Fig. 2.5A, B).

Figure 2.5. Efficacy of *fgf5* splice-blocking MO.
(A) Schematic of *fgf5* mRNA showing intron-exon structure (not to scale). Binding sites for splice-blocking morpholino at intron1-exon2 junction (I1E2-MO) and PCR primers for RT-PCR (forward P1, reverse P2) are shown. (B) RT-PCR results showing the efficacy of I1E2-MO. *fgf5* transcript levels are severely reduced in *fgf5* morphants at 24 hpf. *odc* transcript level was used as a constitutive control.

To address the role of *fgf5* in neuroblast specification we examined *neurog1* expression at various stages in *fgf5* morphants. At 24 hpf no obvious difference was

observed between *fgf5* morphants and control embryos (not shown). By 30 hpf, however, *neurog1* expression was dramatically expanded in *fgf5* morphants (Fig. 2.6A, B, E, F), including a pronounced mediolateral expansion of *neurog1* in the floor of the otic vesicle (Fig. 2.6B, F). Normally, neuroblast specification declines dramatically after 30 hpf [1,20] (Fig. 2.6C). However, *fgf5* morphants continued to show abundant *neurog1*-positive cells at 36 hpf, indicating a prolonged phase of robust specification and delamination (Fig. 2.6G). Neuroblast specification/delamination finally ceased by 48 hpf in *fgf5* morphants (not shown). Knockdown of *fgf5* appeared to affect SAG development in a highly specific manner, as other regional markers in the otic vesicle were expressed normally and development of sensory hair cells was also normal at 32 hpf (Fig. 2.7). Additionally, the *fgf5* morphant phenotype was rescued by strong activation of *hs:fgf8* (39°C) at 24 hpf such that neuroblast specification returned to normal (Fig. 2.6D, H). Such rescue supports the idea that neuroblast specification relies on a proper balance of Fgf signaling, with the morpholino and transgene counter-balancing each other. Overall, these data (summarized in Table 1) support the hypothesis that mature SAG cells become a source of elevated Fgf, which eventually exceeds a signaling threshold that serves to terminate neuroblast specification in a timely manner.

To test this model in another way, mature neurons marked by *isl2b:gfp* transgene expression (99) were killed by serial laser-ablation at 22 hpf and 25 hpf (Fig. 2.6I, J) and *neurog1* expression was examined at 30 hpf. Expression of *neurog1* was expanded on the ablated side relative to the unablated (contralateral) side (Fig. 2.6K, L, Table 1).

Together, these data support the notion that as mature neurons expressing *fgf5* accumulate within the SAG, overall levels of Fgf signaling increase and as a result neuroblast specification is terminated. This also explains the increased susceptibility to misexpression of Fgf8 after 24 hpf, as described above.

Fgf regulates the balance between transit-amplification and differentiation

We next examined the effects of Fgf on post-delamination stages of SAG development. In these experiments heat shock transgenes were activated at high levels (38-39°C) at 24

Table 2.1. Effects of altering Fgf on neuroblast specification.

Condition and stage	*neurog1* domain	Figure
hs:fgf8-high (39°C), 18 hpf	reduced 20 hpf	-
hs:fgf8-low (35°C), 18 hpf	enlarged 24 hpf	4E
hs:dnfgfr1-high (38°C), 14 hpf	reduced 18 hpf	4C
SU5402 (100 μM), 14 hpf	reduced 18 hpf	4B
hs:fgf8-high (39°C), 24 hpf	reduced 30 hpf	4J
hs:fgf8-low (35°C), 24 hpf	reduced 30 hpf	-
hs:dnfgfr1-high, 24 hpf	reduced 30 hpf	4K
hs:dnfgfr1-low (35°C), 24 hpf	enlarged 30 hpf	-
fgf5-MO, 1-cell	enlarged 30,36 hpf	6E–6G
fgf5-MO+*hs:fgf8* (39°C), 24 hpf	normal 36 hpf	6H
Ablate mature SAG 22, 25 hpf	enlarged 30 hpf	6L

hpf and the effects on *neurod*$^{+}$ (transit-amplifying) and Isl1^{+} (mature) populations were examined at 36 hpf and 48 hpf. Summing *neurod*$^{+}$ cells in serial sections of control embryos indicated that there are approximately 200-250 transit-amplifying cells in the

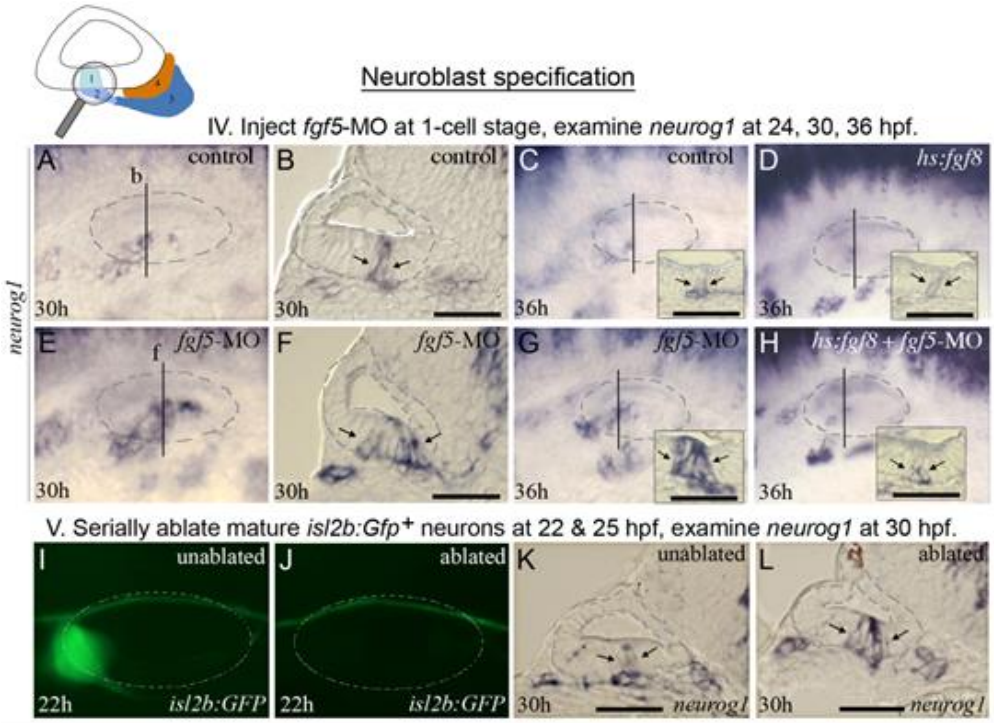

Figure 2.6. *fgf5* from mature neurons terminates the phase of neuroblast specification.
The icon at the top of the figure indicates that analysis focuses on initial formation of neuroblasts. Experimental manipulations in groups IV and V are briefly summarized at the tops of the corresponding data panels. (A-H) Expression of *neurog1* in control embryos (A-C), a *hs:fgf8* embryo (D), *fgf5* morphants (E-G), and a *hs:*fgf8 embryo injected with *fgf5*-MO (H) at the indicated stages. Transgenic embryos (D, H) were heat shocked for 30 minutes at 39°C beginning at 24 hpf. Vertical lines in (A, C-E, G, H) indicate the plane of transverse sections in (B, F, and insets in C, D, G and H). (I-L) Expression of *isl2b:Gfp* at 22 hpf (I, J) and *neurog1* at 30 hpf (K, L) in a specimen in which mature (*fgf5*-expressing) neurons were laser-ablated. The same specimen is shown in all panels. Mature SAG neurons expressing *isl2b:Gfp* were serially ablated on the left side at 22 hpf (J) and 25 hpf (not shown), and the embryo was fixed and sectioned at 30 hpf to examine *neurog1* expression (L). Images of the unablated right side (I, K) were inverted to facilitate comparison. The surface of the otic vesicle is outlined in all panels. Arrows in sections indicate the edges of *neurog1* domain in the otic floor. Note that the amount and duration of delamination of *neurog1*$^{+}$ neuroblasts is strongly enhanced by knockdown of *fgf5* (F, G) or ablation of mature neurons (L). Activation of *hs:fgf8* reverses the effects of *fgf5*-MO (H). Scale bar, 25 µm. Transverse sections are shown with lateral to the left and dorsal up. Wholemount images show dorsolateral views with anterior to the left.

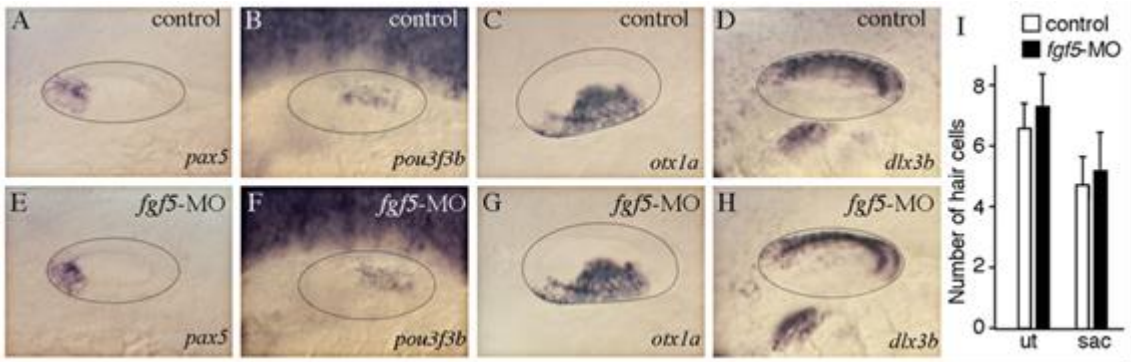

Figure 2.7. Normal axial patterning in *fgf5* morphants. (A-H) Expression of regional patterning markers in control embryos (A-D) and *fgf5* morphants (E-H). Expression of *pax5* (A, E) and *pou3f3b* (B, F) labels anterior and posterior regions, respectively. Expression of *otx1a* (C, G) and *dlx3b* (D, H) labels ventromedial and dorsolateral regions, respectively. The otic vesicle is outlined. Images show dorsolateral views with anterior to the left. (I) The total number of hair cells in the utricular (ut) and saccular (sac) maculae of control embryos and *fgf5* morphants at 32 hpf. Data were obtained by counting GFP-positive hair cells (mean of total number ± standard deviation) in the sensory epithelia of *brn3c:Gfp* transgenic embryos. Data show means and standard deviations from 20 specimens each. Differences between control and experimental specimens were not statistically significant (p=0.16 for the utricle, p=0.67 for the saccule) based on Student's *t* tests.

SAG at these stages (Fig. 2.1B). Because this approach proved laborious and was prone to occasional loss of tissue sections, changes in the *neurod* domain were assessed by measuring mean cross-sectional areas in the three AP regions of the SAG in transgenic and control embryos. Strong activation of *hs:fgf8* at 24 hpf (39°C for 30 minutes) increased the *neurod*$^{+}$ precursor domain by 31% in the largest, middle region of the SAG at 36 hpf (Fig. 2.8A, B, I). A similar trend was observed in the anterior region, although the difference was not statistically significant (Fig. 2.8I). Under these conditions, the smallest, posterior part of the SAG was truncated in *hs:fgf8* embryos and therefore wasnearly devoid of *neurod*$^{+}$ cells in most specimens (Fig. 2.8I). This is possibly because the posterior SAG forms later and elevated Fgf prematurely terminates specification of neuroblasts that might otherwise contribute to this region. Despite, the

increased population of transit-amplifying cells in the middle region, the total number of Isl1^{+} neurons in the SAG was reduced in *hs:fgf8* embryos by 30% at 36 hpf (Fig. 2.8E, F, J) and the hourly rate of neuron production between 24 hpf and 36 hpf was reduced by half (Fig. 2.8K). For loss of function studies, *hs:dnfgfr1* was activated at 24 hpf (38°C for 30 minutes) to impose a strong block to Fgf signaling. This resulted in a decrease of 26% in the *neurod*$^{+}$ domain in the middle region at 36 hpf, and a decrease of 50% in the posterior region (Fig. 2.8C, I). Again, the anterior region showed a similar but non-significant trend. Under the same conditions, there was a 30% increase in the total number of mature Isl1^{+} SAG neurons (Fig. 2.8G, J). The relative effects of *hs:fgf8* and *hs:dnfgfr1* on the transit-amplifying population persisted through at least 48 hpf (Fig. 2.8L). Differences in the total number of mature neurons also persisted at 48 hpf (Fig. 2.8M). However, most of the differences seen at 48 hpf appeared to reflect changes occurring before 36 hpf because the rate of production of new Isl1^{+} neurons after 36 hpf was nearly normal in *hs:fgf8* and *hs:dnfgfr1* embryos (compare Fig. 2.8K, N). This presumably reflects the transient nature of transgene activity and gradual reestablishment of normal SAG regulation. Note that under the conditions used here, we detected little or no cell death in the transit-amplifying or mature regions of the SAG as shown by staining with Acridine Orange or anti-Caspase 3 antibody (not shown). Likewise, we detected no changes in the number of mitotic cells in the SAG, nor in the proportion of cells incorporating BrdU (data not shown), indicating that Fgf does not directly affect cell cycle dynamics. Instead, the data (summarized in Table 2.2) suggest that Fgf slows

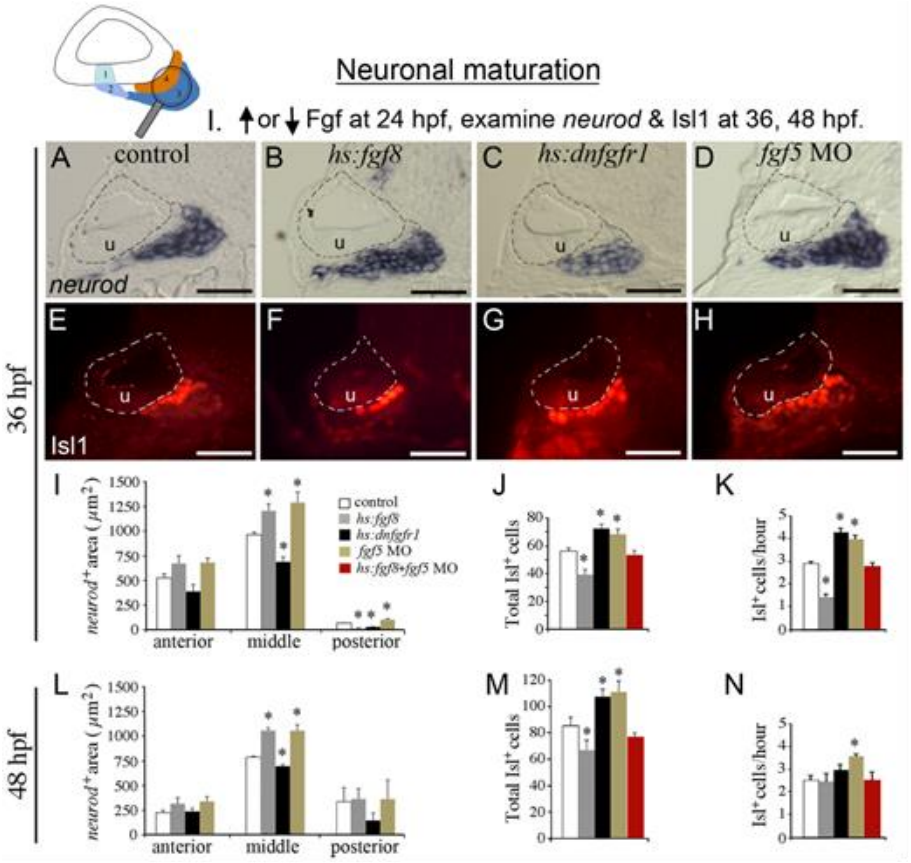

Figure 2.8. Fgf regulates the balance between transit-amplification and differentiation. The icon at the top of the figure indicates that neuronal maturation (*neurod*$^+$ transit-amplifying cells and Isl1$^+$ mature neurons) is the focus of analysis. Manipulations in these experiments (Neuronal maturation group I) are briefly summarized at the top. Embryos were heat shocked for 30 minutes at 39°C (wild-type controls, *hs:fgf8*/+ embryos, and *fgf5*-morphants) or 38°C (*hs:dnfgfr1*/+ embryos) beginning at 24 hpf. (A-H) Transverse sections (lateral to the left, dorsal up) showing *neurod* expression (A-D) or Isl1 staining (E-H) at 36 hpf in control embryo (A, E), *hs:fgf8*/+ embryos (B, F), *hs:dnfgfr1*/+ embryos (C, G) and *fgf5* morphants (D, H). All sections shown pass through the middle region of the SAG at the level of the utricular macula (u). The otic vesicle is outlined. Scale bar, 25 μm. (I-N) Quantitation of transit-amplifying and mature neuronal populations at 36 hpf (I-K) and at 48 hpf (L-N). Panel I shows a color key to facilitate comparison between treatments: White bars, control; gray bars, *hs:fgf8*; black bars, *hs:dnfgfr1*; brown bars, *fgf5* morphants; red bars, activation of *hs:fgf8* in *fgf5* morphants. Analysis of transverse sections was used to measure the mean area of *neurod*$^+$ precursor cells (I, L) in the anterior, middle and posterior regions of SAG. The total number of Isl1+ neurons (J, M) and the mean hourly rate of neuron production from 24 hpf to 36 hpf (K) and from 36 to 48 hpf (N) was measured by counting neurons in stained wholemount specimens. Error bars in I, J, L, M indicate standard deviations (n=3 or greater for sectional areas; n=15 for Isl1$^+$ cell counts). *$p < 0.05$ in comparison to control, analyzed with Student's *t* test. Error bars in K, N indicate standard errors.

the rate at which transit amplifying cells differentiate into mature SAG neurons, whereas blocking Fgf accelerates differentiation.

We next assessed the role of Fgf5 in restraining maturation of precursor cells. In *fgf5* morphants, the size of *neurod*$^{+}$ domain was increased in both the middle and posterior regions of SAG in the embryos at 36 and 48 hpf (Fig. 2.8D, I, L). Note that the increase in the transit-amplifying region seen in *fgf5* morphants was different from what was observed following activation of *hs:dnfgfr1*. This is presumably because the prolonged phase of robust specification seen in *fgf5* morphants (Fig. 2.6G, H) continues to replenish the transit-amplifying population. Additionally, *fgf5* morphants also produced more Isl1^{+} neurons than normal (Fig. 2.8H, J, K, M, N). However, despite the enlargedpool of precursors *fgf5* morphants did not produce more mature neurons than did *hs:dnfgfr1* embryos (Fig. 2.8J, M). This is possibly because redundant factors (possibly macular Fgfs) continue to restrain the enlarged pool of progenitors in *fgf5* morphants. Finally, we observed that strong activation of *hs:fgf8* (39°C) at 24 hpf in *fgf5*-morphants restored neuron production to normal (Fig. 2.8J, K, M, N). Thus, as during neuroblast specification, the rate of neuronal maturation is also regulated by a proper balance of Fgf signaling. Moreover, these data (summarized in Table 2.2) support a role for Fgf5 as a feedback inhibitor released by mature SAG neurons to restrict the rate of neuronal differentiation.

Table 2.2. Effects of altering Fgf on SAG maturation.

Condition and stage	Size *neurod* domain	Number Isl1$^+$ cells	Figure
hs:fgf8-high (39°C), 24 hpf	increased 36, 48 hpf	reduced 36, 48 hpf	8B, 8F, 8I–8N
hs:dnfgfr1-high (38°C), 24 hpf	reduced 36, 48 hpf	increased 36, 48 hpf	8C, 8G, 8I–8N
fgf5-MO, 1-cell	increased 36, 48 hpf	increased 36, 48 hpf	8D, 8H, 8I–8N
fgf5-MO+*hs:fgf8* (39°C), 24 hpf	not determined	normal 36, 48 hpf	8J, 8K, 8M, 8N
Ablate mature SAG 30, 32 hpf	reduced 44 hpf normal 56 hpf	normal 34–44 hpf* increased 56–80 hpf*	9A
hs:fgf8-high (39°C), 34 hpf	normal 56 hpf	reduced 34–56 hpf*	9B
hs:dnfgfr1-high (38°C), 34 hpf	normal 56 hpf	increased 34–56 hpf*	9B
Ablate SAG+*hs:fgf8* (39°C), 34 hpf	normal 56 hpf	normal 34–56 hpf*	9B
Ablate SAG+*hs:dnfgfr1* (38°C), 34 hpf	normal 56 hpf	increased 34–44 hpf*	9B

* rate of mature neuron production during the indicated interval.

Neuronal maturation following ablation of mature SAG neurons

To further explore regulation of SAG maturation, we assessed whether laser-ablation of mature SAG neurons affects the rate of new neuron production. This analysis was conducted after 30 hpf to minimize the impact of neuroblast specification on overall cell number. Using the *isl2b:Gfp* line, mature SAG neurons on one side of the head were targeted for serial ablation at 30 hpf and 32 hpf, with the contralateral side serving as a non-ablated control. We observed that a single round of ablation was inefficient, allowing a substantial fraction of neurons to survive. However, serial ablation successfully eliminated over 90% of mature neurons, as confirmed by anti-Isl1 staining just after the second ablation (not shown). Analysis of the transit-amplifying population revealed that the number of *neurod*$^+$ cells declined by 10-20% on the ablated side during the first 12 hours following neuronal ablation, probably reflecting collateral damage, but the number returned to normal by 56 hpf (24 hours post-ablation) (data not shown). Despite the initial decrease in transit-amplifying cells, new Isl1$^+$ neurons accumulated at a rate comparable to the non-ablated contralateral side for the first 12

hours after ablation, (Fig. 2.9A). The rate of neuron production briefly declined during the next 12-hour period, but then increased to a rate 60% greater than normal through at least 80 hpf (Fig. 2.9A, Table 2). Co-ablation of both mature and transit-amplifying cells (the latter were targeted based on position and morphology) nearly eliminated production of new Isl1^{+} cells through at least 56 hpf (Fig. 2.9A), confirming the vital importance of transit-amplifying cells for producing new mature SAG neurons. Together these data suggest that loss of feedback inhibition from mature neurons leads to accelerated differentiation of cells from a pool of self-renewing progenitors.

We next examined whether altering Fgf signaling influences neuron production after 30 hpf, with and without laser-ablation of mature neurons. Ablations were conducted in transgenic embryos carrying both *isl2b:Gfp* and either *hs:fgf8* or *hs:dnfgfr1*. Again, *isl2b:Gfp*$^{+}$ cells were serially ablated on one side at 30 hpf and 32 hpf, and embryos were then heat shocked at 38°C or 39°C (strong activation) at 34 hpf. The contralateral side served as a non-ablated control. On the non-ablated side, the effects of activating *hs:fgf8* or *hs:dnfgfr1* at 34 hpf were similar the effects of activating these transgenes at 24 hpf: Specifically, strongly elevating Fgf impaired production of new neurons whereas blocking Fgf accelerated production of new neurons (Fig. 2.9B, Table 2). On the ablated side, activation of *hs:dnfgfr1* (38°C) accelerated production of new neurons to more than twice the normal rate through 44 hpf, after which the rate flattened out as in non-transgenic ablations (Fig. 2.9B). Moreover, the rate of neuron production in ablated *hs:dnfgfr1* embryos was 50% greater than in non-ablated *hs:dnfgfr1* embryos. Surprisingly, strong activation of *hs:fgf8* (39°C) resulted in a rate

of neuronal accumulation on the ablated side that was nearly normal (comparable to the non-ablated control). Thus, misexpressing Fgf8 counterbalances the effects of eliminating mature neurons (and hence Fgf5) such that there is no net change in the rate of neuron production. This is similar to the ability of *hs:fgf8* to counterbalance the effects of *fgf5*-MO on neuroblast specification (Fig. 2.6H) and maturation of SAG neurons (Fig. 2.8J, K, M, N). Analysis of the *neurod*$^{+}$ domains showed that transgene activity had no significant effect on the size of the transit-amplifying pool at these stages (Table 2.2). Thus, blocking Fgf accelerates production of new neurons and enhances the effects of neuronal ablation whereas misexpressing Fgf8 offsets the effects of neuronal ablation (summarized in Table 2.2). These data further support the hypothesis that Fgf5 from mature neurons acts as a feedback inhibitor to slow the rate of maturation of new SAG neurons.

DISCUSSION

The data presented here support a model in which changing levels of Fgf differentially regulates distinct stages of SAG development (Fig. 2.10). Initially a moderate level of Fgf in a spatial gradient specifies the neurogenic domain within the otic vesicle. Subsequently, Fgf levels gradually rise as differentiating SAG neurons accumulate and express Fgf5, eventually terminating neurogenesis in the otic vesicle. It is likely that the expanding macular source of Fgf also contributes to termination of neurogenesis. Terminal differentiation of SAG neurons initially occurs rapidly following delamination from the otic vesicle. However, the developmental increase in

Fgf delays neuronal differentiation, maintaining the transit-amplifying phase. This allows the developing SAG to achieve a steady state in which the rate of progenitor growth just matches the rate of neuronal differentiation. This property of the SAG is presumably necessary to provide sufficient neurons to innervate growing sensory epithelia, which continue to expand throughout larval and early adult stages in zebrafish (111). Knockdown of *fgf5* prolongs the phase of neuroblast specification and also accelerates the rate of neuronal differentiation. Neuroblast specification eventually ceases in *fgf5* morphants, possibly in response to elevated Fgf from the growing utricular macula. We cannot assess the long-term effects of *fgf5* knockdown because morpholino efficacy dissipates after 3-5 days. However, once specification/delamination ceases, accelerated neural differentiation in the absence of *fgf5* function would be expected to deplete the transit-amplifying pool, leading to a neural deficiency in the long-run. Cell cycle dynamics are likely to be rather complex in the transit-amplifying population. With a steady state of 180-200 progenitors producing 50-60 neurons per day, the average cell cycle length could be unusually long assuming that most progenitors continue to cycle. However, patterns of BrdU incorporation suggest cell cycle dynamics are not uniform amongst progenitors. A 6-hour incorporation period labels roughly 40% of *neurod*$^{+}$ progenitors, with labeling being especially prominent in distal regions of the SAG (Fig. 2.1E, F, and data not shown). It is therefore possible that a substantial fraction of progenitors enter a quiescent state. We detected no overt effect of Fgf signaling on the pattern of BrdU incorporation or the incidence of mitotic cells (not shown), although we cannot exclude the possibility that our heat shock lines act too

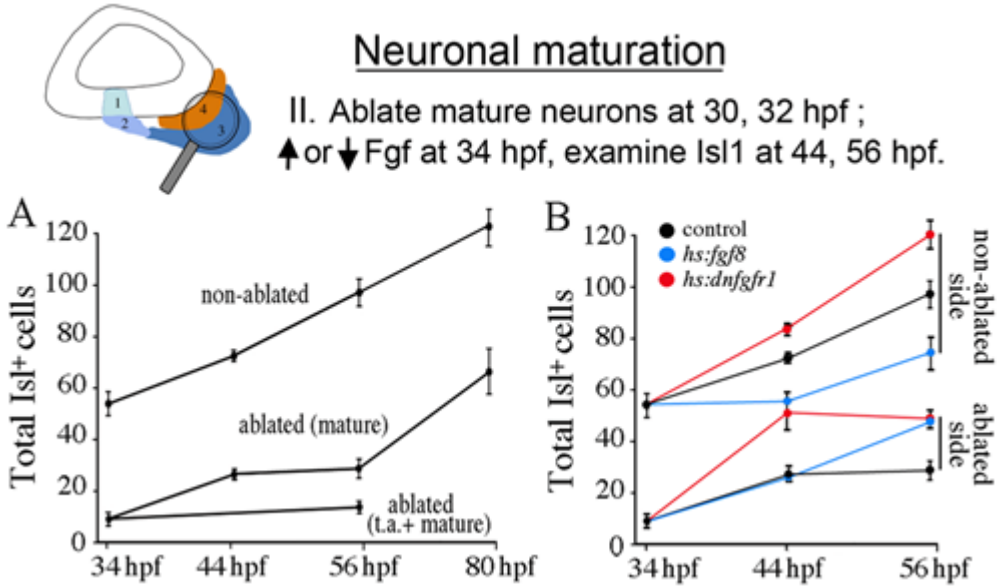

Figure 2.9. Regeneration following SAG ablation. The icon at the top of the figure indicates that neuronal maturation is the focus of analysis. Manipulations in these experiments (Neuronal maturation group II) are briefly summarized at the top. (A) Accumulation of Isl1^{+} SAG neurons in *isl2b:Gfp/+* embryos after serial ablation of Gfp-positive neurons (mature) or ablation of Gfp-positive neurons and transit-amplifying cells (t.a. + mature) at 30 hpf and 32 hpf. Neuronal accumulation on the contralateral (non-ablated) side served as a control. (B) Effects of modulating Fgf after serial ablations at 30 hpf and 32 hpf on the total number of Isl1^{+} neurons. Embryos were heat shocked for 30 minutes at 39°C (+/+ and *hs:fgf8*/+ embryos) or 38°C (*hs:dnfgfr1*/+ embryos) beginning at 34 hpf. Data show means and standard deviations of 2-5 specimens per time point.

transiently to detectably alter cell cycle dynamics. Nevertheless, modulating Fgf clearly had a rapid effect on the rate of production of mature neurons (Figs. 2.8 and 2.9),thereby indirectly affecting the progenitor pool. Interestingly, activating *hs:fgf8* or *hs:dnfgfr1* at 24 hpf caused lasting changes in the size of the progenitor pool (Fig. 2.8), whereas no such change was seen when the transgenes were activated at 34 hpf (data not shown). This difference likely reflects the greater relative impact of changing the rate of neuronal differentiation at early stages when the progenitor pool is still small. In contrast, with nearly 200 progenitors at 32 hpf, it is not surprising that altering the rate of neuronal differentiation by 1-2 cells per hour for several hours had little impact on the progenitor

pool. Although the model in Figure 2.10 depicts the influence of macular Fgfs on SAG specification in the otic vesicle, it must be emphasized that a lateral gradient of Fgf from the hindbrain acts much earlier to coordinate formation of sensory and neural progenitors in adjacent domains during placodal stages. The prosensory gene *atoh1b* is induced at 10.5 hpf in the nascent otic placode in medial cells closest to the

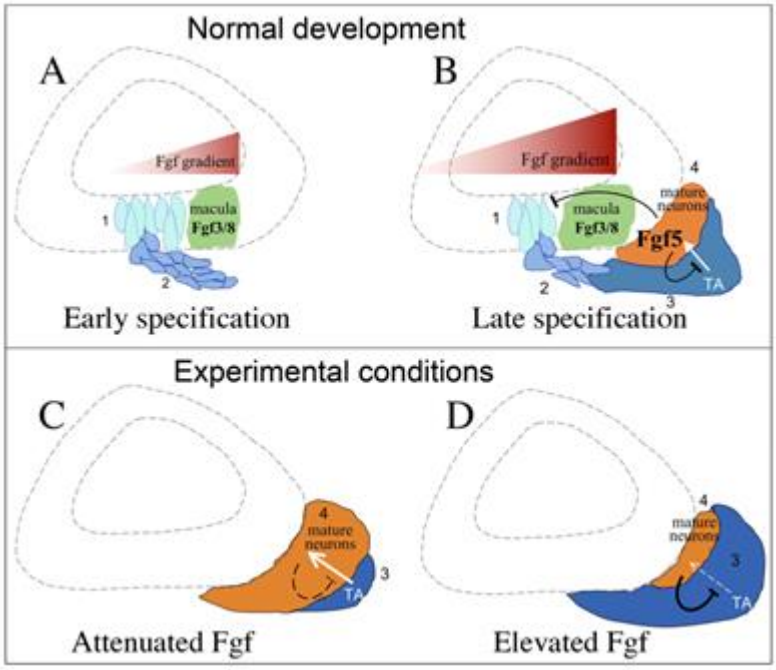

Figure 2.10. Model for regulation of SAG development by Fgf.
(A) Neuroblast specification at early stages. A moderate level of Fgf3 and Fgf8 in a gradient generated by the utricular macula specifies neuroblasts in the floor of the otic vesicle (step 1), and nascent neuroblasts quickly delaminate from the otic vesicle (step 2). (B) As development proceeds, neuroblasts establish a pool of transit-amplifying (TA) progenitors (step 3), which eventually differentiate into mature neurons and express Fgf5 (step 4). Rising levels of neuronal Fgf5, combined with Fgf3 and Fgf8 from the growing utricular macula, exceeds an upper threshold that serves to terminate specification of new neuroblasts within the otic vesicle. Neuronal Fgf5 also slows differentiation of progenitors into mature neurons. (C, D) At stages immediately following establishment of the transit-amplifying pool, experimental attenuation of Fgf signaling promotes maturation of neurons at the expense of progenitors (C) whereas elevating Fgf inhibits maturation, expanding the size of the transit-amplifying pool (D).

Fgf-source (95), and elevating Fgf expands this domain laterally (our unpublished observations). Expression of *neurog1* begins in more lateral tissue by 16 hpf (14 somites) and is initially influenced by the same hindbrain source of Fgf (73, 97). We have confirmedhere that neuroblast specification requires Fgf whereas excess Fgf inhibits *neurog1* expression, consistent with the notion that the neurogenic domain is established by intermediate levels of Fgf in a diffusion gradient. After formation of the otic vesicle, the utricular macula provides the strongest source of Fgf in the otic vesicle and the neurogenic domain forms an arc wrapping around the lateral and posterior edges of this source (14). Later the saccular macula begins to expand and expresses more Fgf (95, 112), with a corresponding posterior extension of the neurogenic domain to form a narrow band just lateral to the saccule (14). Soon thereafter Fgf levels exceed the upper threshold and terminate neuroblast specification.

In zebrafish, it is currently unclear whether the spatial distribution of neuroblasts within the otic vesicle is directly tied to later distribution of mature neurons in the SAG. However, fate mapping studies in chick and mouse reveal that the spatial-temporal progression of neuroblast formation in the otic vesicle presages the spatial-temporal accumulation of vestibular and auditory neurons outside the ear (113, 114). It is likely that a similar progression occurs in zebrafish, though fate mapping studies have yet to confirm this relationship. Mechanism of SAG subtype specification has not been well characterized in any species, though several studies in zebrafish suggests that Shh is involved. Disruption of Hedgehog signaling ablates posterior fates in the otic vesicle, including the saccule and posterior (presumptive auditory) neurons (19, 107). Fgf

signaling acts in opposition to Shh by promoting anterior fates in the otic vesicle (73, 74, 97), though altering Fgf does not appear to cause wholesale redistribution of SAG neurons. However, we found that activating *hs:fgf8* at 24 hpf caused premature termination of neuroblast specification and also blocked later production of posterior/auditory neurons, supporting a link between spatial/temporal cues and SAG subtype-specification.

Are the distinct roles of Fgf conserved in amniotes?

Numerous studies support a role for Fgf in SAG neuroblast specification in the chick and mouse. In chick, misexpression of Fgf8 or Fgf10 during placodal stages causes expansion of the neurogenic domain in the otic vesicle, whereas blocking Fgf signaling dramatically reduces the neurogenic domain (76, 77). In mouse, knockout of *Fgf3* or receptor isoform *Fgfr-2 (IIIb)* causes severe deficiencies of delaminating neuroblasts and neurons (82, 115). Explant cultures of chick or mouse otocysts treated with exogenous Fgf2 produce 5- to 10-fold more delaminated neuroblasts compared to controls, whereas blocking Fgf2 with a neutralizing antibody severely reduces the number of neuroblasts (84, 116). Thus the requirement for Fgf in neuroblast specification appears broadly conserved. However, the spatial gradient of Fgf that we propose coordinates sensory and neural development in zebrafish is unlikely to operate in mammals. Unlike the situation in zebrafish, in mouse the neurogenic and sensory domains overlap spatially but are specified at slightly different times. Neuroblast specification occurs first, but as the phase of neuroblast specification/delamination

begins to wane sensory epithelia begin to form in the same region. The transition from neural to sensory development partly reflects mutual repression between Neurog1 and Atoh1, the principal initiators the proneural and prosensory pathways, respectively (86). Whether Fgf also influences this transition is not known.

Despite the above studies showing a requirement for Fgf, it is not clear whether high levels of Fgf are inhibitory in birds and mammals as we have shown here, nor whether Fgf delays maturation of cells in the transit-amplifying pool. In explants of chick or mouse otocysts, exposure to Fgf accelerates the appearance of mature neurons compared to cultures lacking exogenous Fgf (84, 116). At first glance, these results appear to contradict our findings that Fgf delays differentiation. However, Fgf levels used in the above explant studies were based on dose-response curves and were selected to optimize growth of the explant. Hence potential inhibitory effects of higher doses of Fgf were not evaluated. Furthermore, neuroblasts in culture disperse after delamination rather than accumulating against the otocyst wall where they might facilitate feedback inhibition. This possibly explains why otic explants continue to produce neuroblasts for many days, far longer than during normal embryonic development. In rodent embryos, differentiating auditory neurons express Fgf1, Fgf2, Fgf5 and Fgf10 (82, 117-120), which could help mediate feedback inhibition. Unfortunately, relevant functional studies are lacking. In adult rodents, neuronal Fgf is thought to play a role in maintenance of the spiral ganglion. Augmenting Fgf mitigates neural degeneration following nerve injury or noise-induced trauma (121, 122). Additionally, conditional knockout of Fgf receptor genes *Fgfr1* and *Fgfr2* in glial cells in the spiral ganglion leads

to progressive loss of auditory neurons beginning around 2 months of age, suggesting a role in promoting trophic support from glia (123). In cultures of spiral ganglion from adult mouse, exogenous Fgf2 can promote neuronal survival and neurite outgrowth (124). Unexpectedly, such cultures were also found to contain quiescent progenitors that could be induced to reenter the cell cycle by incubation with EGF and Fgf2, with some cells differentiating into neurons after removal of EGF and Fgf2 (124). These latter data are consistent with the possibility that Fgf maintains progenitors and inhibits neural differentiation, though it remains to be seen whether such a mechanism operates in vivo.

The developing SAG can be compared to the developing olfactory epithelium (OE). Fgf8 expression around the rim of the olfactory pit stimulates proliferation of OE progenitors, which differentiate into mature neurons deeper inside the pit away from the Fgf8 source (125). Conditional knockout of Fgf8 results in severe deficiency of neurons due to failure of progenitors to expand. Development of the OE neurons is also regulated by feedback inhibition from mature neurons, though the mechanism differs from the SAG. Specifically, mature OE neurons secrete the TGFβ factor GDF11, which inhibits further proliferation of progenitors by antagonizing Fgf8 (126). In the eye, too, GDF11 acts as a feedback inhibitor of retinal ganglion cells, though in this case GDF11 blocks further differentiation of progenitors rather than restricting proliferation (127). In numerous other settings, Fgf regulates the balance between growth and differentiation of neural progenitors. In cultures of human or rat cortical progenitors, high levels of Fgf stimulate proliferation and block neuronal differentiation (128, 129). In the developing midbrain-hindbrain region in mouse, conditional knockdown of Fgf receptors results in

an increase in differentiated neurons and a concomitant loss of progenitor cells in the ventricular zone (130). During earlier stages of mouse development, Fgf induces embryonic stem (ES) cells to form epiblast, which begin to express Fgf5. Subsequently, Fgf maintains the epiblast as a stable intermediate by preventing reversion back to the ES ground state and blocking further differentiation into neural ectoderm (131). Thus, maintenance of stable progenitor pools by Fgf appears to be a broadly conserved mechanism utilized in many aspects of neural development. A relatively novel aspect of SAG development is that Fgf coordinates the entire process, initially specifying neuroblasts and, at a higher level, also mediates feedback from mature neurons to inhibit further differentiation. How changing levels of Fgf achieve this balance remains an important unresolved question.

CHAPTER III

TFAP2A PROMOTES SPECIFICATION AND MATURATION OF NEURONS IN THE INNER EAR THROUGH MODULATION OF BMP, FGF AND NOTCH SIGNALING[2]

INTRODUCTION

Vestibular and auditory information is transmitted from the inner ear to the hindbrain via neurons of VIII.th cranial ganglion, also known as the stato-acoustic ganglion (SAG). SAG neurons are formed by a complex but poorly understood multi-step process that begins in the otic vesicle, the precursor of the inner ear. In the first step, SAG neuroblasts are specified in the floor of the otic vesicle and are marked by the expression of proneural gene *neurogenin1* (*ngn1*) (60, 61). After specification, neuroblasts delaminate from the otic epithelium via epithelial-mesenchymal transition and migrate to a region between the otic vesicle and hindbrain. In zebrafish, markers of later stages of differentiation are usually not expressed within the otic epithelium. Upon delamination, however, neuroblasts quickly lose expression of *ngn1* and upregulate the related factor *neurod* (61, 90). *neurod*-expressing cells form a population of migrating

[2]Reprinted with permission from "Tfap2a promotes specification and maturation of neurons in the inner ear through modulation of Bmp, Fgf and notch signaling." by Kantarci H., Edlund R.K., Groves A.K., & Riley B.B., 2015, *PLoS genetics* 11, 3:e1005037. Copyright [2015] by Kantarci et al.

and proliferating precursors called the transit-amplifying (TA) pool (93). As cells in the TA pool differentiate into mature neurons they lose expression of *neurod* and upregulate early neuronal markers *islet1* and *islet2b* (132). Newly formed neurons extend processes bi-directionally to connect sensory epithelia with central targets in the hindbrain. SAG development in chick and mouse embryos follows a similar course except that transit-amplification and expression of *NeuroD* and *Isl1/2* begin while neuroblasts still reside within the otic epithelium (60, 77, 133).

We previously showed that Fgf signaling regulates each step in SAG development in zebrafish (132). Specification of SAG neuroblasts is initiated by a low level of Fgf signaling. As SAG neurons mature they begin to express *fgf5* such that rising levels of Fgf eventually become inhibitory to *ngn*1 expression in the otic vesicle. Consequently, neuroblast specification starts to decline after 24 hpf and ceases entirely by 42 hpf (14, 132). Elevated Fgf also delays terminal differentiation of cells in the TA pool. The TA pool is thereby maintained as a relatively stable population in which the rate of proliferation closely matches the rate of terminal differentiation.

The otic vesicle originates from an ectodermal thickening called the otic placode. The otic placode, along with all other cranial placodes, emerges from a contiguous region of pre-placodal ectoderm (PPE) that forms around the anterior neural plate by the end of gastrulation (9, 134). In zebrafish competence to form PPE is regulated by four transcription factors: Tfap2a, Tfap2c, Gata3 and Foxi1 (9, 135). These transcription factors are also essential for later development of a subset of cranial placodes, including the otic placode. For example, in response to inductive Fgf signaling *foxi1* expression

upregulates in nascent otic/epibranchial placodes; and disruption of *foxi1* leads to severe deficiencies of epibranchial and otic tissue in zebrafish (136-138). A similar role has been shown recently for *Foxi3* in mouse and chick (139, 140). Expression of *gata3* also regulates otic development, becoming localized to the nascent otic placode (141) and to discrete regions of the otic vesicle (142-144). Disruption of *Gata3* in mouse causes severe defects in otic vesicle development (142), including deficiencies of sensory epithelia and improper wiring of auditory neurons (145-147). In contrast, less is known about later roles of *tfap2a/c*. *tfap2a* is best known for its role in the early differentiation and survival of neural crest cells (148-156) and together with *tfap2c* is indispensible for neural crest specification in zebrafish (150, 152). However, whether *tfap2a/c* genes regulate later development in the otic placode and vesicle has not been investigated. Here we report that *tfap2a* is expressed throughout the nascent otic placode and is later restricted to a ventrolateral region in the otic vesicle overlapping with the neurogenic domain. Misexpression of *tfap2a* leads to excess specification and precocious differentiation of SAG neurons whereas knockdown of *tfap2a* causes reduced neurogenesis and delayed differentiation of SAG precursors. Further investigation revealed that *tfap2a* acts non-autonomously through upregulation of *bmp7a*, which in turn restricts Fgf and Notch signaling to promote specification and differentiation of SAG precursors.

MATERIAL AND METHODS

Fish strains and developmental conditions

The wild type strains were derived from AB line (Eugene, OR). Transgenic lines used in this study include *Tg(hsp70:tfap2a)*^{x24} (135), *Tg(hsp70:fgf8a)*^{x17} (19), *Tg(hsp70I:dnfgfr1-EGFP)*^{pd1} (98), *Tg(hsp70I:gal41.5)*^{kca4} (157), *Tg(UAS:myc-Notch1a-intra)*^{kca3} (158) and *Tg(brn3c:gap43-GFP)*^{s356t} (159). These transgenic lines are referred as *hs:tfap2a*, *hs:fgf8*, *hs:dnfgfr1*, *hs:gal4/UAS-NICD* and *brn3c-GFP* respectively. Mutant line *tfap2a*^{m819} (160) was used for most loss of function studies. Mutants were identified by characteristic phenotypes showing expected Mendelian frequencies. Except where noted, embryos were maintained at 28.5 °C in fish water containing 0.008% Instant Ocean salts, methylene blue and PTU (1-phenyl 2-thiourea, 0.3 mg/ml, Sigma) to block melanin formation. Embryos were staged according to standard protocols (100).

Gene misexpression and morpholino injection

To activate heat-shock inducible transgenic lines, heterozygous transgenic embryos were incubated at 39ºC for 30 minutes except where noted. Under this condition, activation of *hs:tfap2a* at 24 hpf led to a detectable increase in *tfap2a* levels by the end of the heat-shock period. Maximal *tfap2a* expression was seen at 25.5 hpf and the *tfap2a* levels remained elevated in the otic vesicle thorough at least 29 hpf (Fig. 3.S1). Since the complete blockage of Fgf signaling inhibits neurogenic specification in the otic vesicle (132), weak attenuation of Fgf signaling was achieved by activation of

hs:dnfgfr1 at 35 ºC for 30 minutes (Fig. 3.6) or at 36.5 ºC for 30 minutes (Fig. 3.7). After the heat-shock, embryos were incubated at 33 ºC until fixation.

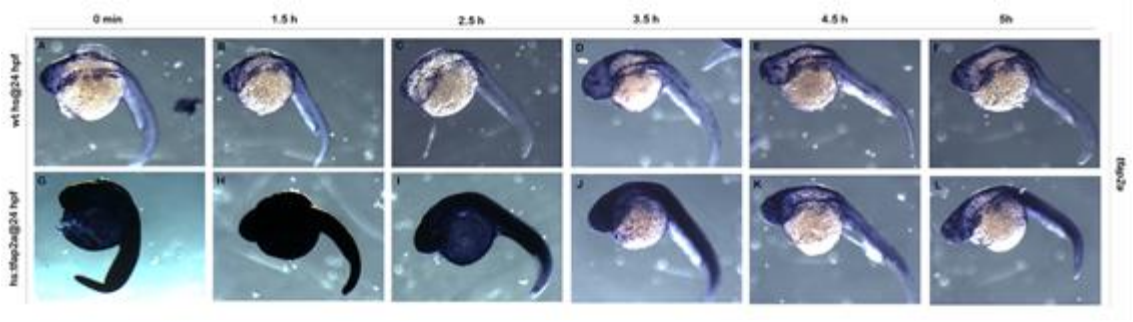

Figure 3.S1: Heat-shock activation of *hs:tfap2a* transgene leads to transient misexpression of *tfap2a*. (A-L) Whole-mount images (dorsal up, anterior left) showing *tfap2a* expression in wild-type and *hs:tfap2a* embryos. Embryos were fixed and stained at indicated intervals after the end of a 30-minute heat-shock initiated at 24 hpf.

In some loss of function experiments, *tfap2a* was knocked down by injecting embryos at the 1-cell stage with approximately 5 ng of *tfap2a* morpholino oligomer (MO). The sequence of *tfap2a* MO has been tested previously for specificity and efficiency (161).

Pharmacological treatments

Notch signaling was blocked by treating embryos with LY411575 diluted from a 10 mM stock in DMSO to a final concentration of 30 μM in fish water. Bmp signaling was blocked by Dorsomorphin (Sigma, P5499) diluted from a 10 mM stock solution into a final concentration of 100 μM in fish water. Treatments were carried in a 24-well plate with a maximum of 15 embryos per well in a volume of 500 μl each.

In situ hybridization and immunohistochemistry

In situ hybridization and antibody staining was carried out as described previously (72, 101, 102). In situ TUNEL assay was performed by using Promega terminal deoxynucleotidyl transferase (M828A) according to the manufacturer's protocol. Following primary and secondary antibodies were used in this study: anti-Islet1/2 (Developmental Studies Hybridoma Bank 39.4D5, 1:100 for whole-mount, 1:250 for cryo-sections), anti-BrdU (Beckton-Dickinson, 1:250) and Alexa 546 goat anti-mouse IgG (Invitrogen A-11003, 1:50 for whole-mount, 1:250 for cryo-sections). Cryo-sectioning and BrdU labeling were carried out as described previously (132). Whole-mount stained embryos were sectioned except for Figures 3.1, 3.7 and 3.S4 where anti-islet1/2 staining was performed on sections using standard whole mount protocols.

Cell transplantation

Wild-type donor cells were injected with the lineage tracer (tetramethylrhodamine labeled, 10,000 MW, lysine-fixable dextran in 0.2 M KCl) and transplanted into non-labeled *hs:tfap2a* embryos at blastula stage.

Chick experiments

Embryonic day 3 (E3) and E4 chick embryos were fixed and embedded in gelatin (7.5% gelatin, 15% sucrose in PBS). 14μm thick sections were collected on Superfrost Plus slides. For AP2a and Jagged-1 co-detection, slides were boiled in 10mM citric acid

for 10 minutes prior to antibody application and then incubated in 0.012% hydrogen peroxide for 15 minutes at room temperature. The 3B5 AP2α monoclonal antibody developed by Trevor Williams was obtained from the Developmental Studies Hybridoma Bank developed under the auspices of the NICHD and maintained by the University of Iowa, Department of Biology, Iowa City, IA 52242. AP2α antibody was diluted 1:100 and Jagged-1 polyclonal antibody (Santa Cruz Biotechnology H-114) was diluted 1:200 in blocking buffer (PBS with 0.02% Tween-20, 0.1% Triton X-100, and 10% goat serum). Staining was detected with biotinylated mouse secondary antibody (Mouse Vectastain ABC kit) in conjunction with PerkinElmer TSA Plus Cyanine-3 System and AlexaFluor 488 conjugated rabbit secondary antibody diluted 1:500 in A+B substrate solution (AlexaFluor goat anti-rabbit, Invitrogen). All slides were mounted in Fluoromount G (Southern Biotech).

Statistics

For pairwise comparisons, student's t-tests were used to evaluate significance. For experiments involving more than two groups significance was evaluated using one-way ANOVA and Tukey post-hoc HSD tests

RESULTS

Expression of *tfap2a* during otic development

To begin to assess potential functions of *tfap2a* in otic development, we examined expression of *tfap2a* in the otic placode and early otic vesicle in zebrafish. At

14 hpf (10 somites) when otic cells first form a morphological placode, *tfap2a* is expressed broadly throughout the placode as shown by co-staining for the early otic marker *pax2a* (Fig. 3.1A-B). The level of *tfap2a* expression varies, with higher levels in dorsal and lateral otic cells. Otic expression in general appears much weaker than in surrounding neural crest cells. By 24 hpf, expression of *tfap2a* in the otic vesicle is restricted to ventrolateral cells. This domain partially overlaps with the neurogenic domain of the otic vesicle, marked by the proneural gene *ngn1* (Fig. 3.1C-D). Neurogenesis declines sharply by 30hpf and ceases entirely by 42 hpf (14, 132). Similarly, the level of *tfap2a* gradually declines in the neurogenic domain after 30 hpf and is no longer detectable by 48 hpf (Fig. 3.1E-I). Despite initial expression of *tfap2a* in at least some neuroblasts in the otic vesicle, expression is lost in most neural precursors as they delaminate from the otic vesicle. Mature neurons of the statoacoustic ganglion (SAG), marked by expression of Isl1, show no detectable expression of *tfap2a* (Fig. 3.1J). These data are consistent with the possibility that *tfap2a* is involved in at least some aspects of neurogenesis in the otic vesicle. Expression patterns of *tfap2a*, *ngn1*, and other key genes involved in SAG development are summarized in Fig. 3.1K. To examine the possibility that expression is conserved in amniote vertebrates, we examined expression of Tfap2a in chick embryos. In agreement with the patterns observed in zebrafish, chick embryos also show expression in ventrolateral regions of the otic vesicle (Fig. 3.1L-Q). Moreover, in chick as in zebrafish, the domain of Tfap2a expression abuts the sensory domain with little or no overlap. The similar expression

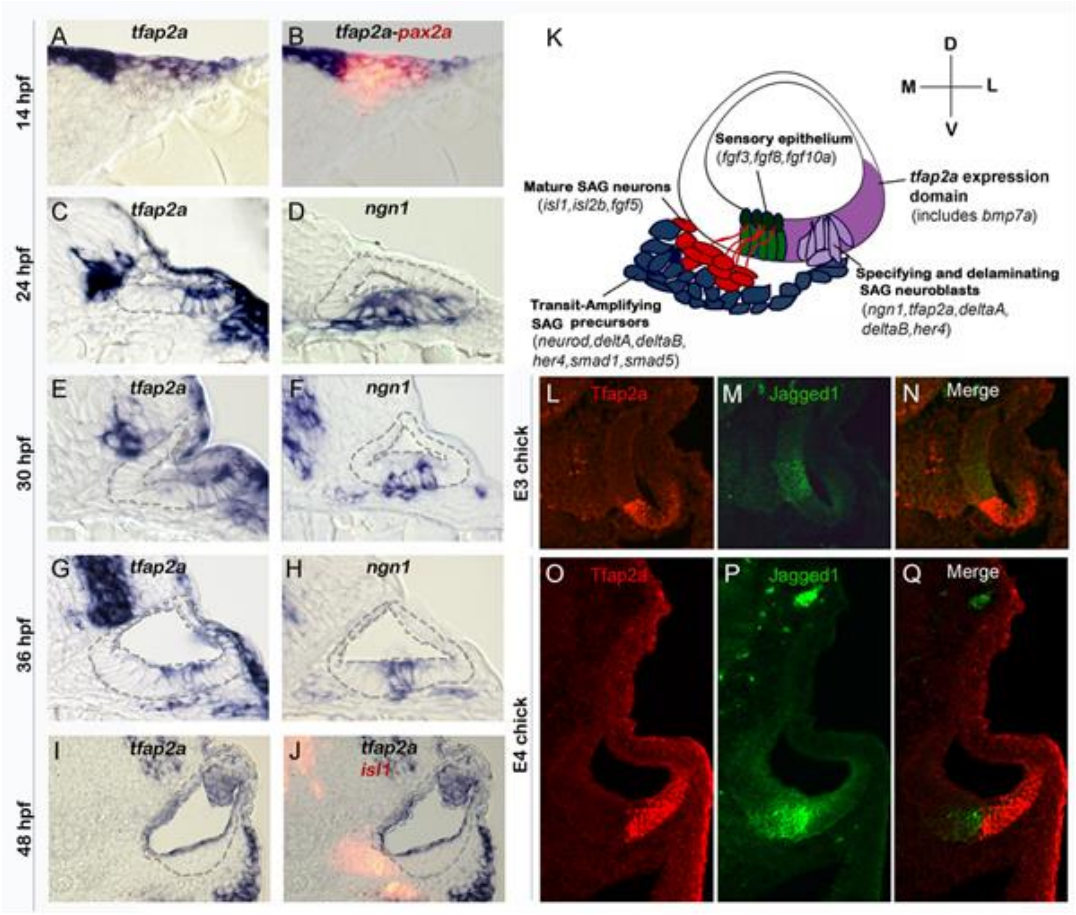

Figure 3.1: Conserved expression of *tfap2a* during otic neurogenesis. All images show cross-sections of the otic placode or vesicle in wild type zebrafish embryos (A-J) or chick embryos (L-Q) with a dorsal up and medial to the left. (A, B) At 14 hpf (10 somites) *pax2a* (red) marks the precursor cells in the emerging otic placode that are co-labeled with *tfap2a* (blue). (C-H) Cross-sections through the widest part of the neurogenic domain of the otic vesicle, just posterior to the utricular macula. The outer and inner edges of the otic vesicle are outlined. Patterns of *ngn1* or *tfap2a* are shown at the indicated times. *tfap2a* is expressed in the ventrolateral part of the otic vesicle, which partially overlaps the domain of *ngn1* expression. (I-J) Cross-sections passing through the utricular macula of specimens co-stained for Isl1 (red) and *tfap2a* (blue) at 48 hpf. Expression of *tfap2a* is not detected in the floor of the otic vesicle or in the mature SAG neurons at this time. (K) Schematic summary of SAG development in zebrafish, including regional markers. Neuroblasts are specified and delaminate from the otic vesicle (light purple) adjacent to nascent sensory epithelia (green). Recently delaminated neuroblasts migrate towards hindbrain and continue to proliferate, forming the transit-amplifying pool (blue). Neuroblasts then stop dividing and differentiate into mature neurons (red). Relevant genes expressed in each domain are indicated. Expression of *tfap2a* (dark purple) overlaps the neurogenic domain, as well as the domain of *bmp7a* expression. Note that all of the tissues indicated express Fgf-target genes (*etv5b* and *spry4*) and transducers of Bmp (*smad1* and *smad5*), but transit amplifying SAG precursors show specific upregulation of *smad1* and *smad5* (162). (L-Q) Cross-sections through the otic vesicle of chick embryos at days 3 and 4 (E3 and E4). The sensory region is labeled with Jagged-1 (green). Tfap2a (red) is expressed in the ventrolateral otic domain in chick embryos similar to the pattern observed in zebrafish.

patterns seen in zebrafish and chick potentially reflect a broadly conserved role in early otic development.

Effects of Tfap2a on neurogenesis in the otic vesicle

To explore the role of *tfap2a*, we characterized the effects of *tfap2a* loss of function or misexpression on neurogenesis in the otic vesicle in zebrafish. Disruption of *tfap2a* causes no overt defects in morphogenesis of the otic vesicle (151). However, *tfap2a*$^{-/-}$ (*lockjaw*) mutants produced only half the normal number of *ngn1*-positive neuroblasts in the otic epithelium at 24 hpf, the stage when neurogenesis normally peaks in wild-type embryos (Fig. 3.2A, C). At later stages, too, *tfap2a*$^{-/-}$ mutants continued to show significant deficiencies in neuroblast specification (Fig. 3.2D, F, M). Similar results were seen in *tfap2a* morphants (*tfap2a*-MO, Fig. 2M). We next used a heat-shock inducible transgenic line, *hs:tfap2a*, to misexpress *tfap2a* at various developmental stages. Activation of *hs:tfap2a* at 20 hpf increased the peak number of neuroblasts in the otic vesicle at 24 hpf by 30% (58.33±3.21 *ngn1*+ cells in *hs:tfap2a* embryos vs. 44.5±2.65 cells in controls, Fig. 3.2B). Activation of *hs:tfap2a* at 24 hpf prolonged the phase of peak neurogenesis, resulting in twice the normal number of neuroblasts at 28 hpf (Fig. 3.2D, E, M). Despite the initial surge, however, the number of *ngn1*+ neuroblasts subsequently declined sharply in transgenic embryos, dropping below the level seen in control embryos at 30 hpf and thereafter (Fig. 3.2G, H, M). Because transgene activity decays 5 hours after heat shock (Fig. 3.S1), we tested the effects of serial heat shocks at 24 hpf and 29 hpf. This resulted in elevated neurogenesis

through at least 32 hpf, when transgenic embryos had twice as many *ngn1*+ cells in the otic epithelium as in control embryos (Fig. 3.2G, I, N). Neurogenesis in the ear normally ceases by 42 hpf (14, 132), prompting us to investigate whether termination of

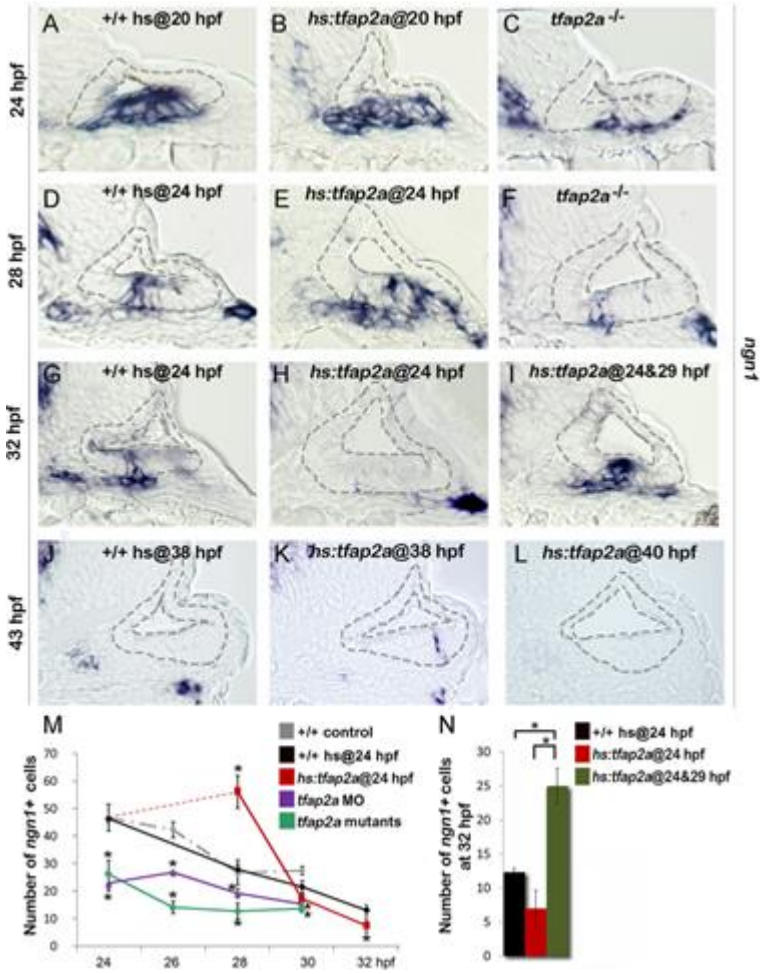

Figure 3.2: Tfap2a enhances otic neurogenesis. (A-L) Cross-sections (medial left, dorsal up) through the otic region just posterior to the utricular macula showing *ngn1* expression in +/+ control embryos, *hs:tfap2a* embryos and *tfap2a*$^{-/-}$ mutants at the indicated times. Wild-type and *hs:tfap2a* embryos were heat shocked as indicated in each panel. Overexpression of *tfap2a* increases the number of neuroblasts in the otic vesicle whereas loss of *tfap2a* slows down and decreases otic neurogenesis. The outer and inner edges of the otic vesicle are outlined in each image. (M, N) Mean and standard deviation of the total number of *ngn1* positive cells in the otic epithelium from 24 to 32 hpf for the genotypes indicated in the color key (counted from serial sections, n=3-7 ears per time point). Asterisks (*) indicate statistically significant differences between groups indicated by brackets (N) or compared to control embryos (M).

neurogenesis could be altered by later misexpression of *tfap2a*. Indeed, activation of *hs:tfap2a* at 38 hpf prolonged specification of neural precursors, as *ngn1*+ neuroblasts were still present in the otic vesicle through at least 43 hpf (Fig. 3.2J, K). In contrast, activation of *hs:tfap2a* at 40 hpf was not sufficient to prevent or delay the cessation of neurogenesis in the otic vesicle (Fig. 3.2L). Overall these results indicate that *tfap2a* enhances neurogenesis in the ear but cannot induce ectopic neurogenesis beyond the floor of the otic vesicle nor reactivate neurogenesis after it has stopped.

Effects of Tfap2a on later stages of SAG development

We next examined whether altered levels of neuroblast specification caused by manipulating *tfap2a* function were followed by changes in later stages of neuronal differentiation. Normally, newly specified neuroblasts delaminate from the otic vesicle, lose expression of *ngn1* and initiate expression of *neurod*, a marker of the "transit-amplifying" (TA) stage of development (61, 132) (Fig. 3.1K). Surprisingly, despite reduced neurogenesis in *tfap2a*$^{-/-}$ mutants and *tfap2a* morphants, the number of *neurod*+ TA cells was greater than normal at every time point examined (Fig. 3.3B, E, H, J). Conversely, despite the large increase in neurogenic specification caused by overexpression of *tfap2a* at 24 hpf, the number of *neurod*-expressing TA cells was reduced at all time points through 48 hpf (Fig. 3.3C, F, I, J). We hypothesized that changes in the size of the TA pool reflect changes in the overall pace of neuronal differentiation. To test this we examined expression of Isl1, a marker of mature SAG neurons. We observed that *tfap2a*$^{-/-}$ mutants and *tfap2a* morphants produced fewer than

normal neurons despite the increased number of *neurod*+ cells (Fig. 3.4E-H, T). The deficiency in neuronal maturation persisted in *tfap2a*$^{-/-}$ mutants through at least 72 hpf (Fig. 3.S2) In contrast, activation of *hs:tfap2a* had the opposite effect. Activation of *hs:tfap2a* during placodal stages elevated accumulation of Isl1+ neurons at 30 hpf, and

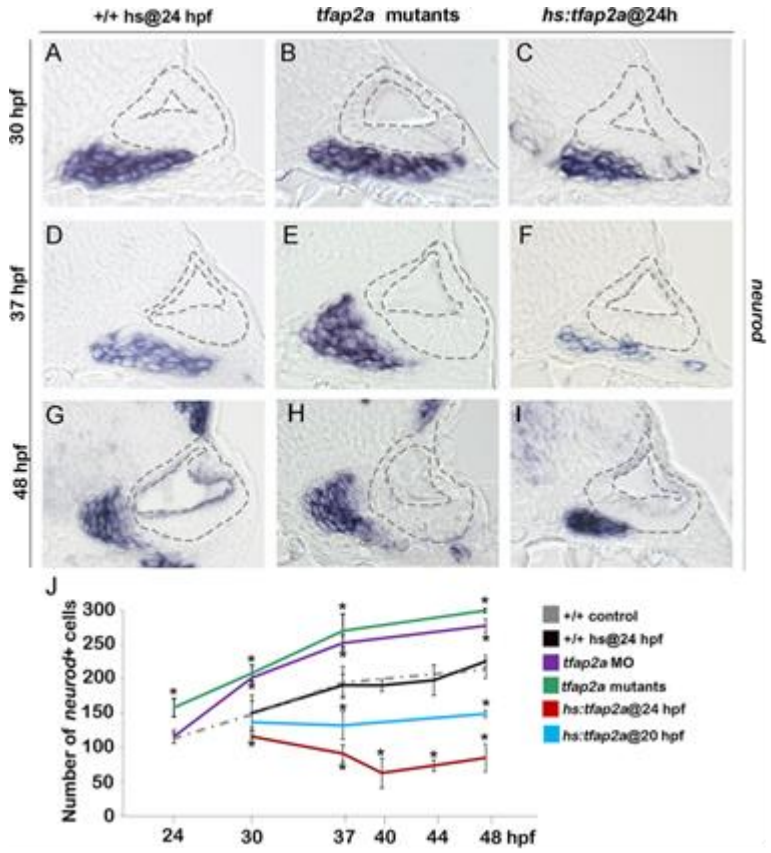

Figure 3.3: Tfap2a regulates the number of transit-amplifying SAG precursors. (A-I) Cross-sections (medial left, dorsal up) at the level of the utricular macula showing *neurod* expression in +/+ control, *tfap2a* mutants and *hs:tfap2a* embryos. Wild-type and *hs:tfap2a* embryos were heat shocked at 24 hpf. Disruption of *tfap2a* leads to accumulation of excess TA cells whereas *tfap2a* overexpression decreases the number of the TA cells. The outer and inner edges of the otic vesicle are outlined in each image. (J) Mean and standard deviation of the total number of *neurod* positive SAG precursors for the genotypes and conditions indicated in the color key (counted from serial sections, n=3-6 ears per time point). Asterisks (*) indicate significant differences from control specimens.

the fold-stimulation was progressively increased with successively later stages of activation (Fig. 3.4M). Activation of *hs:tfap2a* at 24 hpf led to maximal accumulation of neurons, with nearly twice the normal number of Isl1+ neurons observed in transgenic embryos at 30 hpf and 37 hpf (Figure 3.4I-L, M, T). Interestingly, transgene activation at these early stages enhanced accumulation of anterior (vestibular) SAG neurons but not posterior (auditory) neurons (Fig. 3.4D, L). However, activating *hs:tfap2a* expression at 29 hpf increased accumulation of both anterior and posterior neurons (Fig. 3.4N-P), consistent with our previous findings that auditory neurons are specified at later stages than vestibular neurons (132). Together these data indicate that disruption of *tfap2a* inhibits neurogenesis and slows neural maturation, whereas misexpression of *tfap2a* stimulates neuroblast specification and accelerates subsequent differentiation. Importantly, although activation of *hs:tfap2a* at 24 hpf led to elevated accumulation of mature neurons through 37 hpf, the number of mature neurons fell dramatically thereafter to roughly half normal by 48 hpf (Fig. 3.4T). This decline was preceded by a marked increase in the rate of apoptosis amongst mature neurons (Fig. 3.4Q-S, U). Elevated cell death possibly reflects insufficient duration of earlier stages of differentiation and consequent misregulation of factors required for neuronal survival.

Effects on patterning in the otic vesicle

To determine whether the above changes in SAG development resulted from mis-patterning of the otic vesicle, we examined expression of several regional markers.

In *tfap2a*$^{-/-}$ mutants and *tfap2a* morphants, domains of the dorsal marker *dlx3b* and the ventrolateral marker *otx1b* were slightly contracted (Fig. 3.5B, E). Domains of *pax5*, an

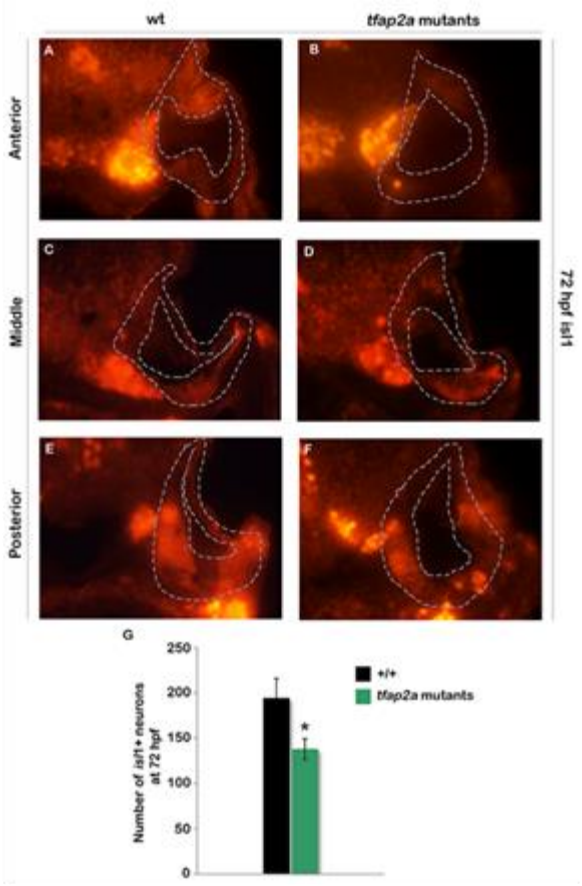

Figure 3.S2: Maturation of SAG neurons remains deficient in *tfap2a* mutants at 3 dpf. (A-F) Cross-sections (dorsal up, medial left) pass through the anterior (A, B), middle (C, D), and posterior (E, F) parts of the otic vesicle and show *isl1* staining in a wild-type embryo (A, C, E) and a *tfap2a* mutant (B, D, F) embryo at 72 hpf. (G) Mean and standard deviation of the total number *Isl1+* SAG neurons in wild-type (n=3) and *tfap2a* mutant (n=4) embryos at 72 hpf (counted on serial sections). Asterisk (*) indicate statistically significant difference compared to wild-type embryos.

anterior-ventral marker of the utricular macula, and *pou3f3b*, a posterior-medial marker of the saccular macula were not altered (Fig. 3.5H, K). Additionally, sensory epithelia

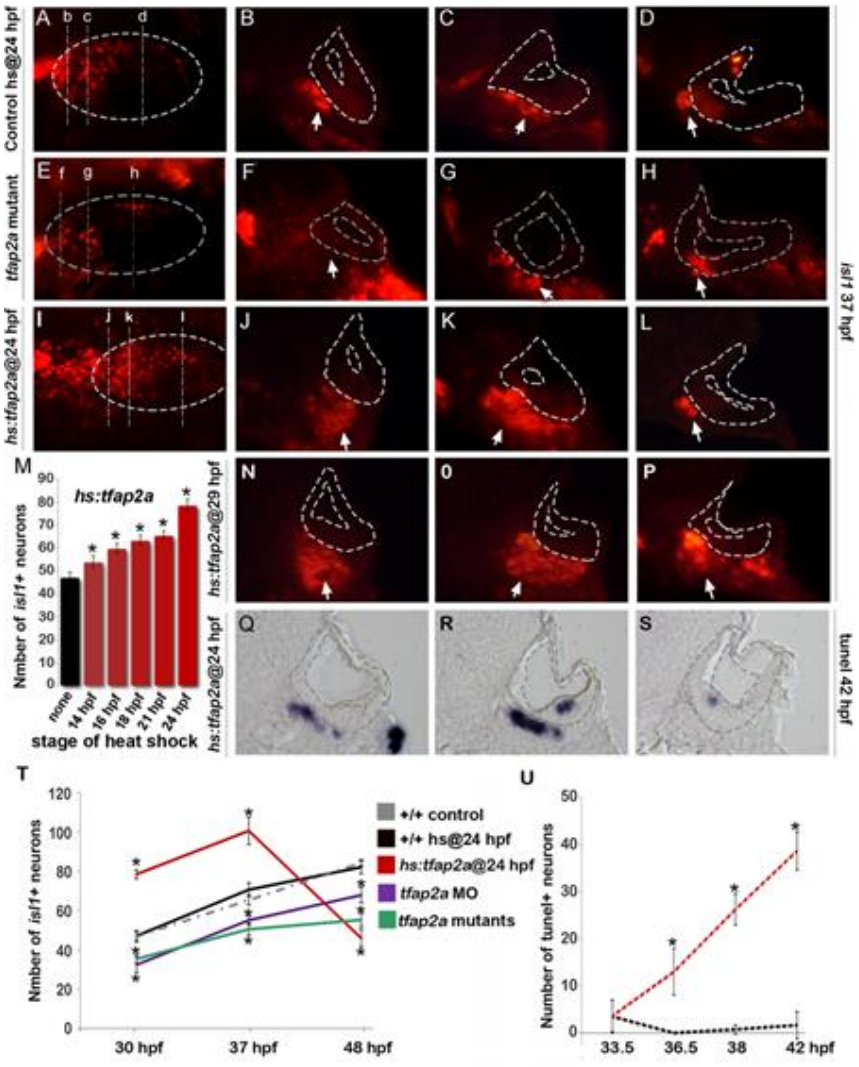

Figure 3.4: Tfap2a regulates maturation of SAG neurons. (A-L) Images of anti-Isl1 antibody staining in control embryos (A-D), *tfap2a*$^{-/-}$ mutants (E-H) and *hs:tfap2a* embryos (I-L) at 37 hpf. Control and *hs:tfap2a* embryos were heat shocked at 24 hpf. Whole-mount specimens (A, E, I) show dorsolateral (anterior to the left) and indicate planes of cross-section in (B-D), (F-H) and (J-L). Cross-sections are oriented with dorsal up and medial to the left. The otic vesicle is outlined in each image. White arrows indicate the SAG population to help distinguish it from other Isl1+ populations present in some sections. (M) Total number of Isl1+ neurons in *hs:tfap2a* embryos at 30 hpf following heat shock at the indicated times (n=10-15 each). (N-P) Cross-sections of a *hs:tfap2a* specimen at 37 hpf following heat shock at 29 hpf. Planes of section are similar to those shown in (I). (Q-S) Cross-sections of a *hs:tfap2a* embryo stained for TUNEL positive SAG neurons at 42 hpf. (T) Mean and standard deviation of the total number of Isl1+ SAG neurons at the indicated times in +/+ embryos, *hs:tfap2a* embryos, *tfap2a*$^{-/-}$ mutants and *tfap2a* morphants (n=7-34 embryos per time point). (U) Mean and standard deviation of the total number of TUNEL positive SAG neurons at the indicated times in control embryos and *hs:tfap2a* embryos (counted from serial sections, n=3-6 ears per time point). Asterisks (*) indicate statistically significant differences compared to control embryos.

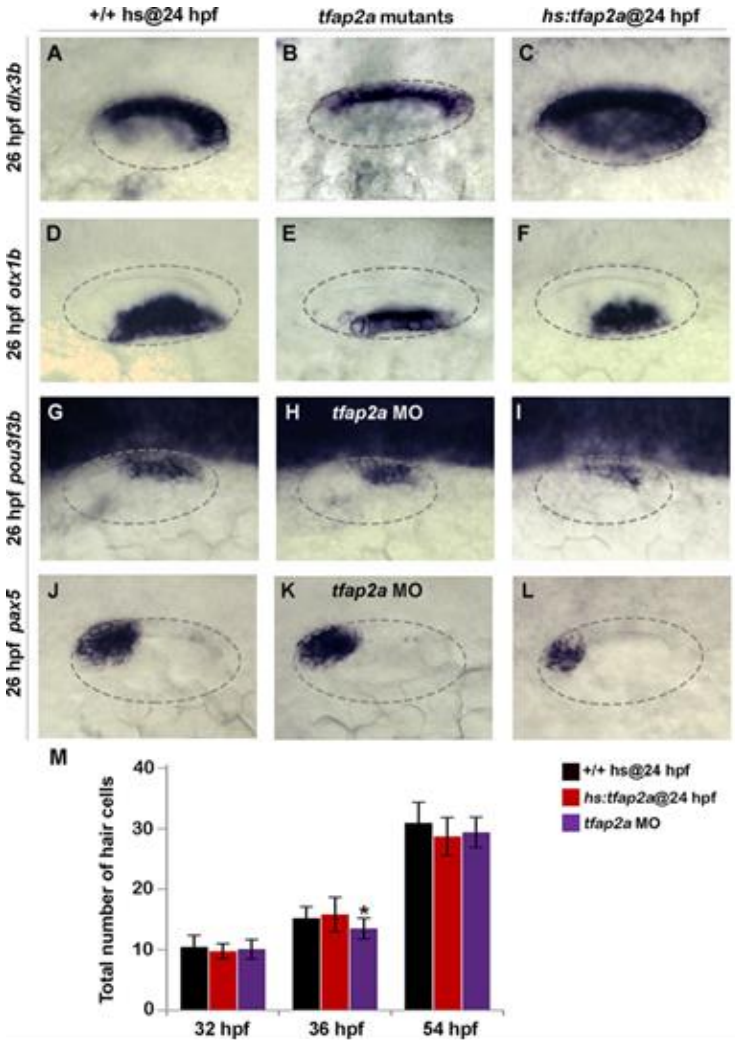

Figure 3.5: Effects of *tfap2a* knockdown and overexpression on otic vesicle patterning. (A-L) Whole-mount images (dorsal up, anterior left) showing dorsolateral views of the otic vesicle (outlined) in control embryos, *tfap2a*$^{-/-}$ mutants and *tfap2a* morphants, and *hs:tfap2a* embryos for the indicated genes at 26 hpf. (M) Mean and standard deviation of the total number of hair cells in utricular and saccular maculae of control and *hs:tfap2a* embryos and *tfap2a* morphants at the indicated times (n=24 embryos each). Data were obtained by counting GFP-positive hair cells in the sensory epithelia of *brn3c:Gfp* transgenic embryos. Accumulation of hair cells was normal except in *tfap2a* morphants at 36 hpf (*), which showed a small but significant decrease relative to the control.

appeared to develop normally and there were no obvious changes in hair cell development through 54 hpf (Fig. 3.5M). Activation of *hs:tfap2a* at 24 hpf led to weak contraction *otx1b* but a substantial expansion of the *dlx3b* (Fig. 3.5C, F). *pax5* was

expressed in its normal domain but at a reduced level (Fig. 3.5L). Expression of *pou3f3b* was normal (Fig. 3.5I) and there were no changes in accumulation of hair cells

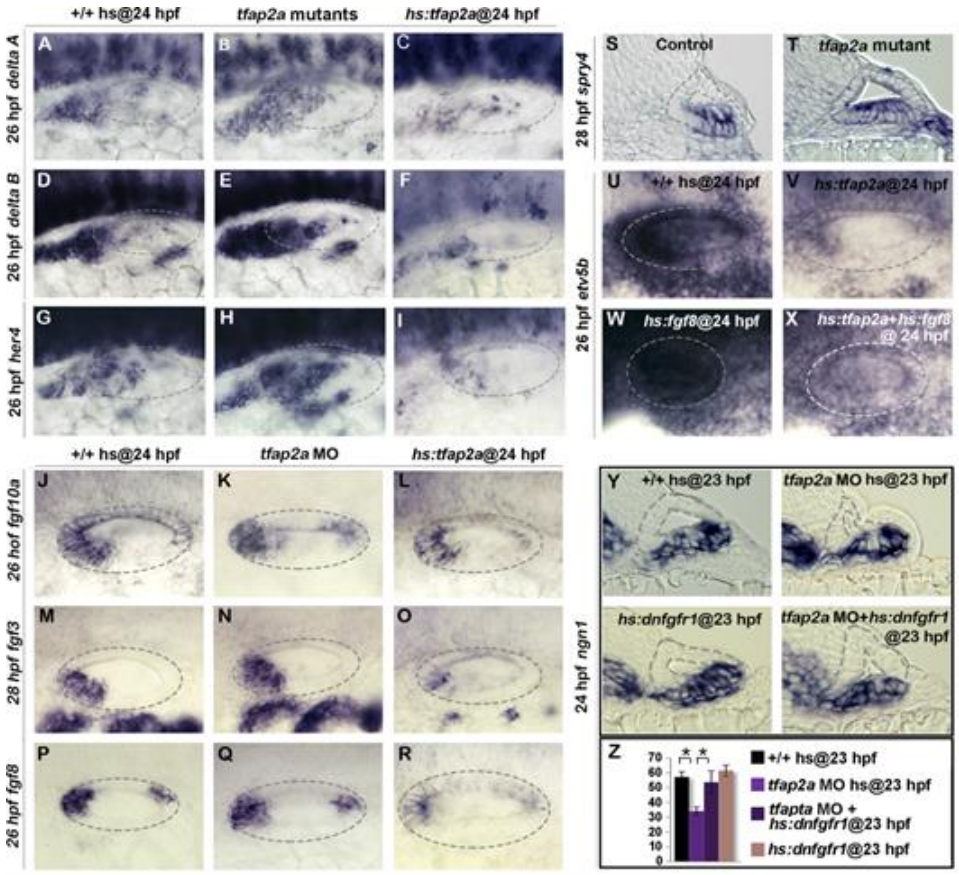

Figure 3.6: Tfap2a regulates the level of Fgf and Notch Signaling in the otic vesicle. (A-V) Whole-mount images (dorsal up, anterior left) showing dorsolateral views of the otic vesicle (outlined). (A-R) Expression of the indicated genes in wild-type embryos, *hs:tfap2a* embryos and *tfap2a*$^{-/-}$ mutants (A-I) or *tfap2a* morphants (J-R) at 26 hpf (A-L, P-R) and 28 (M-O) hpf. (S, T) Cross-sections (dorsal up, medial left) passing through the utricular macula show *spry4* expression at 28 hpf in a control embryo and *tfap2a*$^{-/-}$ mutant. (U-X) Whole-mounts showing expression of *etv5b* at 26 hpf. Activation of *hs:tfap2a* diminishes *etv5b* expression (U, V), activation of *hs:fgf8* leads to global upregulation of *etv5b* (W), and co-activation of *hs:fgf8* and *hs:tfap2a* restores *etv5b* to near normal (X). (Y) Cross-sections (dorsal up, medial left) passing just posterior to the utricular macula showing *ngn1* at 24 hpf following a 35°C heat shock at 23 hpf. Reduction in the *ngn1* domain caused by knockdown of *tfap2a* is rescued by weak activation of *hs:dnfgfr1*. (Z) Mean and standard deviation of the total number of *ngn1* positive cells in the otic epithelium at 24 hpf for the genotypes and knockdowns indicated in the color key (counted from serial sections, n=3-6 ears per time point). Asterisks (*) indicate statistically significant differences between the groups indicated in brackets.

through 54hpf (Fig. 3.5M). Thus, gross patterning in the otic vesicle was nearly normal in *tfap2a*$^{-/-}$mutants and morphants, though substantial changes were seen in one marker (*dlx3b*) following overexpression of *tfap2a*. Such changes in gene expression likely reflect changes in cell signaling as described below.

Effects on Notch and Fgf signaling

We next investigated whether Tfap2a activity influences Notch and Fgf signaling, pathways known to regulate development of SAG neurons. For example, Delta-Notch signaling is normally activated by neurogenic factors Ngn1 and Neurod and serves as a feedback inhibitor of neurogenesis (60, 86, 163). Disruption of Delta-Notch signaling leads to excess neural specification and precocious differentiation (89), similar to the effects of misexpression of *tfap2a*. Here we observed that expression of *deltaA* and *deltaB* was increased in *tfap2a*$^{-/-}$ mutants and, conversely, *delta* gene expression was strongly impaired following overexpression of *tfap2a* (Fig. 3.6A-F). Similar changes were observed for the Notch target gene *her4*, which increased in *tfap2a*$^{-/-}$ mutants and decreased following activation of *hs:tfap2a* (Fig. 3.6G-I). Thus Tfap2a appears to inhibit Notch activity during development of SAG neurons by inhibiting expression of Notch ligands. Fgf signaling has a more complex role in neural development in the ear. At early stages specification of neuroblasts requires Fgf. As development proceeds, however, rising levels of Fgf5 secreted by mature SAG neurons terminates specification of new neuroblasts and delays differentiation of TA cells into mature neurons (132) (Fig. 3.1K). Weak impairment of Fgf signaling can prolong neurogenesis and accelerate

neural differentiation, mimicking aspects of the *tfap2a* overexpression phenotype. We therefore examined expression of various *fgf* genes in the otic vesicle. Knockdown of *tfap2a* did not appear to alter expression of *fgf3*, *fgf8*, or *fgf10a* (Fig. 3.6K, N, Q). Activation of *hs:tfap2a* at 24 hpf led to reduced expression of *fgf3* and *fgf8*, but expression of *fgf10a* was not altered (Fig. 3.6L, O, R). To look for changes in Fgf signaling, we examined expression of Fgf-target genes *spry4* , *etv4* (*pea3*) and *etv5b* (*erm*). Although *etv4* and *etv5b* expression appeared normal in *tfap2a* morphants (Fig. 3.S3D, H), *spry4* was expressed at higher levels and in a broader domain than normal in

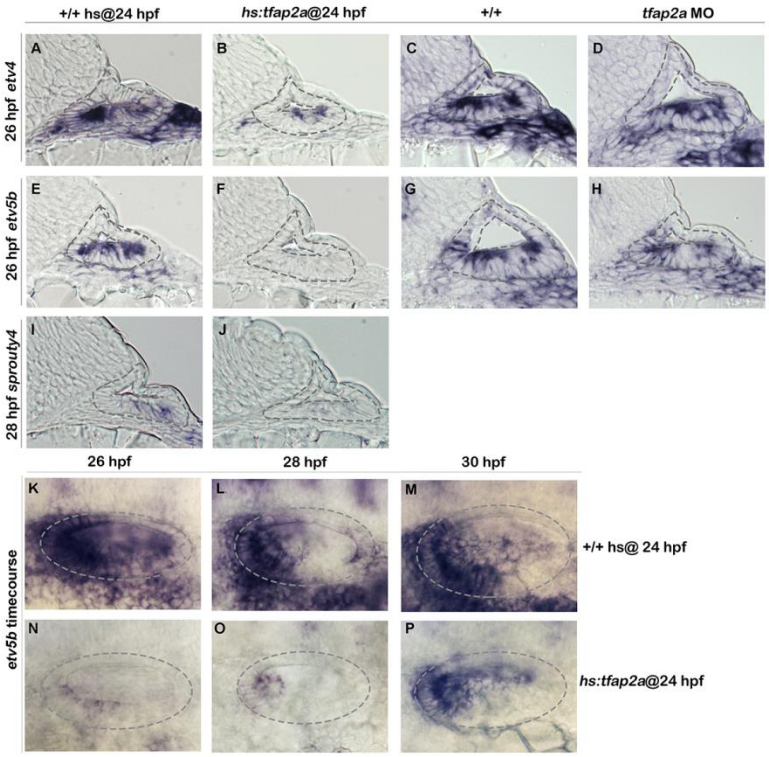

Figure 3.S3: *tfap2a* inhibits Fgf signaling in the otic vesicle. (A-J): Cross-sections (dorsal up, medial left) passing through the otic vesicle just posterior to the utricle showing expression of *etv4* (A-D), *etv5b* (E-H) and *sprouty4* (I, J) in heat-shocked wild-type (A, E, I), *hs:tfap2a* (B, F, J), non-heat shocked wild-type (C,G) and *tfap2a* morphant (D,H) embryos at indicated time points. (K-P): Whole-mount images (dorsal up, anterior left) showing dorsolateral views of the otic vesicle (outlined) stained for *etv5b* expression in heat-shocked wild-type and *hs:tfap2a* embryos at indicated times.

tfap2a$^{-/-}$ mutants, indicating that Fgf signaling was elevated (Fig. 3.6S-T). Conversely, activation of *hs:tfap2a* at 24 hpf reduced expression of *etv4*, *etv5b* and *spry4* by 26 hpf,

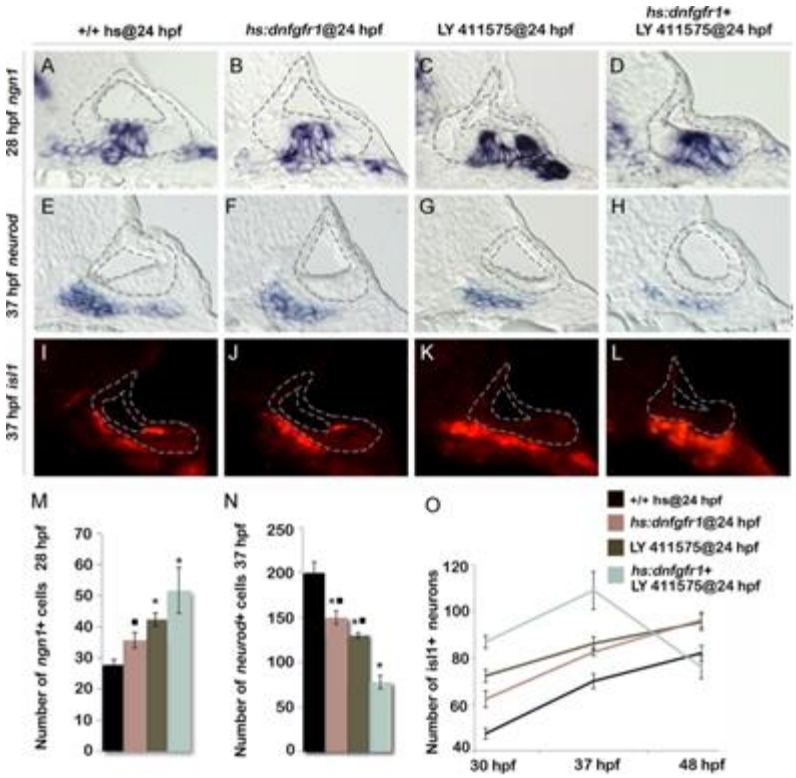

Figure 3.7: Reducing Fgf and Notch levels mimics the effects of *tfap2a* overexpression. (A-L) Cross-sections (medial left, dorsal up) passing just posterior to the utricular macula and showing expression of *ngn1* at 28 hpf (A-D), or sections passing through the utricular macula and showing *neurod* at 37 hpf (E-H) or Isl1 at 37 hpf (I-L) in wild-type control (A, E, I), *hs:dnfgfr1* embryos (B, F, J), LY411575 inhibitor treated wild-type embryos (C, G, K) and LY411575 inhibitor treated *hs:dnfgfr1* embryos (D, H, L). All specimens were treated with 0.3% DMSO and heat-shocked at 24 hpf. The otic vesicle is outlined in each image. (M, N) Mean and standard deviation of the total number of *ngn1* positive cells in the otic epithelium at 28 hpf (M) and total *neurod* positive SAG precursors at 37 hpf (N) for the genotypes and treatments indicated in the color key (counted from serial sections, n=3-6 ears per time point). Asterisks (*) indicate significant differences from control embryos and filled squares indicate significant differences relative to *hs:dnfgfr1* embryos treated with LY411575. (O) Mean and standard deviation of the total number of Isl1 positive SAG neurons at different times for the genotypes and treatments indicated in the color key (n=6-15 embryos each). In (O) differences between control and experimental specimens were significant at each time point. In addition, LY411575 treated *hs:dnfgfr1* embryos were significantly different from *hs:dnfgfr1* alone or LY411575 treatment alone.

indicating a reduced level of Fgf signaling (Fig. 3.6U-V, Fig. 3.S3A-J). Fgf signaling remained reduced through 28 hpf but started to recover after 30 hpf as transgene activity decayed (Fig. 3.S3K-Q). Thus, Tfap2a appears to limit Fgf signaling, in part through reducing expression of *fgf* genes.

To test whether Tfap2a can influence Fgf signaling independently of ligand expression, we co-misexpressed *tfap2a* and *fgf8*. While activation of *hs:fgf8* led to global upregulation of *etv5b*, co-activation of *hs:tfap2a* with *hs:fgf8* at 24 hpf partially suppressed expression of *etv5b* (Fig. 3.6W-X). This indicates that *tfap2a* can inhibit Fgf signaling at a level downstream of ligand accumulation.

To test the functional significance of elevated Fgf signaling in *tfap2a* morphants, we examined whether weakly inhibiting Fgf signaling could rescue the neurogenic deficiencies in *tfap2a* morphants. Indeed, reducing the level of Fgf signaling via low-level activation of *hs:dnfgfr1* (dominant-negative Fgf receptor) at 35 °C restored *ngn1*+ cell counts to normal in *tfap2a* morphants (Fig. 3.6Y-Z). This suggests that elevated Fgf signaling partially accounts for the reduced neuroblast specification in *tfap2a* morphants and mutants.

Because Tfap2a appears to dampen both Fgf and Notch signaling, we tested whether weakening both pathways by other means could mimic the effects of *tfap2a* overexpression. Low level activation of *hs:dnfgfr1* at 36.5°C increased the number of *ngn1*+ neuroblasts in the ear by ~30% (Fig. 3.7B, M). Similarly, reducing the level of Notch signaling by treatment with the gamma-secretase inhibitor LY411575 increased

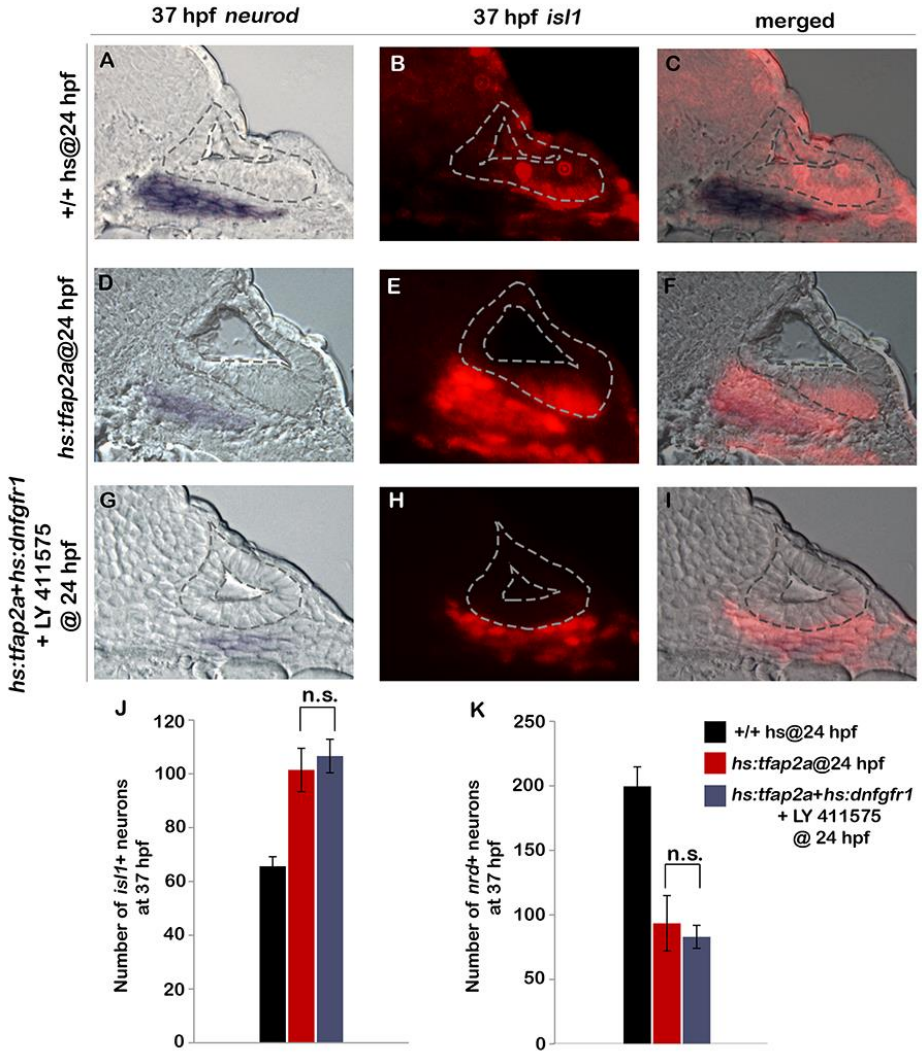

Figure 3.S4: Inhibition of Notch and Fgf signaling in *hs:tfap2a* embryos does not enhance the effects of *hs:tfap2a* activation. (A-I): Cross-sections at the level of utricular macula (medial to the left, dorsal up) show bright field (A, D, G), fluorescent (B, E, H) and merged (C, F, I) images for *neurod* (blue) and *isl1* (red) in heat-shocked wild-type, *hs:tfap2a* and LY 411575 treated *hs:tfap2a+ hs:dnfgfr1* embryos at 37 hpf. All specimens were treated with 0.3% DMSO and heat-shocked (39 °C, 30 minutes) at 24 hpf. (J) Mean and standard deviation of the total number of *is1*+ neurons at 37 hpf under the conditions indicated in the color key (n=10-15 specimens each). (K) Mean and standard deviation of the total number of *nrd*+ neuroblasts at 37 hpf under the conditions indicated in the color key (n=3-6 ears each, counted from serial sections). Both experimental conditions were significantly different compared to controls. n.s., no statistical difference between the groups indicated in brackets.

the number of *ngn1*+ cells in the otic vesicle by ~50% (Fig. 3.7C, M). Combining these conditions to reduce both Fgf and Notch signaling further increased neuroblast specification, closely mimicking the effects of activating *hs:tfap2a* at 24 hpf (Fig. 3.7D, M). Likewise, inhibiting both Fgf and Notch together reduced the number of *neurod*+ cells in the TA pool and increased accumulation of Isl1+ neurons through 37 hpf in amanner similar to activating *hs:tfap2a* at 24 hpf (Fig. 3.7E-O). Moreover, embryos inhibited for both Fgf and Notch signaling showed a dramatic loss of mature SAG neurons after 37 hpf, again mimicking the effects of *hs:tfap2a* activation (Fig. 3.7O). Interestingly, inhibition of either Fgf or Notch alone caused similar but more modest acceleration of neural differentiation, but such conditions did not lead to subsequent loss of mature neurons after 37 hpf (Fig. 3.7O). This is possibly because differentiation, though accelerated relative to control embryos, is still slow enough to allow expression of all factors essential for survival. Finally, activating *hs:tfap2a* at 24 hpf combined with conditions to inhibit Fgf and Notch did not further increase accumulation of Isl1+ neurons at 37 hpf (Fig. 3.S4). Thus, reducing both Fgf and Notch signaling is sufficient to recapitulate all observed effects of *tfap2a* overexpression.

Tfap2a regulates transit amplification independently of earlier stages

We considered the possibility that the ability of Tfap2a to alter development of SAG cells outside the ear could arise secondarily from perturbation of earlier developmental stages within the otic vesicle. To test whether Tfap2a can specifically influence cells after delamination (without altering early development within the otic

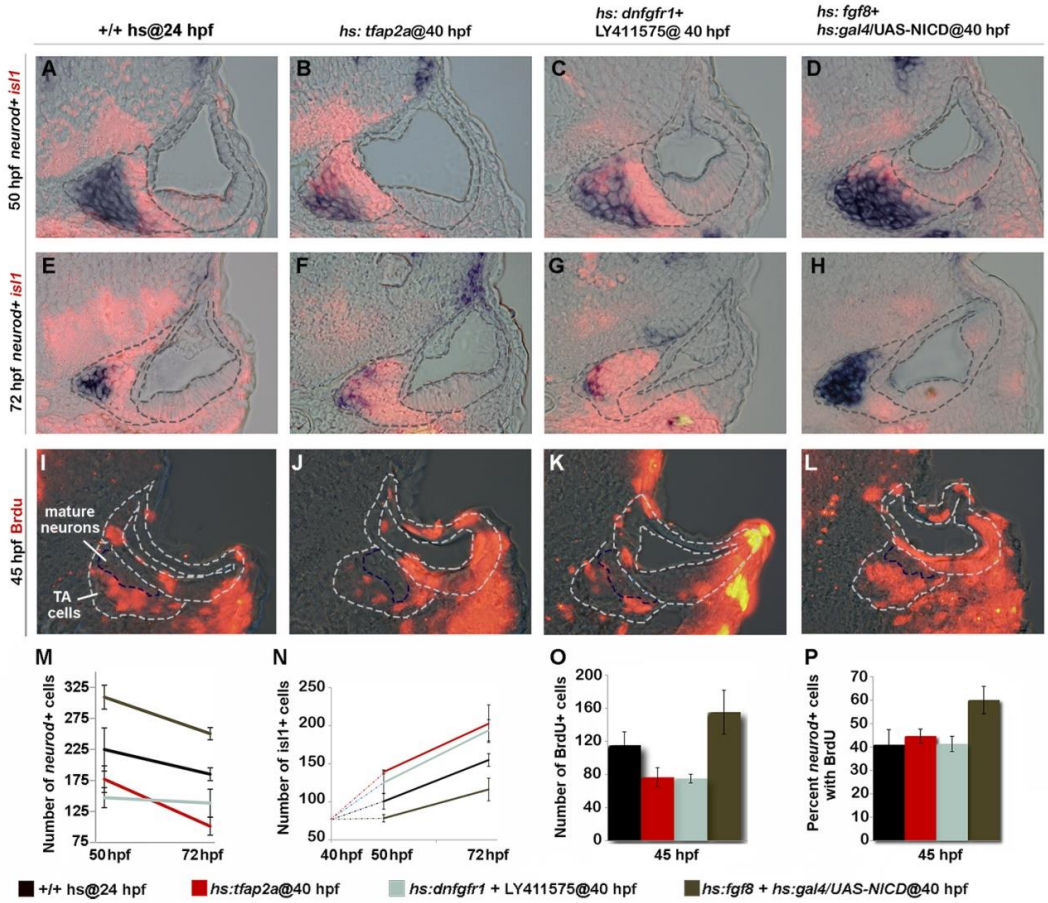

Figure 3.8: Tfap2a regulates development of TA cells independent of earlier stages. (A-L) Cross-sections (medial left, dorsal up) at the level of utricular macula. The otic vesicle and regions occupied by mature SAG neurons and TA cells are outlined in each image. Co-staining for Isl1 (red) and *neurod* (blue) at 50 hpf (A-D) and 72 hpf (E-H) under conditions indicated across the top of the figure. All specimens were treated with 0.3% DMSO and heat-shocked (39 °C) at 40 hpf. (I-L) BrdU staining in embryos exposed to BrdU for 5 hours, from 40 to 45 hpf. The region containing mature SAG neurons is indicated. (M-O) Mean and standard deviation for the total number of *neurod*+ TA cells (M), total Isl1+ mature neurons (N) and total BrdU+ TA cells (O) for the indicated genotypes and treatments (counted from serial sections, n=3-6 ears per time point). Differences between control and experimental specimens were significant at all time points, except that *hs:fgf8+hs:gal4/UAS-NICD* embryos were not significantly different from control embryos at 72 hpf in (N). (P) Percentage of *neurod*+ TA cells that are also BrdU positive (counted from serial sections, n=3-6 ears per time point). Only *hs:fgf8+hs:gal4/UAS-NICD* embryos were significantly different from the control in (P).

vesicle), we activated *hs:tfap2a* at 40 hpf when neurogenesis has ceased in the otic vesicle. Recall that transgene activation fails to prolong or reinitiate neuroblast specification at this stage (Fig. 3.2L). Regardless, overexpression of *tfap2a* at 40 hpf still reduced the number of *neurod*+ cells and led to an increase in Isl1+ neurons at 50 hpf (Fig. 3.8B, F, M, N). Misexpression of *tfap2a* also reduced the total number of cells in the TA pool that incorporated BrdU (Fig. 3.8J, O). However, this was proportional to the reduction in the total number of *neurod*+ cells (Fig. 3.8P), consistent with acceleration of the entire TA pool. A notable difference from earlier activation is that activating *hs:tfap2a* at 40 hpf did not lead to apoptosis of SAG neurons at later stages, as the number of Isl1+ cells remained elevated and in fact continued to increase through at least 72 hpf (Fig. 3.8B, F, N). The same effects were obtained by directly inhibiting both Fgf and Notch signaling after 40 hpf (Fig. 3.8C, G, K M-P). Conversely, misexpressing Fgf8 and NICD (Notch intracellular domain) by heat shock activation at 40 hpf led to accumulation of more TA cells and fewer mature neurons than normal at 50 and 72 hpf, indicating a delay in neuronal differentiation (Fig. 3.8D, H, M, N). Moreover, activating Fgf and Notch together increased the percentage of *neurod*+ cells that continue to incorporate BrdU (Fig. 3.8L, O, P), suggesting that the majority of cells in the TA pool persist in a relatively immature stage of SAG development. Thus, manipulating *tfap2a*, or Fgf and Notch signaling directly, can alter the rate of differentiation of TA cells even when earlier development within the otic vesicle has occurred normally. On the other hand, survival of mature SAG neurons requires normal development at early stages.

Tfap2a acts non-autonomously

It is noteworthy that *tfap2a* is not normally expressed in the TA pool or mature neurons, yet knockdown or misexpression of *tfap2a* alters the rate of differentiation and survival of these cells. This raised the possibility that Tfap2a could act non-

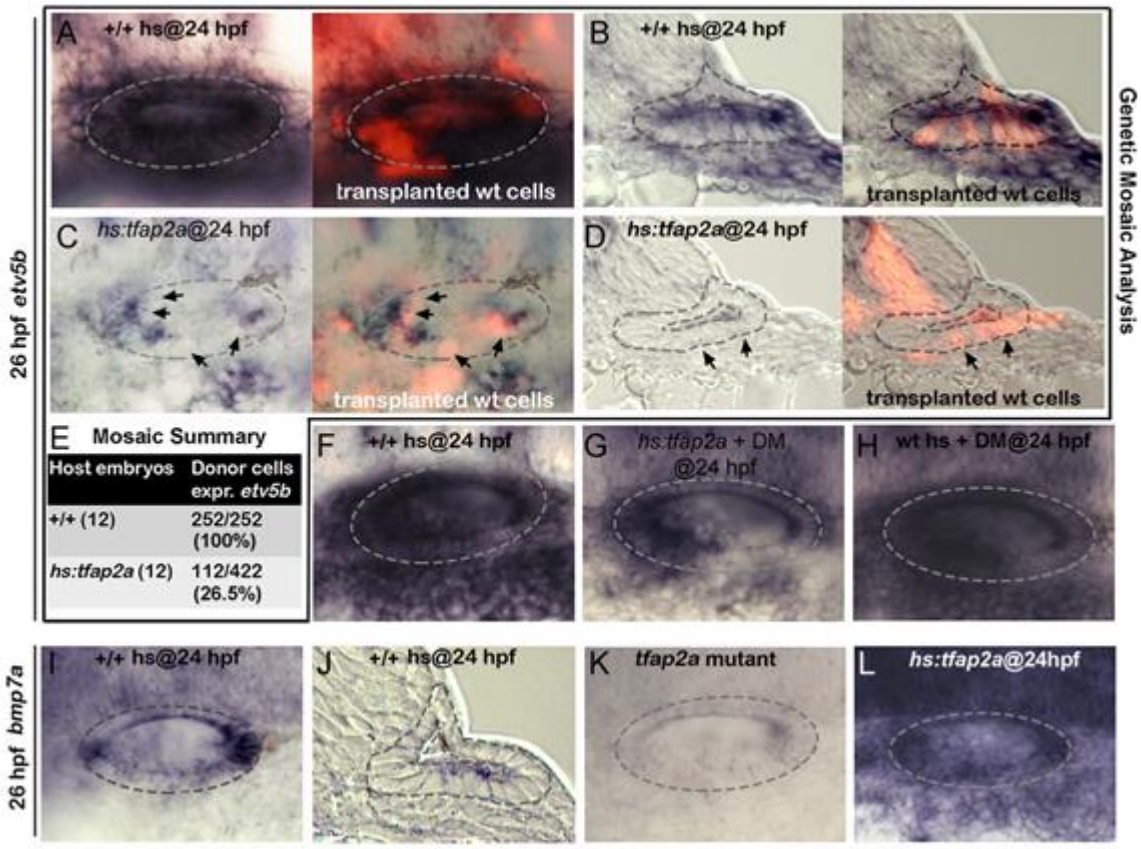

Figure 3.9: Tfap2a regulates SAG development non-autonomously. (A-D) Whole-mounts (dorsal up, anterior left) and cross-sections (just posterior to utricular macula, medial to the left) showing both bright-field and corresponding fluorescent images of +/+ host embryos (A, B) and *hs:tfap2a* host embryos stained for *etv5b* expression (blue) and showing transplanted wild-type donor cells (red). Positions of wild-type cells that fail to express *etv5b* are highlighted with arrows in (C, D). (E) Summary of mosaic analysis showing the number of +/+ or *hs:tfap2a* host embryos examined and the number of +/+ donor cells expressing *etv5b* over the total number of donor cells that populated the ventral half of the otic vesicle. (F-H) Expression of *etv5b* at 26 hpf in a control (F), a DM-treated *hs:tfap2a* embryo (G) and DM-treated wild-type embryo (H). All specimens were treated with 1% DMSO and heat-shocked at 24 hpf. (I-L) Expression of *bmp7a* at 26 hpf in a control (I, J), *tfap2a*$^{-/-}$ mutant (K) and *hs:tfap2a* embryo (L). Wild-type and *hs:tfap2a* embryos were heat shocked at 24 hpf.

autonomously on cells outside the ear. To test directly whether *tfap2a* can act non-autonomously, we generated genetic mosaics by transplanting wild-type cells into *hs:tfap2a* host embryos.

We reasoned that if *hs:tfap2a* were to act non-autonomously, activating the transgene in host cells should be able to prevent wild-type cells from responding to Fgf sources in the otic vesicle. In support, activation of *hs:tfap2a* at 24 hpf suppressed *etv5b* expression in the majority (73.5%) of transplanted wild-type cells by 26 hpf (Fig. 3.9C-E), indicatingthat *tfap2a* acts non-autonomously to modulate the response to Fgf. In contrast, all wild-type donor cells transplanted into wild-type host embryos showed normal expression of *etv5b* in the otic vesicle (Fig. 3.9A, B, E). Thus Tfap2a non-autonomously inhibits Fgf signaling in the otic vesicle (Fig. 3.9H).

Bmp7a mediates the effects of Tfap2a

We next surveyed expression of various *bmp* genes following activation of *tfap2a* and identified *bmp7a* as a likely candidate for mediating its effects on Fgf signaling. *bmp7a* is normally expressed in cells at the anterior and posterior ends of the otic vesicle, and at a lower level in a ventrolateral domain that overlaps the *tfap2a* Bmp signaling is well known to antagonize Fgf signaling in a variety of developmental contexts. Here we found that blocking Bmp signaling with the pharmacological inhibitor dorsomorphin (DM) (164) strongly suppressed the ability of *hs:tfap2a* to reduce Fgf signaling. For example, *etv5b* expression was nearly normal in the otic vesicle 2 hours after the activation of *hs:tfap2a* when embryos were also treated with

DM (Fig. 3.9F, G). DM treatment alone had negligible effects on expression of *etv5b* expression domain (162) (Fig. 3.9I-J, compare with Fig. 3.1C). Expression of *bmp7a* was nearly abolished in *tfap2a*$^{-/-}$ mutants (Fig. 3.9K). In contrast, activation of *hs:tfap2a* strongly upregulated *bmp7a* expression in the otic vesicle as well as in surrounding tissues (Fig. 3.9L). In contrast to *bmp7a*, we observed no consistent changes in expression of *bmp2b* or *bmp4* following manipulation of *tfap2a* function (Fig. 3.S5), indicating that changes in *bmp7a* are relatively specific. Together, these data suggest that *tfap2a* positively regulates *bmp7a*, which in turn restricts the level of Fgf signaling during otic development.

We next examined whether Bmp signaling mediates the effects of *tfap2a* on Notch activity. In support, blocking Bmp with DM rescued expression of *deltaB* and *her4* following activation of *hs:tfap2a* at 24 hpf (Fig. 3.10A-L, M-P). Treatment with DM alone caused a slight but significant increase in the number of cells expressing *deltaB* and *her4* (Fig. 3.10D, H, I-L). Thus the ability of *tfap2a* to restrict Notch signaling requires elevated Bmp signaling.

Finally, we tested whether the effects of *tfap2a* on SAG development also require Bmp signaling. Blocking Bmp after activating *hs:tfap2a* at 24 hpf restored neuroblast specification to normal in 6 out of 8 specimens (Fig. 3.10I-L, Q). Similarly, accumulation of mature Isl1+ neurons was nearly normal in 12 out of 15 embryos at 30 hpf (Fig. 10R) and was restored to normal in all specimens at 37 hpf (n=15) (Fig. 3.10S). DM treatment alone caused a slight but significant reduction in neuroblast specification and accumulation of mature SAG neurons (Fig. 3.10Q-S). Together, these findings

support a model in which *tfap2a* regulates the level of *bmp7a* expression in the otic vesicle, which in turn restricts Fgf and Notch signaling to control the amount, duration and speed of SAG development.

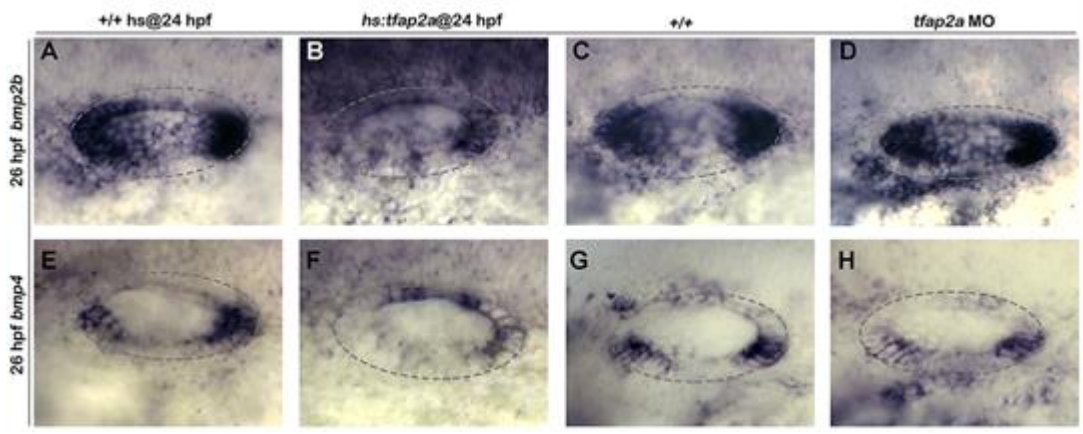

Figure 3.S5: The effects of *tfap2a* overexpression and knock-down on *bmp2b* and *bmp4* expression. (A-H): Whole-mount images (dorsal up, anterior left) showing dorsolateral view of the otic vesicle (outlined) for *bmp2b* (A-D) and *bmp4* (E-H) expression for the indicated genotypes and conditions. Activation of *hs:tfap2a* appears to reduce expression of both genes in portions of the otic vesicle, but *bmb2b* is upregulated in the hindbrain (B) and *bmp4* is upregulated in the dorsal part of the otic vesicle (F). Knocking down *tfap2a* had little or no effect on either gene (D, H).

DISCUSSION

We have shown that Tfap2a regulates development of SAG neurons by modulating Fgf, Notch and Bmp signaling. Tfap2a overexpression promotes neurogenic specification in the otic vesicle and accelerates subsequent differentiation of TA precursors into mature neurons. Conversely, disruption of *tfap2a* reduces the number of *ngn1*+ neuroblasts and decreases the rate of neuroblast differentiation. The neurogenic effects of *tfap2a* overexpression result from inhibition of Notch and Fgf signaling, which normally serve to restrict neuroblast specification and delay differentiation. The effects

of Tfap2a appear to be mediated by Bmp7a, which is upregulated in response to Tfap2a activity. Bmp signaling in turn antagonizes Fgf and Notch signaling to promote specification and terminal differentiation of SAG precursors. These findings are novel and clarify several aspects of SAG development, which are discussed further below.

Coordination of Fgf and Notch

The interplay between Fgf and Notch is complex and dynamic, and levels must be precisely balanced for proper development of the SAG. A low-to-moderate level of Fgf is required to initiate neurogenesis by activating expression of *ngn1* (76, 77, 82, 115, 132), which in turn activates expression of Notch ligands (60, 86). Notch activity serves to limit and slow neurogenesis (86, 163). Neurogenesis is also inhibited at later stages by rising levels of Fgf5 derived from mature neurons (132) (Fig. 3.1K). Without proper modulation by *tfap2a*, both Fgf and Notch signaling quickly become overactive, which terminates specification prematurely and impedes maturation of neuroblasts in the TA pool, thereby leading to under-production of mature SAG neurons.

While too much Fgf and Notch activity clearly impairs neurogenesis, insufficient levels are ultimately far more damaging to SAG development. Conditions that reduce Fgf and Notch signaling (e.g. overexpression of *tfap2a*) cause dramatic acceleration of differentiation and overproduction of neurons, most of which later die upon maturation. Neuronal death appears to arise secondarily from acceleration of early stages within the otic vesicle, as accelerating later stages does not lead to neuronal death. It is likely that

early neuroblast differentiation is especially sensitive to acceleration due to insufficient buildup of factors needed for survival and function of mature neurons. In contrast, an

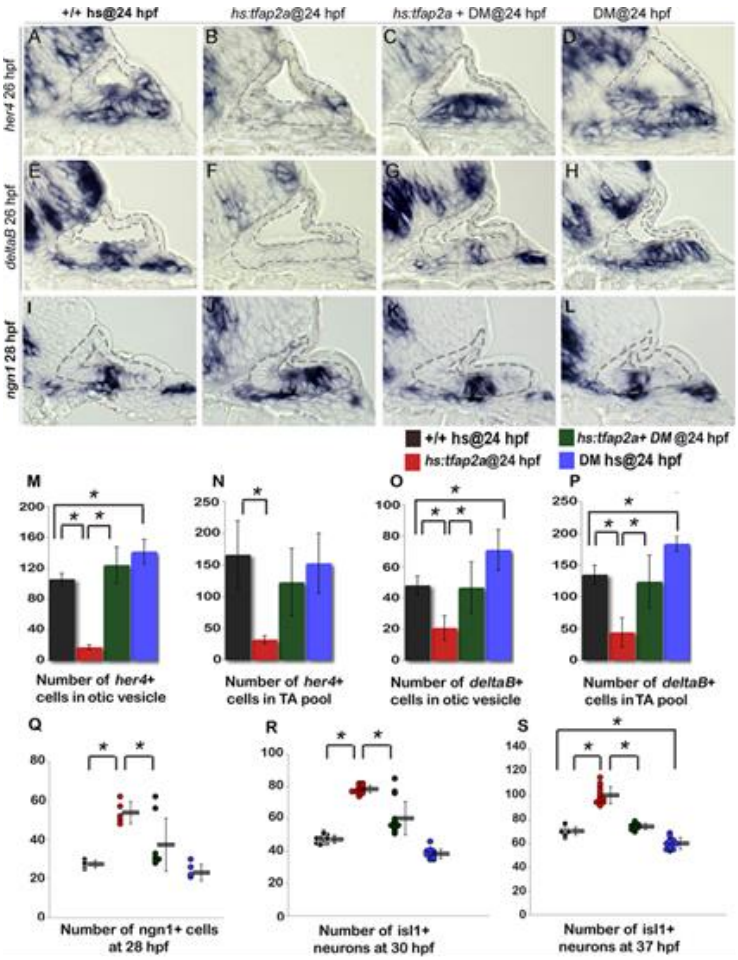

Figure 3.10: Bmp signaling mediates the effects of Tfap2a on SAG development. (A-L) Cross sections (medial left, dorsal up) through the otic vesicle just posterior to the utricular macula showing expression of *her4* (A-D) and *deltaB* (E-H) at 26 hpf and *ngn1* (I-L) at 28 hpf in control embryos (A, E, I), *hs:tfap2a* embryos (B, F, J), DM-treated *hs:tfap2a* embryos (C, G, K) and DM-treated wild-type embryos (D, H, L). All specimens were treated with 1% DMSO and heat-shocked at 24 hpf. (M-P) Mean and standard deviation of the total number of *deltaB* or *her4* expressing cells inside the otic vesicle or in the TA pool at 26 hpf under conditions indicated in the color key (counted from serial sections, n=3-6 ears per time point). (Q-S) Mean and standard deviation of the total number of *ngn1*+ cells at 28 hpf (Q) and Isl1+ SAG neurons at 30 hpf (R) and 37 hpf (S) under the conditions indicated in the color key. Asterisks (*) indicate statistical differences between the groups indicated in brackets.

important attribute of the TA pool is that the rate of differentiation can be regulated without compromising subsequent neuronal survival. The TA pool represents a relatively stable population of slowly cycling progenitors that must be maintained to meet the needs of the growing larva or to regenerate new neurons following damage (132). It is likely that *tfap2a* is needed only transiently in the otic vesicle to prolong specification and establish a healthy progenitor population. Once neuroblast specification has terminated, however, downregulation of *tfap2a* appears necessary to allow Fgf and Notch signaling to rise sufficiently to balance rates of proliferation vs. differentiation in the TA pool.

The role of Bmp

We have shown for the first time a role for Bmp in SAG development. Numerous earlier studies have shown that Bmp regulates morphogenesis of semicircular canals (165-168) and numerous aspects of development of sensory epithelia (169-173). Bmp has also been found to promote SAG survival and neurite outgrowth in chick explant cultures (174). However, no previous studies have detected a role in specification or differentiation of SAG neurons. Abello et al. (76) reported that blocking Bmp signaling did not alter the size of the neurogenic domain in the chick otic vesicle; and mosaic misexpression of an activated form of Bmp receptor did not inhibit neurogenesis, though the possibility that it may have accelerated neurogenesis was not examined. In comparison, we find that *tfap2a* activates expression of *bmp7a* and that blocking Bmp signaling reverses the effects of *tfap2a* overexpression. Treating wild-

type embryos with DM partially mimics the effects of disrupting *tfap2a*. The more severe defects caused by *tfap2a* loss of function could indicate that additional factors help mediate the effects of Tfap2a. Alternatively, Bmp7a could act partly through non-canonical signaling, similar to the role of Bmp7 in establishing tonotopy in the organ of Corti in mouse (170). The specific requirement for Bmp7a in SAG development cannot be assessed by examining *bmp7a* mutants because development of the otic placode is severely compromised (175). Development of lines to conditionally disrupt or misexpress *bmp7a* could resolve many of these issues.

Interestingly, in zebrafish Bmp effectors Smad1 and Smad5 are specifically upregulated in delaminated SAG cells (112, 162) (Fig. 3.1K). This constitutes an unusual form of regulation because *smad1/5* genes are broadly expressed with relatively little variation in the level of expression. Elevated levels of Smad1/5 accumulation could render SAG precursors outside the ear especially sensitive to Bmp, explaining how Bmp expressed within the otic vesicle could have such a profound effect on development of TA cells.

Regulation of *tfap2a*

We do not yet know how *tfap2a* is regulated in the otic vesicle. We detect no changes in expression after manipulating levels of Fgf, Notch, Bmp, Wnt or *ngn1*. It is possible that expression of *tfap2a* in the otic placode and otic vesicle reflects auto-regulatory maintenance from earlier stages. During gastrulation *tfap2a* is induced by Bmp in non-neural ectoderm where it functions as a competence factor for preplacodal

development (9). Once induced Tfap2a acts to maintain its own expression even if Bmp is subsequently blocked (135). This is an important aspect of regulation because dorsally expressed Bmp-antagonists are required to initiate preplacodal development near the end of gastrulation (7-9, 176). Although expression of *tfap2a* could simply persist in the otic placode through self-maintenance, it is not clear how expression becomes restricted to ventrolateral cells in the otic vesicle. A similar pattern is seen in the chick otic vesicle, possibly indicating a conserved mechanism ((177); Fig. 3.1). Identifying factors that regulate *tfap2a* in zebrafish and chick will likely shed light on general mechanisms of otic patterning and specific mechanisms of otic neurogenesis.

CHAPTER IV

THE SPEMANN ORGANIZER GENE GOOSECOID PROMOTES DELAMINATION OF NEUROBLASTS FROM THE OTIC VESICLE[3]

INTRODUCTION

The Stato-Acoustic Ganglion (SAG) connects the inner ear to the brain and transmits hearing and balance information. SAG neurons are generated by a stepwise program that starts in the otic vesicle, the precursor of the inner ear. Initially, a subset of the cells in the otic epithelium is specified for neural fate by the upregulation of the proneural gene *neurogenin1* (*ngn1*) (60, 61). Otic expression of *ngn1* is first detected by 16 hpf, peaks at around 24 hpf and then gradually declines, ceasing entirely by 42 hpf (132). Throughout this period, a subset of newly specified neuroblasts undergoes epithelial-mesenchymal transition (EMT) and delaminates from the otic vesicle (14) (14, 178, 179). In zebrafish, most neuroblasts lose *ngn1* expression after leaving the otic vesicle and subsequently upregulate the related proneural factor *neurod* (64, 65, 180).

---

[3]Reprinted with permission from "Spemann organizer gene Goosecoid promotes delamination of neuroblasts from the otic vesicle." by Kantarci H., Gerberding A., & Riley B.B., 2016, *Proceedings of the National Academy of Sciences of the United States of America*, 113, 44:E6840-E6848. Copyright [2016] by National Academy of Sciences.

neurod expressing cells form a group of proliferating and migrating precursors called the transit-amplifying (TA) pool (66, 132). As TA cells differentiate into mature SAG neurons, they lose *neurod* expression and upregulate mature neuronal markers such as Islet1 and Islet2b (67, 68). The first mature Isl1+ SAG neurons are detected by 20 hpf and subsequently accumulate at a linear rate through at least 72 hpf (132). At the same time, the TA pool is maintained as a stable population by proliferative renewal, assuring further growth of the SAG as larvae develop (132).

Specification of the neurogenic domain is established by a low threshold level of Fgf signaling (132, 181). However, nothing is known about the mechanisms regulating delamination of neuroblasts from the otic vesicle. Ngn1 is required for neuroblast fate specification (60, 61), but *ngn1* is not sufficient to induce delamination. In mouse, many cells that initially express *Ngn1* ultimately remain in the otic vesicle and contribute to developing sensory epithelia (86). In zebrafish, too, delamination of cells within the *ngn1* domain appears highly restricted. Clearly additional factors are required to initiate EMT in the otic epithelium during SAG development.

In addition to positive regulation, other factors appear to stabilize the otic epithelium and prevent inappropriate EMT. In zebrafish, chick and mouse, Pax2 marks the nascent otic placode and is later restricted to the medial half of the otic vesicle (137, 182-185). Loss of Pax2 and related factor Pax8 compromises epithelial integrity, leading to faulty morphogenesis of the otic vesicle and cell dispersal (184, 185).

EMT is characterized by loss of epithelial markers and upregulation of mesenchymal genes, many of which confer the ability to migrate. This process is critical

for establishment of the vertebrate body plan during gastrulation and is initiated by a unique group of cells originally described as Spemann's organizer. *Goosecoid* (*gsc*) is the most abundantly expressed homeobox gene in the vertebrate organizer (186, 187). Ectopic expression of *Gsc* is sufficient to induce organizer activity (188) and promote cell migration (189). *Gsc* is also expressed in the tissues that undergo tissue remodeling at later stages, such as neural crest derived mesenchymal tissues (190). Loss of *Gsc* function leads to craniofacial defects in mouse and humans (191-193). It has also been found that many aggressive metastatic cancers show strong upregulation of *Gsc*, and experimental misexpression of *Gsc* strongly promotes EMT and enhances metastasis (194, 195). Interestingly, *Gsc* expression has been reported in the developing otic vesicle in mouse (190, 196) but its functional importance has never been investigated. Due to these widespread roles of *Gsc* in regulating epithelial dynamics, we examined whether *Gsc* regulates EMT during otic neurogenesis in zebrafish.

Here we describe a full time course for *gsc* expression in the zebrafish otic vesicle. Disruption of gsc impairs delamination of SAG neuroblasts, whereas misexpression of gsc strongly promotes neuroblast delamination. Although *gsc* is regulated by Fgf in a domain that partially overlaps with *ngn1*, *gsc* does not affect neural fate specification. Thus, *ngn1* and *gsc* act in parallel downstream of Fgf to coordinate neural fate specification with morphogenesis. Further analysis revealed the transcription factor Pax2a functions as a strong epithelializing factor expressed in the non-neurogenic regions of the otic vesicle. Moreover, Pax2a represses *gsc* transcription and function, helping to restrict EMT to the neurogenic domain of the otic vesicle.

MATERIALS AND METHODS

Fish strains and developmental conditions

Wild-type embryos were derived from the AB line (Eugene, OR). Transgenic lines used in this study include *Tg(hsp70:fgf8a)*^{x17}(19), *Tg(hsp70I:dnfgfr1-EGFP)*^{pd1}(98), *TgBAC(neurod:EGFP)*(197), *Tg (hsp70:pax2a)*^{x23}(198), and lines produced for this report *Tg(hsp70:gsc)*^{x58} and *Tg(hsp70:ngn1)*^{x28}. Transgenic lines are named in the text as *hs:fgf8*, *hs:dnfgfr1*, *nrd:GFP*, *hs:pax2a*, *hs:gsc* and *hs:ngn1*, respectively. Mutant lines *gsc*^{x59} and *pax2a* ^{tu29a} (199) were used for loss of function analysis. Homozygous mutants were identified by characteristic morphological changes. Embryos were maintained at 28.5 °C (except where noted) and staged accordingly to standard protocols (100). PTU (1-phenyl 2-thiourea, 0.3 mg/ml, Sigma) was added to block pigment formation.

Gene misexpression and morpholino injections

To activate the heat shock transgenes, heterozygous carriers were incubated in a water bath at 39°C for 60 minutes (except where noted). After heat-shock embryos were kept at 33°C until the fixation. At least 15 embryos were observed for each time point. Transgenic carriers were identified by characteristic phenotypes when available, or by PCR-genotyping as previously described (200). Primer sequences are as follows (5'-3'): *hs:gsc* GCAATGAACAGACGGGCATTTA (F), GAATACACGGACACTGTTGCG (R) ; *hs:pax2a* GCAATGAACAGACGGGCATTTA (F),

TCTGCTTTGCAGTGAATATCCA (R). In some experiments *ngn1* or *gsc* were knocked down by injecting embryos at the one-cell stage with 5 ng of morpholino oligomer (MO) using previously published MO sequences (61, 201).

In situ hybridization and immunohistochemistry

Wholemount in situ hybridization and antibody labeling were performed as previously described (72, 102). The primary and secondary antibodies used in this study are as follows: Anti-Islet1/2 (Developmental Studies Hybridoma Bank 39.4D5, 1:100), anti-GM130 (BD Transduction Laboratories^{TM} 610822, 1:100), anti-ZO1 (ThermoFisher Scientific 33-9100, 1:150), anti-phospho-Paxillin pTyr118 (ThermoFisher Scientific PA5-17828, 1:50), anti-phospho-Histone H3 (EMD MILLIPORE 06-570, 1:350) and Alexa 546 goat anti-mouse or anti-rabbit IgG (ThermoFisher Scientific A-11003/A-11010, 1:50). TUNEL assay was performed by using Promega terminal deoxynucleotidyl transferase (M1871) according to manufacturer's protocol. Whole-mount stained embryos were prepared for cryosectioning as preciously described (132) and cut serially into 10 μm sections.

Statistics

Quantitation of cells expressing genes of interest was performed either in wholemounts (n=6-20 specimens each) or by counting cells in serial sections (n=2-4 specimens each). In experiments to test the effects of altering gene function, homozygous mutants and transgenic embryos were identified by characteristic

morphological changes or PCR-genotyping. Student's t-test was utilized for pairwise comparisons. Comparisons between three or more samples were analyzed by one way ANOVA and Tukey post-hoc HSD test.

RESULTS

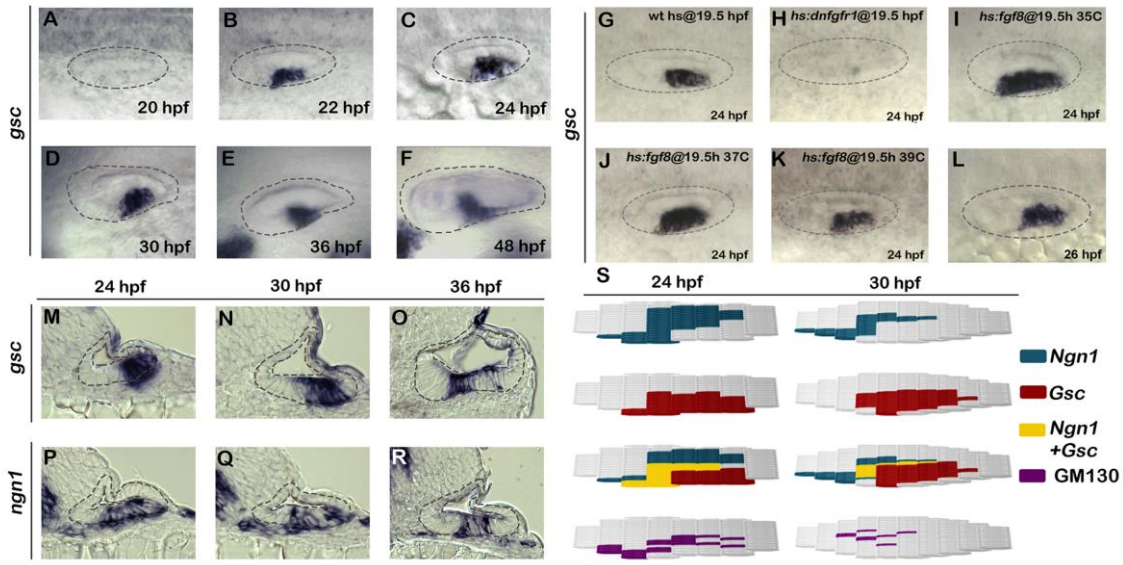

Fig. 4.1. Expression and regulation of *gsc* during otic neurogenesis. (*A-L*) Whole mount images (dorsal up, anterior left) show dorsolateral views of *gsc* expression in the otic vesicle (outlined) at the indicated times. (*M-R*) Cross sections (dorsal up, medial left) passing through the widest part of the neurogenic domain showing expression of *gsc* or *ngn1* at the indicated times. The otic epithelium is outlined in each image. (*S*) Maps of regional markers in the floor of the otic vesicle (medial up, anterior left) generated from serial cross sections of embryos stained for *ngn1*, *gsc*, or GM130 at 24 or 30 hpf. The location and number of cells expressing individual markers (4 embryos each) was normalized and plotted accordingly.

Expression of *gsc* during otic neurogenesis

To assess the function of *gsc* during development of SAG neurons we examined expression of *gsc* in the otic vesicle during relevant stages. *gsc* is first detected in a

small number of ventral otic cells at 20 hpf and becomes strongly upregulated in a ventrolateral domain by 22 hpf (Fig.4.1A, B). This domain lies close to the neurogenic domain of the otic vesicle (61). Ventrolateral expression of *gsc* is maintained in the otic vesicle through at least 48 hpf (Fig. 4.1C-F), beyond the stage when neurogenesis normally ceases (132).

Neurogenesis in the otic vesicle, marked by expression of *ngn1*, is initiated by a low level of Fgf signaling, whereas high-level Fgf signaling blocks expression of *ngn1* (132). Expression of *gsc* shows similar regulation by Fgf. Specifically, blocking Fgf signaling by activation of *hs:dnfgfr1* (dominant-negative Fgf receptor) completely eliminated *gsc* expression in the otic vesicle (Fig. 4.1G, H). Additionally, low level activation of *hs:fgf8* at 35°C expanded the domain of *gsc* expression, with a more modest expansion seen at 37°C (Fig. 4.1I, J). Thus, the requirement for Fgf and response to low-level Fgf appears highly similar for *gsc* and *ngn1*. However, expression of *gsc* does not require *ngn1*: High-level activation of *hs:fgf8* at 39°C represses *ngn1* expression (132) but did not abolish *gsc* expression (Fig. 4.1K). Additionally, expression of *gsc* was normal in *ngn1* morphants (Fig. 4.1L). Similarly, *ngn1* expression does not require *gsc*, as shown below. Thus *gsc* and *ngn1* are co-induced by low-level Fgf signaling but are not dependent on each other.

We next compared the spatial patterns of *gsc1* and *ngn1* expression in serial sections. This confirmed that expression of *gsc* partially overlaps with *ngn1* in the otic floor at least through 36 hpf (Fig. 4.1M-R). *gsc* expression can also be detected in a small number of cells just ventral to the otic vesicle (Fig. 4.1M), presumably marking

recently delaminated neuroblasts. After leaving the otic vesicle, these cells quickly lose *gsc* expression: Neither transit-amplifying neuroblasts (marked by *neurod*) nor mature SAG neurons (marked by Isl1) show detectable expression of *gsc* (Fig. 4.S1). To further examine the degree of overlap between *gsc* and *ngn1* expression domains, we mapped the locations of cells expressing either *gsc* or *ngn1* in the otic floor based on data from serial sections. *ngn1* is expressed in the otic floor adjacent and lateral to the developing sensory epithelia (Fig. 4.1S). Expression of *gsc* overlaps with lateral portions of the *ngn1* domain but extends to more lateral and posterior regions of the otic floor (Fig. 4.1S). Because Gsc is known to regulate epithelial-mesenchymal transition (EMT) (189, 195), we also examined expression of GM130, a Golgi marker that undergoes a dramatic basal relocalization as cells undergo EMT (202, 203). The pattern of GM130-staining in the otic floor revealed that the highest rate of EMT occurs in the region where *ngn1* and *gsc* are coexpressed. (Fig. 4.1S).

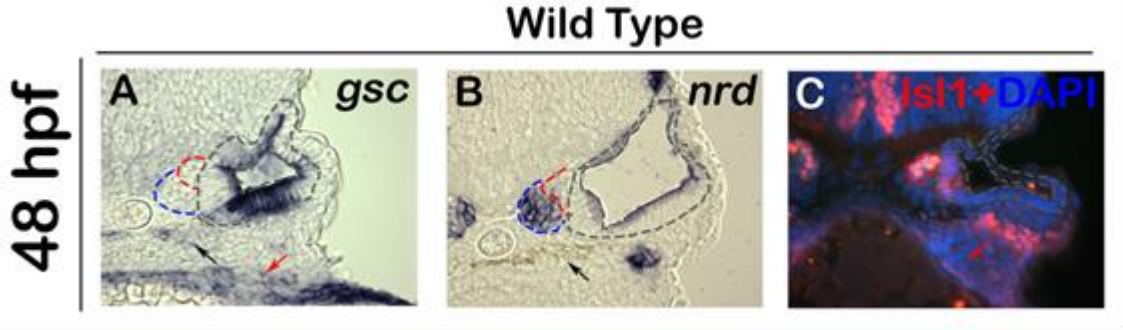

Fig. 4. S1. Expression of *gsc* during later stages of SAG development. (*A*-*C*) Images show expression of *gsc* (*A*), *nrd* (*B*) and immuno detection of Isl1 in DAPI stained (*C*) cross sections passing through the middle of the otic vesicle in wild type embryos. The otic epithelium is outlined with black, TA cells are outlined with blue and mature SAG neurons are outlined in red. *Gsc* expression is absent from the TA cells or mature SAG neurons. *gsc* is also expressed in the pharyngeal endoderm (red arrows) and neural crest derived pigment cells (black arrows).

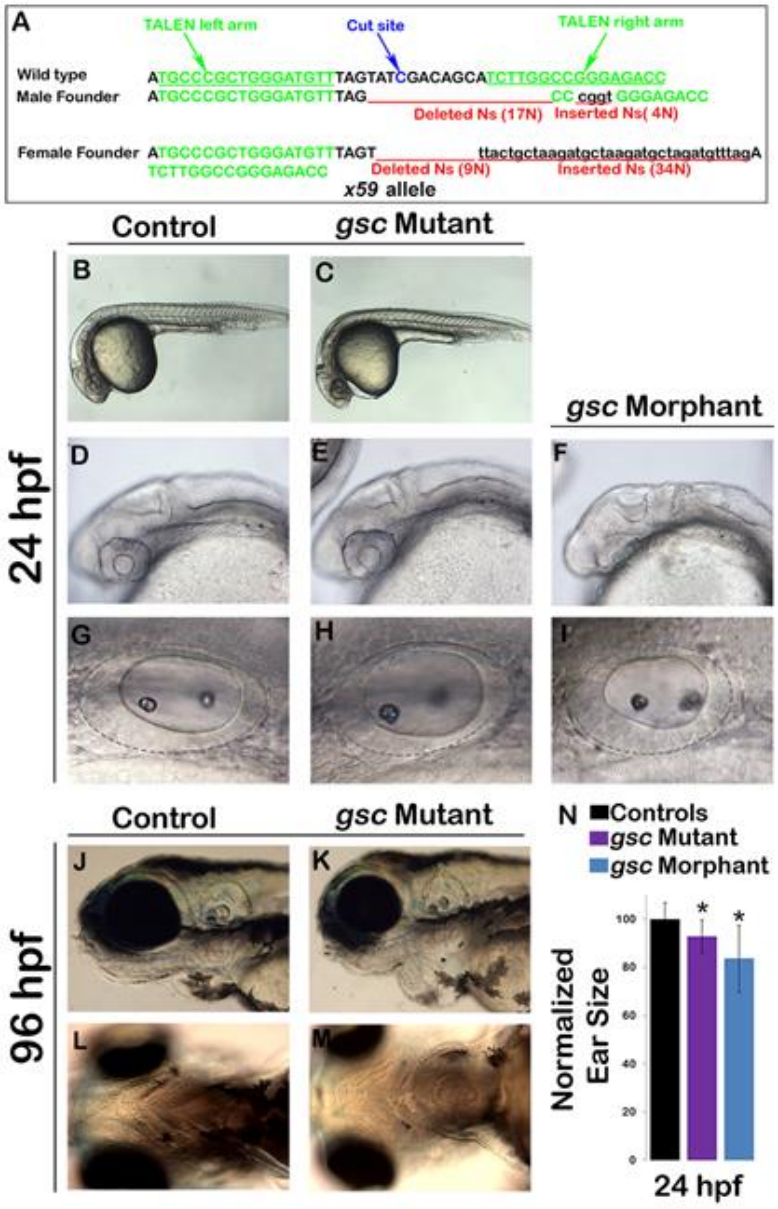

Fig. 4.S2. Generation of *gsc* mutants via TALEN-targeting. (*A*) A summary of the TALEN target sequences on the first exon of the *gsc* locus (marked in green) and the resulting lesions (marked in red) at the predicted cut site (marked in blue) are shown for the two F1 founders isolated during the screening process. (*B-I*) Live specimens at 24 hpf were viewed at low magnification to show general morphology (*B*, *E*) and at higher magnifications to show cranial development (*D-F*) and the otic vesicle (*G-I*) in controls, *gsc* morphants and *gsc* mutants. (*J-L*) Live specimens at 96 hpf viewed from lateral (*J*, *K*) or ventral (*L*, *M*) reveal cardiac edema and jaw hypoplasia in *gsc* mutants. (*N*) Mean and standard deviation of surface area of the otic vesicles, normalized to control embryos, are indicated for *gsc* mutants and *gsc* morphants at 24 hpf.

Role of Gsc during otic neurogenesis

We next tested the effects of disrupting or misexpressing *gsc* on otic neurogenesis. Using TALEN-mediated targeting, we recovered two lesions predicted to eliminate *gsc* function (Fig. 4.S2A). Disruption of *gsc* did not cause axial defects or any overt changes in the gross morphology at 24 hpf (Fig. 4.S2B, C). However, *gsc* mutants did show a slight (~7%) reduction in the size of the otic vesicle (Fig. 4.S2G-I, N) and impaired neural delamination as described below. At later stages *gsc* mutants also developed cardiac edema and a severe jaw defect (Fig. 4.S2J-M).
Similar phenotypes were seen in *gsc* morphants, although *gsc* morphants also showed mild brain necrosis not observed in mutant embryos (Fig. 4.S2D-F).

Despite the reduced size of the otic vesicle in *gsc* mutants, most aspects of otic patterning appeared normal, including expression of various regional markers and accumulation of sensory hair cells (Fig. 4.S3). In addition, *gsc* mutants produced a normal number of the *ngn1+* neuroblasts in the otic epithelium (Fig. 4.2A, B, G). However, the number of *ngn1+* neuroblasts outside the otic vesicle was reduced by more than 50% at all stages of neurogenesis, suggesting a reduced rate of neuroblast delamination. A similar deficiency of recently delaminated *ngn1+* neuroblasts was seen in *gsc* morphants (Fig. 4.2G).

To overexpress *gsc*, we generated a heat-shock inducible transgenic line, *hs:gsc* (Fig. 4.S4). Overexpression of *gsc* at 22 hpf led to a dramatic decrease in the number of *ngn1+* neuroblasts in the otic epithelium within 60 minutes, with a concomitant increase in the number of *ngn1+* cells outside the otic vesicle (Fig. 4.2C, H, I). The number of

ngn1+ cells outside the ear remained elevated in *hs:gsc* embryos for several hours but then returned to control levels by 25 hpf (Fig. 4.2I), presumably reflecting the decline in transgene activity (Fig. 4.S4). Activation of *hs:gsc* at 30 hpf or 36 hpf gave results similar to those observed following activation at 22 hpf (Fig. 4.2H, I). Otic neurogenesis normally ends by 42 hpf (132), so we tested whether activation of *hs:gsc* at this stage could reinitiate neuroblast specification. Activation of *hs:gsc* at 42 hpf failed to reinitiate *ngn1* expression in the otic vesicle, but nevertheless caused a substantial increase in the number of *ngn1+* cells outside the otic vesicle (Fig. 4.2D-F, H, I). This latter increase appears to result from a stage-specific effect on proliferation of transit-amplifying neuroblasts, as shown below.

Together, these data suggest that Gsc does not affect neuroblast specification but instead enhances the ability of neuroblasts to leave the otic vesicle. The effect of Gsc on neuroblast delamination was highly specific, as other aspects of otic vesicle development appeared largely normal several hours after activating *hs:gsc* (Fig. 4.S3).

We next examined the effects of Gsc on the epithelial and mesenchymal cell markers. Zonula Occludens (ZO)-1 is expressed apically in epithelial otic cells but is lost upon transition to the mesenchymal state (Fig. 4.S5A, D, G), whereas the transition is marked by activation of the focal adhesion protein p-Paxillin at the leading edge of migrating cells (Fig. 4.2K, N; Fig. 4.S5A). Delaminating otic cells also show dramatic redistribution of golgi marker GM130 to the basal surface as cells transition to the mesenchymal state (Fig. 4.2Q, T). *gsc* mutants showed more ZO-1 staining in the otic

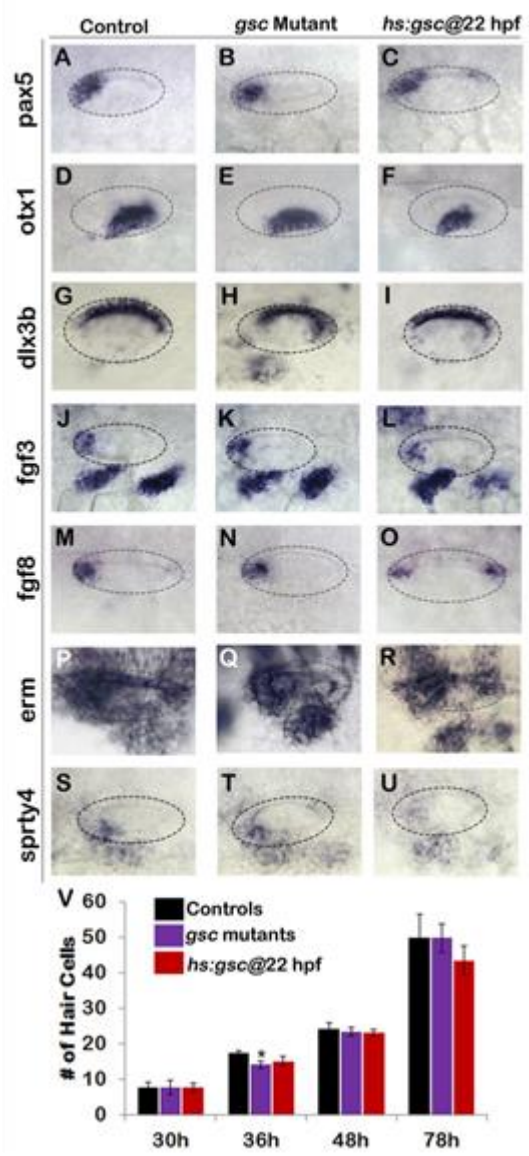

Fig. 4.S3 . Effects of altering *gsc* function on otic vesicle patterning. (*A-U*) Whole-mount images (dorsal up, anterior left) show dorsolateral views of the otic vesicle (outlined) in controls, *gsc* mutants and *hs:gsc* embryos for the indicated genes at 24 hpf. Patterning of the otic vesicle is not affected in *gsc* mutants. *Hs:gsc* embryos show a slight decrease in the expression of ventral-lateral otic marker *otx1* (*F*) but otherwise appear normal. (*V*) Mean and standard deviation of the total number of hair cells in utricular and saccular maculae of control embryos, *gsc* mutants and *hs:gsc* embryos at the indicated times (n= 3 embryos each). Data were obtained by counting hair cells in the serial sections. Accumulation of the hair cells was normal except that *gsc* mutants showed a small but significant decrease relative to the control at 36 hpf. There was also a slight decrease in the number of hair cells (though not statistically significant) in *hs:gsc* embryos at 78 hpf.

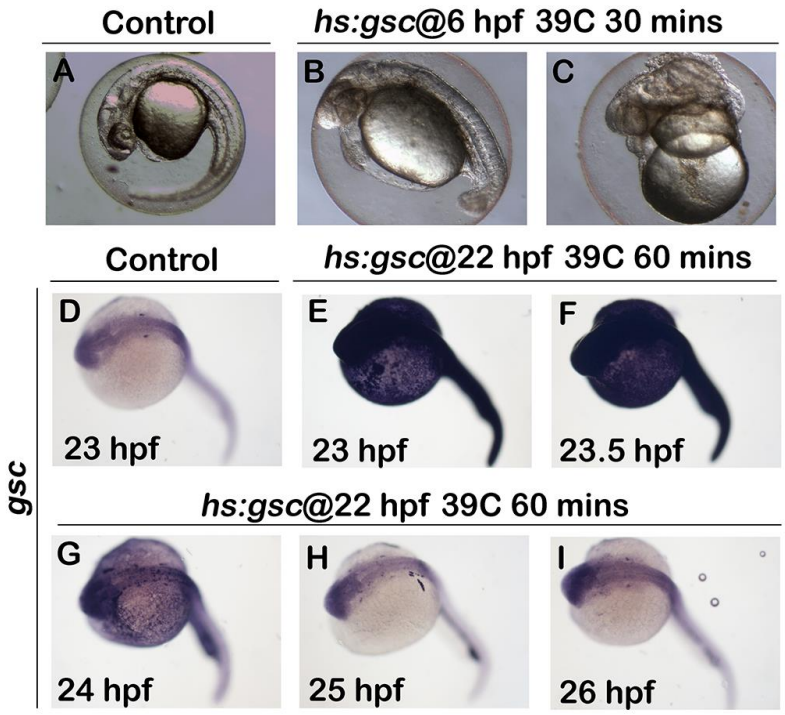

Fig. 4.S4. Heat-shock activation of *hs:gsc* during gastrulation or otic development. (*A*-*C*) Whole mount live images at 24 hpf (dorsal up, anterior left) show the phenotypic effects of a 30 min 39°C heat-shock initiated at 6 hpf in control and *hs:gsc* embryos. Activation of *hs:gsc* under these standard heat-shock conditions dorsalized the embryos to varying degrees (*B, C*). (*D*-*I*) Whole-mount images (dorsal up, anterior left) showing *gsc* expression in controls and *hs:gsc* embryos. Embryos were fixed and stained at indicated times after the end of a 60-minute heat-shock initiated at 22 hpf. Activation of *hs:gsc* at 22 hpf led to a strong increase in the *gsc* level by the end of the heat-shock period (*E*). The level of *gsc* expression was maximal at 23.5 hpf (*F*) but declined rapidly thereafter, returning to normal by 25 and 26 hpf (*H, I*).

epithelium (Fig. 4.S5B, E, H) and a loss of cells with p-Paxillin staining (Fig. 4.2L, O). *gsc* mutants also showed a reduced number of cells with basal GM130 staining (Fig. 4.2R, U). Conversely, activation of *hs:gsc* reduced the ZO-1 staining in the otic epithelium (Fig. 4.S5C, F, I) and increased the number of cells with p-Paxillin staining (Fig. 4.2M, P; Fig. 4.S5C). Activation of *hs:gsc* also increased the number of cells with basal GM130 staining (Fig. 4.2S, V). Overall, these results suggest that *gsc* stimulates EMT of neural progenitors in the otic vesicle without affecting cell fate specification.

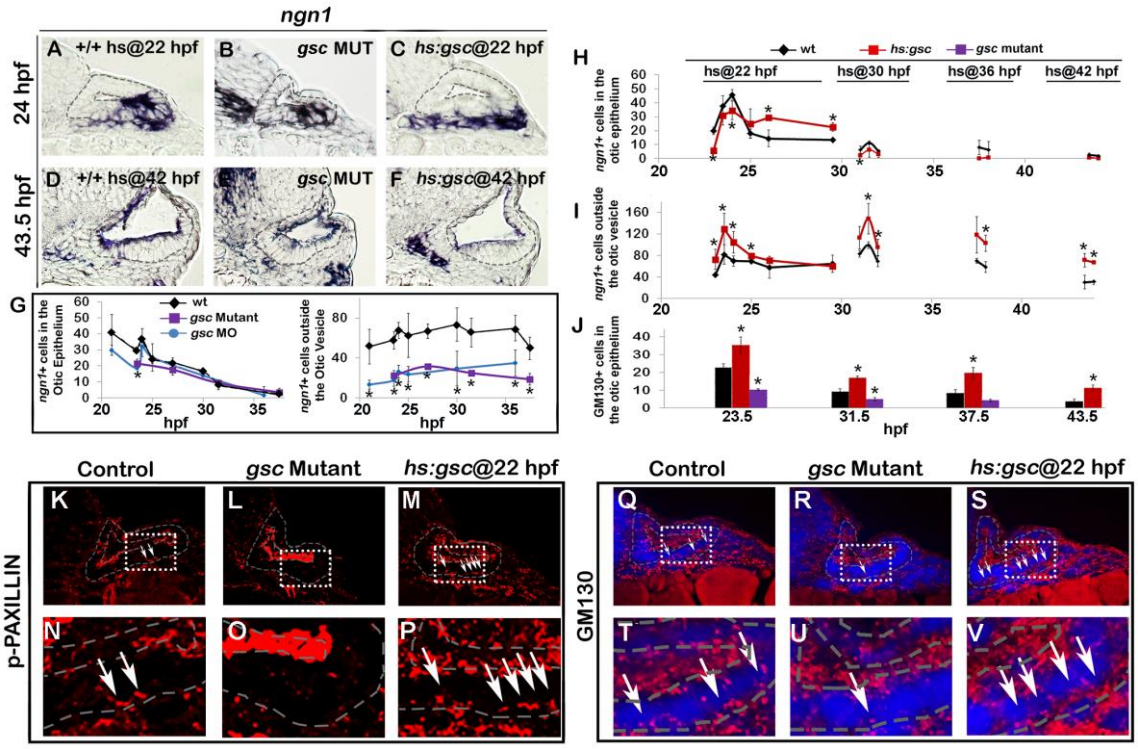

Fig. 4.2. Gsc promotes EMT of otic neuroblasts. (*A-F*) Expression of *ngn1* in cross sections passing through the widest part of the neurogenic domain (dorsal up, medial left) just posterior to the utricular sensory epithelium expression in controls, *gsc* mutants and *hs:gsc* embryos at 24 hpf (*A-C*) or 43.5 hpf (*D-F*). Control and transgenic embryos were heat shocked at 22 hpf (*A*, *C*) or 42 hpf (*D*, *F*). The otic epithelium is outlined in each image. (*G*) Mean and standard deviation of the total number of *ngn1*+ cells in the otic epithelium and outside the otic vesicle for the genotypes indicated in the color key (counted from the serial sections, n=3 or 4 otic vesicles per time point). The number of *ngn1*+ neuroblasts in the otic epithelium was normal in *gsc* mutants and morphants at all stages, except for a small but significant reduction seen in *gsc* morphants at 24 hpf (asterisk). (*H-J*) For the genotypes indicated in the color key, embryos were heat shocked at the indicated times and fixed several hours later to stain for *ngn1* (*H*, *I*) or basal relocalization of GM130 (*J*). Data show the mean and standard deviation of the total number of stained cells in the otic epithelium or delaminated cells outside the otic vesicle (counted from the serial sections, n=3 otic vesicles per time point). Asterisks (*) indicate significant differences from control specimens. (*K-V*) EMT markers in cross sections (dorsal up, anterior left) passing through the neurogenic domain of control embryos, *gsc* mutants or *hs:gsc* embryos immuno-stained for p-Paxillin (*K-P*) or GM130 (red) and DAPI (blue) (*Q-V*). Controls and transgenic embryos were heat shocked at 22 hpf. Boxed regions in *K-M* are magnified in *N-P*, and boxed regions in *Q-S* are magnified in *T-V*. White arrows indicate elevated basal staining in cells undergoing EMT.

Consistent with this idea, we observed a ~12% decrease in the size of the otic vesicle at 24 hpf following activation of *hs:gsc* at 22 hpf (Fig. 4.S6A, B), likely caused by the increased number of cells leaving the otic vesicle. This size reduction persisted through

at least 31 hpf (Fig. 4.S6), suggesting a limited capacity to compensate for earlier cell loss.

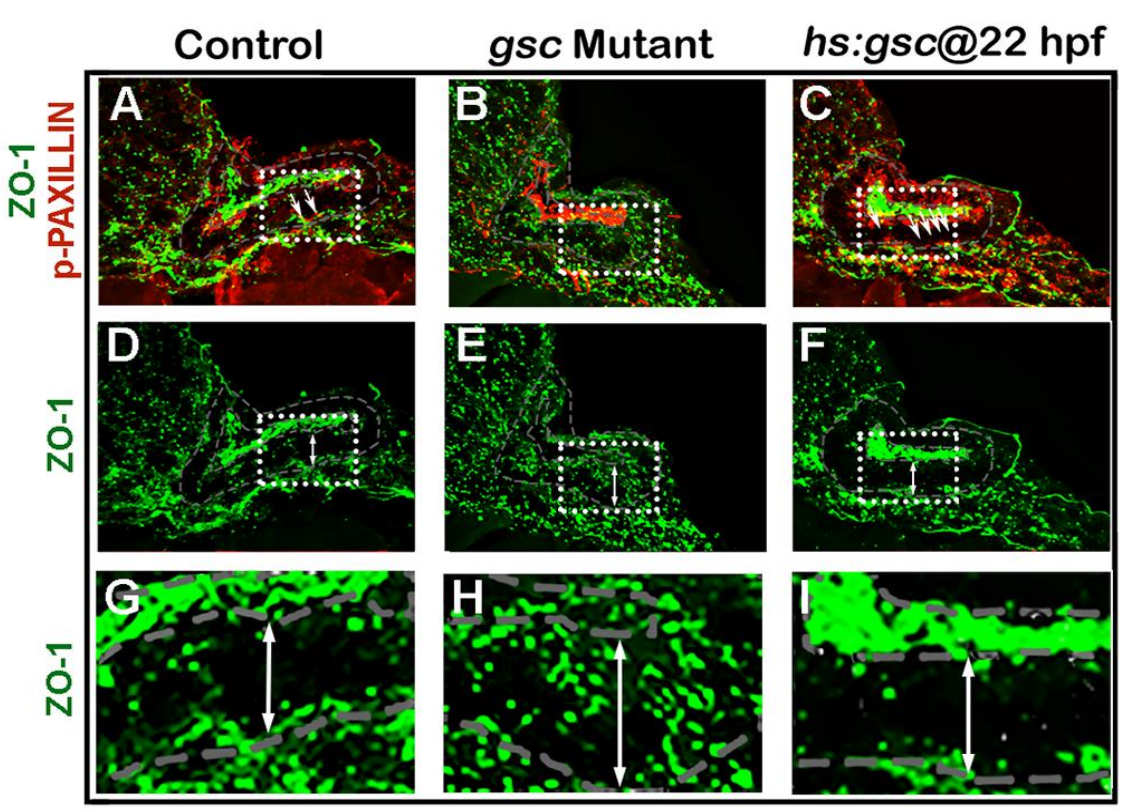

Fig. 4.S5. Effects of altering *gsc* function on ZO-1 and p-Paxillin. (*A-I*) Cross sections through the neurogenic domain just posterior to the utricular macula in a control embryo (*A, D, C*), *gsc* mutant (*B, E, H*) and *hs:gsc* embryo (*C, F, I*) at 24 hpf. These are the same sections depicted in Fig. 2K-P but showing co-staining for p-Paxillin (red) and ZO-1 (green) (*A-C*), or ZO-1 alone (*D-I*). The boxed regions in (*A-F*) are enlarged in (*G-I*). White arrows (*A-C*) indicate cells undergoing EMT with elevated basal accumulation of p-Paxillin, whereas double-headed arrows (*D-I*) span the otic epithelium to highlight changes in ZO-1 staining.

Effects of Gsc on later stages of SAG development

Next, we examined whether altered delamination of neuroblasts affected later stages of neural development. Normally, newly delaminated neural progenitors quickly lose expression of *ngn1* and upregulate *neurod*, marking the transit-amplification (TA)

stage of SAG development (64-66, 132, 180). TA cells migrate towards the hindbrain as they proliferate and then differentiate into mature neurons, marked by Isl1 staining. The number of *neurod*+ TA cells and mature neurons was significantly reduced in *gsc* mutants and morphants at every time point examined (Fig. 4.3B, E, G, H). This is consistent with impairment of neuroblast delamination seen in these embryos. Conversely, activation of *hs:gsc* at 22 hpf led to a ~30% increase in the number of *neurod*+ TA cells and mature neurons (Fig. 4.3C, F, G, H).

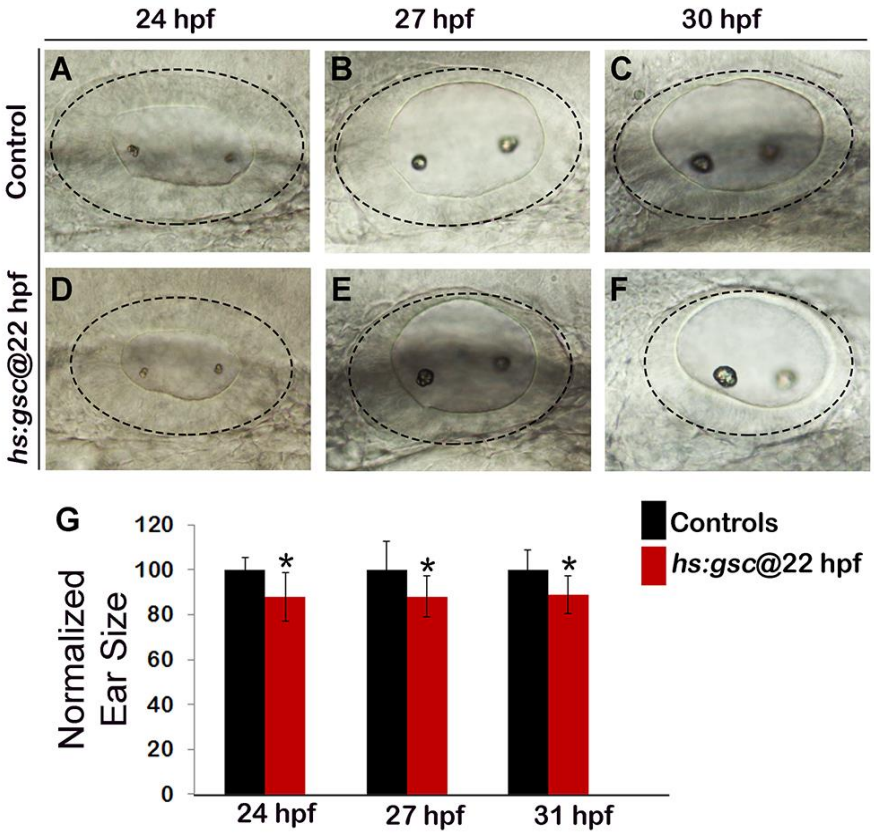

Fig. 4.S6. The size of the otic vesicle declines following activation of *hs:gsc*. (*A-F*) Whole mount live specimens show dorsolateral views of the otic vesicle in controls (*A-C*) and *hs:gsc* embryos (*D-F*). (*G*) Mean and standard deviation of surface area of the otic vesicle, normalized to control embryos, are indicated for *hs:gsc* embryos at the indicated time points

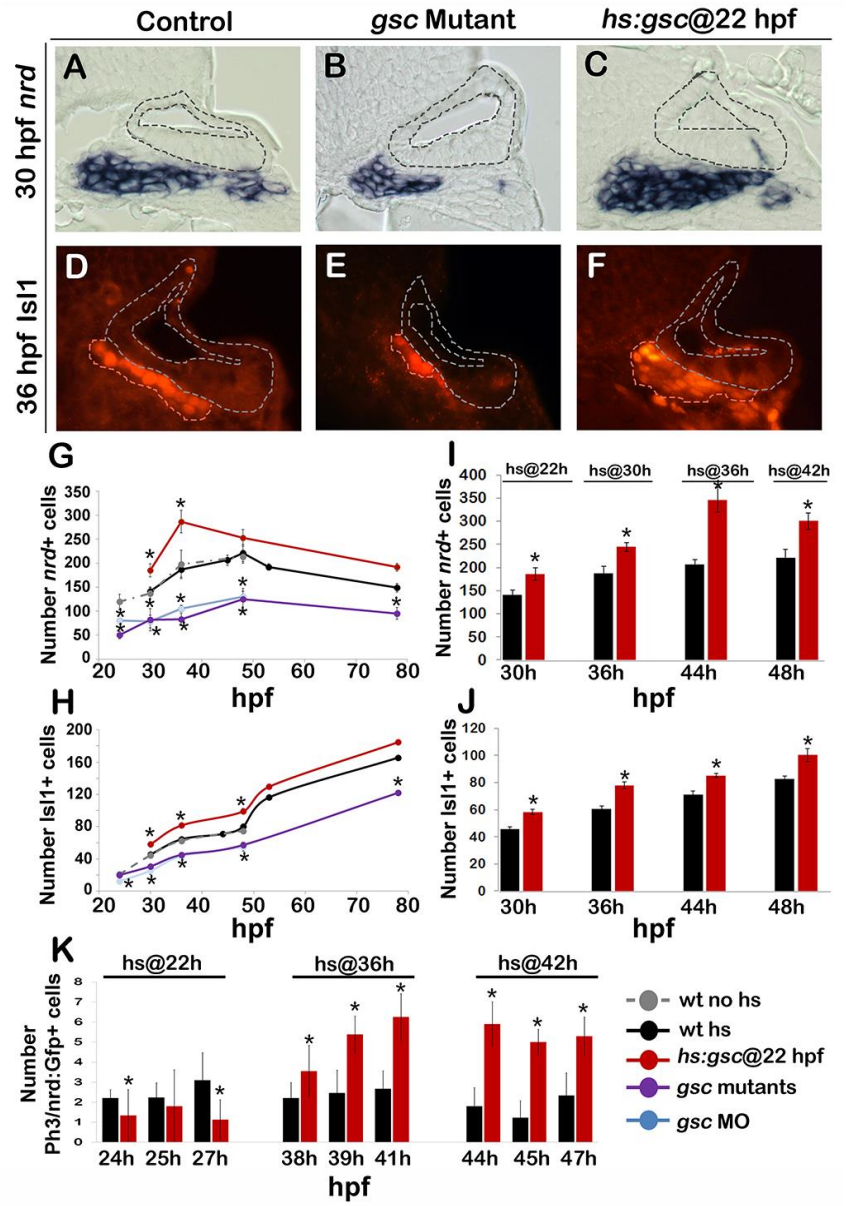

Fig. 4.3. Effects of Gsc on later stages of SAG development. (*A-F*) Cross sections passing through the utricular sensory epithelium (dorsal up, medial left) in controls, *gsc* mutants and *hs:gsc* embryos showing expression of *nrd* (*A-C*) or Isl1 (outlined in orange, *D-F*). The otic epithelium is outlined in all images. (*G-J*) Mean and standard deviation of the total number of *nrd*+ (G, I) or Isl1+ (H, J) cells for the genotypes indicated in the color key at times presented on the X-axes. *nrd*+ cells were counted on serial sections (n=3-5), Isl1+ cells were counted on whole mounts for time points between 30-48 hpf (n=10-17) and on serial sections for 53 and 78 hpf (n=2-3). (*K*) Mean and standard deviation of the total number of Phospho-Histone H3 (Ph3)+ cells within the *nrd:Gfp*+ domain (which marks TA cells) at the indicated times in control and *hs:gsc* embryos. Embryos were heat shocked at the indicated times. Asterisks (*) indicate statistically significant differences compared to control embryos.

Furthermore, the number of mature SAG neurons remained elevated in these embryos through at least 50 hpf before returning to control levels (Fig. 4.3H). Overexpression of *gsc* during earlier placodal stages also increased accumulation of Isl1+ neurons at 30 hpf, though to a lesser degree than activation at 22 hpf (Fig. 4.S7C). Activation of *hs:gsc* at 30 hpf gave results similar to activation at 22 hpf (Fig. 4.3I, J; Fig. 4.S7A, B). Interestingly, activation of *hs:gsc* at 36 or 42 hpf caused a disproportionately greater increase in the number of *neurod*+ TA cells compared to earlier activation (Fig. 4.3I). This was unexpected because rates of neuroblast specification are very low at these later stages, suggesting another source of supernumerary *neurod*+ cells. Analysis of the cell proliferation revealed that activation of *hs:gsc* at 36 or 42 hpf dramatically increased the rate of mitosis in TA cells (Fig. 4.3K), likely accounting for increased numbers of TA cells expression *ngn1* and *neurod* (Figs. 4.2F and 4.3I). In contrast, activation of *hs:gsc* at 22 hpf reduced the rate of proliferation amongst TA cells (Fig. 4.3K). Thus, activation of *hs:gsc* increases the number of TA cells by different mechanisms at different stages: Gsc increases the rate of neuroblast delamination during early stages of neurogenesis, whereas it increases the rate of proliferation in TA cells during later stages of neurogenesis. Activation of *hs:gsc* did not alter the rate of proliferation in the otic epithelium (Fig. 4.S7D). *gsc* mutants showed normal proliferation in the otic epithelium and in TA cells at all stages (Fig. 4.S7E).

Despite the initial surge in *neurod*+ cells following activation of *hs:gsc* at 36 or 42 hpf, the number of *neurod*+ TA cells subsequently returned to the level seen in control embryos by 78 hpf (Fig. 4.S7A). The decline in TA cells occurred

concomitantly with a corresponding increase in the number of mature Isl1+ neurons (Fig. 4.S7B).

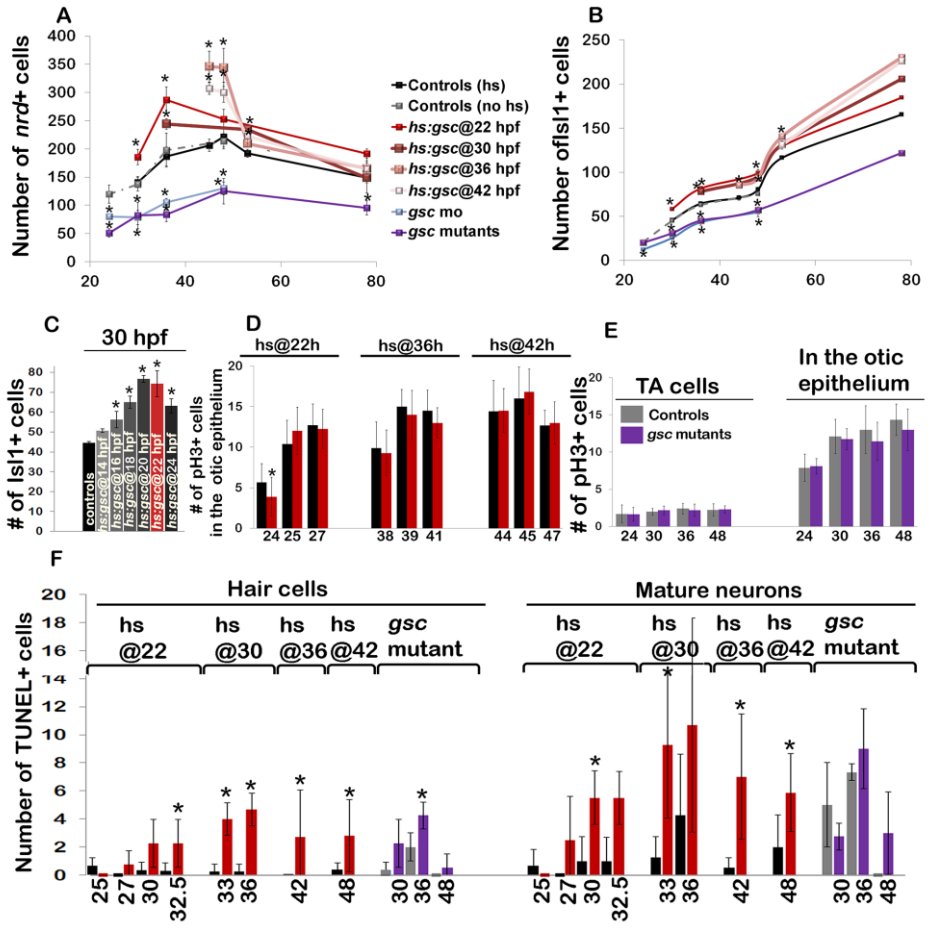

Fig. 4.S7. Effects of Gsc on development of SAG neurons and sensory epithelia. (*A-C*) Mean and standard deviation of the total number of *nrd*+ TA cells (*A*) or Isl1+ (*B, C*) SAG neurons for the genotypes indicated in the color key. *Nrd*+ cells were counted on serial sections, Isl1+ cells were counted on wholemounts for time points between 30-48 hpf (n=10-17) and on serial sections for 53 and 78 hpf (n=2-3). (*D, E*) Mean and standard deviation for the number of pH3+ cells in the otic epithelium of *hs:gsc* embryos (*D*) or in the otic epithelium or TA cells in *gsc* mutants (*E*) at the indicated times. (*F*) Mean and standard deviation of the total number of TUNEL+ hair cells or SAG neurons at the indicated times in controls, *gsc* mutants or *hs:gsc* embryos. TUNEL+ cells were counted from serial sections (n=3 or 4 otic vesicles per time point) except at 42 and 48 hpf when counts were performed on whole mounts for *hs:gsc* and control embryos (n=10-15). Asterisks (*) indicate significant differences compared to control embryos.

gsc loss of function and overexpression led to a modest increase in the rate of apoptosis amongst hair cells and mature neurons (Fig. 4.S7F). The elevated cell death possibly reflects the detrimental effects of altering epithelial integrity or non-autonomous effects of *gsc* function (See discussion).

Cooperation between Gsc and Ngn1 in regulating EMT

We noted that the ability of Gsc to promote EMT appeared to be restricted to the otic floor near the domain of *ngn1* expression. This prompted us to examine the role of *ngn1* in EMT. In *ngn1* morphants, the number of *ngn1*+ cells that accumulated outside the otic vesicle was severely reduced (Fig. 4.S8A), although a small number of delaminated cells was still observed. The fate of these cells is unclear, but they are unable to continue SAG development since *ngn1* morphants produce no TA cells or mature SAG neurons. The number of delaminated cells nearly doubled in *ngn1* morphants following activation of *hs:gsc*, but remained far below normal (Fig. 4.S8B, C). These data suggest that Gsc provides otic cells with a limited capacity for undergoing EMT in the absence of proper fate specification, but the capacity for delamination is strongly enhanced by *ngn1*. To test this further, we tested the effects of simultaneous overexpression of *gsc* and *ngn1*. Co-activation of *hs:ngn1* and *hs:gsc* resulted in additive increases in the number of *neurod*+ TA cells and mature SAG neurons by 30 hpf, and these increases persisted through at least 48 hpf (Fig. 4.S8D-I). Interestingly, activation of *hs:ngn1* induced ectopic *neurod*+ neuroblasts in the medial wall of the otic vesicle, but these neuroblasts were not observed to undergo delamination

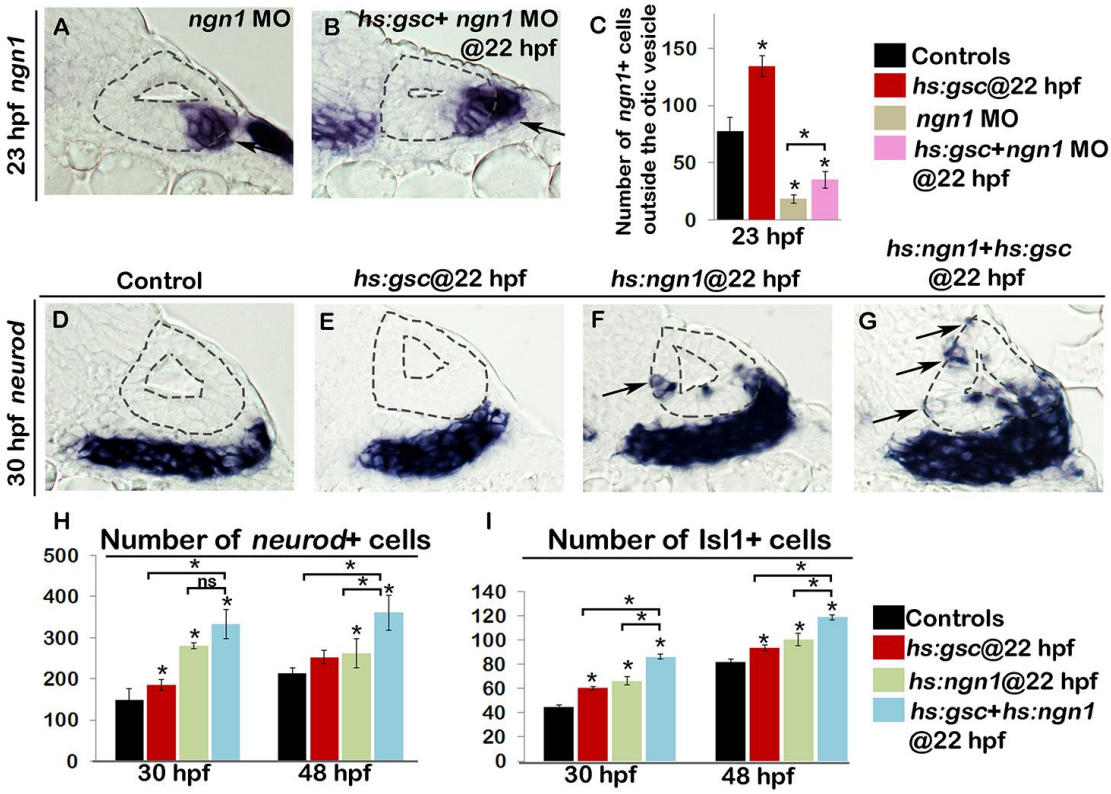

Fig. 4.S8. Ngn1 and Gsc work in concert during otic neurogenesis. Transgenic embryos were heat shocked at 22 hpf. (*A, B*) Cross sections passing through the neurogenic domain of the otic vesicle just posterior to the utricular macula show *ngn1* expression in the indicated genotypes. Black arrows indicate delaminated cells outside the otic vesicle. (C) Mean and standard deviation for the total number of *ngn1*+ cells outside the otic vesicle. Genotype of the embryos is indicated in the color key. (*D-G*) Cross sections show *nrd*+ cells in embryos with indicated phenotypes. Black arrows point to the ectopic expression of *nrd* in the medial otic vesicle (*F, G*) including delamination from the medial wall of the otic vesicle in *hs:gsc* embryos (*G*). (*H, I*) Mean and standard deviation for the total number of *nrd*+ cells (*H*) and Isl1+ mature SAG neurons (*I*) in embryos with genotypes indicated in the color key. Asterisks (*) indicate statistically significant differences between groups indicated by brackets or compared to control embryos.

(Fig. 4.S8F). In contrast, co-activation of *hs:ngn1* and *hs:gsc* appeared to promote delamination of ectopic *neurod*+ neuroblasts from the medial wall (Fig. 4.S8G). Thus, *ngn1* and *gsc* synergize to promote EMT in the otic floor and to a lesser degree the medial wall. However, the ability to promote neurogenesis and delamination from

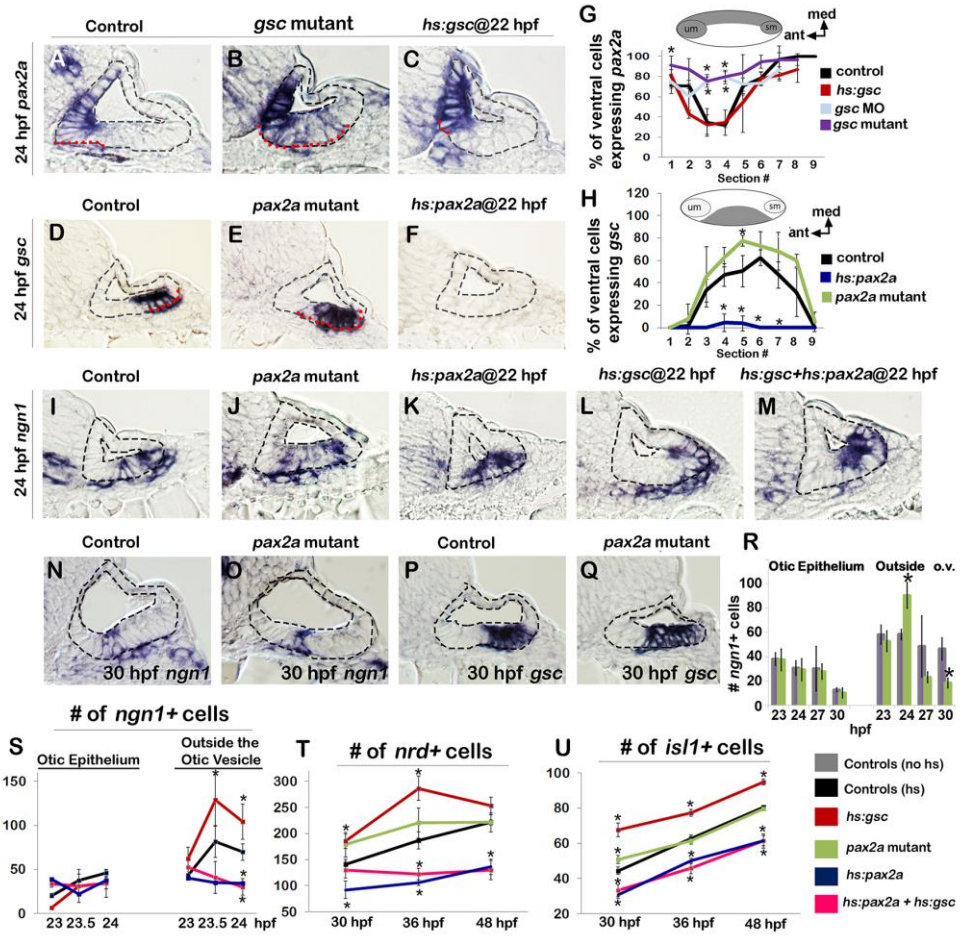

Fig. 4.4. Pax2a opposes the function of Gsc in the otic epithelium. (*A*-F) Cross sections (dorsal up, medial left) passing through the widest part of the neurogenic domain of the otic vesicle just posterior to the utricular macula showing expression of *pax2a* or *gsc* at 24 hpf (outlined in red) in embryos with indicated genotypes. Control and transgenic embryos were heat shocked at 22 hpf. The otic epithelium is outlined black in each image. (*G*, *H*) Mean and standard deviation of the percentage of cells expressing *pax2a* or *gsc* in successive sections through the otic floor in the embryos with indicated genotypes. Data were obtained by counting the number of stained and unstained cells in each section (n=3-4 specimens). Illustrations of typical domains of *pax2a* and *gsc* (medial up, anterior left) are provided above each graph to help clarify spatial patterns within each section of the otic floor. (*I*-*M*) Expression of *ngn1* at 24 hpf in embryos with indicated genotypes. Transgenic embryos were heat shocked at 22 hpf. (*N*-*Q*) Expression of *ngn1* (*N*, *O*) and *gsc* (*P*, *Q*) in controls and *pax2a* mutants at 30 hpf. (*R*-*U*) Mean and standard deviation of the total number of *ngn1*+ cells inside the otic epithelium or outside the otic vesicle (*R*, *S*; counted on serial sections, n=3-4), *nrd*+ TA cells (*T*; counted on serial sections, n=3-4) and Isl1+ cells (*U*; counted on whole mounts, n=6-12). Control (hs) and transgenic embryos were heat shocked at 22 hpf and fixed at time points indicated. Asterisks (*) indicate significant differences compared to control embryos. *Hs:gsc+hs:pax2a* embryos were significantly different than *hs:gsc* embryos at all time points but showed no statistical difference compared to *hs:pax2a* embryos.

ectopic sites was quite limited, suggesting that other regional factors act to oppose these functions in non-neurogenic regions.

Pax2a opposes Gsc function in the otic vesicle

We hypothesized that *pax2a*, which is expressed in the medial half of the otic vesicle, acts to oppose *gsc* function and block EMT. Pax2 has been shown to stabilize the otic epithelium during placodal stages in zebrafish, chick and mouse (110, 184, 185, 204), raising the possibility that this function persists after expression becomes restricted to the medial wall of the otic vesicle (Fig. 4.4A). We therefore examined the functional relationship between *pax2a* and *gsc* in the otic vesicle. Normally, *pax2a* expression abuts but does not overlap the neurogenic domain in the otic floor. In *gsc* mutants, *pax2a* expression expanded laterally into the neurogenic domain, albeit at a relatively low level (Fig. 4.4B, G), whereas activation of *hs:gsc* caused the domain of *pax2a* to recede slightly from the otic floor in regions near the sensory maculae (Fig. 4.4C, G). Conversely, in *pax2a* mutants the domain of *gsc* expression showed a weak medial expansion whereas activation of *hs:pax2a* completely eliminated *gsc* expression within 2 hours (Fig. 4.4D-F, H). These data suggest that *gsc* and *pax2a* mutually repress each other's expression in the otic floor, with a especially prominent role of *pax2a* in repressing *gsc*. Next we examined whether *pax2a* function affects neurogenesis or EMT in the otic vesicle. Loss of *pax2a* function did not alter *ngn1* expression in the otic epithelium yet transiently increased the number of delaminated *ngn1*+ neuroblasts at 24 hpf (Fig. 4.4J, R), consistent with the observed expansion of *gsc* expression in these

embryos (Fig. 4.4E, H). However, the number of delaminating cells in *pax2a* mutants subsequently fell to less than half of normal at 27 and 30 hpf (Fig. 4.4R). Consistent with dynamic changes in delamination, accumulation of TA cells and mature neurons was initially elevated in *pax2a* mutants but subsequently returned to normal after 30 hpf (Fig. 4.4T, U). The later decline probably reflects sporadic cell death in otic neurons and epithelia as previously noted in zebrafish and mouse mutants lacking Pax2 (204-206). In contrast to the effects of disrupting *pax2a*, activation of *hs:pax2a* at 22 hpf strongly suppressed delamination of *ngn1*+ neuroblasts by 23-24 hpf (Fig. 4.4K, S), consistent with loss of *gsc* expression (Fig. 4.4F). Accumulation of TA cells and mature SAG neurons was also severely impaired following activation of *hs:pax2a*, and these deficiencies persisted through at least 48 hpf (Fig. 4.4T, U). Importantly, co-activation of *hs:gsc* and *hs:pax2a* at 22 hpf completely masked the effects of *hs:gsc*, causing a phenotype similar to activation of *hs:pax2a* alone: Specifically, neuroblast delamination was strongly suppressed (Fig. 4.4S), and there was a lasting deficit in accumulation of TA cells and mature SAG neurons (Fig. 4.4T, U). Thus, in addition to repressing *gsc* transcription, Pax2a antagonizes transgenic Gsc activity.

EMT is typically induced by repression of genes encoding Cadherins. We therefore surveyed expression of various *cadherin* genes in relation to *gsc* and *pax2a* function in the otic vesicle. During normal development the E-cadherin gene *cdh1* is expressed throughout the otic vesicle, but expression levels varied markedly in the otic floor, with low-expressing cells potentially corresponding to cells undergoing EMT (Fig. 4.5A). In *gsc* mutants, *cdh1* was expressed at uniformly high levels throughout the otic

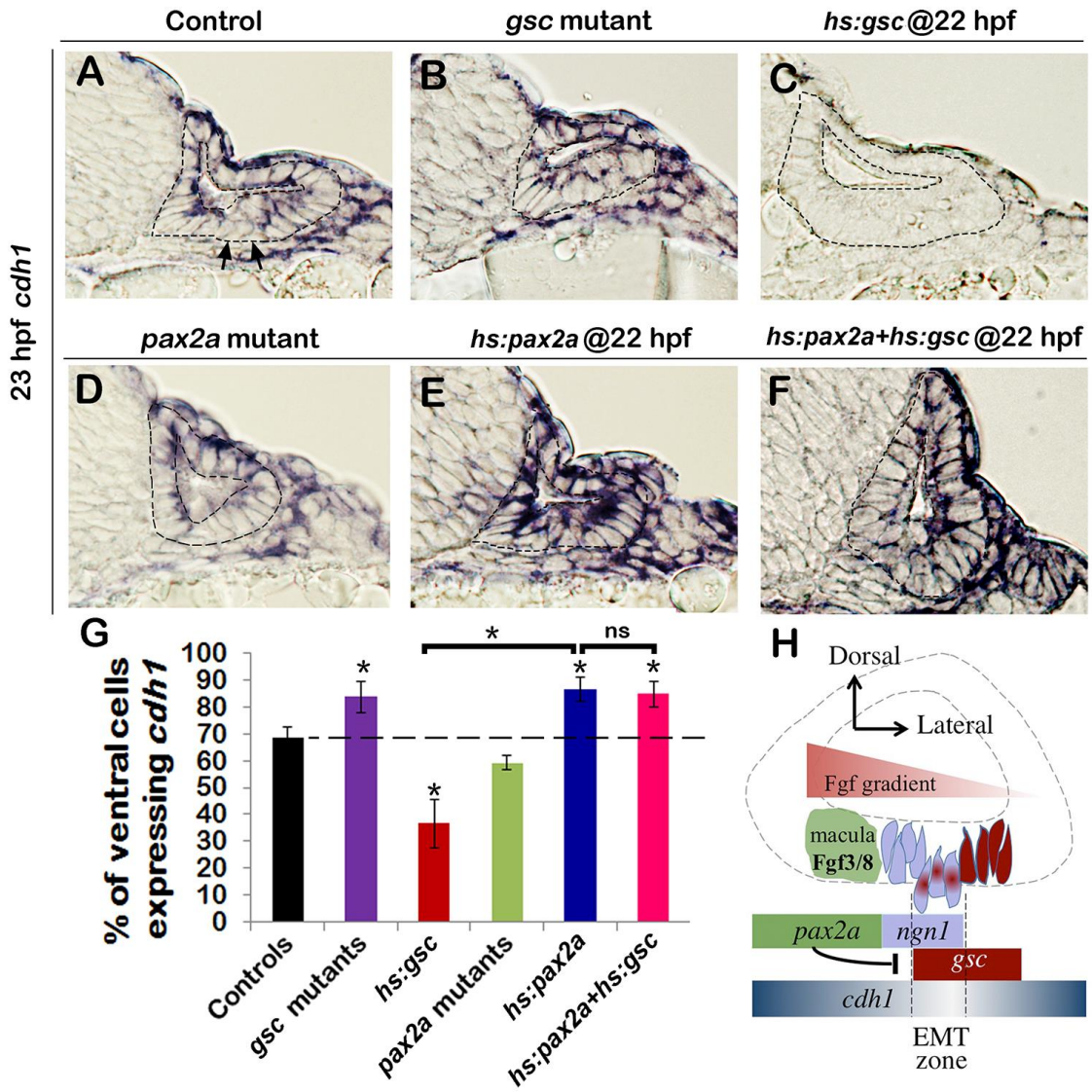

Fig. 4.5. Gsc and Pax2a differentially regulate *cdh1*. (*A-F*) Cross sections passing through the neurogenic domain of the otic vesicle just posterior to the utricular macula showing *cdh1* expression at 23 hpf in embryos with indicated genotypes. The otic epithelium is outlined in each image. Arrows in (*A*) indicate cells with very low *cdh1* expression interspersed with cells showing high *cdh1* expression. (*G*) Mean and standard deviation of the percentage of cells in the otic floor expressing *cdh1* in the embryos with indicated genotypes. Data were obtained by counting the number of stained and unstained cells in serial sections (n=3-4). Transgenic embryos were heat shocked at 22 hpf. Asterisks (*) indicate significant differences between groups indicated by brackets or compared to control embryos. (*H*) A model for regulation of epithelial tissue dynamics during otic neurogenesis. See text for details.

floor (Fig. 4.5B), whereas activation of *hs:gsc* at 22 hpf caused global downregulation of *cdh1* in the otic epithelium (Fig. 4.5C). The opposite relationship was seen with regard to Pax2a function: *pax2a* mutants showed little change in *cdh1* expression, although levels appeared slightly reduced in the otic floor (Fig. 4.5D). Activation of *hs:pax2a* caused substantial upregulation of *cdh1* throughout the otic vesicle, including uniformly high expression in the otic floor (Fig. 4.5E). Co-activation of *hs:pax2a* and *hs:gsc* led to uniformly high expression of *cdh1* throughout the otic vesicle, similar to activation of *hs:pax2a* alone (Fig. 4.5E, F). Changes in the percentage of cells in the otic floor expressing *cdh1+* cells, determined by counting cells in serial sections, confirmed the above trends (Fig. 4.5G). Overall these results suggest that Gsc and Pax2a have opposing effects on tissue architecture mediated in part by differential regulation of *cdh1* transcription.

Global loss of E-cadherin transcription does not lead to widespread cell dispersal in *hs:gsc* embryos. This prompted us to analyze the expression of other *cadherin* genes that might have redundant functions in the otic vesicle. Indeed, expression of *cdh2* remained unaffected in the otic vesicle upon loss of function or overexpression of *gsc* and/or *pax2a* (Fig. 4.S9A-F). *Cdh11* is expressed in the non-neurogenic regions of the otic vesicle such as the medial and lateral walls (Fig. 4.S9G) and did not show any changes in *gsc* mutants or *hs:gsc* embryos (Fig. 4.S9H, I). However, *cdh11* transcript was lost from part of the medial wall in *pax2a* mutants whereas activation of *hs:pax2a* induced *cdh11* expression in ectopic locations including the otic floor (Fig. 4.S9J-L). Conceivably, *cdh11* also helps to mediate Pax2a's role in stabilizing epithelial integrity.

Cdh6 is predominantly expressed in the delaminated otic neuroblasts in the TA pool (Fig. 4.S9M). In keeping with the effects of *gsc* on delamination, *gsc* mutants had fewer *cdh6*+ cells outside the otic vesicle and *gsc* overexpression increased accumulation of *cdh6*+ cells in the TA pool (Fig. 4.S9N, O, S). In contrast, overexpression of *pax2a* reduced the number of *cdh6*+ otic neuroblasts outside the ear and suppressed the effects of activating *hs:gsc* (Fig. 4.S9P, Q, S). *pax2a* mutants showed a statistically normal number of *cdh6*+ neuroblasts at 24 hpf (Fig. 4.S9P, S), possibly because elevated cell death counterbalances the transient spike in neuroblast delamination seen at 24 hpf in these embryos (Fig. 4.4R).

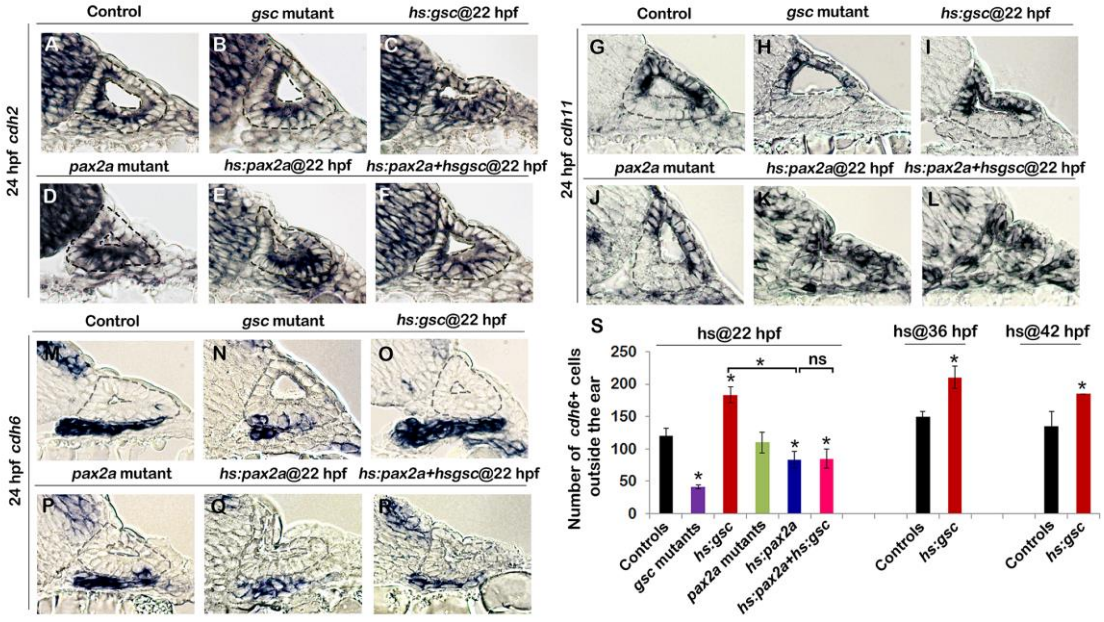

Fig. 4.S9. Expression of cadherin genes in relation to Pax2a or Gsc function in the otic vesicle. Transgenic embryos were heat shocked at the indicated times. (*A-R*) Cross sections (dorsal up, medial left) passing through the middle of the neurogenic domain showing expression of *cdh2* (*A-F*), *cdh11* (*G-L*) and *cdh6* (*M-R*) in embryos with indicated phenotypes. (S) Mean and standard deviation of the total number of *cdh6* expressing cells outside the otic vesicle. Asterisks (*) indicate significant differences between groups indicated by brackets or compared to control embryos.

DISCUSSION

Delamination from the otic vesicle is a vital step in otic neurogenesis that has heretofore been described only at the morphological level. Here we elucidate for the first time a molecular mechanism for this process (Fig. 4.5H). First, we describe a novel role for the organizer gene *gsc* in promoting delamination of neuroblasts from the otic vesicle. Loss of *gsc* function impairs delamination of SAG neuroblasts and leads to a significant loss of mature SAG neurons whereas misexpression of *gsc* enhances neuroblast delamination and increases the size of the mature SAG. Second, Gsc's ability to promote EMT requires coexpression of *ngn1* as a parallel output of Fgf signaling. Co-misexpression of *gsc* and *ngn1* stimulates neuroblast delamination from ectopic sites within the otic vesicle. Third, we document a new role for Pax2a in stabilizing the otic epithelium in opposition to Gsc. Pax2a not only represses *gsc* transcription, but it also suppresses Gsc protein function and blocks EMT. The opposing activities of Pax2a and Gsc correlate with their differential regulation of the *cdh1*, which is downregulated in delaminating neuroblasts in zebrafish as well as mouse (207).

In this model, distinct regulation of *ngn1* and *gsc* assures orderly delamination coupled with ongoing renewal of neuroblasts within the otic epithelium: As *gsc*+ neuroblasts delaminate, adjacent neuroblasts presumably move into the *gsc* domain in preparation for their own EMT. In early stages of neurogenesis, the domain of *ngn1* expands, allowing replacement of cells lost through EMT. Eventually Fgf levels rise to block further *ngn1* induction (132), terminating the ability to replenish neuroblasts as they delaminate. This mechanism is reminiscent of Gsc's role in driving cellular

dynamics and replenishment in the vertebrate organizer (186-189). An important goal of future research will be to conduct detailed cell-labeling experiments to elucidate patterns of epithelial rearrangement implied in our current study.

In addition to promoting EMT, overexpression of *gsc* had unexpected stage-specific effects on proliferation of TA cells. When activated at 22 hpf, *hs:gsc* caused a slight decrease in proliferation in the TA pool. This is understandable since *hs:gsc* causes virtually all *ngn1*+ neuroblasts to delaminate at once, temporarily disrupting the normal steady flow of cycling progenitors into the TA pool. The sudden bolus of TA cells would then continue to develop synchronously and shift the population mean towards a post-mitotic state, reducing the overall rate of proliferation. In contrast, activation of *hs:gsc* at 36 hpf or later caused a dramatic increase in proliferation of TA cells (Fig. 4.3K). The mechanistic basis for this is unclear but could reflect the changing status of Fgf signaling during successive stages of SAG neurogenesis (132, 181). During early stages of otic vesicle development, the level of Fgf signaling is relatively low, which stimulates specification of neuroblasts in the otic epithelium but is not sufficient to affect development of TA cells. As development proceeds, mature SAG neurons begin to accumulate and express *fgf5*, which eventually exceeds an upper threshold to terminate specification of neuroblasts in the otic epithelium. Elevated Fgf5 also delays terminal differentiation and promotes proliferation of TA cells. We speculate that forced expression of *gsc* in TA cells reinforces this effect of Fgf5, thereby increasing the TA pool disproportionately at later stages. This does not reflect a normal function of *gsc* since it is not normally expressed in TA cells. Indeed, proliferation of

TA cells was normal at all stages in *gsc* mutants (Fig. 4.S7E). Further studies will be required to rigorously test the relationship between *gsc* and *fgf5* during later stages of otic development.

Conservation and diversity of Gsc function

The function of *gsc* in the zebrafish inner ear is likely to be conserved in other vertebrates. In mouse, *Gsc* is expressed in the developing otocyst in a pattern similar to that in zebrafish (190, 196), although its function has not been investigated. Loss of *Gsc* function in humans causes SAMS syndrome, characterized by mandibular hypoplasia similar to that seen in zebrafish *gsc* mutants, as well as loss of the auditory canal. These defects reflect deficiencies in neural crest-derived pharyngeal arches 1 and 2, known sites of *Gsc* expression, but it is unknown whether auditory neurons are also affected. Although a recently reported human chromosomal deficiency spanning *Gsc* causes auditory neuropathy, the deficiency also removes other genes that potentially affect the trait (208). Thus, additional studies are needed to clarify the role of *Gsc* in otic neurogenesis in mammals.

Interestingly, the role of Gsc in otic neurogenesis in zebrafish appears similar to the role of Gsc in regulating the stomatogastric nervous system (SNS) in *Drosophila*. SNS neuroblasts in fly initially form in the foregut epithelium and subsequently delaminate and migrate significant distances to form the equivalent of vertebrate enteric neurons. Epithelial SNS neuroblasts express *Gsc*, and delamination is strongly impaired in *Gsc* mutants (209, 210). Additionally, delamination requires Egfr and the RAS-

MAPK pathway (211, 212). Together, these findings suggest that a broadly conserved pathway, acting through RAS-MAPK and *Gsc*, functions to localize neuroblast delamination in these widely divergent species.

In addition to *gsc*, it is likely that additional factors regulate EMT in the otic vesicle. We note that neuroblasts normally begin to delaminate from the otic epithelium by 17 hpf, several hours before the onset of *gsc* expression (Fig. 4.1), and delamination is not completely lost in *gsc* mutants (Fig. 4.2G). A number of transcription factors known to regulate EMT in other tissues, including Snail and Zeb proteins, are also expressed in the otic vesicle at appropriate stages (213-215). These might help promote delamination from the otic vesicle, but functional studies are yet to be reported.

Pax2 as an epithelial stabilizer

Pax2 appears to coordinate cell fate specification and epithelial integrity in several contexts. In zebrafish, combinatorial knockdown of redundant genes *pax2a*, *pax2b* and *pax8* leads to progressive dispersal of otic cells soon after formation of the otic vesicle (185). Similarly, loss of both *Pax2* and *Pax8* in mouse impairs placode invagination and severely reduces otic vesicle size, apparently due to abnormal cell migration (204). Studies in chick show that Pax2 is required for proper expression of NCAM and N-cadherin to stabilize epithelial integrity during placode invagination (184). A continuing role in epithelial maintenance at later stages of otic development might explain why mouse and zebrafish embryos lacking Pax2 or Pax5 function show elevated cell death in the otic vesicle, especially in sensory epithelia (205, 206).

Similarly, Pax2 plays a role in epithelial maintenance during kidney development. Mouse Pax2 mutants display severe renal defects resulting from loss of epithelial structure in the nephric duct, accompanied by formation of irregular outgrowths and increased cell motility (216, 217).

Regulation of Cadherin dynamics

The functions of Gsc and Pax2a counter each other in regulating the level of *E-cadherin* (*cdh1*) transcription (Fig.4.5A-F). E-cadherin is classically associated with epithelia and its downregulation is a common signature of EMT. Hence the ability of Pax2a to totally suppress the effects of Gsc can be explained partly through its ability to maintain *cdh1* expression. However, this mechanism is likely not sufficient. Activation of *hs:gsc* downregulates *cdh1* throughout the otic vesicle yet does not induce widespread dispersal of the otic epithelium. This is probably because other cell adhesion molecules like *cdh2* and *cdh11* are coexpressed in the otic epithelium and are not affected by Gsc activity. The physical arrangement and functional relationships between coexpressed CAMs remain poorly understood aspects of epithelial structure, but partial redundancy likely explains the limited effects of Gsc activity.

Another factor limiting Gsc's ability to promote EMT is the requirement for co-expression of Ngn1. These factors probably regulate different subsets of genes to facilitate EMT. Gsc acts as a transcriptional repressor (218-221) likely explaining its ability to downregulate *cdh1* in the otic vesicle (Fig. 4.5C) as well as in a diverse array of aggressive metastatic cancers in which Gsc promotes EMT (194, 195, 222). In

contrast, Ngn1 acts predominantly as a transcriptional activator. Relevant targets of Ngn1 might include factors that regulate f-actin dynamics, or proteases that degrade basement membrane. All of these processes are potentially coordinated under the combinatorial control of Gsc and Ngn1 to ensure a robust EMT response.

EMT is typically associated with Cadherin switching. For example, *cdh6* is upregulated in neuroblasts after delamination, with weak expression first appearing in scattered cells within the otic epithelium (Fig. 4.S9). Such switching may help weaken epithelial junctions and/or inhibit re-epithelialization of neuroblasts after delamination while facilitating collective migration. Interestingly, the role of specific Cadherins often differs according to context. For example, *cdh11* is often associated with mesenchymal cells (223, 224) yet is expressed in the most stable parts of the otic epithelium in zebrafish (Fig. 4.S9). Conversely, *cdh6* is expressed in migrating otic neuroblasts in zebrafish, whereas it marks premigratory neural crest in chick ectoderm and must be downregulated to allow neural crest delamination (225, 226). The otic vesicle promises to be a useful model for future functional studies to determine how diverse cell adhesion molecules interact and contribute to tissue architecture and dynamics.

CHAPTER V

GLYCOLYSIS MEETS FGF SIGNALING: THE GLYCOLYTIC ENZYME PGK1 IS REQUIRED NON-AUTONOMOUSLY FOR FGF-DEPENDENT SPECIFICATION OF OTIC NEURONS IN ZEBRAFISH

INTRODUCTION

In all vertebrates; hearing and balance related information is transmitted from the inner ear to the brain via the neurons of the Stato-Acustic Ganglion (SAG). SAG neurons are formed by a complex, stepwise program that starts in the otic vesicle, the progenitor of the mature vertebrate ear. At the first step, SAG neural progenitors are specified in the otic epithelium and marked by the expression of the proneural gene *neurogenin1* (*ngn1*). Ngn1 is a basic helix-loop-helix transcription factor, crucial for the cell-fate specification of the otic neuroblasts such that *ngn1* loss of function causes complete loss of SAG neurons and other cranial neurons (60). Next, a subset of specified otic neuroblasts undergoes epithelial-mesenchymal transition and delaminates from the otic vesicle (14). Soon after leaving the otic epithelium, neuroblasts turn of *ngn1* expression and upregulate a related proneural factor called *neurod*. *Neurod* expressing cells migrate towards the hindbrain as they continue to proliferate and form a stable transit-amplifying (TA) progenitor pool (132). TA cells differentiate into mature

SAG neurons upon reaching their final destination and turn on the expression of mature neuronal markers such as Isl1/Isl2b (133, 227). The mature SAG segregates into two functional subunits: the anterior patch of the SAG sends projections to the utricular macula and semicircular canals to mediate balance related information, whereas the posterior subunit of the SAG transmits auditory information from the saccule and lagena to the hearing centers in the hindbrain. Very little is the known about the mechanisms that govern functional segregation and axonal navigation of the distinct SAG subunits. Significant progress has been made to identify and characterize the signaling pathways and genes that regulate distinct steps of SAG development. First, we showed that a threshold level of Fgf signaling is paramount for the specification of SAG progenitors in the otic vesicle, hence the conditions that completely block Fgf signaling impair otic neurogenesis and reduce the size of the mature SAG (132). However, a high level of Fgf signaling is also detrimental to otic neurogenesis, such that, high level overexpression of the Fgf ligands blocks *ngn1* expression in the otic vesicle and leads to production of fewer SAG neurons (132). Accordingly, during the normal progression of SAG development, the rise of Fgf signaling originating from the local sources and mature SAG neurons shuts down otic neurogenesis at around 42 hpf (132). The level of Fgf signaling in the otic vesicle is partially regulated via the action of the transcription factor Tfap2a which dampens Fgf signaling through upregulation of Bmp7 to promote specification of SAG neuroblasts. Thus, the mechanism of SAG development is highly sensitive and tuned to the rise of the level of Fgf signaling in the otic vesicle, yet, how a

threshold level of Fgf signaling is initially set and maintained during the early stages of SAG progenitor specification is very poorly understood.

We conducted an ENU mutagenesis screen in zebrafish to identify novel genes that regulate SAG development. We identified two lethal mutations, named *sagd1* and *sagd2*, that showed no gross morphological defects but both strongly reduced a subset of SAG neurons. *Sagd1* mutants showed a specific reduction in the number of vestibular neurons required for balance, whereas auditory neurons developed normally. Further characterization of *sagd1* mutants revealed that the otic neurogenesis was impaired due to defective Fgf signaling during early SAG development. Fgf signaling recovers as development proceeds and otic neurogenesis resumes to normal, enabling auditory neurons to develop as usual.

Whole genome sequencing revealed the affected locus in *sagd1* mutants as *pgk1* (Phospho-glycerate kinase1). The best known role for Pgk1 is to catalyze the transfer of high energy phosphate from the 1, 3-diphospoglycerate to ADP and to generate 3-phosphoglycerate and ATP during glycolysis. Interestingly, Pgk1 also has an mRNA stabilization function such that the translation of the sequences in the first two thirds of the pgk1 transcript has been shown to stabilize *pgk1* mRNA (228-230).

Here we describe a novel role for Pgk1 during SAG neurogenesis. First we show that *pgk1* is strongly upregulated in the sensory epithelium and vestibular neurons which are the tissues affected by the s*agd1* mutation. Targeted knockdown of the *pgk1* gene using CRISPR technology phenocopies *sagd1* mutants. Further analysis with the use of the genetic mosaics showed that Pgk1 non-autonomously regulates Fgf signaling in the otic

vesicle. Furthermore, the impairment of the Fgf signaling in *pgk1* mutants were not rescued by overexpression of Fgf ligands, indicating that Pgk1 affects Fgf signaling at a step downstream of the ligand production. Further experiments show a novel role for Pgk1 and glycolysis in regulation of MAPK signaling independently from Fgf ligands and through lactate production.

MATERIALS AND METHODS

Fish strains and developmental conditions

Wild-type embryos were derived from the AB line (Eugene,OR). The following transgenic lines were used in this study: Tg*(hsp70:fgf8a)*^{x17}(19), *Tg(Brn3c:GAP43-GFP)*^{s356t}(159), Tg*(-17.6isl2b:GFP)*^{zc7}(99), Tg*(hsp70:pgk1.1)*^{x57}.Mutant lines *sagd1*^{x40} and *pgk1.1*^{x54} were used for loss of function analysis. Homozygous mutants were identified by a characteristic decrease in the expression of Isl2b-GFP in SAG. Embryos were maintained at 28.5°C except after a heat-shock regimen embryos were placed at 33°C. Embryos were staged according to standard protocols (100). PTU (1-phenyl 2-thiourea, 0.3 mg/ml, Sigma) was included in the fish water to inhibit pigment formation.

Gene misexpression and morpholino injections

Heat-shock regimens were carried in a water bath at indicated temperatures and durations. Embryos were kept in a 33°C incubator after the heat-shock. Transgenic carriers were identified by morphological characteristics. Knockdown of Plasminogen

was performed by injecting morpholinos (5 ng/ul) at one cell stage using the following MO sequence: 5'-AACTGCTTTGTGTACCTCCATGTCG.

Statistics

Student's t-test was used for pairwise comparisons. Analysis of 3 or more samples was carried by one way ANOVA and Tukey post-hoc HSD test.

In situ hybridization and immunohistochemistry

Whole mount in situ hybridization and immunohistochemistry protocols used in this study were previously described (72, 102). Whole mount stained embryos were cut into 10 μm thick sections using a cryostat (132). The following antibodies were used in this study: Anti-Islet1/2 (Developmental Studies Hybridoma Bank 39.4D5, 1:100), Anti-GFP (Invitrogen A11122, 1:250), Alexa 546 goat anti-mouse or anti-rabbit IgG (ThermoFisher Scientific A-11003/A-11010, 1:50). Promega terminal deoxynucleotidyl transferase (M1871) was used according to manufacturer's protocol to perform the TUNEL assay.

Pharmacological treatments

Glycolysis was blocked by treating embryos with 2-deoxy-glucose diluted from a 10 mM stock in DMSO to a final concentration of 100 μM in fish water. Lactate production from pyruvate was inhibited by galloflavin diluted from a 10 mM stock solution into a final concentration of 100 μM in fish water. Lactate treatments were

performed with 60% stock sodium DL-lactate solution (Sigma, L1375) diluted 1 to 1000 in fish water containing 10 mm MES. Treatments were carried in a 24-well plate with a maximum of 15 embryos per well in a volume of 500 µl each.

RESULTS

To identify and characterize the novel genes that regulate development of the SAG neurons we have conducted a mutagenesis screen with more than 50 founders in *isl2b*-GFP transgenic background. Initial screening for the 50 mutagenized founders and their families yielded 2 lethal mutations, termed *sagd1* and *sagd2*. SAG neurons form 2 functionally distinct subunits. Anteriorly located SAG neurons project to the vestibular apparatus of the inner ear and mediate balance related information, whereas the posterior subunit of the SAG is required for transmitting auditory information. *sagd1* mutants were initially recovered for a specific defect in the vestibular neurons, whereas auditory neurons develop normally (Fig. 5.1A-R). Quantification of the *isl2b*:GFP staining on serial sections revealed a ~60% deficiency in the number of vestibular SAG neurons located in the anterior portion the otic vesicle (adjacent to the utricular macula) at 24 and 30 hpf (Fig. 5.1A-D, Q).The number of vestibular SAG neurons remained lower compared to controls through at least 48 hpf. The number of auditory SAG neurons, located in the posterior sections of the otic vesicle abutting the saccular macula, was not significantly altered compared to control embryos (Fig. 5.1I- R). There were no overt morphological defects in *sagd1* mutants, and the size and the axial patterning of the otic vesicle was also unaffected (Fig. 5.2A-J). It is also noteworthy that the defect in the

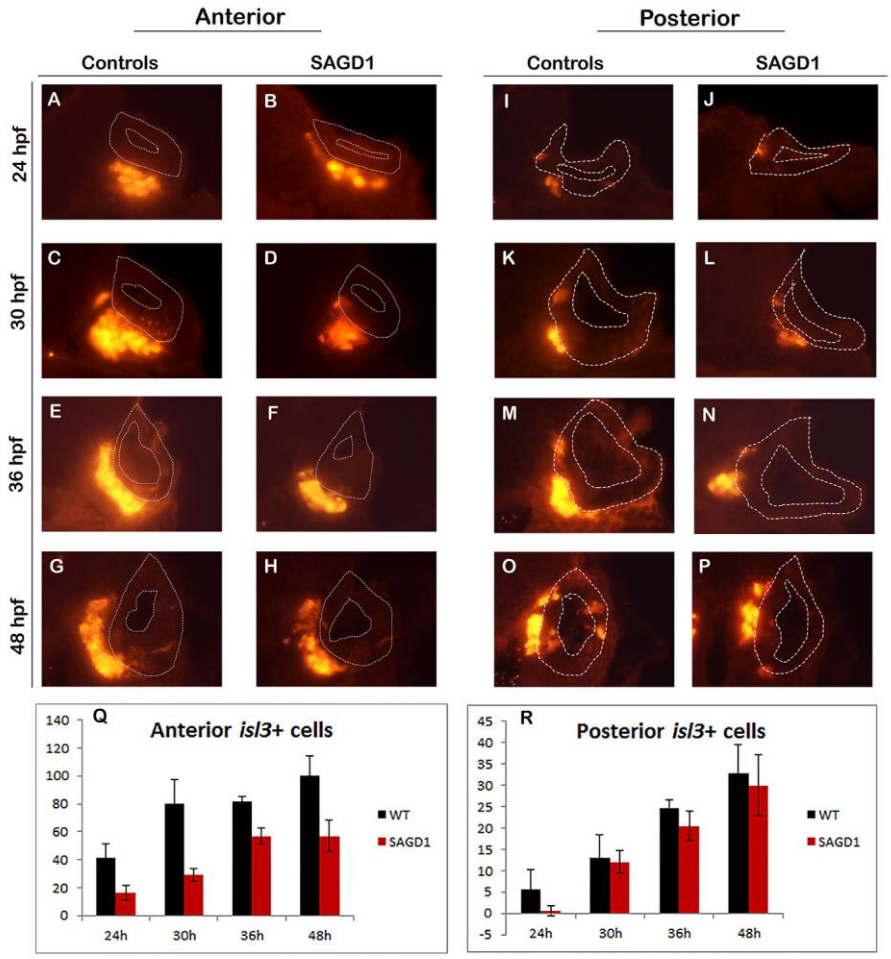

Figure 5.1. *sagd1* mutants produce fewer vestibular SAG neurons. (A-P) Cross sections passing through the utricle (A-H) and saccule (I-P) of the otic vesicle in isl2b-GFP expressing controls and *sagd1* mutants label the mature SAG neurons at indicated time points. Embryos were stained for GFP prior to cryo-sectioning. (Q,R) Mean and standard deviation for the total number of Isl2b+ SAG neurons in controls versus *sagd1* mutants. Asterisks (*) indicate statistically significant differences compared to control embryos ($p \leq 0.05$).

number of vestibular SAG neurons does not stem from an increased rate of apoptosis (Fig. 5.2K), suggesting the impairment of an early step during SAG formation in *sagd1* mutants. Next, we examined earlier stages of SAG development in *sagd1* mutants. Normally delaminated neural progenitors lose expression of *ngn1* and upregulate expression of the related proneural gene, *neurod*, which marks transit-amplification (TA)

stage of SAG development. TA cells migrate towards the hindbrain and subsequently differentiate into Isl+ neurons.

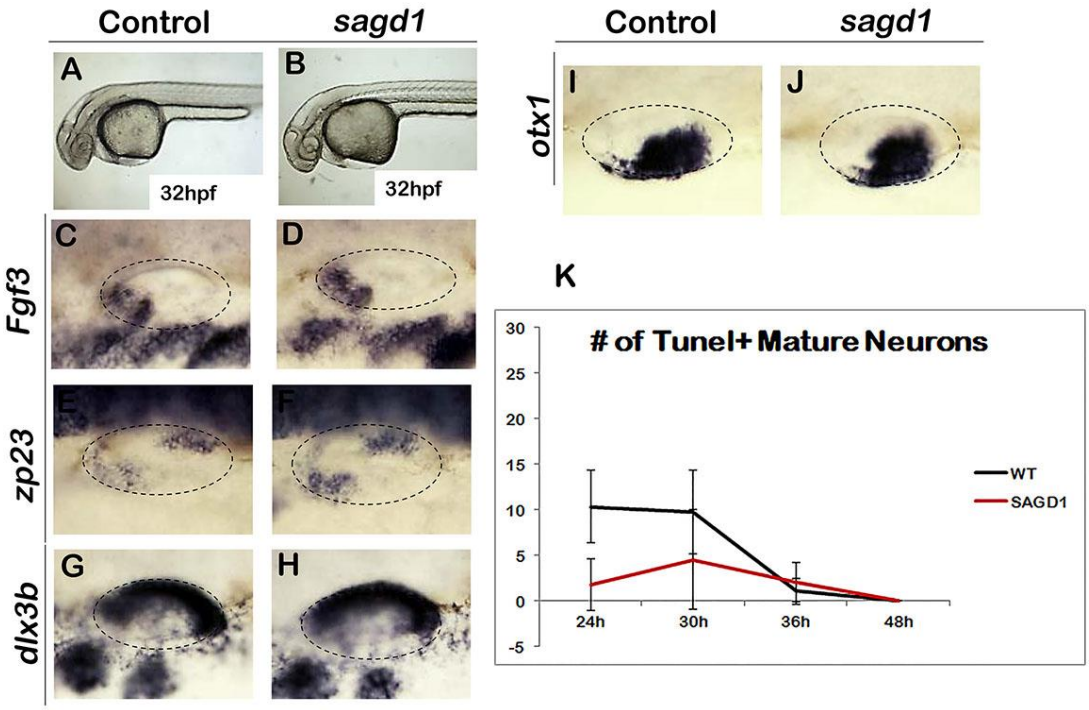

Figure 5.2. Gross morphology and otic vesicle patterning is normal in *sagd1* mutants. (A, B) Live specimens at 32 hpf viewed from dorsolateral view reveal no gross morphological differences between controls and *sagd1* mutants. (C-D) Whole-mount images (dorsal up, anterior left) show dorsolateral views of the otic vesicle (outlined) in controls and *sagd1* embryos for the indicated genes at 30 hpf. (K) Mean and standard deviation for the total number of TUNEL+ SAG neurons in controls versus *sagd1* mutants at indicated time points. There is no significant differences compared to control embryos ($p \leq 0.05$).

Accumulation of *neurod*+ SAG neuroblasts in the anterior portion of the otic vesicle was impaired in *sagd1* mutants (Fig. 5.3A-E). This deficit was more pronounced at 36 hpf (~60% decrease) than at 48 hpf (~20% decrease). Despite the deficiency in the number of anterior TA cells, accumulation of the TA neuroblasts in the posterior regions of the otic vesicle was normal in *sagd1* mutants (Fig. 5.3F-J). We hypothesized that the

decrease in the size of the anterior TA pool reflects impairment of neuroblast specification in the otic vesicle. To test this we examined expression of *ngn1*, a marker of the specified neuroblasts.

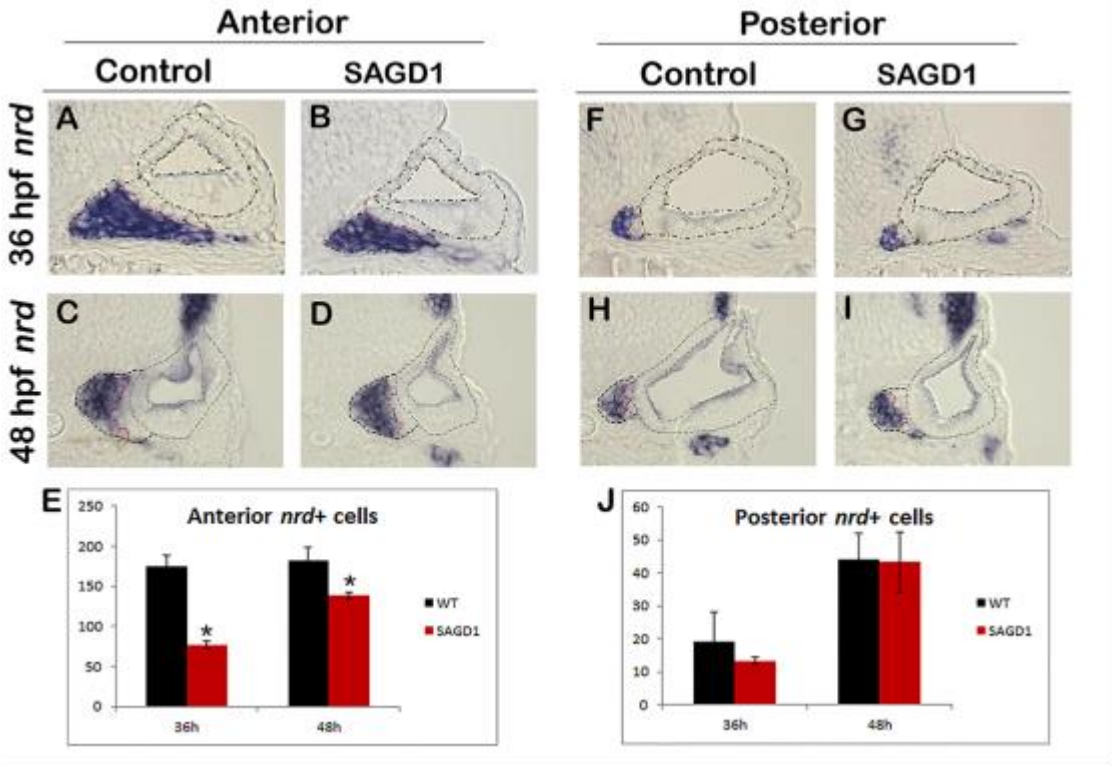

Figure 5.3. *sagd1* mutants produce fewer TA neuroblasts. (A-D, F-I) Cross sections (dorsal up, medial left) passing through the utricle (A-D) and saccule (F-I) show *neurod* staining in controls and *sagd1* embryos. (Q,R) Mean and standard deviation for the total number of *neurod*+ cells in controls versus *sagd1* mutants in utricular (E) versus saccular (J) sections. Asterisks (*) indicate statistically significant differences compared to control embryos ($p \leq 0.05$).

We observed that specification of neuroblasts was reduced during early SAG development between 20-30 hpf (Fig. 5.4A, B, E), with the most severe effect observed at 24 hpf, the peak stage of otic neurogenesis. Interestingly, specification of neural progenitors returned to normal after 30 hpf (Fig. 5.4C, D, E). The number of the

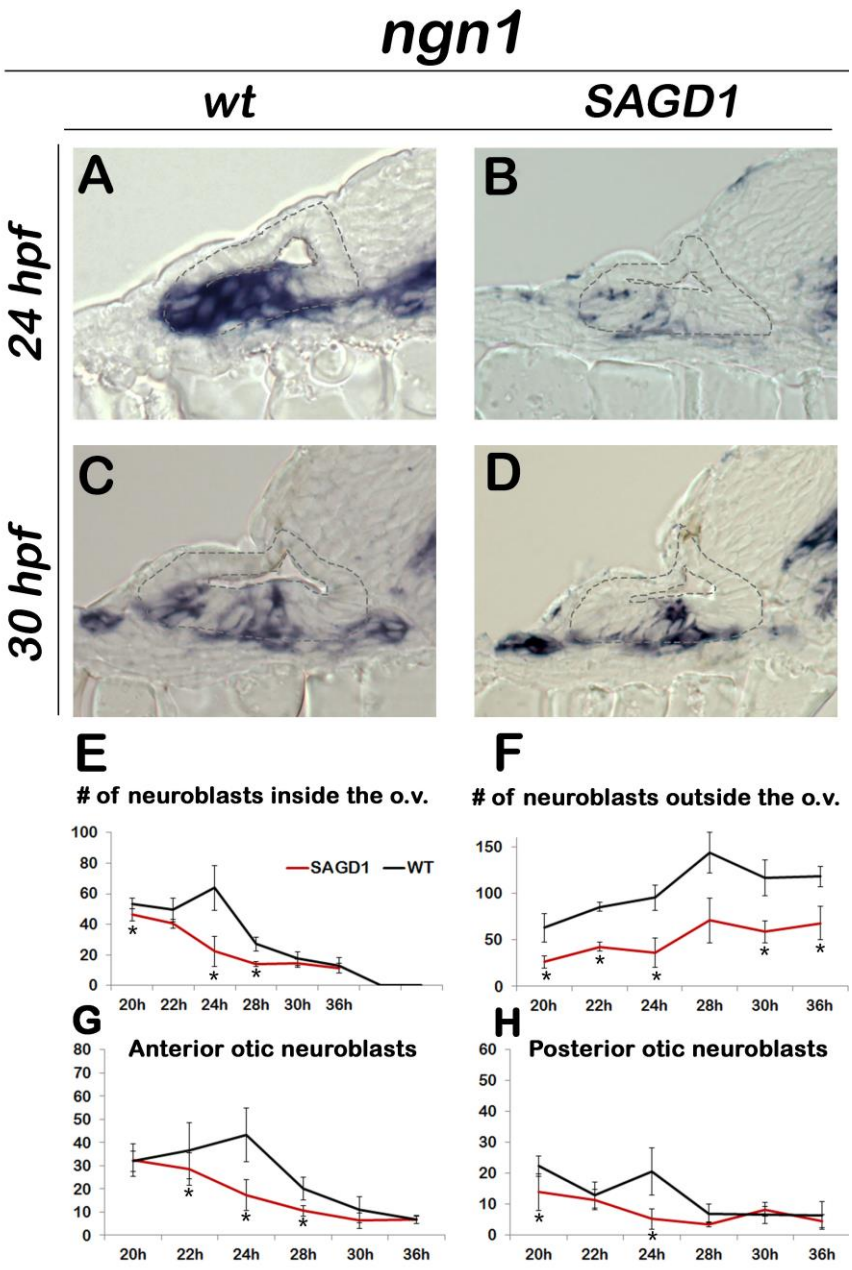

Figure 5.4. Specification of neuroblasts is impaired in *sagd1* mutants during early neurogenesis. (A-D) Cross sections passing through the widest part of the neurogenic domain (dorsal up, medial left) just posterior to the utricular sensory epithelium show *ngn1* staining in controls and sagd1 embryos at indicated time points. (E-H) Mean and standard deviation for the total number of *ngn1*+ cells in controls versus *sagd1* mutants in the inside (E), outside (F), anterior half (G) and posterior half (H) of the otic vesicle. Asterisks (*) indicate statistically significant differences compared to control embryos ($p \leq 0.05$).

delaminated neuroblasts outside the otic vesicle remained deficient at every stage examined, possibly reflecting the early impairment of neurogenesis (Fig. 5.4.F). Recent studies from cell-tracing experiments in mice suggest that the early delaminating neuroblasts form the anteriorly located vestibular SAG population whereas later forming neuroblasts mostly contribute to the auditory portion of the SAG. We previously showed that conditions that enhance otic neurogenesis at early stages lead to an increase only in the size of the vestibular SAG population (132, 181, 231). Overall, these studies suggest that the subtype specification of SAG neurons is regulated temporally. This is consistent with the phenotype of the *sagd1* mutants, where an early deficit in neuroblast specification affects only the vestibular SAG neurons.

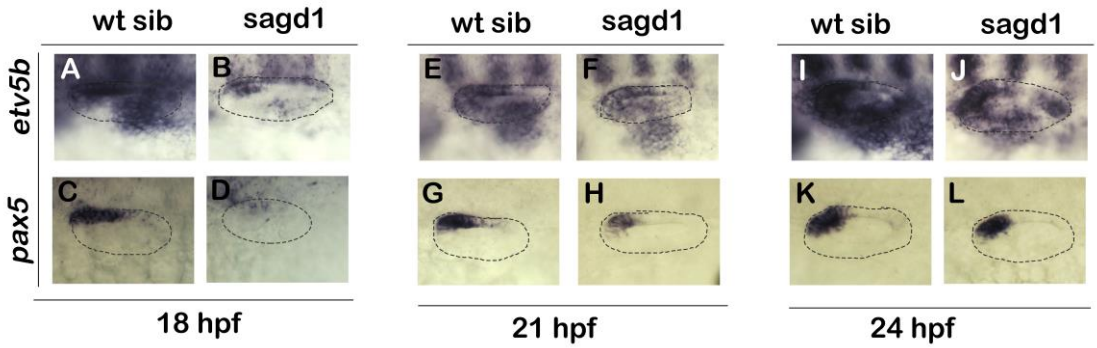

Figure 5.5. Effects of *sagd1* mutation on Fgf signaling. (*A-L*) Whole-mount images (dorsal up, anterior left) show dorsolateral views of the otic vesicle (outlined) in controls and *sagd1* mutants for the expresson of *etv5b* and *pax5* at indicated time points

Next, we sought to understand the reasons for the early impairment of otic neurogenesis in *sagd1* mutants. We previously showed that specification of the otic neuroblasts requires a threshold level of Fgf signaling and conditions that completely block Fgf

signaling halt otic neurogenesis (132). To test whether Fgf signaling was impaired in *sagd1* mutants, we analyzed the expression of the Fgf responding gene *etv5b* and ear-specific Fgf target gene *pax5*. Expression of both markers was markedly reduced at 18 hpf in *sagd1* mutants (Fig. 5.5A-D), but partially recovered at later stages (Fig. 5.5E-L). Overall these data suggest that early impairment of Fgf signaling leads to a deficiency in otic neurogenesis and results in a lower number of mature vestibular SAG neurons.

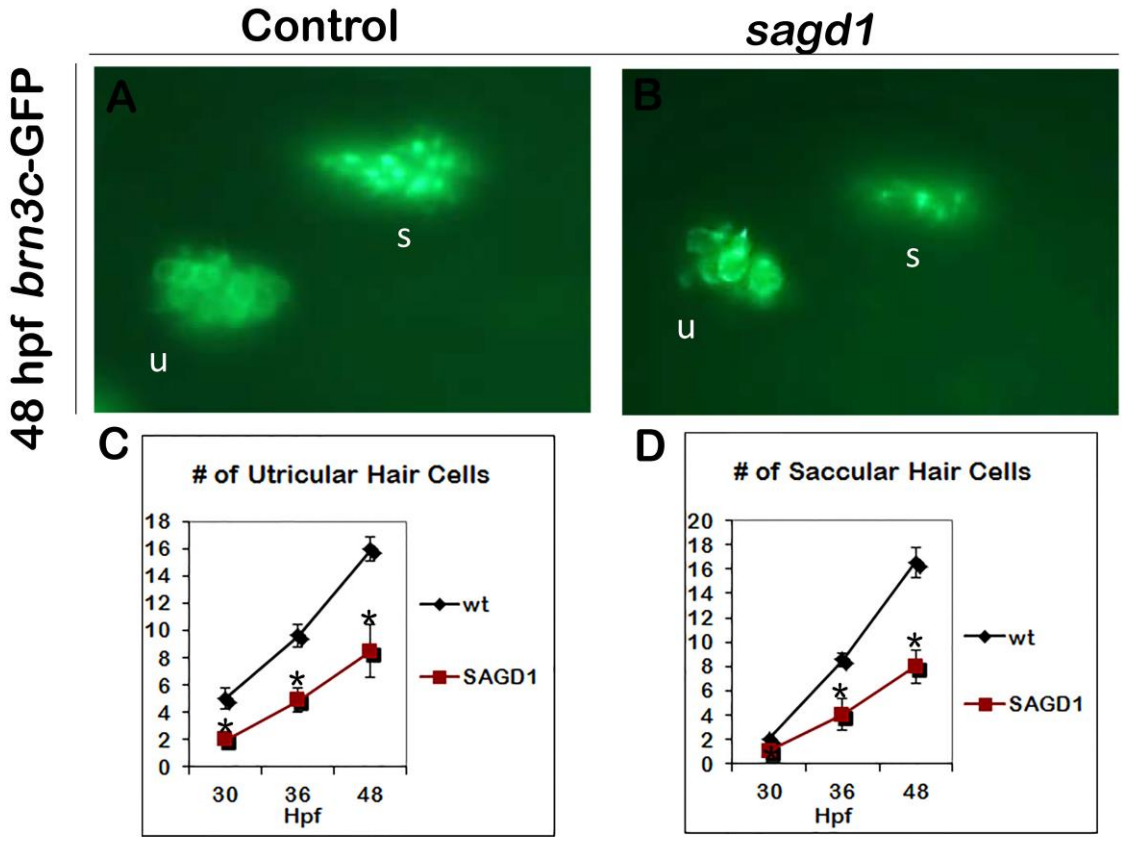

Figure 5.6. ***sagd1*** **mutants produce fewer otic hair cells.** (A,B) Whole-mount images (dorsal up, anterior left) show dorsolateral views of the otic vesicle (outlined) in Brn3c:GFP+ controls and *sagd1* mutants and label the hair cells. Mean and standard deviation for the total number of Brn3c:GFP+ cells in control versus *sagd1* mutant otic vesicles. Asterisks (*) indicate statistically significant differences compared to control embryos ($p \leq 0.05$).

However, Fgf signaling recovers and enables normal neuroblast specification at later stages such that formation of auditory neurons remains unaffected. Most likely due to the impairment of Fgf signaling, sensory hair cell development in both utricular and saccular macula is also deficient in *sagd1* mutants (Fig. 5.6A-D).Impairment of the Fgf signaling could stem from the changes in the expression of Fgf ligands in *sagd1* mutants. To test whether overexpression of an Fgf ligand could rescue the *sagd1* phenotype we generated a *sagd1* mutant line that carries a heat-shock inducible *fgf8* construct. Interestingly, high(39 °C) or low level (35 ºC) activation of *hs:fgf8* at multiple time points including 18 and 24 hpf did not rescue the *sagd1* phenotype, development of SAG neurons remained deficient (Fig. 5.7A-F, data not shown). This data suggests that the *sagd1* lesion impairs Fgf signaling at a step downstream of Fgf ligand-receptor binding, such that cells remain unresponsive even when the level of the fgf ligands was elevated with the activation of the *hs: fgf8* transgene.

To identify the affected locus in *sagd1* mutants, we analyzed the whole genome sequencing data with homozygosity mapping approaches (232) and revealed that the *sagd1* mutation affects the glycolytic enzyme Pgk1 (Phosphoglycerate kinase-1). There are 2 predominant transcripts expressed from the zebrafish *pgk1* locus (Fig. 5.8) (233). The primary transcript is highly conserved in vertebrates and consists of 10 exons (233). However, zebrafish has a unique alternative *pgk1* transcript that harbors 2 novel exons resulted from the integration of a DNA transposon sequence into *pgk1* locus (233). Transcribed from a unique promoter, the alternate *pgk1* transcript also a seventh exon that includes a stop codon (233). Thus the protein product of alternate *pgk1*

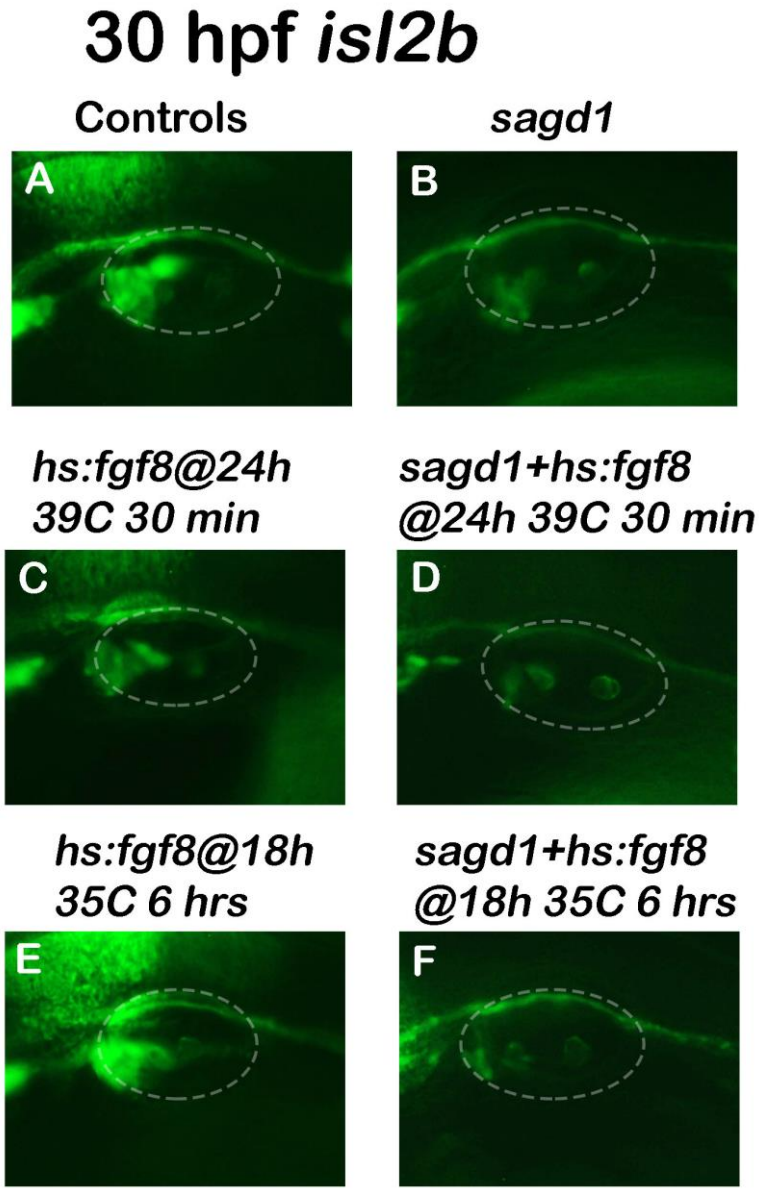

Figure 5.7. Overexpression of *fgf8* does not rescue *sagd1* mutants. (*A-F*) Whole-mount images (dorsal up, anterior left) show dorsolateral views of the otic vesicle (outlined) in *isl2b: GFP*+ controls and *sagd1* mutants, *hs:fgf8* embryos and *hs:fgf8* + *sagd1* mutants. *hs:fgf8* transgene was activated at 39°C or 35°C for indicated durations.

transcript is smaller compared to that of primary *pgk1* transcript (Fig. 5.7). Thus, the alternate Pgk1 protein lacks a significant portion of the nucleotide binding and catalytic domains of Pgk1 such that it is unable to catalyze the glycolytic functions.

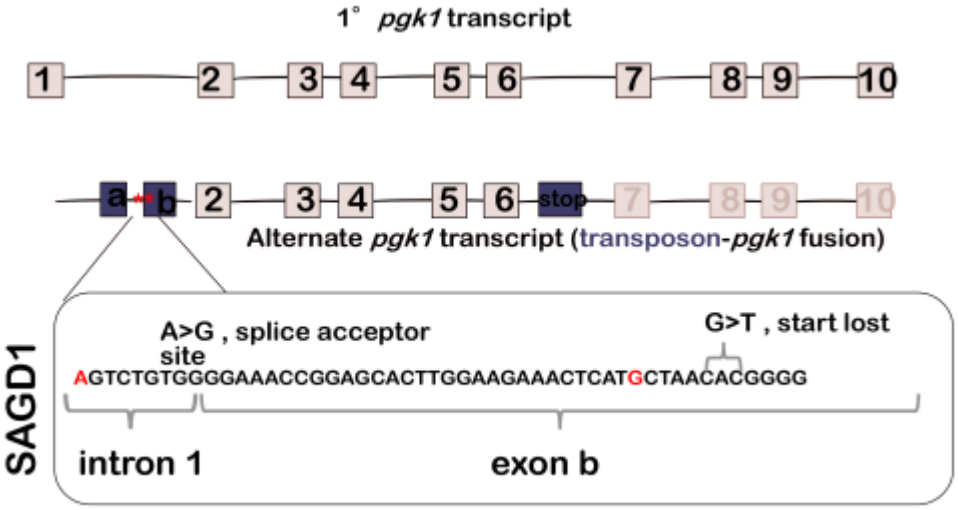

Figure 5.8. Schematic representation of the *pgk1* locus in zebrafish. Zebrafish *pgk1* has 2 different splice variants. *sagd1* mutation affects the alternate pgk1 transcript with indicated lesions.

We identified 2 linked nucleotide substitutions in the *pgk1* locus of *sagd1* mutants that affect only the alternate pgk1 transcript leading to both loss of a splice acceptor site and the start codon. First, we isolated the primary *pgk1* cDNA and produced a RNA probe which could potentially detect the presence of both of the transcripts. A low level of *pgk1* transcript was detected through the embryo, however, the expression was significantly upregulated in tissues that are affected in *sagd1* mutants such as utricular and saccular hair cells, and vestibular SAG neurons (Fig. 5.9A-F).

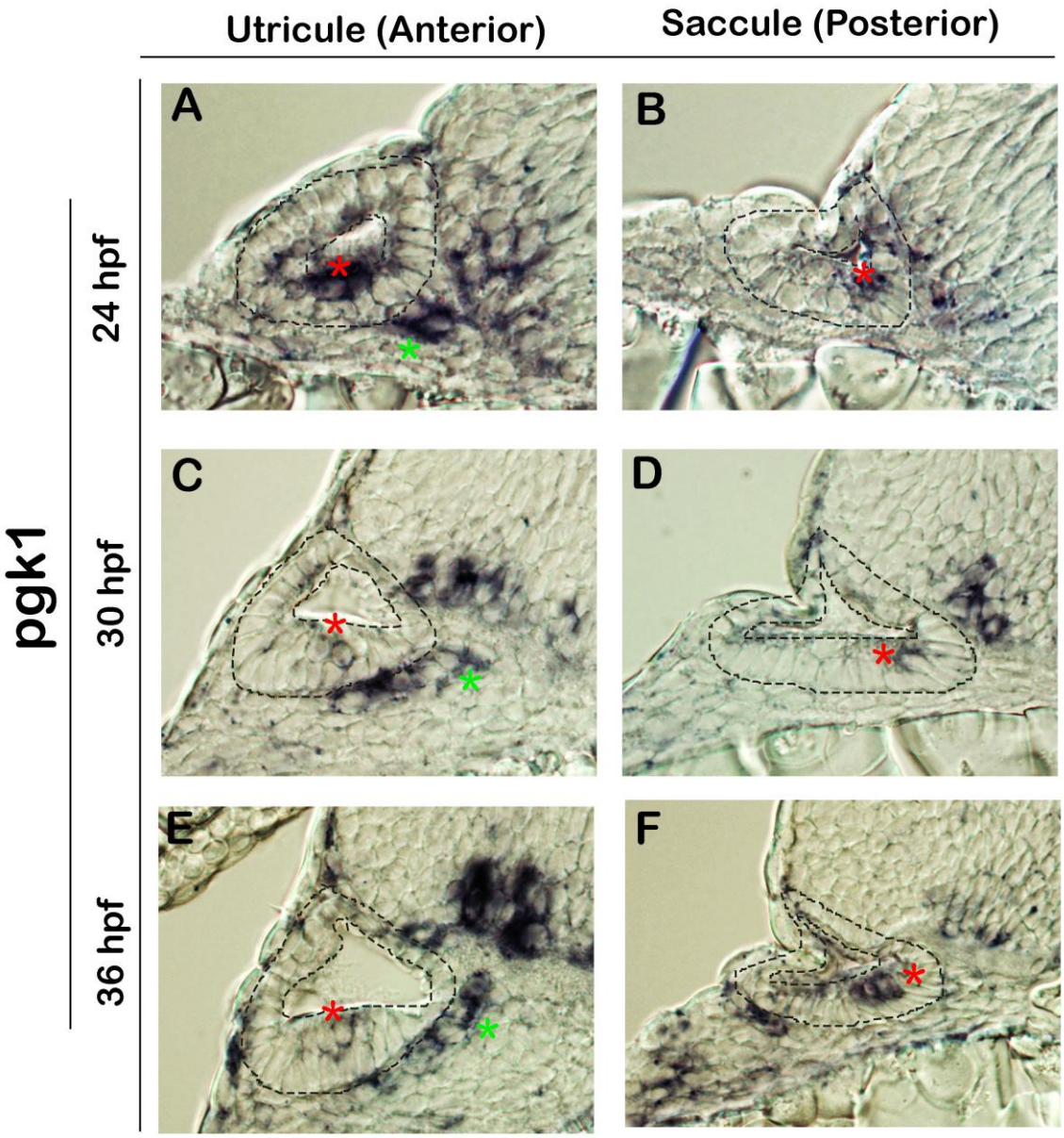

Figure 5.9. Expression of *pgk1* in the otic vesicle. (A-F) Cross sections (dorsal up, lateral left) passing through the utricle (A, C, F) and saccule (B, D, F) show *pgk1* staining in wild type embryos at indicated time points. Red asterisks indicate hair cells, green asterisks indicate vestibular SAG neurons.

We next tested the effects of disrupting and overexpressing the primary *pgk1* transcript on the development of SAG neurons. Using CRISPR-Cas9 targeting we

recovered a mutation that is predicted to eliminate only the primary *pgk1* transcript, hereby referred as *pgk1.1*. Similar to *sagd1* mutants, *pgk1.1* mutants also showed a lower level of *etv5b* expression, reduction in neurogenesis and a deficiency in the number of mature SAG neurons (Fig. 5.10A-F). Thus, the *pgk1.1* mutation strongly recapitulated all the aspects of *sagd1* mutants and resulted in a strikingly similar reduction of the total number of SAG neurons (Fig. 5.10G). We also generated a heat-shock inducible transgene to overexpress *pgk1.1* transcript and showed that the overexpression of *pgk1.1* rescues the number of SAG mature neurons to normal in *sagd1* mutants (Fig. 5.10G). We next tested whether the *pgk1.1* and *sagd1* lesions complement each other and the transcripts affected by these mutations have different functions. To examine this idea, we performed a complementation experiment by crossing a heterozygous *sagd1* carrier to a heterozygous *pgk1.1* carrier. To our surprise, the transheterozygous embryos (*sagd1*/*pgk1.1*) did not display the SAG phenotype. This result suggests the employment of unique functions for the primary and alternate *pgk1* transcripts in regulation of SAG development. Since the alternate transcript contains the segments that are predicted to regulate the stabilization of *pgk1* mRNA, we hypothesized that the main role of the alternate transcript is to protect *pgk1.1* mRNA from degradation. Consistent with this idea, *sagd1* mutants showed a decrease in the total level of *pgk1* mRNA compared to wt embryos (data not shown).

We next sought out the mechanism by which Pgk1 protein regulates Fgf signaling during SAG development. First, we examined whether Pgk1 regulates Fgf signaling cell autonomously. To test this directly we generated genetic mosaics by

transplanting wild-type donor cells into *pgk1.1* mutant host embryos. We reasoned that if Pgk1 were to act non-autonomously, wild-type donor cells would be prevented from

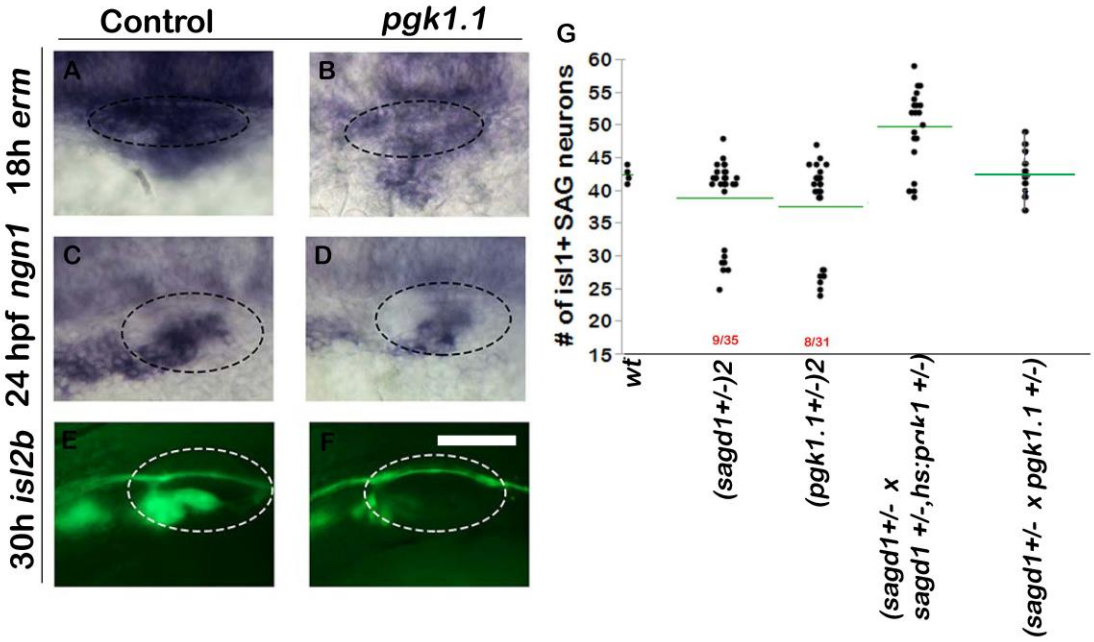

Figure 5.10. ***pgk1.1*** **mutants recapitulate the main aspects of** ***sagd1*** **mutants** (*A*,*B*) Whole-mount images (dorsal up, anterior left) show dorsolateral views of the otic vesicle (outlined) in controls and *pgk1.1* mutants for the indicated genes. Mean for the total number of *Isl1+* SAG neurons, each dot represents an embryo from the indicated crosses. 9/36 and 8/31 embryos display the mutant phenotype in a cross between two heterozygous *sagd1* and *pgk1.1* carriers, respectively. Mutant phenotype was not observed in other crosses.

responding to Fgf sources when transplanted into *pgk1.1* mutant host embryos. In support, the majority of the wt cells lost *etv5b* expression when transplanted into *pgk1.1* host embryos, indicating that Pgk1 acts non-autonomously to regulate the response to Fgf signaling (Fig. 5.11B, D, F, G). In contrast, wild-type cells showed a normal expression of *etv5b* when transplanted into wild-type host embryos (Fig. 5.11A, C, E, and G). Hence, Pgk1 non-autonomously impairs Fgf signaling in the otic vesicle.

The only well-studied function of the secreted Pgk1 protein is that it acts as a disulfide reductase and cleaves the kringle 5 domain of Plasmin to release the angiogenesis

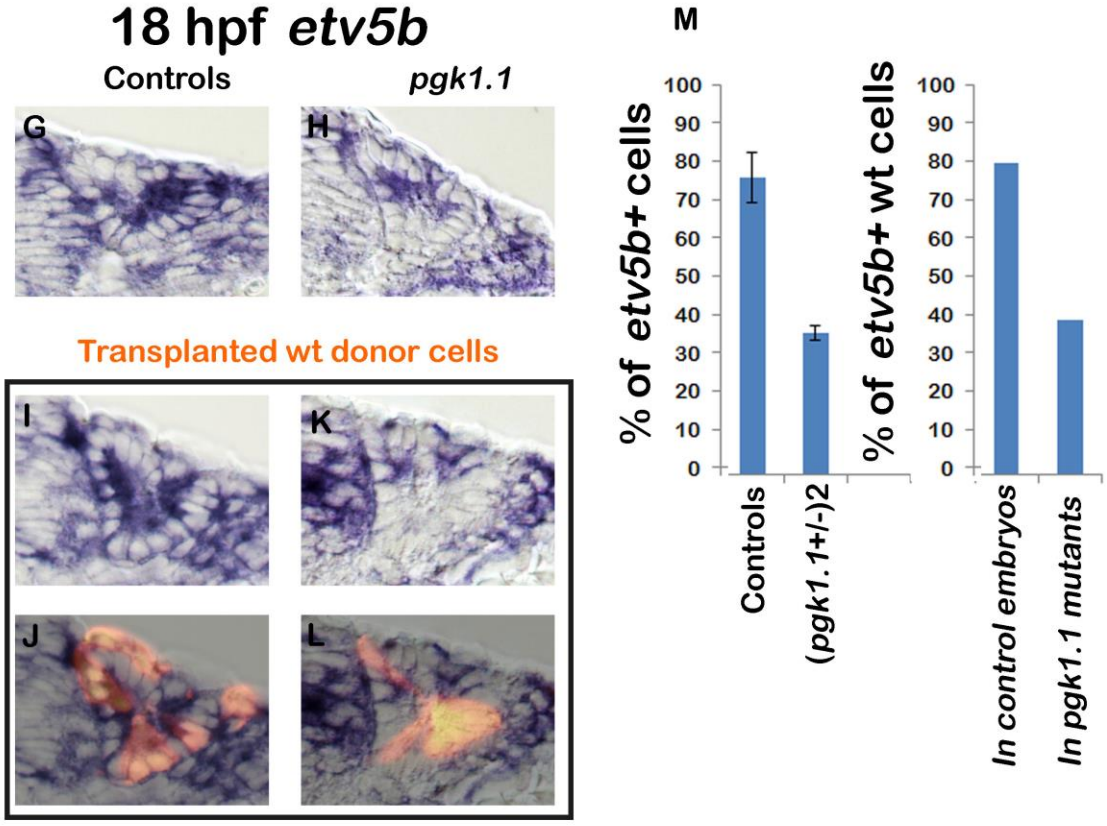

Figure 5.11. Pgk1 acts non-autonomously. (A, B) Cross sections passing through the widest part of the neurogenic domain (dorsal up, medial left) just posterior to the utricular sensory epithelium show *etv5b* staining in controls (A, C, C') and *pgk1.1* mutant embryos (B, D, D') at 18 hpf. (C, D) Dextran labelled wt cells are transplanted into control (C) or pgk1.1 mutant (D) embryos show red fluorescence. (E) Mean and standard deviation for the percentage of *etv5b*+ cells in the otic vesicle of control or *pgk1.1* embryos. (F) Mean and standard deviation for the percentage of *etv5b*+ wt cells transplanted to the otic vesicle of control or *pgk1.1* mutant embryos.

inhibitor Angiostatin (234). Plasmin is released from the liver as an inactive zymogen called plasminogen which is converted to the active form by a variety of activator enzymes. Plasmin is a serine protease that is best known for its ability to dissolve blood

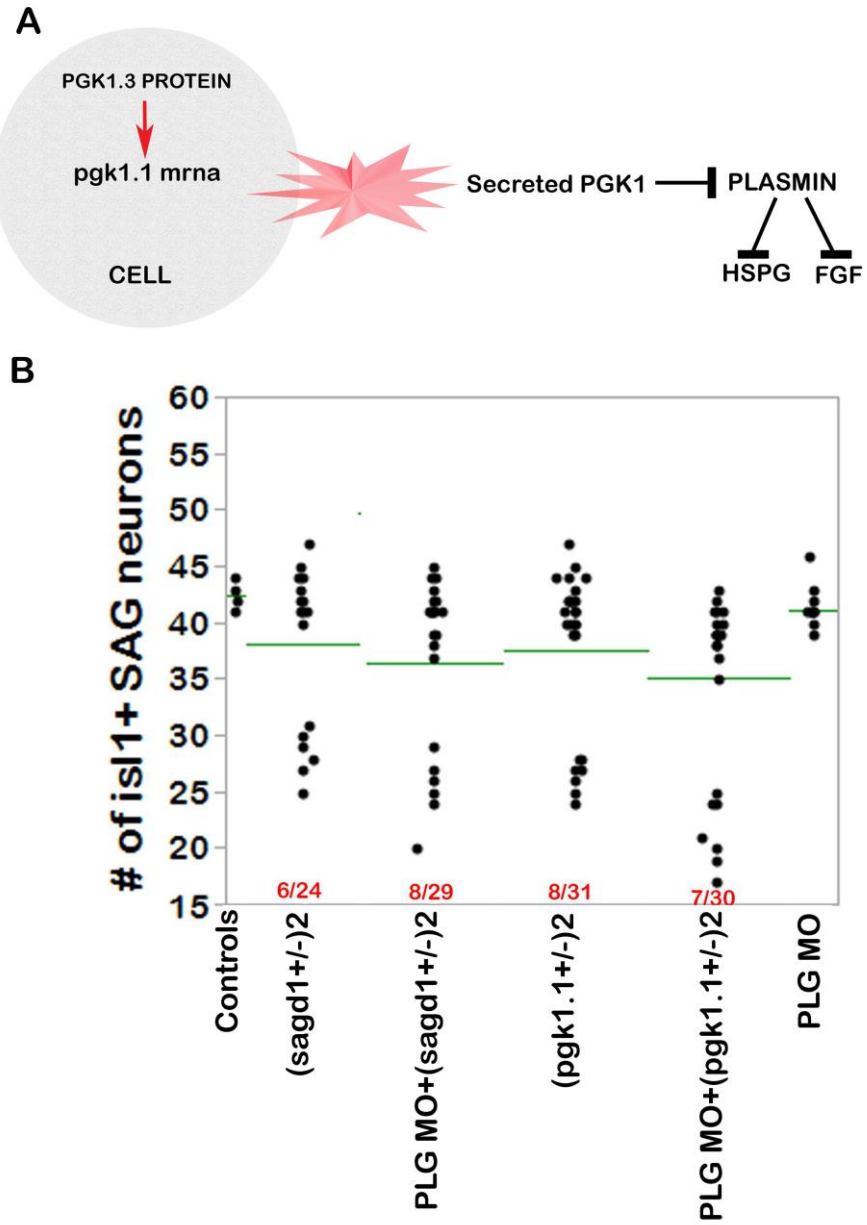

Figure 5.12. A possible mechanism for the otic function of Pgk1. A schematic respresenting the predicted role of Pgk1 in regulation of Fgf signaling during otic vesicle neurogenesis. Mean for the total number of *Isl1*+ SAG neurons, each dot representing an embryo from the indicated crosses. The number of embryos displaying the mutant phenotype in indicated crosses are shown in red.

clots by cleaving fibrin and remodeling extracellular matrix through its proteolytic activity. Interestingly, plasmin has also been shown to digest the active heparin sulfate proteoglycan (HSPG)-Fgf complexes in vitro (235). We suspected that the accumulation of plasmin in the *pgk1.1* mutants could result in the degradation of Fgf ligands and thereby lead to the deficiency of Fgf signaling observed in these mutants (Fig. 5.5). To test this, we block translation of the plasminogen (PLG) gene in *sagd1* and *pgk1.1* mutants with morpholinos to block formation and accumulation of Plasmin in these embryos. However, injection of the PLG morpholino did not rescue the number of mature SAG neurons to normal in *sad1* or *pgk1.1* mutants (Fig. 5.12).

We next investigated whether the glycolytic function of the Pgk1 plays a role in SAG development. Pgk1 activity is required for glycolysis which is a major mechanism by which cells produce ATP from degradation of glucose into pyruvate. When oxygen is available, pyruvate is shuttled into mitochondria to be further broken down for cellular ATP needs. In the absence of oxygen pyruvate is converted into lactate, in a process called fermentation. First described in cancer cells, cells with high proliferative needs undergo fermentation and produce lactate despite the abundant levels of available oxygen in a process called “aerobic glycolysis” or the “Warburg effect”. It is thought that the Warburg effect serves to generate the building blocks required for biosynthesis of the materials needed for proliferation in rapidly dividing tumor cells. However, a growing body of studies suggests that increased glycolytic activity can be a feature of normal cells and have important developmental roles (236-238).

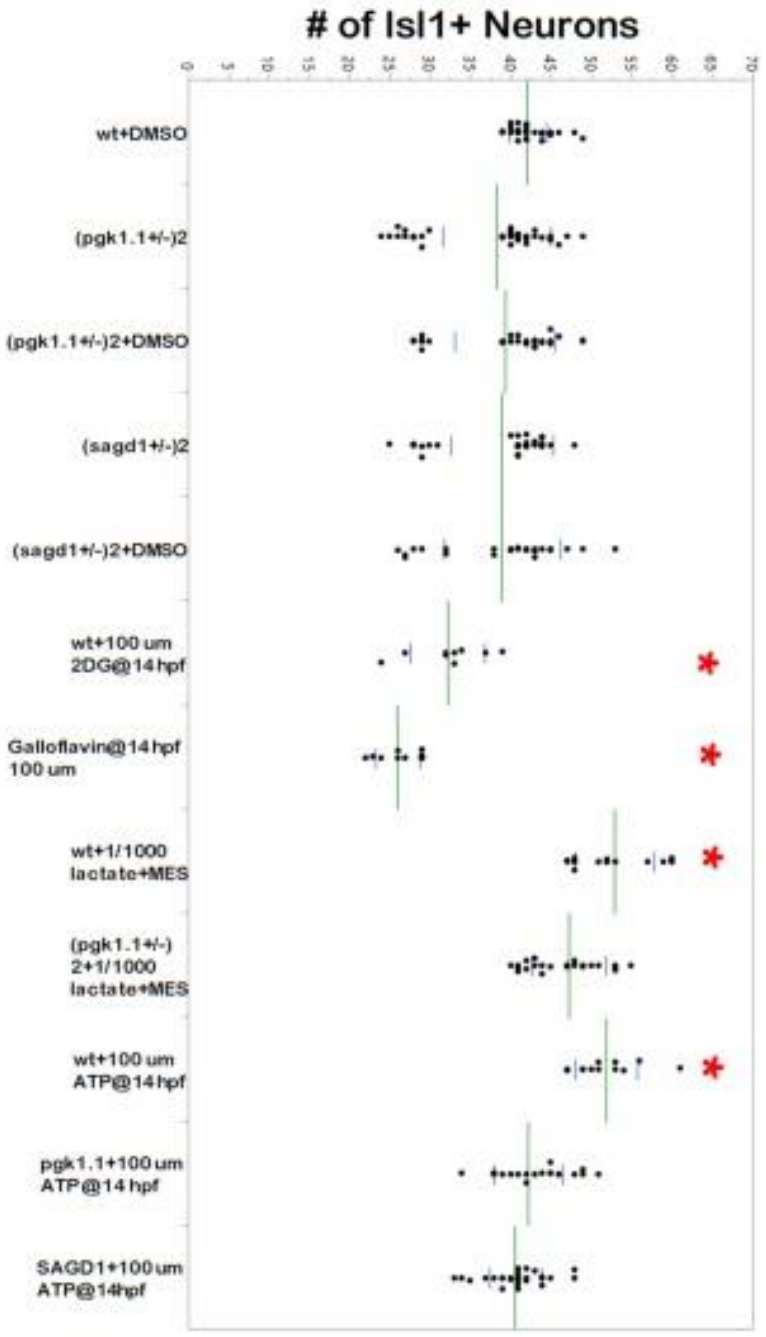

Figure 5.13. Role of Glycolysis in SAG development. Mean and standard deviation for the total number of *Isl1+* SAG neurons, each dot represents an embryo from the indicated crosses or treatments. Asterisks (*) indicate statistically significant differences compared to control embryos ($p \leq 0.05$).

To test if glycolytic activity is required for normal SAG development, we used an inhibitor of glycolysis called 2-deoxy-glucose (2DG). Treatment with 2DG at 14 hpf reduced the number of mature SAG neurons (Fig. 5.13). The number of the mature SAG neurons in 2DG treated embryos was similar to that of *pgk1* or *sagd1* mutants (Figure 13). This result suggests that impairment of glycolysis can be the causative for the SAG phenotype observed in *pgk1* or *sagd1* mutants. Glycolysis could be utilized in otic cells to produce ATP or lactate. Both deficiencies in lactate or ATP levels have been shown to affect MAPK signaling, despite each molecule regulate the pathway via different mechanisms (239, 240). Interestingly, addition of either ATP or lactate rescued the number of SAG neurons to normal in *sagd1* or *pgk1* mutants (Fig. 5.13). Furthermore, lactate or ATP treatments of wild type embryos displayed a significant increase in the number of mature SAG neurons. To test whether production of lactate is required for normal SAG development we used galloflavin, an inhibitor of the enzyme Lactate Dehydrogenase which converts pyruvate into lactate. Galloflavin treatment is predicted to inhibit lactate formation without affecting glycolytic production of ATP through glycolysis. Intriguingly, galloflavin treated embryos displayed a reduction in SAG neurons similar to *pgk1* or *sagd1* mutants (Fig. 5.13).

Because *pgk1* and *sagd1* mutants show a deficiency in accumulation of mature SAG neurons due to impaired MAPK signaling, we tested whether MAPK signaling was impaired in galloflavin treated embryos and investigate the role of lactate in potentiating MAPK signaling. Indeed, galloflavin treated embryos displayed a reduction in *etv5b* expression (data not shown). To further test the role of lactate in MAPK signaling we

treated wild type embryos with lactate and observed a significant upregulation of *etv5b* expression (Fig. 5.14A, B). Next we tested whether lactate can activate MAPK signaling in the absence of Fgf signals. We inhibited the Fgf pathway by overexpression of a dominant negative Fgf receptor construct (*hs: dnfgfr1*), which strongly decreased *etv5b* expression in the otic vesicle (Fig. 5.14C). Importantly, lactate treatment enhanced *etv5b* expression in *hs:dnfgfr1* embryos, showing that lactate can activate the MAPK pathway (Fig. 5.14D). Treatments with ATP fail to produce similar results (data not shown) suggesting that ATP affects SAG development through mechanisms independent of MAPK signaling.

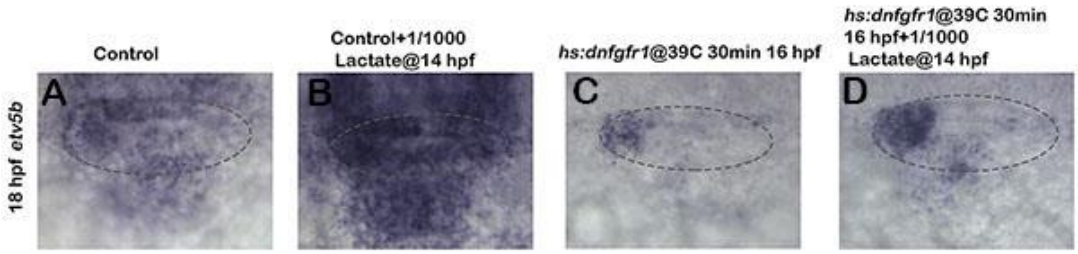

Figure 5.14. Lactate treatment enhances MAPK signaling. (*A-D*) Whole-mount images (dorsal up, anterior left) show dorsolateral views of the otic vesicle (outlined) in indicated phenotypes and treatments for the expression of *etv5b* at 18 hpf.

Overall, our results suggest that glycolytic activity and lactate production is upregulated in the otic vesicle and potentiates MAPK signaling during SAG neurogenesis.

DISCUSSION

Here we report the results from an ENU mutagenesis screen in zebrafish conducted to identify novel regulatory genes of SAG development. First, we describe a

novel mutation, *sagd1*, which impairs development of the vestibular SAG neurons but does not affect auditory neurons. Characterization of the *sagd1* mutants showed a temporary impairment of Fgf signaling during early SAG neurogenesis, yielding a deficiency in the early-forming vestibular neurons. Fgf signaling returns to normal at subsequent stages, allowing normal development of auditory neurons. The *sagd1* mutation is mapped to *pgk1* locus and CRISPR mediated targeted knock down of Pgk1 phenocopies our *sagd1* mutants. Furthermore, overexpression of *pgk1* rescues *sagd1* mutants. Third, we showed that Pgk1 impairs Fgf signaling non-autonomously. Wild-type cells lose expression of the Fgf target gene, *etv5b*, when transplanted into *pgk1.1* mutant host embryos. Moreover, overexpression of *fgf8* fails to rescue SAG neurons to normal in *sagd1* mutants, suggesting that Pgk1 impairs Fgf signaling independently from the amount of the Fgf ligand. The mechanism by which Pgk1 regulates Fgf signaling involves lactate production through a modified form of glycolysis.

Segregation of Auditory and Vestibular Neurons

Fate mapping studies in mouse and chick embryos show that early delaminating *ngn1*-positive neuroblasts contribute almost exclusively to the vestibular ganglion whereas later forming otic neuroblasts generate auditory SAG population (113, 114). It is likely that the signaling environment in the otic vesicle changes from the early to late neurogenesis, inducing transcription factors that condition the otic neuroblasts to generate the auditory SAG lineages. In this regard, inhibition of the Sonic Hedgehog (Shh) pathway has been shown to specifically reduce the auditory SAG population (107,

241). For example, the transcription factor Gata3 has been shown to regulate specification, wiring and maintenance of auditory SAG neurons in mouse and chick embryos (142, 145, 146, 242, 243). Interestingly, ear specific known down of Shh signaling strongly reduces Gata3 expression in the mouse otocyst (241). Future studies might shed light on how Hh signaling regulates segregation of SAG neural lineages in zebrafish and the role of *gata3* in this process.

Many studies also suggest spatial segregation of otic neuroblasts into vestibular and auditory locales in the otic vesicle during SAG formation (114, 242). In this regard, it is suggested that neuroblasts that contribute to the vestibular lineage delaminate from anterior-lateral parts of the otic vesicle whereas auditory precursors delaminate from posterior-medial locations (114, 242). It is important to note that, in zebrafish *ngn1*-positive cells are mostly found in anterior-lateral portions in the otic vesicle early on, however, as the development precedes *ngn1* domain shifts to posterior-medial otic vesicle. This is most likely due to the changes in the level of Fgf signaling in the otic vesicle. Early on, neurogenesis is most active in the regions adjacent to the anterior macula. As development progresses, the macula grows in size and produces a higher level of ligands which increases Fgf levels in the adjacent regions. Since high levels of Fgf signaling inhibits otic neurogenesis, the growth of the macula and the subsequent rise in Fgf signaling most likely pushes the ngn1 domain to further posterior and medial locations in the otic vesicle. This temporal shift in the *ngn1* domain likely accounts for the proposed segregation of auditory and vestibular precursors in the otic epithelium. It is also noteworthy that *sagd1* mutants show a deficiency in the *ngn1*-positive cells at

both the anterior and posterior half of the otic vesicle in the early stages, suggesting that both of these regions contribute to the vestibular ganglion during early neurogenesis. Moreover, during late neurogenesis *sagd1* mutants show a recovery in the number of both anterior and posterior *ngn1*-positive neuroblasts which are assumed to contribute to the auditory SAG population.

Evolution of the Pgk1 Locus

Evolution of new genetic traits by transposon mediated integration into the gene regulatory sequences or coding regions was suggested more than 40 years ago. In this regard, DNA repeat elements were commonly found in the DNA binding regions of many transcription factors, expanding the regulatory repertoire of these elements (244-246). Moreover, integration of transposable elements into cis regulatory regions has been shown to induce new expression patterns for the afflicted genes and contribute to the neofunctionalization and evolution of new characteristics (244-246). Integration of the DNA repeat elements into mRNAs is also commonly seen in mammalian genomes enhancing the versatility and variability of the resulting proteins (244-246). In many cases these integration events are represented in alternate splice variants due to selection against disruption of the intact coding regions (244-246). Here we describe the insertion of a DNA repeat element into *pgk1* locus which resulted in the transcription of an abundant alternative transcript, possibly with an enhancing functionality in the mRNA binding function of Pgk1. The loss of the nucleotide binding domain in the alternate *pgk1* transcript most likely disables glycolytic functions of the resulting peptide, availing

this protein for other functions, such as regulation of mRNA stability (228-230). This described transcription event is unique to the zebrafish genome and is not found in the even closely related fish species (233). Conceivably, other genomes coopted different methods to enhance Pgk1 protein levels such as the modification of the cis regulatory regions or coding sequences. Accordingly, 5' upstream sequences greatly diverge between zebrafish and mammalians and even between some of the closely related fish species (233).

Functions of Pgk1

Pgk1 is characterized as a "moonlighting protein" due to its many diverse, mechanistically different functions. For example, mitochondrial Pgk1 has been shown to inhibit mitochondrial pyruvate metabolism by acting as a protein kinase during tumorigenesis when cellular energy is predominantly produced by a high rate of glycolysis rather than oxidative respiration (Warburg effect) (247). Pgk1 is also identified as a primer recognition protein that participates in the lagging strand DNA replication (248). Pgk1 is secreted from cancer cells as a free soluble protein through oncotic pores in response to a decrease in the extracellular protein concentrations (249). Extracellular Pgk1 cleaves the serine protease plasmin and generates the angiogenesis inhibitor angiostatin (234). Plasmin is a protease and is known to digest Fgf-HSPG complexes in vitro (234, 235). We investigated whether plasmin is involved in the mechanism by which Pgk1 regulates MAPK signaling. This model predicts accumulation of plasmin in *sagd1* and *pgk1.1* mutants which could lead to excess

removal of Fgf-HSPG complexes. To test this model, we injected plasminogen MOs into sagd1 and pgk1.1 mutants and examined SAG phenotypes for a possible rescue. However, injection of plasminogen MOs fails to rescue these mutants, suggesting a different mechanism for regulation of otic development by Pgk1 function.

Pgk1 is best known for oxidizing 1, 3-diphosphoglycerate to 3-phosphoglycerate during glycolysis. Increased glycolytic activity is a hallmark of cancer cells (Warburg effect) and cells with high proliferative needs (aerobic glycolysis) and usually attributed to the need for generation of the required building blocks for molecules. However, recent studies suggest that upregulation of glycolysis is observed in normal cells as a part of the normal developmental program (236-239, 250, 251). Here we discovered a novel mechanism in which otic cells engage in upregulated aerobic glycolysis to boost MAPK levels and enable neuroblast and hair cell formation. We show that *pgk1* is upregulated in the sensory epithelium and mature vestibular neurons. Other glycolytic enzymes also display increased levels in the otic epithelium (252). We investigated role of the two important products of aerobic glycolysis: ATP and lactate and we showed that lactate can enhance MAPK signaling in the otic vesicle, even in the absence of signaling through Fgf ligands. Overall, our results suggest a novel role for glycolysis and lactate in potentiation of MAPK signaling in otic development.

A threshold level of Fgf signaling specifies neural fates in the otic vesicle; however, expression of *ngn1* precedes expression of Fgf ligands in the otic vesicle (132). It is likely that MAPK pathway is activated prior to the onset of Fgf ligand expression in the otic vesicle. In this regard, MAPK activation through lactate signaling could be vital

for accumulation of the Fgf responding genes *etv5b* and *pea3* which also serve as downstream effectors of Fgf signaling. We have shown that lactate can stimulate MAPK pathway following overexpression of *hs:dnfgfr1*, a condition that strongly downregulates signaling through Fgf ligands. It is likely that early accumulation of Etv5b and Pea3 proteins in the otic vesicle through lactate induced MAPK pathway is important for generating a quick and robust signal after Fgf ligands begin to be expressed in the otic vesicle.

CHAPTER VI

CONCLUSIONS AND DISCUSSION

In all vertebrates, SAG neurons connect the ear to the brain and transmit hearing and balance related information. SAG neurons originate in the otic vesicle (the precursor of the vertebrate inner ear) and follow a complex stepwise progression. At the first step neuroblasts turn on expression of the proneural gene *neurogenin1* (*ngn1*) which is necessary and sufficient for specification of the neural fate in the otic vesicle. Accordingly, *ngn1* loss of function leads to loss of all cranial neurons, including those of the SAG, in zebrafish. We first showed that a low level of Fgf signaling is necessary for induction of neurogenesis in the otic vesicle. Inhibition of Fgf signals by a pharmacological inhibitor or by overexpression of a dominant-negative Fgf receptor severely inhibits *ngn1* expression in the otic vesicle and decreases the number of mature SAG neurons. In similar experiments, we showed that misexpression of Fgf signaling at a low level enhances otic neurogenesis at early stages.

FGFS AS A MORPHOGEN IN OTIC SENSORY AND NEURAL DEVELOPMENT

In zebrafish, the sensory epithelium and neurogenic domains develop in adjacent regions. The sensory epithelium is the closest source of Fgf ligands (*Fgf3*/*fgf8*) to the

otic vesicle and likely provides the necessary level of Fgf signals for neurogenic development. Expression of Fgf responding genes in the otic vesicle follows a predicted pattern, where highest levels of *etv5b, pea3* and *sprty4* expression are observed in the sensory epithelium, lower levels of *etv5b, pea3* and *sprty4* are observed in the neurogenic domain (132, 181). It is likely that Fgf ligands act as morphogens in otic development, since a high level of the signal is required for sensory development and a low level of the signal initiates formation of the neurogenic domain. However, whether a high level of Fgf signaling is required for development of hair or support cells has not been thoroughly investigated.

Fgf ligands act as morphogens in several contexts; they diffuse over long distances and encode positional information in target tissues. Injection of Fgf8 recombinant protein into zebrafish embryos at the 30% epiboly stage results in accumulation of the recombinant protein 12 cell diameters away and leads to induction of the Fgf responding gene, *sprty4*, up to 16 cell diameter away from the source (253). In the blastoderm margin, at the stage when *fgf8* is expressed in 8 rows of cells, the Fgf response genes *etv5b, pea3* and *sprty4* are detected in 17, 15 and 13 cell diameters away, respectively, showing that Fgf ligands can induce expression of different genes based on concentration (253).

Fgf signaling is required for proper development and patterning of the sensory epithelium (254-256). Previous studies have shown that high level overexpression of *fgf3* or *fgf8* is insufficient to expand the sensory epithelium (198). Moreover, a mild treatment of Fgf inhibitor SU5402 enhances sensory development and increases the

number of hair cells (255). In addition, increasing the level of Fgf signals is shown to inhibit differentiation of sensory progenitor cells or support cells into hair cells (transdifferentiation) (254). Conceivably, a high level of Fgf signaling is necessary to allow proper patterning of the sensory epithelium such that the correct number and spacing of hair and support cells are established. Fgf signaling likely plays a similar role in the neurogenic otic domain. Lowering the level of Fgf signaling by a pharmacological inhibitor increases the specification events by increasing the number of *ngn1*+ cells in the otic vesicle and also stimulates differentiation of *neurod*+ transit-amplifying cells into mature SAG neurons. Also, high level overexpression of Fgf ligands slows down both production and differentiation of SAG neuroblasts. Regardless, it is unclear whether the amount of Fgf signaling required to correctly pattern sensory epithelium versus neurogenic domain is different. Future studies to examine both sensory and neural development following treatments that lower or rise Fgf signaling could determine whether Fgf ligands act as a morphagen in the otic vesicle.

THE ROLE OF PAX GENES

Differences in Fgf level requirements likely stems from the need for distinct sets of transcription factors for sensory versus neural development in the otic vesicle. For instance, *pax2a* and *pax5* genes are both important for sensory development and respond to a high level of Fgf signaling. Epithelial integrity of the sensory cells is possibly jeopardized in *pax5* or *pax2a* mutants, since sensory cells are either lost from the otic epithelium or undergo apoptosis (205, 206). This could stem from the EMT-inducing

roles of Fgf signaling. Fgf signaling is shown to induce cell migration in several instances and increased Fgf levels are correlated with metastatic properties of tumor cells (257-259). In the third chapter we show that Fgf signaling induces expression of *gsc*, a key player in EMT during otic neurogenesis (231). It is likely that high levels of Fgf signaling become detrimental to epithelial integrity of the sensory cells in the absence of the *pax2* and *pax5* genes. In this regard, examination of the otic epithelial architecture in *pax2*/*pax5* mutants following misexpression of Fgf signals could be informative. We also show that overexpression of *pax2a* stabilizes otic epithelia and inhibits EMT during otic neurogenesis (231). This role of Pax2a is likely indispensable for the development of the sensory cells under high Fgf conditions. The spatial domain of *pax* genes is completely excluded from the neurogenic domain in the otic vesicle and overexpression of *pax2a* in the neurogenic domain has deleterious effects. Overexpression of *pax2a* strongly blocks EMT of SAG neruoblasts and leads to formation of a much smaller SAG (231). We also showed that overexpression of *pax2a* strongly represses *gsc* expression in the otic vesicle and thereby reduces EMT events in the otic epithelium (231). It is likely that *pax* genes are not expressed in the neurogenic domain due to the lack of a high level of Fgf signaling that is required for activation of *pax* genes. Accordingly, in a recent study using microarrays, it was shown that Fgf treated chick otic ectoderm samples display a 7.3 fold upregulation in *pax2a* expression (260).

FORMING AN FGF GRADIENT IN THE OTIC EPITHELIUM

As mentioned earlier, Fgf ligands form a sharp gradient in the otic vesicle; a strong *etv5b* expression is detected in the sensory epithelium whereas *etv5b* level drops dramatically in the neighboring neurogenic domain. Diffusion of the Fgf ligands is controlled at multiple levels. Spreading of the Fgf ligands is shown to be restricted by endocytosis (253). Conditions that block endocytosis increase the extent of the Fgf responding genes whereas conditions that stimulate endocytosis clear Fgf protein from the extracellular space and restrict its spreading (253). Thus, endocytosis determines the concentration of Fgf ligands in the extracellular space and affects the width of the target tissue responding to Fgf signaling. Small GTPases of the Rab family label the clathrin-coated endocytosis vesicles and play a role in the tethering and fusion of the vesicles (261). Accordingly, Rab5a is shown to regulate endocytosis of Fgf ligands and is strongly expressed in the otic vesicle (252, 253). Futures studies to analyze detailed expression of *rab5* and other endocytosis regulators in the otic vesicle could aid in understanding how a sharp Fgf gradient is formed. Additionally, diffusion of Fgf ligands in the extracellular matrix is regulated by heparin sulfate proteoglycans (HSPGs) and the length or sulfation level of heparin sulfate structures associated with Fgf ligands can greatly affect the level of Fgf signaling (262).

IMPORTANCE OF FGF LIGAND SPECIFICITY

Several different Fgf ligands regulate SAG development. A low threshold of Fgf signaling is necessary to initiate neurogenesis. Most likely, *fgf3* and *fgf8* expressed in the

utricular macula meet this requirement as the closest Fgf source. However, Fgf signals from the tissues surrounding the otic vesicle could also contribute to SAG development. Overexpression of *fgf3* or *fgf8* results in similar SAG phenotypes and suggests that Fgf ligand specificity is not critical in SAG development (132). At later stages of SAG development, mature SAG neurons express *fgf5*, which contributes to the increasing levels of Fgf signaling and shuts down neurogenesis in the otic vesicle (132). Similarly, overexpression of *fgf3* or *fgf8* at later stages inhibits neurogenesis, suggesting that the level of Fgf signaling, rather than the specificity of the Fgf ligands, regulates SAG neurogenesis. To shed light on the importance of Fgf ligand specificity in SAG development, gene replacements to swap *fgf5* with *fgf3* or *fgf8* using homologous recombination mediated TALEN or CRISPR-CAS9 editing could be utilized and effects on SAG neurogenesis can be examined. In this regard, it is interesting that mutations in *fgfr2* versus *fgfr3* result in different inner ear phenotypes in mouse (82, 83). Accordingly, ligand specificity of the Fgf receptors and their expression levels has been studied extensively in the mouse inner ear to explain the resulting phenotypes of mutations in different Fgf receptors (81, 82). However, in zebrafish all Fgf receptors are expressed in the developing otic vesicle and it is currently unknown if the ligand specificity of each receptor plays a role in otic development (263-266).

REGULATION OF THE TRANSIT-AMPLIFYING STAGE DURING SAG DEVELOPMENT

Specification of neuroblasts takes place in a very short time window in the otic vesicle. Specified neuroblasts leave the otic vesicle and slowly cycle as they mature and differentiate into SAG neurons. The number of cells in the transit-amplifying pool stays constant throughout early development and the rate of proliferative renewal matches the rate of loss from the TA pool as cells differentiate (132). Thus, once a stable number of TA cells are formed, specification of neuroblasts in the otic vesicle is no longer required and TA cells can serve as a continuous supply for new SAG neurons. Mature SAG neurons help maintain this homeostatic state by expressing *fgf5* which both regulates the rate of differentiation in the TA pool and specification of neuroblasts in the otic vesicle (132). In *fgf5* morphants, the number of specified neuroblasts increases and termination of SAG neuroblast specification is delayed (132). The same phenotype is observed when Fgf signaling levels are lowered by a pharmacological inhibitor of the pathway or overexpression of a dominant-negative Fgf receptor (132). Overall, these data indicate that increasing Fgf levels during SAG neurogenesis regulates termination of the specification events in the otic vesicle. Importantly, laser ablation of the mature neurons also delays termination of neurogenesis in the otic vesicle (132). This confirms that mature neurons play a significant role in regulation of the SAG tissue size.

Fgf signaling also regulates the differentiation rate of the transit amplifying cells: conditions that block Fgf signaling increases the number of mature neurons at the expense of TA cells (132, 181). At later stages, a high level Fgf signaling provided by

mature neurons is likely required to prevent premature differentiation of TA cells to the mature neurons and maintain sufficient cycling progenitors in the TA pool. In *fgf5* morphants, initially a larger TA pool is formed due to failure of termination of neuroblast specification in the otic vesicle (132). However, it is predicted that this condition will result in depletion of TA cells in the long term, since the TA cells will quickly differentiate into mature neurons in the absence of high Fgf signaling and deplete the cycling TA neuroblasts. Future studies to generate *fgf5* mutants or time specific knock down of *fgf5* will likely show the indispensable role of mature neurons in regulating the size of the TA pool.

Notch signaling also plays an important role in regulation of the SAG tissue size. Inhibition of Notch signaling enhances neurogenesis in the otic vesicle and also stimulates differentiation of TA cells into mature neurons (181). Proneural genes expressed by the SAG neuroblasts, *ngn1* and *neurod*, activate expression of Delta ligands to aid in temporal control of the pace of SAG development (181).

We have shown that otic neuroblasts leave the otic epithelium and form a stable stem cell pool to provide new SAG neurons at a constant rate until at least 5 dpf (132). It is currently unknown how long new SAG neurons are produced in zebrafish. Zebrafish forms new hair cells until adulthood and can regenerate lost hair cells (19, 267). Possibly, the ability to produce new SAG neurons to connect newly forming hair cells to the information processing centers also exists in adult zebrafish. Conceivably, TA cells also exist in larval or adult stages of zebrafish to maintain the ability to produce new SAG neurons. Maintenance of the TA cells is regulated by Fgf and Notch signals. We

showed that overexpression of both Fgf and Notch pathways increases the number of proliferating SAG progenitors in the TA pool and delays further differentiation, whereas downregulation of both signals induces premature differentiation of these progenitors into mature neurons and depletion of the TA pool (181). Future studies to examine adult zebrafish SAG neurons could determine whether Fgf and Notch signals are maintained through development to conserve a self-preserving TA pool where the number of proliferating progenitors matches the number of newly forming neurons. However, in fish species of similar size, only a few hundred SAG neurons have been detected in adulthood. It is also likely that the differentiation rate of SAG neuroblasts declines with age and stops when sufficient neurons are produced. High Fgf5 levels provided by mature neurons could also signal for the final tissue size of SAG and regulate the size of the TA pool or differentiation of the TA progenitors accordingly. It is currently unknown whether *fgf5* expression is maintained in mature SAG neurons through larval stages. Future studies to examine the genes expressed in adult SAG neurons and whether the TA precursors exist in mature zebrafish could aid in answering these questions.

NOVEL ROLE OF TFAP2A AND BMP SIGNALING IN OTIC NEUROGENESIS

We show that additional factors aid in regulation of Fgf and Notch signaling during SAG development. For instance, ventral otic cells express *tfap2a*, which indirectly modulates Fgf and Notch pathways by activating the expression of *bmp7a* (181). In *tfap2a* mutants, loss of *bmp7a* expression from the otic epithelium leads to an increase in Fgf and Notch levels that stalls SAG development. Furthermore,

overexpression of *tfap2a* activates *bmp7a* expression and stimulates SAG development through lowering Fgf and Notch levels. It is likely that the level of Fgf and Notch signals quickly rises during development and regulation by *bmp7a* is necessary to avoid premature termination of specification in the otic vesicle or prolonged cycling of the TA precursors. Simultaneous activation of Fgf and Notch pathways at high levels increases the number of the proliferating TA neuroblasts. However, this severely disrupts their differentiation into mature neurons (181). This phenotype is consistent with the increase in the size of the TA pool observed in *tfap2a* mutants, due to the increased level of Fgf and Notch signaling observed (181). Treatment with dorsomorphin, a pharmacological inhibitor of the BMP pathway, blocks the effects of *tfap2a* overexpression suggesting that Tfap2a regulates SAG development through activating BMP pathway. However, a direct analysis of Bmp7a function is currently lacking from our analysis. Future studies to induce time specific knock down or overexpression of *bmp7a* could show a direct function for this gene in regulation of the pace of SAG neurogenesis.

The interplay between the Fgf and Bmp pathways has been shown in several instances. In the otic vesicle, expression of the Fgf ligands does not change in *tfap2a* mutants although *bmp7a* expression is lost and there is a significant increase in the expression level and domain of the Fgf responding gene *sprty4*. This result is consistent with other studies showing that Bmp signaling antagonizes Fgf signaling. In Xenopus animal cap cells, overexpression of the Bmp inhibitor Noggin, results in increased levels of phosphorylated MAPK (ERK), a downstream effector of Fgf signaling (268). Moreover, overexpression of Bmp ligands inhibits expression of Fgf-induced

downstream neural markers (268). The BMP pathway regulates Fgf signaling during early neural patterning by suppressing *flrt3* expression, a positive regulator of the pathway. *flrt3* knockdown inhibits Fgf induced ERK phosphorylation and *flrt3* overexpression recovers inhibition of Fgf pathway by BMP signals (268). Flrt3 is a transmembrane protein that interacts with Fgf receptors and positively modulates MAPK response and expressed in the otic vesicle in zebrafish (265). The temporal and spatial modulation of Fltr3 could serve as the basis for inhibition of Fgf signaling by BMP pathway during SAG development. Functional studies to knock down or overexpress *flrt3* could shed light on the mechanism by which BMP lowers Fgf signal transduction in the otic vesicle.

Even though the crosstalk between the Fgf and Bmp pathways has been studied intensively during early embryonic development and later in tissue modeling, an interaction between the Notch and Bmp pathways has not been studied in detail prior to our study (231). We show that overexpression of *tfap2a* downregulates expression of delta ligands *deltaA* and *deltaB* via regulating BMP pathway (231). Inhibition of Bmp pathway by a pharmacological inhibitor rescues this inhibitory effect of *tfap2a* on Notch signaling. Possibly, *deltaA* and *deltaB* genes share common enhancer element that could be bound by activated BMP effectors.

ROLE OF GSC IN OTIC NEUROGENESIS

We have identified Spemann organizer gene Gsc as a major regulator of epithelial-mesenchymal transition (EMT) during SAG neurogenesis (231).

Overexpression of *gsc* enhances the number of delaminated SAG neuroblasts whereas *gsc* knockdown diminishes the ability of SAG neuroblasts to leave the otic epithelium (231). Most likely, the mechanism by which *gsc* enhances EMT involves repression of *cadherin1* (*E-cadherin*), however, the direct functional link between *cadherin1* downregulation and increase in EMT events is currently lacking from our analysis. Future studies to generate transgenic lines to temporally overexpress or knockdown *cadherin1* could provide additional support for this hypothesis. It is also likely that *gsc* regulates expression of additional genes that are important for EMT during otic neurogenesis. We showed that the tight junction protein ZO1 immunoflourescence is decreases following overexpression of *gsc* (231). This difference in ZO1 protein levels could stem from repression of *zo1* transcription by Gsc. Similarly, other genes that regulate formation and maintenance of the tight or adherens junctions could be regulated by Gsc function in the otic vesicle. Chromatin immunoprecipitation assays could identify potential targets of Gsc in the otic vesicle and help to determine the mechanism by which Gsc enhances EMT.

THE FUNCTION OF PGK1 AND GLYCOLYSIS IN SAG DEVELOPMENT

We identified the glycolytic enzyme Pgk1 as a regulator of neurogenesis in the otic vesicle. *pgk1* mutants produce too few SAG neurons. This effect stems from a transient deficiency in early MAPK signaling. For example, *pgk1* mutants show a lower level of *etv5b* expression between 18-24 hpf in the otic vesicle. With mosaic analysis, we observed that wild type cells lose expression of the Fgf responding gene, *etv5b,* when

transplanted into *pgk1* mutants. This finding suggests that Pgk1 non-autonomously regulates Fgf signaling in the otic vesicle. This finding raised the possibility that a moonlighting function of the secreted Pgk1 could potentiate downregulation of Fgf signaling. The only known role of the secreted Pgk1 protein is the cleavage of the kringle 5 domain of the Plasmin protein, a protease that is known to digest (HSPG)-Fgf complexes in vitro (234, 235). We have examined the possibility of regulation of Fgf signaling by Pgk1 through modulation of Plasmin protein levels. This model predicts that Plasmin protein accumulates in *pgk1* mutants thereby causing the excess removal of active Fgf-HSPG complexes. However, injection of morpholinos against *plasmin* failed to rescue *pgk1* mutants suggesting a different mechanism of action for Pgk1 during otic neurogenesis.

GLYCOLYTIC FUNCTION OF PGK1

The main function of Pgk1 is oxidation of 1, 3-diphosphoglycerate to 3-phosphoglycerate during glycolysis. Pgk1 activity is indispensable for glycolytic activity, which is a major mechanism in cells to produce ATP from degradation of glucose to pyruvate. When oxygen is available, pyruvate is transported into mitochondria and converted into acetyl-coA, which is then further oxidized to generate ATP. In the absence of oxygen, pyruvate is converted to lactate in a process called fermentation.

Through investigation of Pgk1 function , we discovered a novel mechanism in which otic cells engage in a modified form of glycolysis called the “Warburg effect”

(269). First described in metastatic tumors, the Warburg effect describes a metabolic shift into fermentation where pyruvate is converted into lactate instead of being shuttled to mitochondria for ATP production, despite the presence of abundant oxygen (269). Glycolysis can serve to generate the building blocks required for biosynthesis such as acetyl-coA for making fatty acids or ribose for making nucleotides. That is why it is thought that glycolysis is mainly used in cells with high proliferative needs to produce the glycolytic intermediates required for proliferation. However, many recent studies suggest novel roles for glycolysis during the developmental course of normal cells (250, 251). For example, during early development of the mouse embryo a major metabolic shift takes place during implantation when the embryos begin to increase the glycolytic activity and lactate production (270). As development proceeds, this intense glycolytic activity is replaced during organogenesis with oxidative phosphorylation (271). High glycolytic activity is thought to coincide with high proliferative activity during early mouse embryogenesis, however, a high rate of proliferation is also observed during organogenesis when glycolytic activity begins to decrease, thus suggesting another role for this high glycolytic activity.

Growing evidence suggests that the Warburg effect can be a feature of normal cells during embryogenesis and have important developmental roles. For instance, inhibition of the aerobic glycolysis in the Xenopus retina by a pharmacological inhibitor reduces proliferation and differentiation of the retinal progenitors even though ATP levels are maintained normal with oxidative phosphorylation (272). Moreover, Wnt

proteins are shown to regulate glycolytic activity and induce the Warburg effect during bone formation and thereby regulate osteoblast differentiation (250).

ROLE OF GLYCOLYSIS IN OTIC NEUROGENESIS

These studies suggest that the glycolytic function of Pgk1 might have a regulatory role during otic development. Accordingly, expression of many other glycolytic enzymes also increases in the otic epithelium at neurogenic stages suggesting the presence of high glycolytic activity during the development of SAG neurons (252). The enzymes with increased otic expression include central glycolysis regulators such as *pgk1* (Chapter V), *hexokinase 1*, *hexokinase 2* and *phosphofructose kinase* (252). Future studies will aim to test whether knockdown of these genes would also give rise to similar SAG phenotypes as *pgk1* mutants.

A temporal decrease in early Fgf levels in *pgk1* and *sagd1* mutants causes formation of too few SAG neurons. Several recent studies suggest a functional link between upregulation of glycolytic activity and Fgf signaling during development. For instance, in the presomitic mesoderm (PSM) a gradient of glycolytic activity regulates Fgf signaling and plays an indispensable role in posterior elongation of the embryonic axis in an ATP independent manner (251).

A possible link between glycolysis and Fgf signaling is provided by studies of hypoxia induced responses. Hypoxia responses enable cells to adapt to harsh environmental conditions such as low oxygen availability and mainly regulated by hypoxia inducible factors (HIFs) (273). Many of the functions of HIF factors include

regulation of metabolic pathways, oxygen delivery and pH and impact cell proliferation and survival (273). One of the immediate responses to hypoxia, upregulation of glycolysis and inhibition of Kreb's cycle, is mediated by HIFs (273). Many downstream effectors of Fgf signaling is activated in response to hypoxia such as PI3K, AKT and ERK, although, there is no evidence linking activation of these factors to HIFs (274). Thus, the mechanism by which these elements are activated in response to hypoxia remains elusive. However, a recent study shows that a hypoxia induced gene, NDRG3, is expressed independently of HIF levels and binds to lactate to activate the MAPK pathway through Raf-c and Erk1/2 phosphorylation (239). This study provides a novel link between glycolysis and MAPK activation and suggests a novel role for lactate in regulation of hypoxia induced responses (239). Both depletion of NDRG3 and inhibition of lactate production suppress hypoxia induced activation of MAPK pathway (239). It is also shown that lactate can form complexes with NDRG3; however, the mechanism by which these complexes activate phosphorylation of Raf or Erk proteins remains unknown (239).

Lactate was once considered a metabolic waste, an end product of glycolysis. However, growing evidence suggests that it can have critical roles in maintenance of tumor growth and metastasis. Lactate also can act as a signaling molecule and enhance angiogenesis during tumor growth. Elevated levels of Lactate Dehydrogenase A, the enzyme that converts pyruvate to lactate, is a hallmark of many tumors and inhibition of this enzyme can block tumor growth in cell lines in vitro (275) and in transplanted breast tumors in vivo (276). A pharmacological inhibitor of the lactate dehydrogenase

enzymes, galloflavin, also suppresses proliferation of breast cancer cells at high concentrations (277). Lactate can also be secreted into extra cellular matrix and taken up by the cells to be used as a substrate in oxidative phosphorylation. For instance, astrocytes undergoing aerobic glycolysis secrete lactate to be used as a food source by the neurons (278). Furthermore, cancer cells can induce neighboring cells to produce and shuttle lactate to fuel their oxidative metabolism (279). Secreted lactate can also act as a signaling molecule to induce migration, tube formation and angiogenesis (280). Studies show that secreted lactate can lead to acidification of extracellular matrix and activate metalloproteases which modify the extracellular environment and to promote cell motility (281). Overall, these studies emphasize many diverse roles for glycolysis in regulation of signaling pathways during normal development and tumor growth. Our analysis of the role of *pgk1* and lactate in otic development adds to this growing body of literature and provides a concise mechanistic framework for how these studies might be generally related.

To address the role of increased glycolytic activity and lactate production during SAG neurogenesis we used an inhibitor of glycolysis, 2-deoxy-glucose (2DG) and an inhibitor of lactate synthesis, galloflavin. Both pharmacological treatments lead to a decrease in the number of mature SAG neurons, similar to the phenotypes observed in *pgk1* or *sagd1* mutants. Additionally, treatment of *pgk1* or *sagd1* embryos with lactate rescued the observed SAG phenotypes in these embryos. Importantly, multiple homologs of NDRG3 are expressed in the otic vesicle in zebrafish (252), providing further support for a possible interaction between lactate and NDRG3 to induce MAPK

signaling. Future studies to knockdown or overexpress *ndrg3* could further implicate the role of lactate-NDRG3 complexes on neurogenesis and MAPK signaling in the otic vesicle.

A low threshold level of Fgf signaling is required to specify neural fates in the otic vesicle. However, the onset of *ngn1* expression precedes expression of Fgf ligands in the otic epihelium. *ngn1* expression is first detected at ~16 hpf in the otic cells whereas *fgf3* and *fgf8* begin to be expressed at ~18 hpf. It is likely that Fgf signaling from the tissues surrounding the otic placode initiate otic neurogenesis. However, it is also likely that other ligands or signaling molecules activate MAPK pathway prior to the beginning of Fgf ligand expression in the utricle. In this regard, activation of the MAPK pathway by aerobic glycolysis through lactate production could be vital to boost this signal and activate neurogenesis in the otic vesicle. MAPK responding genes such as *etv5b* and *pea3* also serve as the downstream effectors of Fgf signaling. Early accumulation of these transcripts in the otic vesicle is likely important for generating a quick and robust signal following the onset of Fgf ligand expression in the otic vesicle. In this regard, we tested whether lactate can activate expression of *etv5b* in the absence of Fgf signaling and showed that lactate can increase *etv5b* expression following activation of *hs:dnfgfr1* construct. This result suggests a novel role for lactate signaling in activation of MAPK pathway during otic development.

To conclude, we have discovered many new regulatory mechanisms important for SAG development. First we show that a threshold level of Fgf signaling is required to initiate otic neurogenesis in the otic vesicle, however high levels inhibits specification

of otic neuroblasts. In this regard, *fgf5* expressed by the mature SAG neurons aid in termination of otic neurogenesis at late stages and regulate the overall size of the ganglion. In further studies we showed that Tfap2a has an important role in regulating the pace of SAG development such that regimens to overexpress *tfap2a* lower Fgf and Notch signaling and doubles the size of the mature SAG. We also show novel roles for Notch signaling in modulating differentiation of TA neuroblasts. We investigated the mechanism by which SAG neuroblasts leave the otic vesicle and discovered Gsc as a major regulator of the EMT events in the otic epithelium. We also showed that non-neurogenic regions of the otic vesicle are resistant to the EMT promoting function of Gsc due to the presence of the epithelializing factor Pax2a. Gsc and Pax2a have opposing roles in the otic vesicle, partially through modulation of *cadherin1* expression. Also, we conducted a mutagenesis screen and identified 2 novel genes that affect SAG development in unique ways. We identified the first mutated locus to affect the glycolytic enzyme *pgk1*. This finding suggests a novel role for aerobic glycolysis during otic development and emphasizes that Warburg affect can also modulate development of normal cells in addition to its role in promoting tumor growth and metastasis. Our analyses have filled many gaps in our understanding of SAG development through identification of novel roles for the transcription factors such as Tfap2a , Gsc and Pax2a; and through characterizing diverse functions of main signaling pathways such as BMP, Notch and Fgf .

REFERENCES

1. Baker CV & Bronner-Fraser M (2001) Vertebrate cranial placodes I. Embryonic induction. *Developmental biology* 232(1):1-61.

2. Streit A (2007) The preplacodal region: an ectodermal domain with multipotential progenitors that contribute to sense organs and cranial sensory ganglia. *The International journal of developmental biology* 51(6-7):447-461.

3. Schlosser G (2010) Making senses development of vertebrate cranial placodes. *International review of cell and molecular biology* 283:129-234.

4. Brugmann SA, Pandur PD, Kenyon KL, Pignoni F, & Moody SA (2004) Six1 promotes a placodal fate within the lateral neurogenic ectoderm by functioning as both a transcriptional activator and repressor. *Development* 131(23):5871-5881.

5. Mishima N & Tomarev S (1998) Chicken Eyes absent 2 gene: isolation and expression pattern during development. *The International journal of developmental biology* 42(8):1109-1115.

6. Xu PX, Woo I, Her H, Beier DR, & Maas RL (1997) Mouse Eya homologues of the Drosophila eyes absent gene require Pax6 for expression in lens and nasal placode. *Development* 124(1):219-231.

7. Ahrens K & Schlosser G (2005) Tissues and signals involved in the induction of placodal Six1 expression in Xenopus laevis. *Developmental biology* 288(1):40-59.

8. Litsiou A, Hanson S, & Streit A (2005) A balance of FGF, BMP and WNT signalling positions the future placode territory in the head. *Development* 132(18):4051-4062.

9. Kwon HJ, Bhat N, Sweet EM, Cornell RA, & Riley BB (2010) Identification of early requirements for preplacodal ectoderm and sensory organ development. *PLoS genetics* 6(9):e1001133.

10. Ladher RK, O'Neill P, & Begbie J (2010) From shared lineage to distinct functions: the development of the inner ear and epibranchial placodes. *Development* 137(11):1777-1785.

11. Ohyama T, Groves AK, & Martin K (2007) The first steps towards hearing: mechanisms of otic placode induction. *The International journal of developmental biology* 51(6-7):463-472.

12. Schimmang T (2007) Expression and functions of FGF ligands during early otic development. *The International journal of developmental biology* 51(6-7):473-481.

13. Pfeffer PL, Gerster T, Lun K, Brand M, & Busslinger M (1998) Characterization of three novel members of the zebrafish Pax2/5/8 family: dependency of Pax5 and Pax8 expression on the Pax2.1 (noi) function. *Development* 125(16):3063-3074.

14. Haddon C & Lewis J (1996) Early ear development in the embryo of the zebrafish, Danio rerio. *The Journal of comparative neurology* 365(1):113-128.

15. Riley BB & Phillips BT (2003) Ringing in the new ear: resolution of cell interactions in otic development. *Developmental biology* 261(2):289-312.

16. Hilfer SR, Esteves RA, & Sanzo JF (1989) Invagination of the otic placode: normal development and experimental manipulation. *The Journal of experimental zoology* 251(2):253-264.

17. Lewis ER, Leverenz EL, & Bialek WS (1985) *The vertebrate inner ear* (CRC Press, Boca Raton, Fla.) p 248 p.

18. Whitfield TT, Riley BB, Chiang MY, & Phillips B (2002) Development of the zebrafish inner ear. *Developmental dynamics : an official publication of the American Association of Anatomists* 223(4):427-458.

19. Millimaki BB, Sweet EM, & Riley BB (2010) Sox2 is required for maintenance and regeneration, but not initial development, of hair cells in the zebrafish inner ear. *Developmental biology* 338(2):262-267.

20. Corwin JT & Oberholtzer JC (1997) Fish n' chicks: model recipes for hair-cell regeneration? *Neuron* 19(5):951-954.

21. Ozeki H, Oshima K, Senn P, Kurihara H, & Kaga K (2007) Development and regeneration of hair cells. *Acta oto-laryngologica. Supplementum* (559):38-44.

22. Edge AS & Chen ZY (2008) Hair cell regeneration. *Current opinion in neurobiology* 18(4):377-382.

23. Kazmierczak P, *et al.* (2007) Cadherin 23 and protocadherin 15 interact to form tip-link filaments in sensory hair cells. *Nature* 449(7158):87-91.

24. Tanaka K & Smith CA (1978) Structure of the chicken's inner ear: SEM and TEM study. *The American journal of anatomy* 153(2):251-271.

25. Lim DJ & Anniko M (1985) Developmental morphology of the mouse inner ear. A scanning electron microscopic observation. *Acta oto-laryngologica. Supplementum* 422:1-69.

26. Riley BB, Zhu C, Janetopoulos C, & Aufderheide KJ (1997) A critical period of ear development controlled by distinct populations of ciliated cells in the zebrafish. *Developmental biology* 191(2):191-201.

27. Kindt KS, Finch G, & Nicolson T (2012) Kinocilia mediate mechanosensitivity in developing zebrafish hair cells. *Developmental cell* 23(2):329-341.

28. Hudspeth AJ & Corey DP (1977) Sensitivity, polarity, and conductance change in the response of vertebrate hair cells to controlled mechanical stimuli. *Proceedings of the National Academy of Sciences of the United States of America* 74(6):2407-2411.

29. Corey DP & Hudspeth AJ (1983) Kinetics of the receptor current in bullfrog saccular hair cells. *The Journal of neuroscience : the official journal of the Society for Neuroscience* 3(5):962-976.

30. Zdebik AA, Wangemann P, & Jentsch TJ (2009) Potassium ion movement in the inner ear: insights from genetic disease and mouse models. *Physiology* 24:307-316.

31. Smith CA & Sjostrand FS (1961) Structure of the nerve endings on the external hair cells of the guinea pig cochlea as studied by serial sections. *Journal of ultrastructure research* 5:523-556.

32. Lenzi D & von Gersdorff H (2001) Structure suggests function: the case for synaptic ribbons as exocytotic nanomachines. *BioEssays : news and reviews in molecular, cellular and developmental biology* 23(9):831-840.

33. Meyer AC, *et al.* (2009) Tuning of synapse number, structure and function in the cochlea. *Nature neuroscience* 12(4):444-453.

34. Hossain WA, Antic SD, Yang Y, Rasband MN, & Morest DK (2005) Where is the spike generator of the cochlear nerve? Voltage-gated sodium channels in the mouse cochlea. *The Journal of neuroscience : the official journal of the Society for Neuroscience* 25(29):6857-6868.

35. Brödel M & Malone PD (1946) *Three unpublished drawings of the anatomy of the human ear* (W. B. Saunders Company, Philadelphia, London,) p 19 p. incl. col. front. (port.) plates.

36. Spoendlin H (1969) Innervation patterns in the organ of corti of the cat. *Acta oto-laryngologica* 67(2):239-254.

37. Brownell WE, Bader CR, Bertrand D, & de Ribaupierre Y (1985) Evoked mechanical responses of isolated cochlear outer hair cells. *Science* 227(4683):194-196.

38. Spoendlin H & Brun JP (1973) Relation of structural damage to exposure time and intensity in acoustic trauma. *Acta oto-laryngologica* 75(2):220-226.

39. Brown MC (1994) Antidromic responses of single units from the spiral ganglion. *Journal of neurophysiology* 71(5):1835-1847.

40. Rubel EW & Fritzsch B (2002) Auditory system development: primary auditory neurons and their targets. *Annual review of neuroscience* 25:51-101.

41. Smith ME, Schuck JB, Gilley RR, & Rogers BD (2011) Structural and functional effects of acoustic exposure in goldfish: evidence for tonotopy in the teleost saccule. *BMC neuroscience* 12:19.

42. Liberman MC (1982) Single-neuron labeling in the cat auditory nerve. *Science* 216(4551):1239-1241.

43. Liberman MC, Dodds LW, & Pierce S (1990) Afferent and efferent innervation of the cat cochlea: quantitative analysis with light and electron microscopy. *The Journal of comparative neurology* 301(3):443-460.

44. Ehret G (1976) Development of absolute auditory thresholds in the house mouse (Mus musculus). *Journal of the American Audiology Society* 1(5):179-184.

45. Ryugo D (1992) The auditory nerve: Peripheral innervation, cell body morphology, and central projections. *The mammalian auditory pathway: Neuroanatomy* The auditory nerve: Peripheral innervation, cell body morphology, and central projections, ed Webster AP, & R. Fay (Springer-Verlag, New York), pp 23 – 65.

46. Nadol JB, Jr., Burgess BJ, & Reisser C (1990) Morphometric analysis of normal human spiral ganglion cells. *The Annals of otology, rhinology, and laryngology* 99(5 Pt 1):340-348.

47. Crozier RLDaRA (The Electrophysiological Signature of Spiral Ganglion Neurons. in *The Primary Auditory Neurons of the Mammalian Cochlea*, eds

Dabdoub A, Fritzsch B, Popper AN, Fay RR, & SpringerLink (Online service), pp XIV, 286 p. 261 illus., 239 illus. in color.

48. Pirvola U, *et al.* (1992) Brain-derived neurotrophic factor and neurotrophin 3 mRNAs in the peripheral target fields of developing inner ear ganglia. *Proceedings of the National Academy of Sciences of the United States of America* 89(20):9915-9919.

49. Ernfors P, Van De Water T, Loring J, & Jaenisch R (1995) Complementary roles of BDNF and NT-3 in vestibular and auditory development. *Neuron* 14(6):1153-1164.

50. Fritzsch B, Silos-Santiago I, Bianchi LM, & Farinas I (1997) The role of neurotrophic factors in regulating the development of inner ear innervation. *Trends in neurosciences* 20(4):159-164.

51. Sun W & Salvi RJ (2009) Brain derived neurotrophic factor and neurotrophic factor 3 modulate neurotransmitter receptor expressions on developing spiral ganglion neurons. *Neuroscience* 164(4):1854-1866.

52. Eatock RA, Xue J, & Kalluri R (2008) Ion channels in mammalian vestibular afferents may set regularity of firing. *The Journal of experimental biology* 211(Pt 11):1764-1774.

53. Goldberg JM (2000) Afferent diversity and the organization of central vestibular pathways. *Experimental brain research* 130(3):277-297.

54. Hebert JM & McConnell SK (2000) Targeting of cre to the Foxg1 (BF-1) locus mediates loxP recombination in the telencephalon and other developing head structures. *Developmental biology* 222(2):296-306.

55. Ohyama T & Groves AK (2004) Generation of Pax2-Cre mice by modification of a Pax2 bacterial artificial chromosome. *Genesis* 38(4):195-199.

56. Bouchard M, Souabni A, & Busslinger M (2004) Tissue-specific expression of cre recombinase from the Pax8 locus. *Genesis* 38(3):105-109.

57. Sandell LL, Butler Tjaden NE, Barlow AJ, & Trainor PA (2014) Cochleovestibular nerve development is integrated with migratory neural crest cells. *Developmental biology* 385(2):200-210.

58. Freter S, Fleenor SJ, Freter R, Liu KJ, & Begbie J (2013) Cranial neural crest cells form corridors prefiguring sensory neuroblast migration. *Development* 140(17):3595-3600.

59. Begbie J & Graham A (2001) Integration between the epibranchial placodes and the hindbrain. *Science* 294(5542):595-598.

60. Ma Q, Chen Z, del Barco Barrantes I, de la Pompa JL, & Anderson DJ (1998) neurogenin1 is essential for the determination of neuronal precursors for proximal cranial sensory ganglia. *Neuron* 20(3):469-482.

61. Andermann P, Ungos J, & Raible DW (2002) Neurogenin1 defines zebrafish cranial sensory ganglia precursors. *Developmental biology* 251(1):45-58.

62. Ma Q, Kintner C, & Anderson DJ (1996) Identification of neurogenin, a vertebrate neuronal determination gene. *Cell* 87(1):43-52.

63. Blader P, Fischer N, Gradwohl G, Guillemot F, & Strahle U (1997) The activity of neurogenin1 is controlled by local cues in the zebrafish embryo. *Development* 124(22):4557-4569.

64. Kim WY, *et al.* (2001) NeuroD-null mice are deaf due to a severe loss of the inner ear sensory neurons during development. *Development* 128(3):417-426.

65. Jahan I, Kersigo J, Pan N, & Fritzsch B (2010) Neurod1 regulates survival and formation of connections in mouse ear and brain. *Cell and tissue research* 341(1):95-110.

66. D'Amico-Martel A (1982) Temporal patterns of neurogenesis in avian cranial sensory and autonomic ganglia. *The American journal of anatomy* 163(4):351-372.

67. Tsuchida T, *et al.* (1994) Topographic organization of embryonic motor neurons defined by expression of LIM homeobox genes. *Cell* 79(6):957-970.

68. Gong Z, Hui CC, & Hew CL (1995) Presence of isl-1-related LIM domain homeobox genes in teleost and their similar patterns of expression in brain and spinal cord. *The Journal of biological chemistry* 270(7):3335-3345.

69. Bok J, Bronner-Fraser M, & Wu DK (2005) Role of the hindbrain in dorsoventral but not anteroposterior axial specification of the inner ear. *Development* 132(9):2115-2124.

70. Shanmugalingam S, *et al.* (2000) Ace/Fgf8 is required for forebrain commissure formation and patterning of the telencephalon. *Development* 127(12):2549-2561.

71. Bok J, *et al.* (2011) Transient retinoic acid signaling confers anterior-posterior polarity to the inner ear. *Proceedings of the National Academy of Sciences of the United States of America* 108(1):161-166.

72. Phillips BT, Bolding K, & Riley BB (2001) Zebrafish fgf3 and fgf8 encode redundant functions required for otic placode induction. *Developmental biology* 235(2):351-365.

73. Kwak SJ, Phillips BT, Heck R, & Riley BB (2002) An expanded domain of fgf3 expression in the hindbrain of zebrafish valentino mutants results in mis-patterning of the otic vesicle. *Development* 129(22):5279-5287.

74. Hammond KL & Whitfield TT (2011) Fgf and Hh signalling act on a symmetrical pre-pattern to specify anterior and posterior identity in the zebrafish otic placode and vesicle. *Development* 138(18):3977-3987.

75. Leger S & Brand M (2002) Fgf8 and Fgf3 are required for zebrafish ear placode induction, maintenance and inner ear patterning. *Mechanisms of development* 119(1):91-108.

76. Abello G, *et al.* (2010) Independent regulation of Sox3 and Lmx1b by FGF and BMP signaling influences the neurogenic and non-neurogenic domains in the chick otic placode. *Developmental biology* 339(1):166-178.

77. Alsina B, *et al.* (2004) FGF signaling is required for determination of otic neuroblasts in the chick embryo. *Developmental biology* 267(1):119-134.

78. Wright TJ, *et al.* (2004) Mouse FGF15 is the ortholog of human and chick FGF19, but is not uniquely required for otic induction. *Developmental biology* 269(1):264-275.

79. Wright TJ & Mansour SL (2003) FGF signaling in ear development and innervation. *Current topics in developmental biology* 57:225-259.

80. Vazquez-Echeverria C, Dominguez-Frutos E, Charnay P, Schimmang T, & Pujades C (2008) Analysis of mouse kreisler mutants reveals new roles of hindbrain-derived signals in the establishment of the otic neurogenic domain. *Developmental biology* 322(1):167-178.

81. Wright TJ, *et al.* (2003) Expression of mouse fibroblast growth factor and fibroblast growth factor receptor genes during early inner ear development. *Developmental dynamics : an official publication of the American Association of Anatomists* 228(2):267-272.

82. Pirvola U, *et al.* (2000) FGF/FGFR-2(IIIb) signaling is essential for inner ear morphogenesis. *The Journal of neuroscience : the official journal of the Society for Neuroscience* 20(16):6125-6134.

83. Colvin JS, Bohne BA, Harding GW, McEwen DG, & Ornitz DM (1996) Skeletal overgrowth and deafness in mice lacking fibroblast growth factor receptor 3. *Nature genetics* 12(4):390-397.

84. Hossain WA, Zhou X, Rutledge A, Baier C, & Morest DK (1996) Basic fibroblast growth factor affects neuronal migration and differentiation in normotypic cell cultures from the cochleovestibular ganglion of the chick embryo. *Experimental neurology* 138(1):121-143.

85. Satoh T & Fekete DM (2005) Clonal analysis of the relationships between mechanosensory cells and the neurons that innervate them in the chicken ear. *Development* 132(7):1687-1697.

86. Raft S, *et al.* (2007) Cross-regulation of Ngn1 and Math1 coordinates the production of neurons and sensory hair cells during inner ear development. *Development* 134(24):4405-4415.

87. Lanford PJ, *et al.* (1999) Notch signalling pathway mediates hair cell development in mammalian cochlea. *Nature genetics* 21(3):289-292.

88. Brooker R, Hozumi K, & Lewis J (2006) Notch ligands with contrasting functions: Jagged1 and Delta1 in the mouse inner ear. *Development* 133(7):1277-1286.

89. Haddon C, Jiang YJ, Smithers L, & Lewis J (1998) Delta-Notch signalling and the patterning of sensory cell differentiation in the zebrafish ear: evidence from the mind bomb mutant. *Development* 125(23):4637-4644.

90. Korzh V, Sleptsova I, Liao J, He J, & Gong Z (1998) Expression of zebrafish bHLH genes ngn1 and nrd defines distinct stages of neural differentiation. *Developmental dynamics : an official publication of the American Association of Anatomists* 213(1):92-104.

91. Begbie J, Ballivet M, & Graham A (2002) Early steps in the production of sensory neurons by the neurogenic placodes. *Molecular and cellular neurosciences* 21(3):502-511.

92. Matei V, *et al.* (2005) Smaller inner ear sensory epithelia in Neurog 1 null mice are related to earlier hair cell cycle exit. *Developmental dynamics : an official publication of the American Association of Anatomists* 234(3):633-650.

93. Camarero G, *et al.* (2003) Insulin-like growth factor 1 is required for survival of transit-amplifying neuroblasts and differentiation of otic neurons. *Developmental biology* 262(2):242-253.

94. Adamska M, *et al.* (2001) FGFs control the patterning of the inner ear but are not able to induce the full ear program. *Mechanisms of development* 109(2):303-313.

95. Millimaki BB, Sweet EM, Dhason MS, & Riley BB (2007) Zebrafish atoh1 genes: classic proneural activity in the inner ear and regulation by Fgf and Notch. *Development* 134(2):295-305.

96. Adamska M, *et al.* (2000) Inner ear and lateral line expression of a zebrafish Nkx5-1 gene and its downregulation in the ears of FGF8 mutant, ace. *Mechanisms of development* 97(1-2):161-165.

97. Lecaudey V, *et al.* (2007) Role of the hindbrain in patterning the otic vesicle: a study of the zebrafish vhnf1 mutant. *Developmental biology* 303(1):134-143.

98. Lee Y, Grill S, Sanchez A, Murphy-Ryan M, & Poss KD (2005) Fgf signaling instructs position-dependent growth rate during zebrafish fin regeneration. *Development* 132(23):5173-5183.

99. Pittman AJ, Law MY, & Chien CB (2008) Pathfinding in a large vertebrate axon tract: isotypic interactions guide retinotectal axons at multiple choice points. *Development* 135(17):2865-2871.

100. Kimmel CB, Ballard WW, Kimmel SR, Ullmann B, & Schilling TF (1995) Stages of embryonic development of the zebrafish. *Developmental dynamics : an official publication of the American Association of Anatomists* 203(3):253-310.

101. Jowett T & Yan YL (1996) Double fluorescent in situ hybridization to zebrafish embryos. *Trends in genetics : TIG* 12(10):387-389.

102. Riley BB, Chiang M, Farmer L, & Heck R (1999) The deltaA gene of zebrafish mediates lateral inhibition of hair cells in the inner ear and is regulated by pax2.1. *Development* 126(24):5669-5678.

103. Alsina B, Giraldez F, & Varela-Nieto I (2003) Growth factors and early development of otic neurons: interactions between intrinsic and extrinsic signals. *Current topics in developmental biology* 57:177-206.

104. Sanchez-Calderon H, Milo M, Leon Y, & Varela-Nieto I (2007) A network of growth and transcription factors controls neuronal differentation and survival in the developing ear. *The International journal of developmental biology* 51(6-7):557-570.

105. Radosevic M, Robert-Moreno A, Coolen M, Bally-Cuif L, & Alsina B (2011) Her9 represses neurogenic fate downstream of Tbx1 and retinoic acid signaling in the inner ear. *Development* 138(3):397-408.

106. Liu M, *et al.* (2000) Essential role of BETA2/NeuroD1 in development of the vestibular and auditory systems. *Genes & development* 14(22):2839-2854.

107. Sapede D & Pujades C (2010) Hedgehog signaling governs the development of otic sensory epithelium and its associated innervation in zebrafish. *The Journal of neuroscience : the official journal of the Society for Neuroscience* 30(10):3612-3623.

108. Raible F & Brand M (2001) Tight transcriptional control of the ETS domain factors Erm and Pea3 by Fgf signaling during early zebrafish development. *Mechanisms of development* 107(1-2):105-117.

109. Roehl H & Nusslein-Volhard C (2001) Zebrafish pea3 and erm are general targets of FGF8 signaling. *Current biology : CB* 11(7):503-507.

110. Padanad MS, Bhat N, Guo B, & Riley BB (2012) Conditions that influence the response to Fgf during otic placode induction. *Developmental biology* 364(1):1-10.

111. Higgs DM, Souza MJ, Wilkins HR, Presson JC, & Popper AN (2002) Age- and size-related changes in the inner ear and hearing ability of the adult zebrafish (Danio rerio). *Journal of the Association for Research in Otolaryngology : JARO* 3(2):174-184.

112. Feng Y & Xu Q (2010) Pivotal role of hmx2 and hmx3 in zebrafish inner ear and lateral line development. *Developmental biology* 339(2):507-518.

113. Koundakjian EJ, Appler JL, & Goodrich LV (2007) Auditory neurons make stereotyped wiring decisions before maturation of their targets. *The Journal of neuroscience : the official journal of the Society for Neuroscience* 27(51):14078-14088.

114. Bell D, *et al.* (2008) Spatial and temporal segregation of auditory and vestibular neurons in the otic placode. *Developmental biology* 322(1):109-120.

115. Mansour SL, Goddard JM, & Capecchi MR (1993) Mice homozygous for a targeted disruption of the proto-oncogene int-2 have developmental defects in the tail and inner ear. *Development* 117(1):13-28.

116. Hossain WA & Morest DK (2000) Fibroblast growth factors (FGF-1, FGF-2) promote migration and neurite growth of mouse cochlear ganglion cells in vitro: immunohistochemistry and antibody perturbation. *Journal of neuroscience research* 62(1):40-55.

117. Goldfarb M, Bates B, Drucker B, Hardin J, & Haub O (1991) Expression and possible functions of the FGF-5 gene. *Annals of the New York Academy of Sciences* 638:38-52.

118. Luo L, Koutnouyan H, Baird A, & Ryan AF (1993) Acidic and basic FGF mRNA expression in the adult and developing rat cochlea. *Hearing research* 69(1-2):182-193.

119. Pauley S, *et al.* (2003) Expression and function of FGF10 in mammalian inner ear development. *Developmental dynamics : an official publication of the American Association of Anatomists* 227(2):203-215.

120. Silva VA, Gomide VC, & Chadi G (2005) Fibroblast growth factor-2 immunoreactivity is present in the central and peripheral auditory pathways of adult rats. *Journal of morphology* 265(2):141-151.

121. Sekiya T, Shimamura N, Yagihashi A, & Suzuki S (2003) Effect of topically applied basic fibroblast growth factor on injured cochlear nerve. *Neurosurgery* 52(4):900-907; discussion 907.

122. D'Sa C, Gross J, Francone VP, & Morest DK (2007) Plasticity of synaptic endings in the cochlear nucleus following noise-induced hearing loss is facilitated in the adult FGF2 overexpressor mouse. *The European journal of neuroscience* 26(3):666-680.

123. Wang SJ, *et al.* (2009) Inactivation of fibroblast growth factor receptor signaling in myelinating glial cells results in significant loss of adult spiral ganglion neurons accompanied by age-related hearing impairment. *Journal of neuroscience research* 87(15):3428-3437.

124. Wei D, Jin Z, Jarlebark L, Scarfone E, & Ulfendahl M (2007) Survival, synaptogenesis, and regeneration of adult mouse spiral ganglion neurons in vitro. *Developmental neurobiology* 67(1):108-122.

125. Kawauchi S, *et al.* (2005) Fgf8 expression defines a morphogenetic center required for olfactory neurogenesis and nasal cavity development in the mouse. *Development* 132(23):5211-5223.

126. Wu HH, *et al.* (2003) Autoregulation of neurogenesis by GDF11. *Neuron* 37(2):197-207.

127. Kim J, *et al.* (2005) GDF11 controls the timing of progenitor cell competence in developing retina. *Science* 308(5730):1927-1930.

128. Tsai RY & Kim S (2005) Fibroblast growth factor 2 negatively regulates the induction of neuronal progenitors from neural stem cells. *Journal of neuroscience research* 82(2):149-159.

129. Nelson AD & Svendsen CN (2006) Low concentrations of extracellular FGF-2 are sufficient but not essential for neurogenesis from human neural progenitor cells. *Molecular and cellular neurosciences* 33(1):29-35.

130. Saarimaki-Vire J, *et al.* (2007) Fibroblast growth factor receptors cooperate to regulate neural progenitor properties in the developing midbrain and hindbrain. *The Journal of neuroscience : the official journal of the Society for Neuroscience* 27(32):8581-8592.

131. Greber B, *et al.* (2010) Conserved and divergent roles of FGF signaling in mouse epiblast stem cells and human embryonic stem cells. *Cell stem cell* 6(3):215-226.

132. Vemaraju S, Kantarci H, Padanad MS, & Riley BB (2012) A spatial and temporal gradient of Fgf differentially regulates distinct stages of neural development in the zebrafish inner ear. *PLoS genetics* 8(11):e1003068.

133. Radde-Gallwitz K, *et al.* (2004) Expression of Islet1 marks the sensory and neuronal lineages in the mammalian inner ear. *The Journal of comparative neurology* 477(4):412-421.

134. Saint-Jeannet JP & Moody SA (2014) Establishing the pre-placodal region and breaking it into placodes with distinct identities. *Developmental biology* 389(1):13-27.

135. Bhat N, Kwon HJ, & Riley BB (2013) A gene network that coordinates preplacodal competence and neural crest specification in zebrafish. *Developmental biology* 373(1):107-117.

136. Nissen RM, Yan J, Amsterdam A, Hopkins N, & Burgess SM (2003) Zebrafish foxi one modulates cellular responses to Fgf signaling required for the integrity of ear and jaw patterning. *Development* 130(11):2543-2554.

137. Padanad MS & Riley BB (2011) Pax2/8 proteins coordinate sequential induction of otic and epibranchial placodes through differential regulation of foxi1, sox3 and fgf24. *Developmental biology* 351(1):90-98.

138. Solomon KS, Kudoh T, Dawid IB, & Fritz A (2003) Zebrafish foxi1 mediates otic placode formation and jaw development. *Development* 130(5):929-940.

139. Edlund RK, Ohyama T, Kantarci H, Riley BB, & Groves AK (2014) Foxi transcription factors promote pharyngeal arch development by regulating formation of FGF signaling centers. *Developmental biology* 390(1):1-13.

140. Khatri SB, Edlund RK, & Groves AK (2014) Foxi3 is necessary for the induction of the chick otic placode in response to FGF signaling. *Developmental biology* 391(2):158-169.

141. Neave B, Rodaway A, Wilson SW, Patient R, & Holder N (1995) Expression of zebrafish GATA 3 (gta3) during gastrulation and neurulation suggests a role in the specification of cell fate. *Mechanisms of development* 51(2-3):169-182.

142. Karis A, *et al.* (2001) Transcription factor GATA-3 alters pathway selection of olivocochlear neurons and affects morphogenesis of the ear. *The Journal of comparative neurology* 429(4):615-630.

143. Lillevali K, Haugas M, Pituello F, & Salminen M (2007) Comparative analysis of Gata3 and Gata2 expression during chicken inner ear development. *Developmental dynamics : an official publication of the American Association of Anatomists* 236(1):306-313.

144. Sheng G & Stern CD (1999) Gata2 and Gata3: novel markers for early embryonic polarity and for non-neural ectoderm in the chick embryo. *Mechanisms of development* 87(1-2):213-216.

145. Appler JM, *et al.* (2013) Gata3 is a critical regulator of cochlear wiring. *The Journal of neuroscience : the official journal of the Society for Neuroscience* 33(8):3679-3691.

146. Duncan JS & Fritzsch B (2013) Continued expression of GATA3 is necessary for cochlear neurosensory development. *PloS one* 8(4):e62046.

147. Luo XJ, *et al.* (2013) GATA3 controls the specification of prosensory domain and neuronal survival in the mouse cochlea. *Human molecular genetics* 22(18):3609-3623.

148. Arduini BL, Bosse KM, & Henion PD (2009) Genetic ablation of neural crest cell diversification. *Development* 136(12):1987-1994.

149. de Croze N, Maczkowiak F, & Monsoro-Burq AH (2011) Reiterative AP2a activity controls sequential steps in the neural crest gene regulatory network. *Proceedings of the National Academy of Sciences of the United States of America* 108(1):155-160.

150. Hoffman TL, Javier AL, Campeau SA, Knight RD, & Schilling TF (2007) Tfap2 transcription factors in zebrafish neural crest development and ectodermal evolution. *Journal of experimental zoology. Part B, Molecular and developmental evolution* 308(5):679-691.

151. Knight RD, *et al.* (2003) lockjaw encodes a zebrafish tfap2a required for early neural crest development. *Development* 130(23):5755-5768.

152. Li W & Cornell RA (2007) Redundant activities of Tfap2a and Tfap2c are required for neural crest induction and development of other non-neural ectoderm derivatives in zebrafish embryos. *Developmental biology* 304(1):338-354.

153. Luo T, Lee YH, Saint-Jeannet JP, & Sargent TD (2003) Induction of neural crest in Xenopus by transcription factor AP2alpha. *Proceedings of the National Academy of Sciences of the United States of America* 100(2):532-537.

154. Nikitina N, Sauka-Spengler T, & Bronner-Fraser M (2008) Dissecting early regulatory relationships in the lamprey neural crest gene network. *Proceedings of the National Academy of Sciences of the United States of America* 105(51):20083-20088.

155. Van Otterloo E, *et al.* (2012) Novel Tfap2-mediated control of soxE expression facilitated the evolutionary emergence of the neural crest. *Development* 139(4):720-730.

156. Wang WD, Melville DB, Montero-Balaguer M, Hatzopoulos AK, & Knapik EW (2011) Tfap2a and Foxd3 regulate early steps in the development of the neural crest progenitor population. *Developmental biology* 360(1):173-185.

157. Scheer N, Riedl I, Warren JT, Kuwada JY, & Campos-Ortega JA (2002) A quantitative analysis of the kinetics of Gal4 activator and effector gene expression in the zebrafish. *Mechanisms of development* 112(1-2):9-14.

158. Scheer N & Campos-Ortega JA (1999) Use of the Gal4-UAS technique for targeted gene expression in the zebrafish. *Mechanisms of development* 80(2):153-158.

159. Xiao T, Roeser T, Staub W, & Baier H (2005) A GFP-based genetic screen reveals mutations that disrupt the architecture of the zebrafish retinotectal projection. *Development* 132(13):2955-2967.

160. Holzschuh J, *et al.* (2003) Noradrenergic neurons in the zebrafish hindbrain are induced by retinoic acid and require tfap2a for expression of the neurotransmitter phenotype. *Development* 130(23):5741-5754.

161. O'Brien EK, *et al.* (2004) Transcription factor Ap-2alpha is necessary for development of embryonic melanophores, autonomic neurons and pharyngeal skeleton in zebrafish. *Developmental biology* 265(1):246-261.

162. Mowbray C, Hammerschmidt M, & Whitfield TT (2001) Expression of BMP signalling pathway members in the developing zebrafish inner ear and lateral line. *Mechanisms of development* 108(1-2):179-184.

163. Abello G, Khatri S, Giraldez F, & Alsina B (2007) Early regionalization of the otic placode and its regulation by the Notch signaling pathway. *Mechanisms of development* 124(7-8):631-645.

164. Yu PB, *et al.* (2008) Dorsomorphin inhibits BMP signals required for embryogenesis and iron metabolism. *Nature chemical biology* 4(1):33-41.

165. Chang W, Nunes FD, De Jesus-Escobar JM, Harland R, & Wu DK (1999) Ectopic noggin blocks sensory and nonsensory organ morphogenesis in the chicken inner ear. *Developmental biology* 216(1):369-381.

166. Gerlach LM, *et al.* (2000) Addition of the BMP4 antagonist, noggin, disrupts avian inner ear development. *Development* 127(1):45-54.

167. Hammond KL, *et al.* (2009) A late role for bmp2b in the morphogenesis of semicircular canal ducts in the zebrafish inner ear. *PloS one* 4(2):e4368.

168. Ohta S, Mansour SL, & Schoenwolf GC (2010) BMP/SMAD signaling regulates the cell behaviors that drive the initial dorsal-specific regional morphogenesis of the otocyst. *Developmental biology* 347(2):369-381.

169. Chang W, *et al.* (2008) Bmp4 is essential for the formation of the vestibular apparatus that detects angular head movements. *PLoS genetics* 4(4):e1000050.

170. Mann ZF, *et al.* (2014) A gradient of Bmp7 specifies the tonotopic axis in the developing inner ear. *Nature communications* 5:3839.

171. Li H, *et al.* (2005) BMP4 signaling is involved in the generation of inner ear sensory epithelia. *BMC developmental biology* 5:16.

172. Ohyama T, *et al.* (2010) BMP signaling is necessary for patterning the sensory and nonsensory regions of the developing mammalian cochlea. *The Journal of neuroscience : the official journal of the Society for Neuroscience* 30(45):15044-15051.

173. Pujades C, Kamaid A, Alsina B, & Giraldez F (2006) BMP-signaling regulates the generation of hair-cells. *Developmental biology* 292(1):55-67.

174. Fantetti KN & Fekete DM (2012) Members of the BMP, Shh, and FGF morphogen families promote chicken statoacoustic ganglion neurite outgrowth and neuron survival in vitro. *Developmental neurobiology* 72(9):1213-1228.

175. Mullins MC, *et al.* (1996) Genes establishing dorsoventral pattern formation in the zebrafish embryo: the ventral specifying genes. *Development* 123:81-93.

176. Linker C, *et al.* (2009) Cell communication with the neural plate is required for induction of neural markers by BMP inhibition: evidence for homeogenetic induction and implications for Xenopus animal cap and chick explant assays. *Developmental biology* 327(2):478-486.

177. Shen H, *et al.* (1997) Chicken transcription factor AP-2: cloning, expression and its role in outgrowth of facial prominences and limb buds. *Developmental biology* 188(2):248-266.

178. Hemond SG & Morest DK (1991) Ganglion formation from the otic placode and the otic crest in the chick embryo: mitosis, migration, and the basal lamina. *Anat Embryol (Berl)* 184(1):1-13.

179. Carney PR & Silver J (1983) Studies on cell migration and axon guidance in the developing distal auditory system of the mouse. *The Journal of comparative neurology* 215(4):359-369.

180. Jahan I, Pan N, Kersigo J, & Fritzsch B (2010) Neurod1 suppresses hair cell differentiation in ear ganglia and regulates hair cell subtype development in the cochlea. *PloS one* 5(7):e11661.

181. Kantarci H, Edlund RK, Groves AK, & Riley BB (2015) Tfap2a promotes specification and maturation of neurons in the inner ear through modulation of Bmp, Fgf and notch signaling. *PLoS genetics* 11(3):e1005037.

182. Riley BB (2003) Genes controlling the development of the zebrafish inner ear and hair cells. *Current topics in developmental biology* 57:357-388.

183. Hans S, Liu D, & Westerfield M (2004) Pax8 and Pax2a function synergistically in otic specification, downstream of the Foxi1 and Dlx3b transcription factors. *Development* 131(20):5091-5102.

184. Christophorou NA, Mende M, Lleras-Forero L, Grocott T, & Streit A (2010) Pax2 coordinates epithelial morphogenesis and cell fate in the inner ear. *Developmental biology* 345(2):180-190.

185. Mackereth MD, Kwak SJ, Fritz A, & Riley BB (2005) Zebrafish pax8 is required for otic placode induction and plays a redundant role with Pax2 genes in the maintenance of the otic placode. *Development* 132(2):371-382.

186. Blumberg B, Wright CV, De Robertis EM, & Cho KW (1991) Organizer-specific homeobox genes in Xenopus laevis embryos. *Science* 253(5016):194-196.

187. Blum M, *et al.* (1992) Gastrulation in the mouse: the role of the homeobox gene goosecoid. *Cell* 69(7):1097-1106.

188. Cho KW, Blumberg B, Steinbeisser H, & De Robertis EM (1991) Molecular nature of Spemann's organizer: the role of the Xenopus homeobox gene goosecoid. *Cell* 67(6):1111-1120.

189. Niehrs C, Keller R, Cho KW, & De Robertis EM (1993) The homeobox gene goosecoid controls cell migration in Xenopus embryos. *Cell* 72(4):491-503.

190. Gaunt SJ, Blum M, & De Robertis EM (1993) Expression of the mouse goosecoid gene during mid-embryogenesis may mark mesenchymal cell lineages in the developing head, limbs and body wall. *Development* 117(2):769-778.

191. Yamada G, *et al.* (1995) Targeted mutation of the murine goosecoid gene results in craniofacial defects and neonatal death. *Development* 121(9):2917-2922.

192. Rivera-Perez JA, Mallo M, Gendron-Maguire M, Gridley T, & Behringer RR (1995) Goosecoid is not an essential component of the mouse gastrula organizer but is required for craniofacial and rib development. *Development* 121(9):3005-3012.

193. Parry DA, *et al.* (2013) SAMS, a syndrome of short stature, auditory-canal atresia, mandibular hypoplasia, and skeletal abnormalities is a unique neurocristopathy caused by mutations in Goosecoid. *American journal of human genetics* 93(6):1135-1142.

194. Hartwell KA, *et al.* (2006) The Spemann organizer gene, Goosecoid, promotes tumor metastasis. *Proceedings of the National Academy of Sciences of the United States of America* 103(50):18969-18974.

195. Xue TC, *et al.* (2014) Goosecoid promotes the metastasis of hepatocellular carcinoma by modulating the epithelial-mesenchymal transition. *PloS one* 9(10):e109695.

196. Vitelli F, *et al.* (2003) TBX1 is required for inner ear morphogenesis. *Human molecular genetics* 12(16):2041-2048.

197. Obholzer N, *et al.* (2008) Vesicular glutamate transporter 3 is required for synaptic transmission in zebrafish hair cells. *The Journal of neuroscience : the official journal of the Society for Neuroscience* 28(9):2110-2118.

198. Sweet EM, Vemaraju S, & Riley BB (2011) Sox2 and Fgf interact with Atoh1 to promote sensory competence throughout the zebrafish inner ear. *Developmental biology* 358(1):113-121.

199. Brand M, *et al.* (1996) Mutations in zebrafish genes affecting the formation of the boundary between midbrain and hindbrain. *Development* 123:179-190.

200. Westerfield M (1993) *The Zebrafish Book: A Guide for the Laboratory Use of Zebrafish (Brachydanio Rerio)* (M. Westerfield).

201. Seiliez I, Thisse B, & Thisse C (2006) FoxA3 and goosecoid promote anterior neural fate through inhibition of Wnt8a activity before the onset of gastrulation. *Developmental biology* 290(1):152-163.

202. Zhao J, Yang C, Guo S, & Wu Y (2015) GM130 regulates epithelial-to-mesenchymal transition and invasion of gastric cancer cells via snail. *Int J Clin Exp Pathol* 8(9):10784-10791.

203. Nakamura N (2010) Emerging new roles of GM130, a cis-Golgi matrix protein, in higher order cell functions. *J Pharmacol Sci* 112(3):255-264.

204. Bouchard M, de Caprona D, Busslinger M, Xu P, & Fritzsch B (2010) Pax2 and Pax8 cooperate in mouse inner ear morphogenesis and innervation. *BMC developmental biology* 10:89.

205. Kwak SJ, *et al.* (2006) Zebrafish pax5 regulates development of the utricular macula and vestibular function. *Developmental dynamics : an official publication of the American Association of Anatomists* 235(11):3026-3038.

206. Burton Q, Cole LK, Mulheisen M, Chang W, & Wu DK (2004) The role of Pax2 in mouse inner ear development. *Developmental biology* 272(1):161-175.

207. Davies D (2011) Cell-extracellular matrix versus cell-cell interactions during the development of the cochlear-vestibular ganglion. *Journal of neuroscience research* 89(9):1375-1387.

208. Schlade-Bartusiak K, Macintyre G, Zunich J, & Cox DW (2008) A child with deletion (14)(q24.3q32.13) and auditory neuropathy. *American journal of medical genetics. Part A* 146A(1):117-123.

209. Hahn M & Jackle H (1996) Drosophila goosecoid participates in neural development but not in body axis formation. *The EMBO journal* 15(12):3077-3084.

210. Hernandez K, Myers LG, Bowser M, & Kidd T (2015) Genetic Tools for the Analysis of Drosophila Stomatogastric Nervous System Development. *PloS one* 10(6):e0128290.

211. Forjanic JP, Chen CK, Jackle H, & Gonzalez Gaitan M (1997) Genetic analysis of stomatogastric nervous system development in Drosophila using enhancer trap lines. *Developmental biology* 186(2):139-154.

212. Gonzalez-Gaitan M & Jackle H (2000) Tip cell-derived RTK signaling initiates cell movements in the Drosophila stomatogastric nervous system anlage. *EMBO reports* 1(4):366-371.

213. Thisse C, Thisse B, Schilling TF, & Postlethwait JH (1993) Structure of the zebrafish snail1 gene and its expression in wild-type, spadetail and no tail mutant embryos. *Development* 119(4):1203-1215.

214. Thisse C, Thisse B, & Postlethwait JH (1995) Expression of snail2, a second member of the zebrafish snail family, in cephalic mesendoderm and presumptive neural crest of wild-type and spadetail mutant embryos. *Developmental biology* 172(1):86-99.

215. Delalande JM, Guyote ME, Smith CM, & Shepherd IT (2008) Zebrafish sip1a and sip1b are essential for normal axial and neural patterning. *Developmental dynamics : an official publication of the American Association of Anatomists* 237(4):1060-1069.

216. Soofi A, Levitan I, & Dressler GR (2012) Two novel EGFP insertion alleles reveal unique aspects of Pax2 function in embryonic and adult kidneys. *Developmental biology* 365(1):241-250.

217. Bouchard M, Souabni A, Mandler M, Neubuser A, & Busslinger M (2002) Nephric lineage specification by Pax2 and Pax8. *Genes & development* 16(22):2958-2970.

218. Danilov V, Blum M, Schweickert A, Campione M, & Steinbeisser H (1998) Negative autoregulation of the organizer-specific homeobox gene goosecoid. *The Journal of biological chemistry* 273(1):627-635.

219. Latinkic BV & Smith JC (1999) Goosecoid and mix.1 repress Brachyury expression and are required for head formation in Xenopus. *Development* 126(8):1769-1779.

220. Yao J & Kessler DS (2001) Goosecoid promotes head organizer activity by direct repression of Xwnt8 in Spemann's organizer. *Development* 128(15):2975-2987.

221. Izzi L, *et al.* (2007) Foxh1 recruits Gsc to negatively regulate Mixl1 expression during early mouse development. *The EMBO journal* 26(13):3132-3143.

222. Taube JH, *et al.* (2010) Core epithelial-to-mesenchymal transition interactome gene-expression signature is associated with claudin-low and metaplastic breast cancer subtypes. *Proceedings of the National Academy of Sciences of the United States of America* 107(35):15449-15454.

223. Kimura Y, *et al.* (1995) Cadherin-11 expressed in association with mesenchymal morphogenesis in the head, somite, and limb bud of early mouse embryos. *Developmental biology* 169(1):347-358.

224. Hadeball B, Borchers A, & Wedlich D (1998) Xenopus cadherin-11 (Xcadherin-11) expression requires the Wg/Wnt signal. *Mechanisms of development* 72(1-2):101-113.

225. Coles EG, Taneyhill LA, & Bronner-Fraser M (2007) A critical role for Cadherin6B in regulating avian neural crest emigration. *Developmental biology* 312(2):533-544.

226. Taneyhill LA, Coles EG, & Bronner-Fraser M (2007) Snail2 directly represses cadherin6B during epithelial-to-mesenchymal transitions of the neural crest. *Development* 134(8):1481-1490.

227. Gay F, Anglade I, Gong Z, & Salbert G (2000) The LIM/homeodomain protein islet-1 modulates estrogen receptor functions. *Molecular endocrinology* 14(10):1627-1648.

228. Ho MY, *et al.* (2010) Nucleotide-binding domain of phosphoglycerate kinase 1 reduces tumor growth by suppressing COX-2 expression. *Cancer science* 101(11):2411-2416.

229. Shetty S, *et al.* (2005) Regulation of urokinase receptor expression by phosphoglycerate kinase is independent of its catalytic activity. *American journal of physiology. Lung cellular and molecular physiology* 289(4):L591-598.

230. Peltz SW, Brown AH, & Jacobson A (1993) mRNA destabilization triggered by premature translational termination depends on at least three cis-acting sequence elements and one trans-acting factor. *Genes & development* 7(9):1737-1754.

231. Kantarci H, Gerberding A, & Riley BB (2016) Spemann organizer gene Goosecoid promotes delamination of neuroblasts from the otic vesicle. *Proceedings of the National Academy of Sciences of the United States of America* 113(44):E6840-E6848.

232. Obholzer N, *et al.* (2012) Rapid positional cloning of zebrafish mutations by linkage and homozygosity mapping using whole-genome sequencing. *Development* 139(22):4280-4290.

233. Aken BL, *et al.* (2016) The Ensembl gene annotation system. *Database (Oxford)* 2016.

234. Lay AJ, *et al.* (2000) Phosphoglycerate kinase acts in tumour angiogenesis as a disulphide reductase. *Nature* 408(6814):869-873.

235. Saksela O & Rifkin DB (1990) Release of basic fibroblast growth factor-heparan sulfate complexes from endothelial cells by plasminogen activator-mediated proteolytic activity. *The Journal of cell biology* 110(3):767-775.

236. Menendez-Montes I, *et al.* (2016) Myocardial VHL-HIF Signaling Controls an Embryonic Metabolic Switch Essential for Cardiac Maturation. *Developmental cell* 39(6):724-739.

237. Bulusu V, *et al.* (2017) Spatiotemporal Analysis of a Glycolytic Activity Gradient Linked to Mouse Embryo Mesoderm Development. *Developmental cell* 40(4):331-341 e334.

238. Ait-Ali N, *et al.* (2015) Rod-derived cone viability factor promotes cone survival by stimulating aerobic glycolysis. *Cell* 161(4):817-832.

239. Lee DC, *et al.* (2015) A lactate-induced response to hypoxia. *Cell* 161(3):595-609.

240. Tzatsos A & Tsichlis PN (2007) Energy depletion inhibits phosphatidylinositol 3-kinase/Akt signaling and induces apoptosis via AMP-activated protein kinase-dependent phosphorylation of IRS-1 at Ser-794. *The Journal of biological chemistry* 282(25):18069-18082.

241. Brown AS & Epstein DJ (2011) Otic ablation of smoothened reveals direct and indirect requirements for Hedgehog signaling in inner ear development. *Development* 138(18):3967-3976.

242. Lawoko-Kerali G, *et al.* (2004) GATA3 and NeuroD distinguish auditory and vestibular neurons during development of the mammalian inner ear. *Mechanisms of development* 121(3):287-299.

243. Yu WM, *et al.* (2013) A Gata3-Mafb transcriptional network directs post-synaptic differentiation in synapses specialized for hearing. *eLife* 2:e01341.

244. Weiner AM, Deininger PL, & Efstratiadis A (1986) Nonviral retroposons: genes, pseudogenes, and transposable elements generated by the reverse flow of genetic information. *Annu Rev Biochem* 55:631-661.

245. Hedges DJ & Batzer MA (2005) From the margins of the genome: mobile elements shape primate evolution. *BioEssays : news and reviews in molecular, cellular and developmental biology* 27(8):785-794.

246. Kazazian HH, Jr. (2004) Mobile elements: drivers of genome evolution. *Science* 303(5664):1626-1632.

247. Li X, *et al.* (2016) Mitochondria-Translocated PGK1 Functions as a Protein Kinase to Coordinate Glycolysis and the TCA Cycle in Tumorigenesis. *Molecular cell* 61(5):705-719.

248. Jindal HK & Vishwanatha JK (1990) Functional identity of a primer recognition protein as phosphoglycerate kinase. *The Journal of biological chemistry* 265(12):6540-6543.

249. Chirico WJ (2011) Protein release through nonlethal oncotic pores as an alternative nonclassical secretory pathway. *BMC cell biology* 12:46.

250. Esen E, *et al.* (2013) WNT-LRP5 signaling induces Warburg effect through mTORC2 activation during osteoblast differentiation. *Cell metabolism* 17(5):745-755.

251. Oginuma M, *et al.* (2017) A Gradient of Glycolytic Activity Coordinates FGF and Wnt Signaling during Elongation of the Body Axis in Amniote Embryos. *Developmental cell* 40(4):342-353 e310.

252. Thisse B, Thisse C. (2004) Fast Release Clones: A High Throughput Expression Analysis. ZFIN Direct Data Submission.

253. Scholpp S & Brand M (2004) Endocytosis controls spreading and effective signaling range of Fgf8 protein. *Current biology : CB* 14(20):1834-1841.

254. Jacques BE, Dabdoub A, & Kelley MW (2012) Fgf signaling regulates development and transdifferentiation of hair cells and supporting cells in the basilar papilla. *Hearing research* 289(1-2):27-39.

255. Maier EC & Whitfield TT (2014) RA and FGF signalling are required in the zebrafish otic vesicle to pattern and maintain ventral otic identities. *PLoS genetics* 10(12):e1004858.

256. Wang J, *et al.* (2015) Fgf-signaling-dependent Sox9a and Atoh1a regulate otic neural development in zebrafish. *The Journal of neuroscience : the official journal of the Society for Neuroscience* 35(1):234-244.

257. Valles AM, Boyer B, Tarone G, & Thiery JP (1996) Alpha 2 beta 1 integrin is required for the collagen and FGF-1 induced cell dispersion in a rat bladder carcinoma cell line. *Cell adhesion and communication* 4(3):187-199.

258. Ciruna B & Rossant J (2001) FGF signaling regulates mesoderm cell fate specification and morphogenetic movement at the primitive streak. *Developmental cell* 1(1):37-49.

259. Sauka-Spengler T & Bronner-Fraser M (2008) A gene regulatory network orchestrates neural crest formation. *Nature reviews. Molecular cell biology* 9(7):557-568.

260. Yang L, *et al.* (2013) Analysis of FGF-dependent and FGF-independent pathways in otic placode induction. *PloS one* 8(1):e55011.

261. Bucci C, *et al.* (1995) Co-operative regulation of endocytosis by three Rab5 isoforms. *FEBS letters* 366(1):65-71.

262. Matsuo I & Kimura-Yoshida C (2013) Extracellular modulation of Fibroblast Growth Factor signaling through heparan sulfate proteoglycans in mammalian development. *Curr Opin Genet Dev* 23(4):399-407.

263. Thisse B, Pflumio, S., Fürthauer, M., Loppin, B., Heyer, V., Degrave, A., Woehl, R., Lux, A., Steffan, T., Charbonnier, X.Q. and Thisse, C. (2001) Expression of the zebrafish genome during embryogenesis. (ZFIN Direct Data Submission).

264. Thisse B, Wright, G.J., Thisse, C. (2008) Embryonic and Larval Expression Patterns from a Large Scale Screening for Novel Low Affinity Extracellular Protein Interactions. (ZFIN Direct Data Submission).

265. Thisse C, and Thisse, B. (2005) High Throughput Expression Analysis of ZF-Models Consortium Clones. (ZFIN Direct Data Submission).

266. Rohs P, Ebert AM, Zuba A, & McFarlane S (2013) Neuronal expression of fibroblast growth factor receptors in zebrafish. *Gene expression patterns : GEP* 13(8):354-361.

267. Cruz IA, *et al.* (2015) Robust regeneration of adult zebrafish lateral line hair cells reflects continued precursor pool maintenance. *Developmental biology* 402(2):229-238.

268. Cho GS, Choi SC, & Han JK (2013) BMP signal attenuates FGF pathway in anteroposterior neural patterning. *Biochemical and biophysical research communications* 434(3):509-515.

269. Vander Heiden MG, Cantley LC, & Thompson CB (2009) Understanding the Warburg effect: the metabolic requirements of cell proliferation. *Science* 324(5930):1029-1033.

270. Clough JR & Whittingham DG (1983) Metabolism of [14C]glucose by postimplantation mouse embryos in vitro. *Journal of embryology and experimental morphology* 74:133-142.

271. Shepard TH, Tanimura T, & Park HW (1997) Glucose absorption and utilization by rat embryos. *The International journal of developmental biology* 41(2):307-314.

272. Agathocleous M, *et al.* (2012) Metabolic differentiation in the embryonic retina. *Nature cell biology* 14(8):859-864.

273. Cassavaugh J & Lounsbury KM (2011) Hypoxia-mediated biological control. *Journal of cellular biochemistry* 112(3):735-744.

274. Seta KA, Spicer Z, Yuan Y, Lu G, & Millhorn DE (2002) Responding to hypoxia: lessons from a model cell line. *Sci STKE* 2002(146):re11.

275. Shim H, *et al.* (1997) c-Myc transactivation of LDH-A: implications for tumor metabolism and growth. *Proceedings of the National Academy of Sciences of the United States of America* 94(13):6658-6663.

276. Fantin VR, St-Pierre J, & Leder P (2006) Attenuation of LDH-A expression uncovers a link between glycolysis, mitochondrial physiology, and tumor maintenance. *Cancer cell* 9(6):425-434.

277. Farabegoli F, *et al.* (2012) Galloflavin, a new lactate dehydrogenase inhibitor, induces the death of human breast cancer cells with different glycolytic attitude by affecting distinct signaling pathways. *European journal of pharmaceutical sciences : official journal of the European Federation for Pharmaceutical Sciences* 47(4):729-738.

278. Pellerin L, *et al.* (2007) Activity-dependent regulation of energy metabolism by astrocytes: an update. *Glia* 55(12):1251-1262.

279. Lisanti MP, *et al.* (2010) Understanding the "lethal" drivers of tumor-stroma co-evolution: emerging role(s) for hypoxia, oxidative stress and autophagy/mitophagy in the tumor micro-environment. *Cancer biology & therapy* 10(6):537-542.

280. Doherty JR & Cleveland JL (2013) Targeting lactate metabolism for cancer therapeutics. *The Journal of clinical investigation* 123(9):3685-3692.

281. Gardner DK (2015) Lactate production by the mammalian blastocyst: manipulating the microenvironment for uterine implantation and invasion? *BioEssays : news and reviews in molecular, cellular and developmental biology* 37(4):364-371.